

**Development of Selective and Sensitive  
Electrodes of an Electronic Tongue for  
Identification of Important Chemical  
Constituents in Green Tea**

**Thesis submitted**

By

**Debangana Das**

Doctor of Philosophy (Engineering)

**Department of Instrumentation and Electronics Engineering**

**Faculty Council of Engineering & Technology**

**Jadavpur University, Kolkata, India**

**2023**



# JADAVPUR UNIVERSITY

KOLKATA- 700032

INDIA

INDEX NO. D-7/E/505/19

Title of the Thesis                      **Development of Selective and Sensitive  
Electrodes of an Electronic Tongue for  
Identification of Important Chemical  
Constituents in Green Tea**

Name, Designation  
& Institution of the  
Supervisor                      ***Dr. Runu Banerjee Roy***  
*Professor*  
*Dept. of Instrumentation and Electronics*  
*Engineering*  
*Jadavpur University, Salt Lake Campus,*  
*Sector-III, Block-LB, Plot-8, Kolkata-*  
*700106, India.*  
*Phone: 08240235742*  
*Fax: 03323357254*





# List of Publications

## Journals

- [1] **Debangana Das**, Trisita Nandy Chatterjee, Runu Banerjee Roy, Bipan Tudu, Ajanto Kr. Hazarika, Santanu Sabhapondit, Rajib Bandyopadhyay, “Titanium oxide nanocubes embedded molecularly imprinted polymer based electrode for selective detection of caffeine in green tea,” *IEEE Sensors Journal*, vol. 20, no.12, pp. 6240-6247, 2020. doi: 10.1109/JSEN.2020.2972773.
- [2] **Debangana Das**, Shreya Nag, Srikanta Acharya, Sanchita Barik, Bipan Tudu, Runu Banerjee Roy, “Discrimination of tea using caffeine sensitive sensor by employing different classifiers and various data analysis techniques,” *Journal of Institution for Engineers, India Series B*, vol.102, pp.939-946, 2021. <https://doi.org/10.1007/s40031-021-00611-8>.
- [3] **Debangana Das**, Don Biswas, Ajanto Kumar Hazarika, Santanu Sabhapondit, Runu Banerjee Roy, Bipan Tudu, Rajib Bandyopadhyay, “CuO nanoparticles decorated MIP-based electrode for sensitive determination of gallic acid in green tea,” *IEEE Sensors Journal*, vol.21, no.5, pp.5687-5694, 2021. doi: 10.1109/JSEN.2020.3036663.
- [4] **Debangana Das**, Shreya Nag, Shubham De, Ajanto Kumar Hazarika, Santanu Sabhapondit, Bipan Tudu, Rajib Bandyopadhyay, Panchanan Pramanik, Runu Banerjee Roy “Electrochemical Detection of Epicatechin in Green Tea Using Quercetin-Imprinted Polymer Graphite Electrode,” *IEEE Sensors Journal*, vol. 21 no. 23, pp. 265226-265234, 2021. doi: 10.1109/JSEN.2021.3122145.
- [5] **Debangana Das**, Shreya Nag, Akansha Adaval, Ajanto Kumar Hazarika, Santanu Sabhapondit, Arup Ranjan Bhattacharyya, Bipan Tudu, Rajib Bandyopadhyay, Runu Banerjee Roy, “Amine Functionalized MWCNTs Modified MIP-Based Electrode for Detection of Epicatechin in Tea, *IEEE Sensors Journal*, vol.22, no.11, pp.10323-10330, 2022. doi: 10.1109/JSEN.2022.3169169.

## Conference Proceedings

- [1] **Debangana Das**, Trisita Nandy Chatterjee, Ajanto Kumar Hazarika, Santanu Sabhapondit, Runu Banerjee Roy, Bipan Tudu, Rajib Bandyopadhyay, Development of a Highly Selective Nickel Cobalt Oxide Nanoparticles Modified

Molecular Imprinted Polymer Based Sensor for Detection of Gallic Acid In Green Tea, IEEE International Symposium on Olfaction and Electronic Nose (ISOEN), 26<sup>th</sup>-29<sup>th</sup> May, 2019, Fukuoka, Japan.

- [2] **Debangana Das**, Shreya Nag, Srikanta Acharya, Srikanta Barik, Bipan Tudu, Runu Banerjee Roy, “Discrimination of Tea using Caffeine-Sensitive Sensor by Employing different Classifiers and Various Data Analysis Techniques”, International Conference on Ubiquitous and Emerging concepts on Sensors and Transducers (UEMCOS), 20<sup>th</sup> May – 22<sup>nd</sup> May, 2020, Kolkata, India.
- [3] **Debangana Das**, Shreya Nag, Upasana Saha, Bipan Tudu and Runu Banerjee Roy, "Development of Molecularly Engraved Polymer Based Sensor for Detection of Theobromine in Tea," IEEE 2<sup>nd</sup> International Conference on Control, Measurement and Instrumentation (CMI), pp. 144-148, 8<sup>th</sup> -10<sup>th</sup> January, 2021, Kolkata, India.

## Journal Publications other than thesis

- [1] **Debangana Das**, Trisita Nandy Chatterjee, Runu Banerjee Roy, Bipan Tudu, Santanu Sabhapondit, Panchanan Pramanik, Rajib Bandyopadhyay, Discrimination of green tea using an Epigallocatechin-3-gallate (EGCG) sensitive molecular imprinted polymer (MIP) based electrode, *Carbon - Science and Technology*, pp. 27 – 37 (2018).
- [2] Trisita Nandy Chatterjee, **Debangana Das**, Runu Banerjee Roy, Bipan Tudu, Ajanto Kumar Hazarika, Santanu Sabhapandit, Pradip Tamuly, Rajib Bandyopadhyay, “Development of a nickel hydroxide nanopetal decorated molecular imprinted polymer based electrode for sensitive detection of epigallocatechin-3-gallate in green tea”, *Sensors and Actuators B: Chemical*, pp. 69-78, March , 2019.
- [3] Trisita Nandy Chatterjee, **Debangana Das**, Runu Banerjee Roy, Bipan Tudu, Santanu Sabhapondit, Pradip Tamuly, Panchanan Pramanik, Rajib Bandyopadhyay, “Molecular Imprinted Polymer Based Electrode for Sensing Catechin (+C) in Green Tea”, *IEEE Sensors Journal*, pp. March 15, 2018.
- [4] Srikanta Acharya, **Debangana Das**, Trisita Nandy Chatterjee, Soumen Roy, Runu Banerjee Roy, Bipan Tudu, and Rajib Bandyopadhyay, “Voltammetric Electrode Array Optimization for Black Tea Discrimination Using Computational

- Intelligence Approach”, *IEEE Sensors Journal*, vol. 21, no. 18, pp. 20589-20595, 2021, doi: 10.1109/JSEN.2021.3098036.
- [5] Shreya Nag, Susmita Pradhan, **Debangana Das**, Bipan Tudu, Rajib Bandyopadhyay, Runu Banerjee Roy, “Fabrication of a Molecular Imprinted Polyacrylonitrile engraved Graphite Electrode for Detection of Formalin in Food Extracts”, *IEEE Sensors Journal*, DOI 10.1109/JSEN.2021.3128520, 2021.
- [6] Shreya Nag, **Debangana Das**, Hemanta Naskar, Bipan Tudu, Rajib Bandyopadhyay, and Runu Banerjee Roy, " Detection of Metanil Yellow Adulteration in Turmeric Powder Using Nano Nickel Cobalt Oxide Modified Graphite Electrode ”, *IEEE Sensors Journal*, vol. 22, no. 13, pp. 12515-12521, 1 July1, 2022, doi: 10.1109/JSEN.2022.3178768.
- [7] D. Bandyopadhyay, S. Nag, **Debangana Das**, S. Acharya, B. Tudu, R. Bandyopadhyay, R. B. Roy, “Voltammetric Detection of Inositol Using A Platinum Based Electrode”, *NanoLife*, March 11, 2022, <https://doi.org/10.1142/S1793984422500040>.
- [8] Shreya Nag, **Debangana Das** and Runu Banerjee Roy, "Voltammetry Application of Molecularly Imprinted Polyacrylamide as Vanillin Receptor in Desserts," *IEEE Sensors Journal*, 2023, doi: 10.1109/JSEN.2023.3235933.
- [9] Madhurima Moulick, **Debangana Das**, Ajanto Kumar Hazarika, Santanu Sabhapondit, Bipan Tudu, Rajib Bandyopadhyay and Runu Banerjee Roy, “Molecularly Imprinted Polymer Based Electrode for Tannic Acid Detection in Black Tea,” *IEEE sensors journal* (Early access), 2023. 10.1109/JSEN. 2023. 3240069



## Statement of Originality

*I, Debangana Das, registered on 25<sup>th</sup> June, 2019, do hereby declare that this thesis entitled “Development of Selective and Sensitive Electrodes of an Electronic Tongue for Identification of Important Chemical Constituents in Green Tea” contains literature survey and original research work done by the undersigned candidate as part of Doctoral studies.*

*All information in this thesis have been obtained and presented in accordance with existing academic rules and ethical conduct. I declare that, as required by these rules and conduct, I have fully cited and referred all materials and results that are not original to this work.*

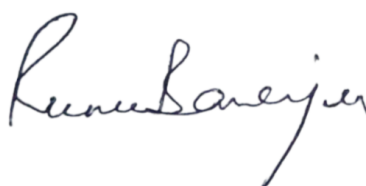
*I also declare that I have checked this thesis as per the “Policy on Anti Plagiarism, Jadavpur University, 2019”, and the level of similarity as checked by iThenticate software is 6%.*



**Debangana Das**

Index No.: **D-7/E/505/19**

Date: 17th Feb, 2023



**Dr. Runu Banerjee Roy**

Professor

Dept. of Instrumentation and Electronics Engineering  
Jadavpur University Salt Lake Campus

Professor  
Dept. of Instrumentation & Electronics Engg  
Jadavpur University  
Saltlake, 2nd Campus  
Kolkata-700 106



## Certificate from the Supervisor

Date: 17th Feb , 2023

*This is to certify that the thesis entitled “Development of Selective and Sensitive Electrodes of an Electronic Tongue For Identification of Important Chemical Constituents in Green Tea”, submitted by Debangana Das, who got her name registered on 25<sup>th</sup> June, 2019, for the award of Ph.D. (Engineering) degree of Jadavpur University, is absolutely based upon her own work under supervision of Prof. Runu Banerjee Roy and that neither her thesis nor any part of the thesis has been submitted for any degree/diploma or any other academic award anywhere before.*



**Dr. Runu Banerjee Roy**

*Professor*

*Dept. of Instrumentation and Electronics Engineering*

*Jadavpur University, Salt Lake Campus*

*Kolkata- 700106. India*

Professor  
Dept. of Instrumentation & Electronics Engg  
Jadavpur University  
Saltlake, 2nd Campus  
Kolkata-700 106





*This thesis is dedicated to*  
*My Parents*



# Acknowledgement

This thesis represents not only my work at the keyboard, but a milestone in more than three year's work at the Research Lab in the Dept. of Instrumentation and Electronics Engineering at Jadavpur University, Kolkata, India. With profound gratitude, the thesis is a remembrance on my part of all the suggestions, guidance and constant reassurances by the Professors, seniors and fellow scholars, which has helped my thesis in seeing the light of day. I have been given unique opportunities and hopefully, have taken advantages of them all.

First and foremost, I would like to extend my sincere gratitude towards my supervisor, Dr. Runu Banerjee Roy, Professor, Jadavpur University, without whose able guidance, support and constant encouragement, this thesis would not have materialized. Her technical expertise, dynamism, vision and motivation have helped me tide over the difficult and disheartening moments during the course of this work. Her kind assistance with the statistical analysis in this dissertation and her patience with my knowledge gaps in the area of this thesis have been second to none. It was a great privilege and honor to work and study under her guidance.

Further, I would like to extend my profound gratitude and heartfelt thanks to Prof. Rajib Bandyopadhyay, Dept. of IEE, Jadavpur University for his priceless advices at important junctures of the project. His lectures have always had a strong impression on me and I have always carried positive memories of his interactions with me. Also, I would like to thank him for being the foundation upon which this laboratory and all the works and emotions therein have been built.

I will always be indebted to Prof. Bipan Tudu, Dept. of IEE, Jadavpur University, whose free soul and ingenious ways of teaching have never failed to inspire me through troubled times during this work. His carefree yet intense way of teaching not only made me absorb my lessons, but also taught me about life.

I would also thank Prof. Arup Ranjan Bhattacharyya, Department of Metallurgical Engineering & Materials Science, Indian Institute of Technology, Bombay, India for helping me with technical details of material characterizations. He has been a constant motivator and advisor throughout my research duration. I thank my colleagues; Ms. Sreya Nag, Dr. Trisita Nandi Chatterjee, Dr. Susmita Pradhan, Dr. Hemanta Naskar, Dr. Saumita Kar, Dr. Sudip Biswas, Mr. Sukanta Ghosh, Mrs. Samhita Dasgupta, Dr. Nilabha Debabhuti for making a cheerful ambience and for their instant participation and effective advices as and when it was required by me.

I would like to thank my friends and juniors Mr. Arpan Bhattacharyya for helping me throughout with proof-reading, Mr. Sudipto Dutta Gupta, Mr. Sourav Bagchi and Mr. Diganta Mandal for sharing knowledge related to electronic circuits. I would like to thank Dr. Tapas Kumar Maji for constantly motivating me to complete my thesis amidst busy work schedule. Also, I would like to thank my one and only sibling, Mrs. Debolina Das Sharma, whose constructive criticisms have always helped me improve in many ways.

Finally, I would like to extend my love and gratitude to my mother and father without whose unwavering support, vigilance and constant words of encouragement, this dissertation, wouldn't have blossomed into a beautiful flower from the bud I started with. It is highly gratifying that they understood the level of stress during my research work and have dealt with my mood fluctuations tactfully. Every time I was ready to quit, my mother and father would not let me and for that, I shall remain forever grateful. This thesis stands as a testament to their sincere love, compassion and support throughout the time of this work. Last but not the least; I thank the Almighty God for His shower of blessings.



Debangana Das  
Department of Instrumentation & Electronics Engineering  
Jadavpur University, Salt Lake Campus  
Sector –III, Block –LB, Kolkata –700 106

Date:17th February, 2023

# Abstract

Green tea is an elixir of life due to its immense contribution towards human health. It is the storage house of anti-oxidants, which protect us from various diseases given that recommended quality and quantity of it is ingested. The quality of tea is assessed normally based on the amount of the phenolic compounds viz. caffeine, gallic acid, epicatechin, catechin, gallic acid, epicatechin gallate, epigallocatechin gallate, theaflavin, etc. present in tea. These compounds are primarily responsible for variation in the taste and flavor of tea. Therefore, determination of the taste-affecting compounds is of utmost necessity. To achieve this aim and to determine only selective compounds which affect the quality of tea, the molecularly imprinted polymer technique has been adopted. Molecular imprinting is a technique to polymerize around a template molecule and remove the template after polymerization. Molecular imprinting polymer (MIP) technology leaves behind recognition sites with the complementary size and shape of the template in the polymer matrix. This technology is evolving into a flexible tool for designing unique molecular recognition sites. MIP has attracted a lot of attention in the world of sensors recently because to its distinctive qualities, which include robustness, a large number of binding sites, low cost, ease of preparation, and excellent stability.

The thesis portrays the development of three electrodes, specific for green tea chemicals, by employing MIP technology. The utilization of MIP enables the detection of a specific target molecule in the analyte. The first molecule that has been chosen for detection in tea is the caffeine molecule. The second molecule that has been chosen is gallic acid (GA). GA serves as a strong anti-oxidant and is the only free phenolic acid present in tea. The third molecule that has been chosen is epicatechin (EC) ( $C_{15}H_{14}O_6$ ) is the most significant bioactive compound amongst all, as takes part in the race of serving tea as a quality health beverage. The epicatechin sensitive electrode has been developed in two ways for cost-effectiveness. A markable reduction in cost has been observed using a dummy template (quercetin) for the detection of EC. The caffeine sensitive electrode demonstrated a linear range from 5  $\mu\text{M}$  to 120  $\mu\text{M}$  with the limit of detection (LOD) being 0.6  $\mu\text{M}$ . An average prediction accuracy of 92.94% is obtained using partial least square regression (PLSR) with root mean square error of calibration (RMSEC) value being as low as 0.07. Additionally for principal component analysis (PCR), an average prediction

accuracy of 93.75% is acquired with RMSEC value being 0.07. The GA sensitive electrode demonstrated two wide linear ranges, i.e., 1  $\mu\text{M}$  – 100  $\mu\text{M}$  and 100  $\mu\text{M}$  to 900  $\mu\text{M}$  with a low detection limit of 12.6 nM. While with PLSR, average prediction accuracy of 88.81 % is obtained with RMSEC as low as 1.36, PCR results in an average prediction accuracy of 87.38 % with RMSEC being 1.37. The EC selective electrode that has been developed using two monomers has wide linear ranges. All the electrodes developed in this work is established to be repeatable, selective, and reproducible, with approximately three-month's stability. Additionally, a three-electrode potentiostat have been developed. The performance of the developed potentiostat has been initially tested with the caffeine electrode. At first, the electrode was subjected to the commercial Autolab Potentiostat (PGSTAT 101) to test the performance of the sensor. On imbibing the electrode, acceptable results were found with a peak current of 167.4  $\mu\text{A}$ . In order to compare the instrument that has been developed in this work with the Autolab potentiostat, the same sensor was dipped in the caffeine stock solution of concentration 1 mM and a peak current of 161.42  $\mu\text{A}$  has been observed.

# Table of Contents

Certificate from Supervisor		xi
Acknowledgement		xv
Abstract		xvii
Table of Content		xix
List of Figures		xxv
List of Tables		xxix
List of Abbreviations		xxxii
<b>Chapter 1: Introduction</b>		<b>1-46</b>
1.1.	Introduction	3
1.2.	The human gustatory system and its perception to taste	5
1.3.	Tea and its taste	7
1.3.1.	Origin of tea	7
1.3.2.	Important taste constituents of tea	8
1.4.	Quality assessment of tea	8
1.4.1.	Instrumental methods	8
1.4.2.	Organoleptic methods	9
1.4.3.	Electronic tongue	10
1.4.4.	Limitations of the above techniques and need for specific sensors	12
1.5.	Electrochemical transduction mechanisms	12
1.6.	Characteristics of electrochemical techniques	13
1.7.	Types of electrochemical techniques	13
1.7.1.	Coulometry	13
1.7.2.	Potentiometry	14
1.7.3.	Voltammetry	14
1.7.3.1.	Traditional types of voltammetric measurements	16
A.	Linear sweep voltammetry	16
B.	Cyclic voltammetry	17
C.	Pulse voltammetry	17

	D. Stripping voltammetry	19
1.8.	Molecularly imprinted polymer (MIP)	19
1.8.1.	Types of imprinting techniques	21
1.8.1.1.	Covalent imprinting	21
	A. Imprinting with readily reversible covalent bond	22
	B. Covalent imprinting with boronate esters	22
	C. Covalent imprinting with Schiff's esters	23
	D. Covalent imprinting with acetals and ketals	23
1.8.1.2.	Non-covalent imprinting	23
	A. Single functional monomer	24
	B. combination of monomers	24
1.8.1.3.	Semi covalent imprinting	25
1.8.1.4.	Imprinting with sacrificial spacers	25
1.9.	Literature survey based on MIP sensors	26
1.10.	Objectives	32
1.11.	Thesis layout	33
	References	34

**Chapter 2: Development of titanium oxide nanoparticles modified MIP electrode for determination of caffeine in green tea** **47-76**

2.1.	Introduction	49
2.2.	Experimental section	51
2.2.1.	Reagents and materials	51
2.2.2.	Equipment and characterization	52
2.2.3.	Synthesis of TiO <sub>2</sub> nanoparticles	52
2.2.4.	Synthesis of the MIP and non-imprinted polymer (NIP)	52
2.2.5.	Preparation of the TiO <sub>2</sub> modified MIP and the NIP electrodes	53
2.3.	Preparation of the green tea liquor for real sample analysis	53
2.4.	Data analysis techniques	54
2.4.1.	Principal component analysis (PCA)	55
2.4.2.	Partial least square regression (PLSR)	57
2.4.3.	Principal Component Regression (PCR)	58
2.5.	Results and discussions	59



2.5.1.	XRD analysis of the prepared TiO <sub>2</sub> nanoparticles	59
2.5.2.	UV-visible spectroscopy	60
2.5.3.	FESEM studies	60
2.5.4.	Optimization of the experimental conditions	61
2.5.4.1.	Supporting electrolyte and pH	61
2.5.4.2.	Influence of scan rate	63
2.5.4.3.	Concentration variation and linearity	64
2.5.4.4.	Sensory characteristics of the MIP- TiO <sub>2</sub> electrode	65
2.6.	Analysis of green tea samples	66
2.6.1.	Principal component analysis (PCA)	67
2.6.2.	Partial least square regression (PLSR)	67
2.6.3.	Principal component regression (PCR)	68
2.6.4.	Validation and prediction using the regression models	69
2.7.	Comparative analysis	70
2.8.	Conclusion	71
	References	72

**Chapter 3: Development of copper oxide nanoparticles embedded MIP electrode for tracing gallic acid in green tea 77-104**

3.1	Introduction	79
3.2	Experimental section	80
3.2.1.	Reagents and materials	80
3.2.2.	Equipment and characterization	81
3.2.3.	GA estimation in HPLC	81
3.2.4.	Synthesis of CuO NPs	81
3.2.5.	Synthesis of GA imprinted polymer and NIP	82
3.2.6.	Fabrication of CuO modified MIP and NIP electrodes	82
3.3	Results and discussions	82
3.3.1.	UV-Visible Spectroscopy	82
3.3.2.	XRD Analysis of the Prepared CuO NPs	83
3.3.3.	SEM and energy dispersive spectroscopy studies	83
3.3.4.	Optimization of the experimental condition	84
3.3.4.1.	Influence of buffer and pH	84

3.3.4.2.	Influence of scan rate	86
3.3.4.3.	Concentration Variation and Linearity	87
3.3.5.	Sensory characteristics of the MIP-CuO Electrode	87
3.4	Analysis of green tea samples	88
3.4.1.	Data clustering using PCA	89
3.4.2.	PLSR analysis	90
3.4.3.	PCR analysis	90
3.4.4.	Validation and prediction using linear regression models	92
3.5	Comparative analysis	92
3.6	Conclusion	93
	References	94
<b>Chapter 4: Development of MIP electrode for tracing epicatechin in green tea</b>		<b>99-134</b>
4.1.	Introduction	101
4.2.	Detection of EC using EC as the target molecule	102
4.2.1.	Chemicals and reagents	103
4.2.2.	Methods and measurement	104
4.2.3.	Synthesis of multi-walled carbon nanotubes	104
4.2.4.	Preparation of the MIP material	104
4.2.5.	Preparation of the electrodes	105
4.2.6.	Results and discussions	105
4.2.6.1.	Morphological characterizations of MIP-EC material	105
	Optical microscopy, Raman spectroscopy and TEM of the prepared MWCNTs	
A.	prepared MWCNTs	105
B.	SEM and TEM of the prepared MIP materials	106
C.	FTIR analysis	110
4.2.6.2.	Influence of buffer and pH	113
4.2.6.3.	Influence of scan rate	112
4.2.6.4.	Concentration variation and linearity	113
4.2.6.5.	Sensory parameters of the MIP-EC electrode	115
4.2.7.	Analysis with real samples	116
4.2.7.1.	PLSR analysis	116
4.2.7.2.	PCR analysis	118

4.2.7.3.	Validation and prediction using the regression models	118
4.3.	Comparison of the present work with existing techniques	119
4.4.	Detection of EC using Q as the target molecule	119
4.4.1.	Chemicals and reagents	120
4.4.2.	Methods and measurement	120
4.4.3.	Preparation of the MIP material	121
4.4.4.	Preparation of the electrodes	121
4.4.5.	Results and discussions	121
	Electrochemical Properties of the MIP-Q@G Electrodes and	
4.4.5.1.	NIP@G Electrodes	121
4.4.5.2.	UV visible spectroscopy	122
4.4.5.3.	Morphological characterizations of MIP-Q material	122
4.4.5.4.	Influence of buffer and pH	123
4.4.5.5.	Influence of scan rate	124
4.4.5.6.	Concentration variation and linearity	124
4.4.5.7.	Sensory characteristics of the developed MIP electrode	126
4.4.6.	Analysis with real samples	128
4.4.6.1.	Partial least square regression	128
4.4.6.2.	Principal component regression	129
4.4.6.3.	Validation and prediction using the developed models	129
4.5.	Comparative analysis	129
4.6.	Conclusion	130
	References	131
<b>Chapter 5: Towards development of a function generator and signal conditioning circuit for voltammetric purpose</b>		<b>135-166</b>
5.1.	Introduction	137
5.2.	The three electrode potentiostat	139
5.3.	Components of the developed cyclic voltammetry three electrode system	140
5.3.1.	Triangular function generator	140
5.3.2.	Filter and level shifter circuit	144
5.3.3.	Potentiostat Circuit	145
5.3.3.1.	Control amplifier	145

5.3.3.2.	Voltage buffer	146
5.3.3.3.	I to V converter	147
5.3.4.	Potentiostat circuit design	148
5.3.5.	PCB routing	149
5.3.6.	Snapshots of the developed system	150
5.3.7.	Power supply unit	150
5.4.	Scan rate variation using the developed system	151
5.5.	Comparison of data	152
5.6.	Conclusion	153
	References	154
<b>Chapter 6: Conclusion and future scope</b>		<b>157-168</b>
6.1.	Introduction	159
6.2.	Summary of findings	160
6.2.1.	Development of titanium oxide nanocubes modified MIP electrode for determination of caffeine in green tea	160
6.2.2.	Development of copper oxide nanoparticles embedded MIP-based electrode for tracing gallic acid in green tea	161
6.2.3.	Development of MIP-based electrode for tracing epicatechin in green tea	161
6.2.4.	Towards development of a function generator and signal conditioning circuit for voltammetric purpose	163
6.3.	Recommendations	164
6.4.	Future scope of this work	164
6.5.	Conclusion	166
	References	166

# List of Figures

<b>Fig. no.</b>	<b>Figure Caption</b>	<b>Pg. No.</b>
Fig.1.1.	The human gustatory reception system	7
Fig.1.2.	Schematic of electronic tongue	10
Fig.1.3.	Three- electrode based electrochemical cell	14
Fig.1.4.	Schematic representation of electrochemical cell	15
Fig.1.5.	Basic electrical circuitry of a potentiostat	16
Fig.1.6.	(a)Cyclic voltammetry waveform (b) Typical cyclic voltammogram showing the different parameters for a reversible reaction	17
Fig.1.7.	(a)Excitation potential waveform for differential pulse voltammetry (b) A typical differential pulse voltammograms	18
Fig.1.8.	Schematic showing MIP technique	21
Fig.1.9.	Schematic explaining the covalent imprinting process	22
Fig.1.10.	Schematic explaining the mechanism of non-covalent imprinting	23
Fig.2.1.	Chemical structure of caffeine	49
Fig.2.2.	Step-wise preparation of the MIP Electrode	50
Fig.2.3.	Optimizations and experimentations performed post-development of the electrode	51
Fig.2.4	(a) Fabricated MIP- electrode (b) Three-electrode configuration along with AutoLab	54
Fig.2.5.	Operational flow chart	54
Fig.2.6	Powder X-ray diffraction pattern of TiO <sub>2</sub>	59
Fig.2.7.	UV-vis absorption spectra of the 1mM CAF solution, before (BRT) and after (ART) removal of the template	60
Fig.2.8.	FESEM images of (a) TiO <sub>2</sub> nanoparticles (b) MIP- TiO <sub>2</sub> and (c) NIP- TiO <sub>2</sub>	61
Fig.2.9.	CV obtained for (a) 1 mM CAF in phthalate, phosphate and acetate buffer solutions (b) 1 mM CAF using phosphate buffer solution of pH values 5, 6 and 7, respectively (c) Comparative CV response of 1 mM CAF solution using MIP- TiO <sub>2</sub> , MIP and NIP-TiO <sub>2</sub> electrode	62
Fig.2.10.	a) CV indicating the variation of peak currents with different scan rates (10 to 100 mVs <sup>-1</sup> ) b) Variation of the anodic peak current with the scan rate c) Relationship between oxidation potential (Ep) and logarithmic scan rate (log v).	64
Fig. 2.11.	(a) Concentration variation of CAF in PBS 5 buffer (DPV) using the MIP- TiO <sub>2</sub> electrode (b) Linear dependency of peak current with concentration	65

Fig. 2.12.	(a) Bar plot indicating the selectivity of the MIP-TiO <sub>2</sub> electrode (b) repeatability of the MIP-TiO <sub>2</sub> electrode (c) reproducibility of the MIP-TiO <sub>2</sub> electrode (d) stability of the MIP-TiO <sub>2</sub> electrode	.66
Fig. 2.13.	PCA plot showing cluster of ten green tea samples	68
Fig. 2.14.	FOR PLSR: (a) RMSEC values of ten components (b) Bar plot indicating the actual and predicted values of CAF; FOR PCR: (c) RMSEC values of ten PCR components (d) Bar plot indicating the actual and predicted values of CAF	70
Fig.3.1.	Chemical structure of GA	79
Fig.3.2.	(a) UV-vis absorption spectra of the 1mM GA solution before (BRT) and after (ART) removal of template (b) Powder XRD pattern of CuO NPs	83
Fig.3.3.	SEM image of a) MIP-CuO b) NIP-CuO c) CuO NPs and d) EDX spectrum of the as prepared CuO NPs	84
Fig.3.4.	Voltammograms obtained for 1 mM GA (a) in citrate, acetate and phosphate buffer solutions (b) with PBS of pH values 5, 6 and 7 (c) with MIP-CuO, MIP and NIP-CuO electrode	85
Fig.3.5.	a) Variation of peak currents with different scan rates (0.01-0.4 Vs <sup>-1</sup> ) b) Plot of peak current with scan rate c) Relationship between oxidation peak current (I <sub>p</sub> ) and square root of scan rate	86
Fig.3.6.	DPV plots obtained on the surface of the MIP-CuO electrode containing different concentrations of GA in PBS 5 (b) Variation of the peak current with concentration; the inset shows the magnified image of the encircled portion	87
Fig.3.7.	Sensory characteristics of the MIP-CuO electrode showing (a) selectivity, (b) reproducibility, (c) repeatability and (d) stability	89
Fig.3.8.	PCA score plot showing cluster of ten green tea samples based on their GA content	90
Fig.3.9.	RMSEC versus number of components (a) PLSR (b) PCR and c) Plot depicting the actual and predicted contents of GA by employing both PLSR and PCR model	91
Fig.4.1.	Chemical structure of (a) EC (b) Q	101
Fig.4.2.	Morphological characterizations of f-MWCNTs: (a) optical microscopic image (scale bar = 100 μm) showing homogeneously dispersed along with 'agglomerates' of f-MWCNTs, (b) TEM image (scale bar = 100 nm) of coiled and entangled 'individualized' f-MWCNTs, (c) the corresponding SAED 'ring pattern' associated with f-MWCNTs, (d,e) FEG-SEM images of highly dense f-MWCNTs network and (f) intensity versus Raman shift of f-MWCNTs	108

Fig.4.3.	FEG-SEM images of (a) MIP before wash (Sample 1),(b) MIP after wash (Sample 2), (c) MIP modified with f-MWCNTs (Sample 3), (d) NIP (Sample 4), (e) and (f) NIP modified with f-MWCNTs (Sample 5)	109
Fig.4.4.	TEM images and the corresponding SAED patterns of Sample 1: MIP before wash (a, b, c), Sample 2: MIP after wash (d, e, f), Sample 3: MIP modified with f-MWCNTs (g, h, i), Sample 4: NIP (j, k, l), and Sample 5: NIP modified with f-MWCNTs (m, n, o)	110
Fig.4.5.	FTIR spectra of MIP before wash (Sample 1), MIP after wash (Sample 2), MIP modified with MWCNTs (Sample 3), NIP (Sample 4), and NIP modified with MWCNTs (Sample 5)	111
Fig.4.6.	Voltammograms obtained for 1 mM EC (a) in citrate, acetate and phosphate buffer solutions (c) with PBS of pH values 5, 6 and 7 (c) with MIP-EC modified, MIP-EC and NIP-modified electrode	113
Fig.4.7.	(a) CV obtained by varying scan rates ( $0.005 - 0.3\text{Vs}^{-1}$ ) (b) deviation of peak current with scan rate (c)plot of Oxidation potential ( $E_p$ ) versus logarithm of scan rate ( $\log v$ )	114
Fig.4.8.	(a) Voltammograms at the MIP-EC electrode surface with different EC concentrations in PBS 5 (b) Deviation of peak current with EC concentration	115
Fig.4.9.	MIP-EC electrode showing (a) selectivity, (b) repeatability, (c) reproducibility and (d) stability	116
Fig.4.10.	RMSEC versus number of components (a) PLSR (b) PCR and (c) Plot depicting the actual and predicted contents of EC by employing both PLSR and PCR model	118
Fig.4.11.	(a) CVs of MIP-Q@G and NIP@G electrode in 0.1 M buffer containing 1mM EC (b) UV-vis absorption spectra of the MIP material before (BW) and after (AW) washing the template	122
Fig.4.12.	SEM image of (a) MIP material and (b) NIP material	123
Fig.4.13.	Voltammograms obtained for 1 mM EC (a) in PBS, acetate and citrate buffer solutions(b) with PBS of pH values 5, 6 and 7	123
Fig. 4.14.	(a) Effect of varying scan rates ( $0.025 - 0.3 \text{Vs}^{-1}$ ) over peak current (b) Peak current deviation with scan rate (c) Oxidation potential vs logarithm of scan rate ( $\log v$ )	125
Fig.4.15.	(a) DPV responses at the MIP-Q@G electrode surface with different EC concentrations in PBS 5 (dipping time 10s before each measurement) (b) Peak current deviation with concentration	125

Fig.4.16.	MIP-Q@G electrode showing (a) selectivity, (b) interference profile	126
Fig.4.17.	MIP-Q@G electrode showing (a) repeatability (b) reproducibility, and (c) stability	127
Fig.5.1.	Block diagram of the developed system	140
Fig.5.2.	First order filter circuit	144
Fig.5.3.	Second order filter circuit	145
Fig.5.4.	Control amplifier circuit	146
Fig.5.5.	Voltage buffer circuit	147
Fig.5.6.	I to V converter	147
Fig.5.7.	Potentiostat circuit design	148
Fig.5.8.	PCB routing done in Proteus 8	149
Fig.5.9.	Display of the triangular-waveform	150
Fig.5.10	Electrochemical response using the developed potentiostat	150
Fig.5.11.	Power Supply Circuit	151
Fig.5.12	Scan rate variation	152
Fig.5.13	Voltammogram obtained with commercial Autolab potentiostat using MIP- caffeine electrode	153
Fig.5.14.	Voltammogram obtained with the developed system using the same electrode	153



## List of Tables

<b>Table No.</b>	<b>Table caption</b>	<b>Pg. No.</b>
Table 1.1.	Types of taste papilla present on human tongue	6
Table 1.2.	Taste affecting compounds in tea	8
Table 1.3.	Comparison of sensors based on natural biomolecules and MIP sensors	21
Table 1.4.	Literature survey on MIP technology	26
Table 2.1.	Actual and predicted CAF content from the LOOCV based PLS and PCR model	69
Table 2.2.	Prediction of CAF concentration in unknown tea samples	69
Table 2.3.	Comparison of the proposed method with existing techniques	71
Table 3.1.	Actual and predicted GA content from PLSR and PCR models.	92
Table 3.2.	Prediction of GA concentration in unknown tea samples	92
Table 3.3.	Comparison of the present method with existing literature	93
Table 4.1.	EC content from PLSR and PCR Model	117
Table 4.2.	Prediction of EC concentration in unknown samples	117
Table 4.3.	Comparison of the present technique with previous literature	119
Table 4.4.	Prediction of EC content from PLSR and PCR model	128
Table 4.5.	Prediction of EC concentration of unknown samples	128
Table 4.6.	Comparison of the present technique with previous literature	129
Table 5.1.	Wave generation parameters	141
Table 6.1.	Summary of findings in the proposed work	163
Table 6.2.	Predictive ability of the fabricated electrodes	163



# List of Abbreviations

ABS	Acetate buffer
Ag/AgCl	Silver/ Silver Chloride
AIBN	2,2'-Azobisisobutyronitrile
AN	Acrylonitrile
BP	Caffeine
CA	Control Amplifier
CAF	Caffeine
CAT	Catechin
CB	Citrate buffer
CE	Counter Electrode
CPE	Carbon Paste Electrode
CTC	Crush Tear Curl
CuO NPs	Copper oxide nanoparticles
CV	Cyclic voltammetry
DPASV	Differential Pulse Anode Stripping voltammetry
DPV	Differential Pulse voltammetry
EC	Epicatechin
ECG	Epicatechin Gallate
EDX	Energy dispersive X-ray spectroscopy detector
EGCG	Epigallocatechin Gallate
EGDMA	Ethylene Glycol Dimethacrylate
EIS	Electrochemical impedance spectroscopy
FESEM	Field emission scanning electron microscope
GA	Gallic acid
GCE	Glassy Carbon Electrode
GO	Graphene oxide
HPLC	High Performance Liquid Chromatography

IA	Itaconic acid
IR spectroscopy	Infrared spectroscopy
LAPV	Large Amplitude Pulse voltammetry
LOD	Limit of detection
LOOCV	leave one out cross validation
LOQ	Limit of quantification
LSV	Linear Sweep Voltammetry
LV	Latent variable
MA	Maleic acid
MAA	Methylacrylic acid
MIP	Molecularly Imprinted Polymer
MIP-TiO <sub>2</sub>	Molecular imprinted polymer electrode modified with TiO <sub>2</sub> nanoparticles
MWCNTs	Multiwalled carbon nanotubes
Ni(OH) <sub>2</sub> NPs	Nickel hydroxide nanoparticles
NIP-TiO <sub>2</sub>	Non- imprinted polymer electrode modified with TiO <sub>2</sub> nanoparticles
NMR spectroscopy	Nuclear Magnetic Resonance spectroscopy
NPV	Normal Pulse Voltammetry
PBS	Phosphate buffer
PC	Principal component
PCA	Principal component analysis
PCR	Principal component regression
PLSR	Partial least square regression techniques
PTh	Phthalate buffer
PV	Pulse Voltammetry
PXRD	Powder X-ray diffraction
Q	Quercetin
RE	Reference Electrode
RMSE	Root mean square error
RMSEC	Root mean square error of calibration
RMSEP	Root mean square error of prediction
RMSEV	Root mean square error of validation

RSD	Relative standard deviation
SAPV	Short Amplitude Pulse Voltammetry
SEM	Scanning electron microscope
SI	Separability index
SWASV	Square wave anode stripping voltammetry
TF	Theaflavin
THB	Theobromine
THP	Theophylline
TiO <sub>2</sub>	Titanium oxide
TLC	Thin Layer Chromatography
WE	Working Electrode
XRD	X-ray diffraction



# Chapter 1

## Introduction

This chapter describes the purpose and exemplifies the goals of this thesis work. The human gustatory system is explained in details. Introduction to origin of tea along with its various compositions have been included. The electrochemical principle of transduction has been discussed. It also focuses on numerous electrochemical techniques used for detection of caffeine, gallic acid and epicatechin. It was followed by a description of how MIP-based recognition systems can be used to overcome the challenges posed by conventional electrochemical identification techniques. Different types of imprinting have also been discussed. Literature survey regarding the usage of MIP technique for detection of various molecules has been done thoroughly

### List of sections

- Introduction
- Human gustatory system and its perception to taste
- Tea and its taste
- Quality assessment of tea
- Electrochemical transduction mechanisms
- Characteristics of electrochemical techniques
- Types of electrochemical techniques
- Molecularly imprinted polymer
- Literature survey based on MIP sensors
- Objectives
- Thesis layout







# Chapter 1

## Introduction

---

### 1.1. Introduction

Tea has captivated the imagination of a huge population as it is the most widely consumed universal beverage in the world, after water, because of its proven benefits towards health [1]. The production, market, and scalability of tea industry are primarily dependent on the quality of the crops. Therefore, serious research has been carried out over the last decade to improve the quality of tea mainly in terms of the plants' health and the color, taste, and flavor of tea leaves. A number of phenolic compounds namely caffeine (CAF), gallic acid (GA), epicatechin (EC), catechin (CAT), epicatechin gallate (ECG), epigallocatechin gallate (EGCG), theaflavin (TF), etc. are the compounds primarily responsible for variation in the color and taste of tea whereas the volatile compounds (such as linalool, geraniol, etc.) affect its flavor. Depending on the tea-processing techniques, there are various kinds of tea like green tea, black tea, purple tea, white tea, oolong tea, etc. Green tea has a befittingly illustrious history of production and consumption. In addition to antioxidants [2], green tea contains health-beneficial compounds such as CAF, GA, and EC. The consumption of green tea can help us prevent numerous harmful diseases including cancer, cardiovascular diseases, diabetes mellitus, Alzheimer's and Parkinson's disease, etc. However, all these benefits can be relished if proper quality of green tea is consumed and in the proper amount. Due to the unique and undeniable role in shaping the modern tea industry, green tea has been used as the real sample throughout this work.

In order to qualitatively discriminate tea on the basis of taste, a group of panelists, known as 'tea tasters' are usually employed by the tea industries [3]. Thereafter, on the basis of colour, aroma and taste of different variants of tea, they assign scores on a scale of 1-10. But these gradations are subjective to a large extent and hence suffer from various inconsistencies owing to the influence of human emotional and psychological attributes [4]. On the other hand, high end instrumental methods like high performance liquid chromatography (HPLC) [5], capillary electrophoresis [6], spectrophotometry [7] provide quality and reproducible information about the tea constituents. These

techniques have various shortcomings like high costs, considerable amount of time required for estimation as well as requirement of skilled personnel with technical know-how. As a result, deployment of these techniques on regular basis by remote tea parlors is unsustainable.

The present thesis titled 'Development of Selective and Sensitive Electrodes of an Electronic Tongue for Identification of Important Chemical Constituents in Green Tea' describes the development of three electrodes, specific for green tea chemicals, by employing molecularly imprinted polymer (MIP) technology. The utilization of MIP enables the detection of a specific target molecule in the analyte. The first molecule that has been chosen for detection in green tea in the thesis is the CAF molecule. The benefits of CAF are advised to 250 mg consumption of CAF per day and overconsumption may lead the human body to develop a tolerance towards it [8, 9] and a human may suffer from several side-effects like anxiety, insomnia, high blood pressure, increased heart rate, and fatigue [10].

Besides helping obese people to lose their weight, green tea is used as an analgesic [11]. As a drug, it stimulates the heart rate, central nervous system [12], and decreases the risk of Type II diabetes mellitus. It also acts as a protective alkaloid against neurodegenerative diseases like Alzheimer's and Parkinson's [13] and is used to cure apnea in premature infants [14]. Due to the structural similarity of CAF with adenosine, it acts an antagonist for the adenosine receptors that helps to aid wakefulness.

The second molecule that has been chosen is GA. GA serves as a strong antioxidant and is the only free phenolic acid present in tea [15]. GA has antibiotic, anti-histaminic, anti-inflammatory, anti-mutagenic and anti-cancer properties. GA also provides protection against cardio-vascular diseases [15-18]. GA is used as a marker for antioxidant capacity and adulteration in any kind of beverage [19]. GA content in tea varies with its degree of fermentation during manufacturing, season and other conditions [20]. Also, the probability of having cardiovascular diseases increases with high consumption of GA as it reacts with hypertension drugs [21]. The determination of GA in green tea is imperative in ensuring its use for beneficial purposes and thus escalates the need for developing low cost and efficient sensors for its detection.

The third molecule that has been chosen is EC ( $C_{15}H_{14}O_6$ ) which is the most significant bioactive compound amongst all, as it takes part in the race of serving tea as a quality health beverage [22]. Distinct properties of EC render protection against

cancer by reducing tumor growth [23, 24]. Moreover, being a shield against carcinogens, it also combats the risk of heart diseases by keeping the serum cholesterol within standard range. Proper consumption of EC improves immunity which is of major concern in today's scenario. Such health benefits motivate the development of a cost-friendly, recyclable, and reproducible sensor for tracing the content of EC.

An additional step has been taken towards the development of a three electrode cyclic-voltammetry (CV) system. The commercial potentiostat is of very high cost because of its precision and provision of various types of voltammetric techniques. The three electrode cyclic voltammetry consists of a triangular wave-form generator, the potentiostat circuit, the synthesized working electrode (WE), platinum counter electrode, Ag/AgCl reference electrode and a digital storage oscilloscope for storing the data and the display of the voltammetric response.

## **1.2. The human gustatory system and its perception to taste**

The primary taste sensing organs in human are called the "taste buds". These are the gustatory organs protruding from the mucous layer of human tongue. Each taste bud is a barrel like structure composed of a number of spindle shaped taste receptor cells bundled within its epithelial sack [25]. A small opening known as "taste pore" is located on top of each taste bud that allows the chemicals of ingested food to come in contact with the receptor cells. Each receptor cell has microscopic hair like protrusions called the "microvilli" extending out through the taste pore. The chemicals of food interact with the receptor cells through the microvilli. A series of complex and multistage biochemical reactions take place when the food chemicals interact with the taste-receptor cells in salivary medium, leading to the generation of electrical potentials within the cell. Such sequence of stages initiated by the physical and chemical interactions of food chemicals with the taste-receptor cells, resulting into the cell potential are termed as "signal transduction pathways". Signal transduction stages are initiated when the molecules of chemicals interact with the taste receptors through physical mechanisms like diffusion or binding. The taste receptor cells are thus, responsible for signal transduction of chemical stimuli obtained from the ingested food. The base of receptor cells are synaptically connected to the nerve cells by many to one relationship. The electrical potentials generated in response to chemical stimuli are then transmitted by the nerve cells to brain for perceptory interpretations. A single taste bud

comprises 50-150 taste receptors. The taste buds are again spatially localized into functional groups called the “papillae”.

The organisation of papillae and taste buds is presented in Fig. 1.1. There are three major types of papillae. Each types of papilla are tuned for detecting a specific taste and are found in the form of localised clusters at the surface of tongue. Table 1.1 describes various types of papilla found on human tongue.

In general, there are considerable differences in the number of taste buds present on a human tongue; it may be as few as 500 or as large as 20,000. This explains why some people can identify subtle differences in taste better than the others. The sense of taste may also diminish with time as the regeneration of taste receptors slows down with age. It has been found that the human gustatory system is very sensitive to the basic taste types [26]. The human beings are endowed with a fairly versatile, highly sensitive and objectively accurate taste perception system and regularly apply their taste buds for quality evaluation of large number of food items on a regular basis.

*Table 1.1. Types of taste papilla present on human tongue.*

<b>Type</b>	<b>Taste detected</b>	<b>Location on tongue</b>
Fungiform papilla	Sweet and salty	Mainly present at the apex of tongue for both sweet and salty taste. Also found to be evenly spread over the tongue towards salty taste
Foliate papilla	Sour	Posterior lateral edges
Circumvallate papilla	Bitter	On the lingual valet and at the rear portion of tongue.

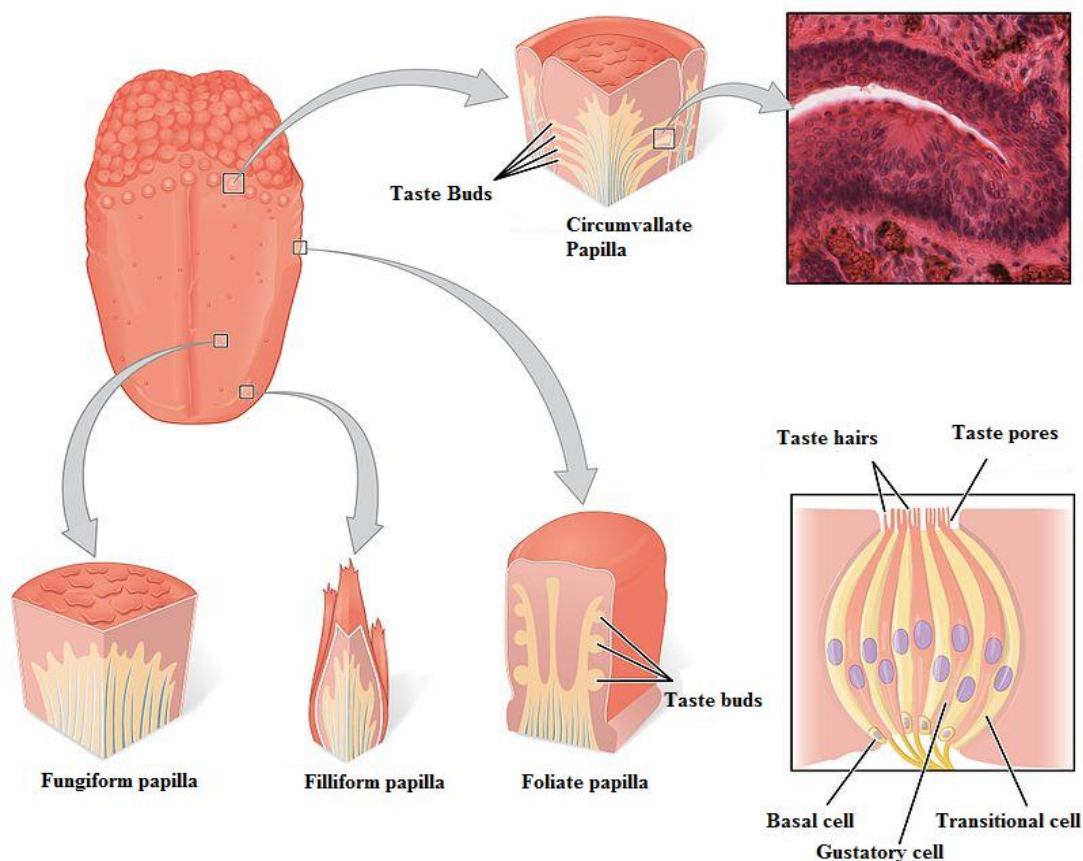


Fig.1.1. The human gustatory reception system.

## 1.3. Tea and its taste

### 1.3.1. Origin of tea

The Portuguese priests and the merchants of China were the first to taste extract of the leaves of *Camellia sinensis*, a plant native to South East Asia more than 5000 years ago [27]. During 17th century, drinking tea became popular in British households which opened the market of tea production and manufacturing in India and to compete with the Chinese monopoly as well. Tea grows under various climatic conditions ranging from the humid tropical landscapes to regions of high latitudes. The tea plant originates in South-East Asian countries, probably in the region incorporating sources and high valleys of the Brahmaputra, the Irrawaddy, the Salween and the Mekong rivers of India, China and Myanmar. The characteristic liquor is the major factor for tea. Assam, China and Darjeeling tea differ in morphological features, quality and degree of fermentation. Assam and the southern part of India are major producer of Crush Tear Curl (CTC) tea (known for its strong gutty liquor), whereas Darjeeling mainly produces orthodox tea, having a strong floral aroma.

### 1.3.2. Important taste constituents of tea

The perceptual consequence of the integration of taste, smell and temperature is referred to as flavor [28]. Tea leaves contain more than 500 compounds which are responsible for their taste and smell. The important taste contributing agents of tea are listed in Table 1.2.

*Table 1.2. Taste affecting compounds in tea.*

Sl. No.	Compounds	Taste
1	Catechin	Strongly Bitter
2	EGCG	Astringent and bitter to a lesser degree
3	Theaflavin	Astringent
4	Thearubigin	Ashy and slight astringent
5	Polyphenol	Astringent
6	Amino acids	Brothy
7	CAF	Bitter

## 1.4. Quality assessment of tea

### 1.4.1. Instrumental methods

In the light of above discussions, it may be stated that the estimation of CAF, GA and EC along with some other compounds like TF, CAT, ECGC, theophylline, etc are the basis for the quality evaluation of tea. Instrumental methods are regularly employed by tea scientists to determine the concentration of non-volatile compounds in tea for gaining knowledge of its qualities. Initial reports on CAF estimation include analytical methods such as gas chromatography, mass spectrometry, and other spectroscopic analyses [29-30]. Some of the traditional methodologies to estimate the GA content in food and beverages comprise reversed phase HPLC, mass spectroscopy [20], chemiluminescence [21] flow injection analysis [31], thin-layer chromatography (TLC) [32] and chronoamperometry. For determination of EC, a pervasive literature survey revealed instrumental methods [33] such as infrared (IR) spectroscopy, liquid chromatography [34-35], Raman spectroscopy [36], nuclear magnetic resonance spectroscopy (NMR) [37], spectrophotometry [38] and capillary electrophoresis [39]. These instruments are capable to estimate the amounts of targeted chemicals and could also separate their fractions. However, in addition to the use of toxic organic solvents while performing experiments, the high-cost factor, long-term performance issue, bulky in size of the instruments, and requirement of skilled technician to operate the instruments lead to their stifled application [40-41]. These

factors create serious challenges to deal with large number of samples. Thus rapid, low-cost, efficient and objective quality analysis is the necessity of the hour from the perspective of industrial applications.

### 1.4.2. Organoleptic methods

Despite the advancements of instrumental quality evaluation techniques, the human perceptions of taste and smell still play a major role to detect the quality of under process or finished tea sample and the price of tea is determined based on their verdict. In the tea tasting process quality, grades are assigned to a tea sample based on the appearance, feel and aroma of dry tea leaves; colour and aroma of infused tea leaves and the taste, colour, and flavour of tea liquor. The quality of dry tea leaves are adjudged after placing the tea leaves on a white paper and observing the colour of leaves, sorting uniformity, feel of texture and aroma emanated from them. The quality of infused leaf is examined after preparing the tea extract by following a standard procedure and separating the infused leaves from the extract. The colour and aroma of the liquor obtained upon sieving from infused leaves are observed. The colour of infused leaves are qualified with linguistic phrases like “bright greenish”, “mixed”, “dull”, “dark”, etc., based on their appearance. The aroma emitted from the hot infused leaves are smelled and quality scores are assigned in terms of adjectives as “delicate”, “fruity”, “burnt”, “smoky” and “sour”. The quality of tea liquor is also sensed using gustation. This can be achieved by sucking in a quantity of liquid and air from a spoon or straight from the tasting cup. In this way, the flavour of the tea is perceived in terms of aroma and taste.

The quality of any type of tea is defined by tea traders that give maximum profit, while consumers define the quality of tea as based on its overall taste and class. The limitations of tasters’ scores are particularly apparent when very small turnaround time is desired due to increased production volume. Thus, the need for good, unbiased, reliable and rapid quality evaluation methodologies become more and more essential due to increasing demand of tea. It has already been indicated that the taste of a food is contributed by the taste of different chemical constituents present and tea is not an exception to it. In this regard, it may be stated that, the instrumental means of tea quality estimation based on the chemical analysis of compounds, both volatile and non-volatile, present in tea, and is more accurate and reliable.



### 1.4.3. Electronic tongue

An electronic tongue is a biologically inspired sensory-electrical system in which intelligent multivariate statistical models are used to record and interpret the responses received from electrodes with overlapping sensitivities. The sample analytes from natural sources are classically examined by complex chemical matrix of innumerable compounds. Electrochemical sensors for specific detection of different types of chemicals are available in large number. However, the effectiveness of using such electrodes for each type of chemical is strictly restricted by the number of chemical compounds that constitute the analytes from natural sources e.g. tea. Under such situations, the electrodes with overlapping affinities yield information about most of the compounds but with different levels of sensitivities, for example, the noble metal electrodes. To extract the required quantity from the electrical signatures collected from the electrodes, the multivariate statistical methods are utilised. The functional schematic of electronic tongue is presented in Fig. 1.2. The electronic tongue systems are classified into two major types based on the principle of operation:

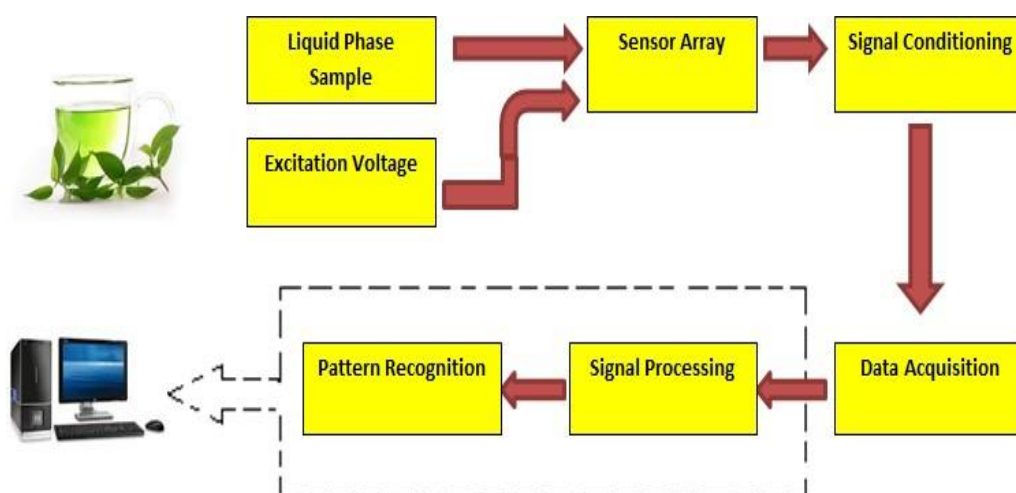


Fig.1.2. Schematic of electronic tongue.

➤ **Potentiometric:** In potentiometric technique, the electric potential developed across the interface of electrode and sample is measured with respect to the potential of a reference electrode under the absence of current. Potentiometric electronic tongue consists of an array of electrodes made of different sensing membranes producing a broadly selective response when subjected to a mixture of chemicals [42-44]. As this kind of electronic tongue is targeted for selective



compounds hence their responses are limited by the number of charged species present in the analyte sample.

➤ **Amperometric:** Here, the electrodes are subjected to a fixed level of voltage corresponding to the redox potentials of constituent chemicals. The steady value of current flowing through the electrodes due to the electrochemical reactions occurring at the surface of working electrode is measured. The amplitude of measured current gives an indication of the concentration of species undergoing redox reaction. In chronoamperometry, the shape of the temporal profile of current also conveys information about the constituents of the analyte under test.

Voltammetry is a subclass of amperometry. In voltammetric methods, changing levels of voltage is given to the working electrode, the resulting current spectra is recorded and represented with respect to the independent variables like time or voltage for analysis purposes. In CV, the voltage signal that is applied to the working electrodes is in triangular shape and the current is analyzed with reference to the applied voltage. In pulse voltammetry, voltage pulses of various amplitudes changing with respect to time are applied. The output current signal with respect to time also yields valuable information about the chemodynamic characteristics of the test electrolyte. In a chemical solution which contains large number of constituents, it is difficult to design electrodes with good selectivity to each of the compounds. In such a scenario, it is prudent to consider the use of a voltammetric electronic tongue [45]. This type of electronic tongue generally contains a set of working electrodes, a reference electrode (RE) and a counter electrode (CE). In voltammetric measurement, potential is applied amidst WE and RE. Also, the current flowing between the WE and CE is recorded. The applied waveforms can be of different shapes and amplitudes. Accordingly, the type of voltammetry can be large amplitude pulse voltammetry (LAPV), short amplitude pulse voltammetry (SAPV) or staircase voltammetry. LAPV is generally used when low threshold of detection is required, while SAPV yields fast response and good sensitivity. The idea of voltammetry is to obtain large amount of information in the form of transient (capacitive current) and steady state (faradaic current) portions of the response. This information when properly analyzed yield sufficient indications regarding the chemical nature of constituents and their contributions to overall quality. The analysis procedure using an electronic tongue is rapid and objective. It not only requires simple sample preparation procedures but also generates large amount of information characterizing the constitution of a complex

multi-component sample. The onus of intelligent data analysis module is to uncover the desired information regarding the parameter or process under study from the complicated electrical spectra obtained from the electrode array.

#### **1.4.4. Limitations of the above techniques and need for specific sensors**

The above techniques discussed for quality gradation of tea has certain limitations, which are discussed below.

- Human tasters normally assign score after tasting. But this type of tea quality analysis is highly subjective because the score given can differ from one person to another depending on the taster's individual choice, mental state, health, etc. Thus, the score so obtained, suffers from various inconsistencies.
- The high-end analytical instruments are sophisticated and costly. Despite of producing accurate results, they are time consuming, complicated, requires skilled operator. Cost effectiveness and simplicity is a major factor in the research area. Due to these practical difficulties, these methods cannot be adopted for quality analysis in the daily evaluation process in the tea industries located in the remote areas.
- The analysis by means of electronic tongue is governed by the overall response of the array of noble metal electrodes followed by suitable pattern recognition techniques. Thus, the response so obtained is non-specific. Moreover, electronic tongue requires a large number of sensors and also it is not able to provide the proper chemical information of the analyte.

### **1.5. Electrochemical transduction mechanism**

Electrochemical transduction mechanisms mainly involve the principle of electro-chemistry to quantify volatile and non-volatile compounds conceivably. Important information regarding the sample can be obtained through the redox reaction process through the detection of current corresponding to the target species and the potential difference between the electrodes; which help to quantify the sample quantitatively. Because of low cost of fabrication, stability, sensitivity, ease of recovery and lesser interferences [46-47], the electrochemical techniques are used extensively in practice.

### **1.6. Characteristics of electrochemical techniques**

The regulatory factors of an electrochemical reaction are potential, current, charge and time. The distinct characteristics of the electrochemical techniques are discussed below:

- i) The potential of the electrode determines the form of the analyte at its surface.
- ii) The analyte may be involved in other reactions along with the conventional oxidation and the reduction processes.
- iii) Current is a measure of the analyte's oxidation and reduction rate.
- iv) Current and potential across an electrode cannot be controlled simultaneously.

## **1.7. Types of electrochemical techniques**

### **1.7.1. Coulometry**

This type of electro-analytical method involves the amount of electricity (coulomb), essential for a substance to get converted into a different oxidation state. This underlying principle for this method is the Faraday's first law of electrolysis [48]. The weight of the substance ( $w$ ) produced or consumed in electrolysis can be obtained by the following Eq. (1.1) considering the charge transfer of  $Q$  coulomb-

$$W = \frac{MQ}{96487n} \quad (1.1)$$

where,  $M$  indicates the molecular mass of the substance liberated or consumed and during the electrochemical process, number of electrons transferred is denoted by  $n$ .

For coulometric analysis, two generalized techniques are normally used, namely the potentiostatic (controlled potential) coulometry and amperostatic (controlled current) coulometry. In case of controlled potential type, the working potential of the electrode is kept at constant level. The oxidation or the reduction of the analyte can be performed without the involvement of less reactive species in the sample or the solvent. On the other hand, in controlled current type coulometry, the respective signal can be obtained in terms of current until the completion of the reaction. Further, the quantity of the output charge can be obtained from the current magnitude and the time during which the current passes.

### **1.7.2. Potentiometry**

In the case of potentiometry, the measurement of potential of an electrochemical cell comes into account without drawing considerable amount of current. The two-electrode system consists of an indicator electrode (measuring electrode) and a RE. The potential signal can be obtained upon dipping the measuring electrode into the target analyte contained solution with respect to a fixed reference electrode. Potentiometry technique can also be subdivided into direct potentiometry and potentiometric titrations. The potentiometry determines the cell potential and relates it to the concentration of the active chemical species. In potentiometric titrations, the cell potential is estimated as an element of the volume of reagent [48].

### 1.7.3. Voltammetry

The most widely used electrochemical techniques involve the principle of voltammetry, where the current is measured using the electrode within a variable potential window [48-49].

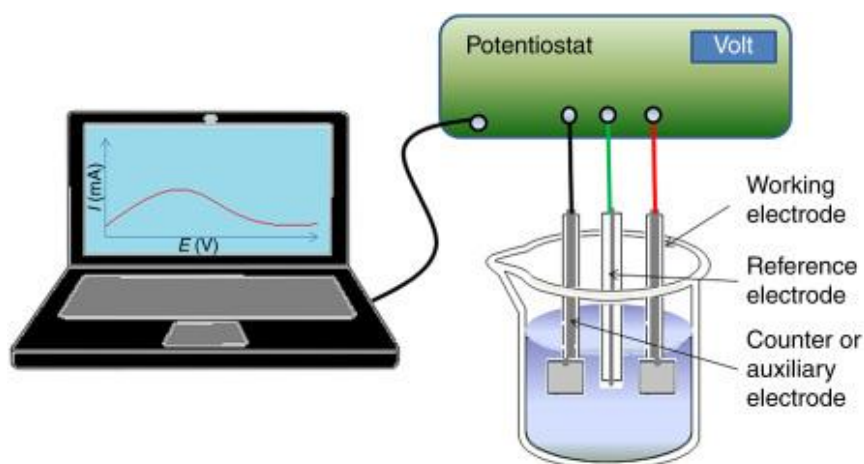


*Fig.1.3. Three- electrode based electrochemical cell.*

The potential is varied within a specified range in order to keep the electroactive chemical species at the surface of the WE. The quantitative information of the target species can be obtained in terms of the peak current generated due to absorption of molecules at the surface of the WE. Fig.1.3. depicts the three electrode based electrochemical cell [49-50], consisting of a RE, such as the saturated calomel electrode or Silver- Silver Chloride electrode (Ag/AgCl) RE, a platinum CE, and a measuring electrode or WE. Unlike potentiometry, RE comes into play in order to maintain a reference potential against the WE with the help of power source or potentiostat. The potentiostat bears an analogy with the controlled voltage source in an electrical system.

It measures and controls the voltage applied across the working electrode by inducing redox reactions at the electrode interface and hence produces current. The generated current flowing through the CE and WE contains meaningful information about the reaction kinetics of the system and the electrochemical properties. The connections and the three electrode setup [48] and the possible configuration of these electrodes viz. CE, RE and a WE are depicted in Fig. 1.3. Here, the direction of current flow is between the CE and WE.

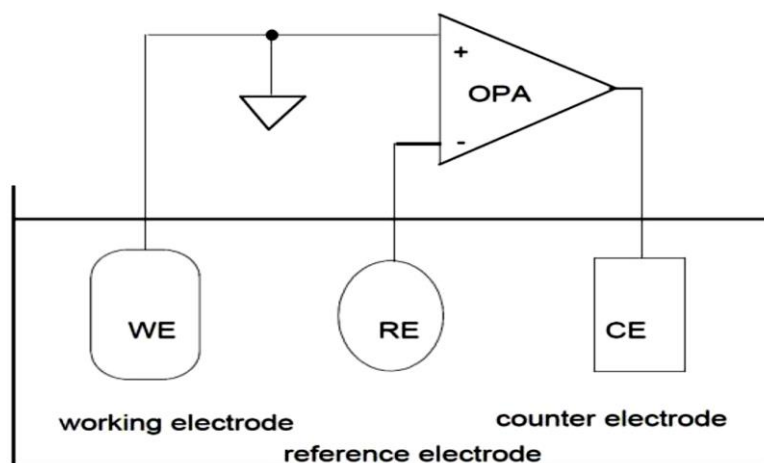


Fig. 1.4. Schematic representation of electrochemical cell.

**Potentiostat:** Fig. 1.4 shows a simple op-amp-based electronic device designed to control a three-electrode cell that can operate most of the electro-analytical experiments. The third electrode (CE) is used to keep a fixed potential difference between the RE and WE. Whenever current passes, potential between the electrodes is changed which simply means, the electrodes are polarised. The current at the CE is adjusted to keep the potential of the WE at a constant level with respect to RE. Therefore, to achieve a stable potential, no current should be allowed to pass through the reference electrode. In this regard, a potentiostat should have a very high input resistance to meet this desired null condition.

Fig. 1.5 shows the basic electrical circuitry of potentiostat. Control amplifier (CA) block is connected to CE, which hinders the flow of current through the electrochemical cell. On the other hand, WE is connected to the current follower circuit. A commercial potentiostat has some additional elements:

- An input resistor is used as a protective element in the reference electrode input (at open condition) to prevent the potential amplifier from being destroyed by static high voltage shocks.

- A phase correction capacitor is connected between RE and CE.
- The input current signal is sent from the reference electrode input through a potential buffer for amplification, while the voltage remains unchanged. Therefore, the reference electrode is charged with negligibly small currents only, and the output is able to feed appreciable loads.
- Potentiostatic CA with high open-loop gain.
- A high precision operational amplifier is used as trans-impedance amplifier to convert the current into equivalent voltage.

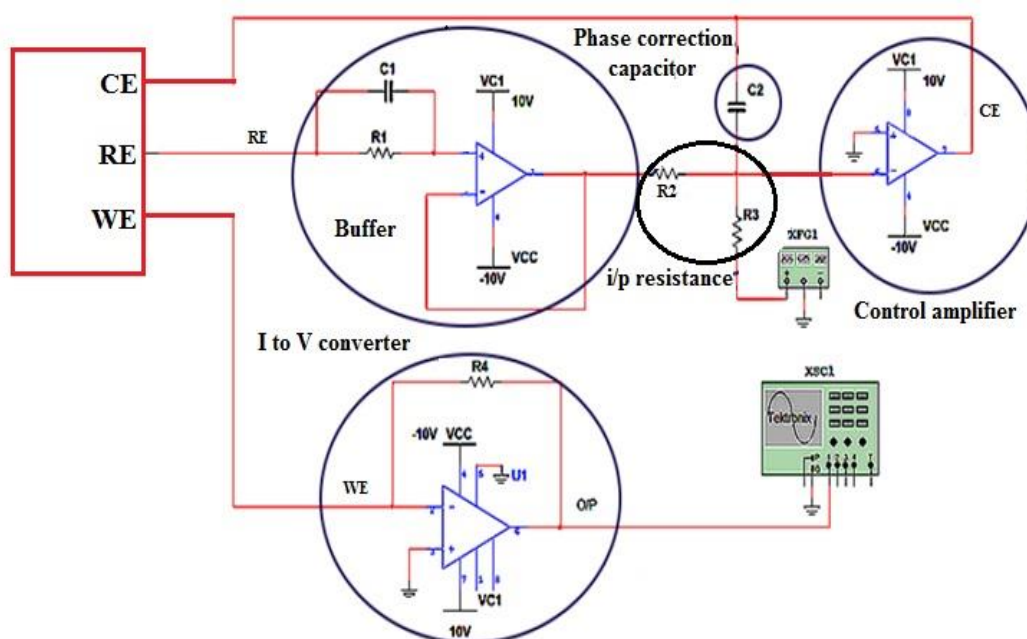


Fig 1.5. Basic circuitry of a potentiostat.

### 1.7.3.1. Traditional types of voltammetric measurements

#### A. Linear sweep voltammetry (LSV)

As suggested by the name, the current produced in an electrochemical cell is scanned with reference to the linearly varied potential between the WE and RE with time. Characteristics such as the electron transfer reactions' rate, the reactivity of the electroactive species and the scan rate, dominate the LSV [48]. With regard to this, upon increasing the scan rate, the capacitive current generates, which cannot be compensated electrochemically.

#### B. Cyclic voltammetry

CV is the most commonly used potentiodynamic electrochemical measurement, wherein potential is varied linearly with respect to time [48]. After reaching the saturation potential, potential of the WE ramps in reverse way to return to the initial potential value.

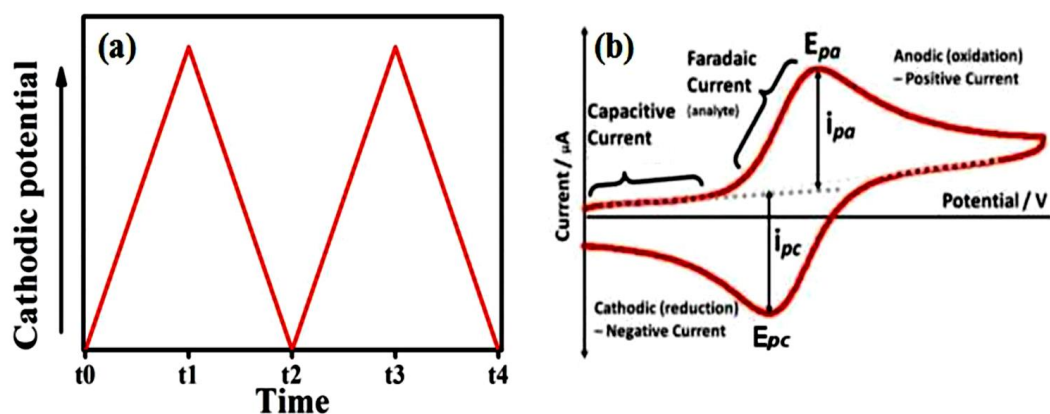


Fig. 1.6.(a) Cyclic voltammetry waveform; (b) Typical cyclic voltammogram showing the different parameters for a reversible reaction.

The typical cyclic voltammogram is depicted in Fig. 1.6 (a) and 1.6 (b) thereby showing the cathodic ( $I_{pc}$ ) and the anodic currents ( $I_{pa}$ ) corresponding to the oxidation and the reduction process, respectively, in response to different time intervals. As shown in Fig. 1.6 (a), the reaction is triggered by the triangular pulse [51]. The current increases with input potential during the forward scan ( $t_0$ - $t_1$ ). At this point, the process of oxidation takes place rapidly due to substantial amount of reactants present. On further applying voltage, the reactants' supply become diffusion limited and the current value decreases to a lower or often, to a constant value. On the reverse sweep ( $t_1$  to  $t_2$ ), the cathodic peak is monitored by means of the reduction of the oxidized species.

### C. Pulse voltammetry (PV)

PV operates in relation to a potential pulse based on the deviation in the rate of charging and faradaic currents. The Faradaic current decays at a slower rate than the charging current, which itself decays exponentially with a function of  $1/(\text{time})^{1/2}$ . This voltammetry techniques were developed by Barker and Jenkin [52] and it detects analyte up to  $10^{-8}$  M concentration level. On the basis of the applied waveform and the corresponding current profile, PV is classified as appended:

#### ➤ Normal pulse voltammetry (NPV)

A series of monotonically increasing potential pulses trigger the output current at the end of each pulse hence allowing some time for the charging current decay. The duration of the pulse time ( $t$ ) in response to the potential ( $E_i$ ) ranges from 1 to 100 ms with the corresponding interval being 0.1 s to 5 s. The voltammogram is represented as the sampled current on the vertical axis corresponding to a stepped pulse on the horizontal axis.

### ➤ Differential pulse voltammetry (DPV)

Fig.1.7. represents a typical DPV technique [53]. Apart from the applied potential (whose amplitude in this case is increased in an incremental manner), there are some similarities between NPV and DPV methods. The baseline potential follows the change of application of consecutive pulses which is held for certain duration until the next application of pulse.

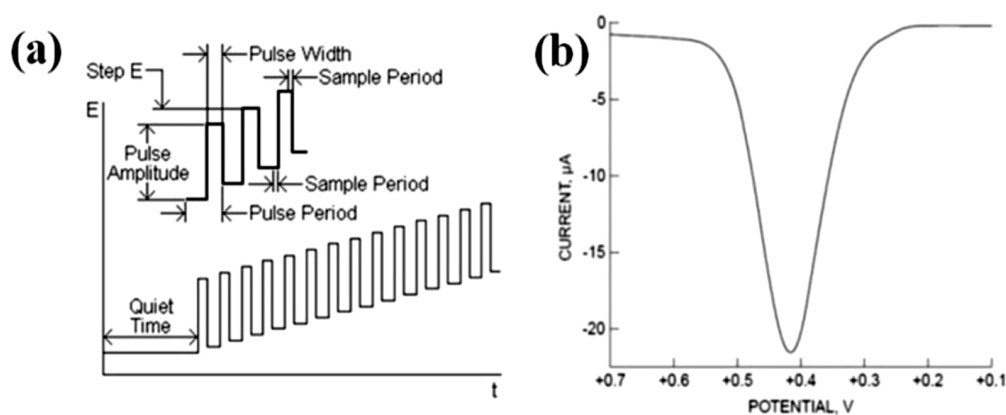


Fig. 1.7. (a) Excitation potential waveform for differential pulse voltammetry; (b) A typical differential pulse voltammograms.

The corresponding sequential current is sampled before and at the end of each pulse, as shown in Fig. 1.7 (a). The resulting deviation between these two values of sampled current are further recorded for quantitative analysis of the target analyte. Therefore, DPV seems to be the most sensitive technique with lower limit of detection compared to the other type of PVs.

### ➤ Square wave voltammetry



In this type of voltammetry, the sequence of symmetrical square wave pulses of amplitude  $E_{sw}$  is superimposed in such a way that the forward pulse of the square wave corresponds with the phase of the staircase [53]. The resulting current is found out based on the deviation between the oxidation and reduction currents. The amplitude of the peak and the concentration of the electroactive species are linearly dependent on each other and the lower detection level is up to the order of 0.1 nM.

#### **D. Stripping voltammetry**

Sensitive stripping voltammetry technique is mainly employed to detect trace amounts of metals in a solution [53]. Firstly, to trigger the deposition of the target metal ions on the surface of the electrode, certain potential is applied onto it. The solution is constantly stirred in order to maximize the number of metal ions for deposition. The stirring process is discontinued after the deposited ions are settled on the electrode surface. In the final stripping state step, the deposited metal ions are stripped from the electrode by scanning the potential and the current which is produced is proportional to the amount of the metal present in the mixture or experimental solution. Depending upon the positive or negative potential scan of the stripping process, there are two different kinds of voltammetry: cathodic stripping voltammetry and anodic stripping voltammetry, respectively.

It is important for us to note that the choice of voltammetry technique depends on the specific application, the nature of the analyte, and the goals of the analysis. Each technique has its advantages and limitations, and selecting the appropriate method is crucial for obtaining reliable and meaningful results. Throughout the thesis, cyclic voltammetry and differential pulse voltammetry have been used. The cyclic voltammetry has been used to investigate the kinetics of the electrochemical system and the differential pulse voltammetry being much more sensitive has been used for investigating the concentration variation.

### **1.8. Molecularly imprinted polymer (MIP)**

MIPs are a feasible approach in regards to the design and development of a selective and sensitive electrode. MIP materials are prepared through the use of functional monomers and a target molecule which are collected and cross linked to each other around the target molecule. An imprinted matrix is formed by polymerization of

the template and the functional monomers (which are assembled around the template molecule). Under specific conditions, the target particle is removed from the structure, hence forming a pit integral fit to the layout as fiddle. The active binding site of the enzyme has a particular geometric structure which is appropriate for a substrate. A substrate which only matches to the binding site is recognised and then it selectively binds to the enzyme. The experiments related to molecular imprinting was first performed by Dickey in the 1940s and 1950s [54-55] wherein the affinity for dye molecules in silica gel was established in combination with a theory of Linus Pauling [56]. The basic schematic of an MIP process is depicted in Fig. 1.8.

MIP synthesis method can be summarised in 3 steps [57]:

- a) Association: Target molecule and monomers are assembled with the help of covalent and non-covalent binding.
- b) Polymerization: Various kinds of polymerization methods are performed, because of which cross-linked copolymers entrapped with the template molecules are acquired.
- c) Elution: Template molecules trapped inside the polymer network are removed by utilizing the proper elution agent. Thus, cavities of comparable fit are formed which is a requisite for molecular recognition purposes.
- d) There are two factors that contribute to the underlying principles owing to which the molecular recognition takes place [58]. These are namely:
  - The complementary functional groups in the polymer are pre-organized by the template.
  - A cavity is imprinted which is complementary to the shape and size of the template molecule.

MIPs are advantageous as they are flexible, adaptable methods having great mechanical stability. Additionally, because of the wide availability of the practical monomers, MIP sensors reasonable to any objective analyte can be structured effectively. In addition, MIP method can be used as an alternative to unstable bio molecules like enzymes and antibodies in biosensors. The advantages of MIP sensors over natural bio-molecules [58] have been recorded in Table 1.3. Active sites in any polymer matrix are formed through different chemical routes, viz., covalent imprinting, semi-covalent imprinting, imprinting with sacrificial spacers, and non-covalent imprinting. The various sorts of imprinting forms are appended in the following sub-sections.

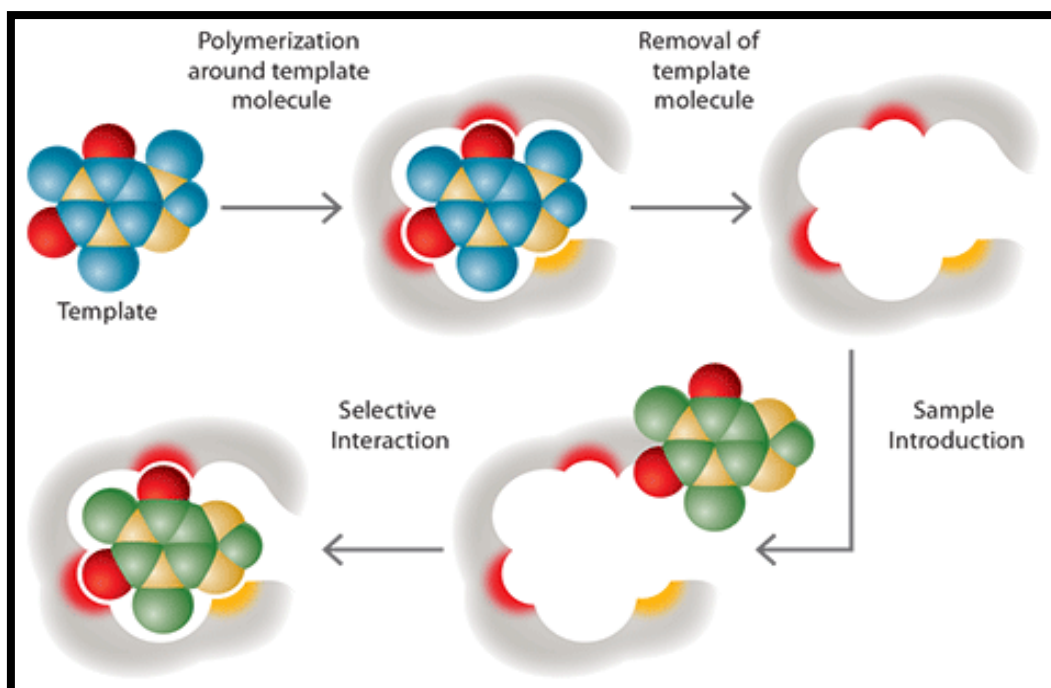


Fig 1.8. Schematic showing MIP Technique

Table. 1.3. Comparison of sensors based on natural biomolecules and MIP sensors

Sl. No.	Sensor based on natural biomolecules	MIP sensors
1	Stability is poor	Stability is comparatively higher
2	Enzymes and receptors are expensive	It is low cost and easy to handle
3	Perform poorly in non-aqueous media	They can respond in organic solvents
4	Poor compatibility with micromachining technology and miniaturization	Polymers are fully compatible with micromachining technology.

### 1.8.1. Types of imprinting techniques

#### 1.8.1.1. Covalent imprinting

In this technique, by means of a chemical step which is not dependent of polymer formation, the template and at least one polymerizable unit are conjoined by reversible covalent bonds to form a template monomer complex. From the outset, a pre-polymerization derivative is formed from the target and the monomer, followed by the polymerization process. Post polymerization, after expulsion of the template from the polymer, the covalent linkage between the polymer and the template is cut. A similar linkage is again settled on rebinding of the template atom inside MIP [59], the main highlight of the approach being evacuation of the template molecule that was

formed during polymerization. The covalent imprinting process [60] is portrayed as a schematic appeared in Fig. 1.9.

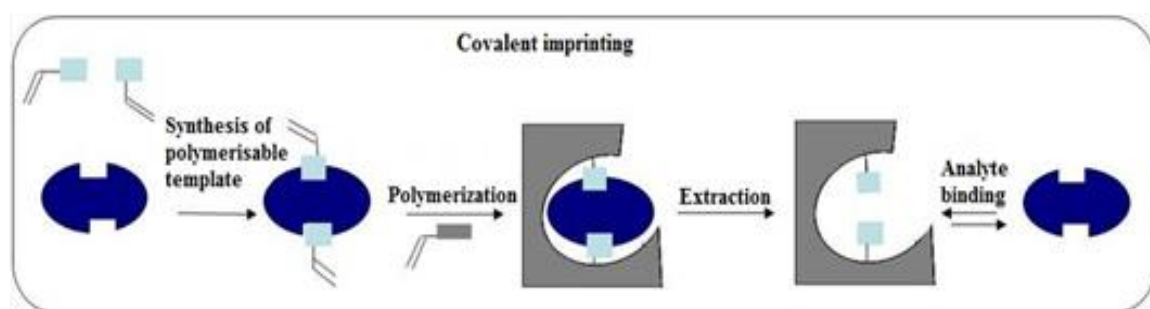


Fig. 1.9. Schematic explaining the covalent imprinting process.

### A. Imprinting with readily reversible covalent bond

This kind of covalent bonding advances the planning of the monomer-template bindings for promptly reversible binding responses. Delicate liquid conditions are required for improvement of these bindings in order to hydrolyze the organization molecule from the polymer[61,62]. The specific assistant essential of covalent strategies definitely limits the amount of arrangements that can be imprinted. One definite purpose of this method is that the bounce back state is undefined from the as prepared polymer in which each coupling site practically looks somewhat like one another. In the same way, unclear confining may be totally reduced as the monomer quantity is less. The hindrance of any covalent etching methodology is the prerequisite for amalgamation of the organization monomer. Additionally, the format monomers of this sort may be delicate to the closeness of water. Further, the reactions occurring in the imprinted polymer regions force extra steric necessities, which in this manner ruin the system of the template particle exchange.

### B. Covalent imprinting with boronate esters

This approach is the best reversible covalent strategy, since it is relevant to the imprinting of starch or carbohydrate subsidiaries. This strategy, being first actualized by Gunter Wulff et al., incorporates the formats, in particular, glyceric corrosive, subordinates of mannose, galactose and fructose, sialic corrosive, castasterone, L-Dopamine and nucleotides [63] for the imprinting procedure. A number of researchers have demonstrated the joining of boronate esters in MIPs for detection of fluorescence [64-66], in imprinted hydrogels of polyelectrolyte [64] and functionalized coatings of polyaniline [68]. In addition to the usage of monomers based

on boron ophthalide [69-70] has extended this method to the engraving of different spatially isolated hydroxyl gatherings and monoalcohol formats. In the same way, utilising this process, particular derivation of sterols by polymeric securing bunches has been accomplished by the polymers [71].

### C. Covalent imprinting with Schiff's esters

The chemistry of Schiff's base essentially encompasses the build-up of a carbonyl (generally an aldehyde) and an amine compound. To imprint amine or aldehyde comprising templates, this method is of use. The derivatives of amino acid have been imprinted by this same strategy [72].

### D. Covalent imprinting with acetals and ketals

Shea et al. [73-75] extensively studied the mono and di-ketone templates where a polymerizable diol has been utilized as the binding group for the readiness of the MIP. Also, focus has been put on for the study of cyclic hemi-acetals [76].

#### 1.8.1.2. Non-covalent imprinting

This method overcomes the constraints of covalent imprinting. Mosbach's group, in 1980s built it up as a practical technique for creating imprinted receptors in engineered polymers. The scheme of the process of non-covalent engraving is shown in Fig. 1.10. In this method, monomer-template complex is shaped in a properly dissolvable solvent dependent upon different interactive forces. The template is thereafter expelled from the polymerized test and can be recovered using the same interactive forces. The force of attraction involved between atoms is due to Van der Waals forces. Also, dipole-dipole interactions play a huge role. This helps to create adducts of layout and monomers in arrangement. Now-a-days, non-covalent imprinting method widely used for its robustness in regards to the functionalities on a template.

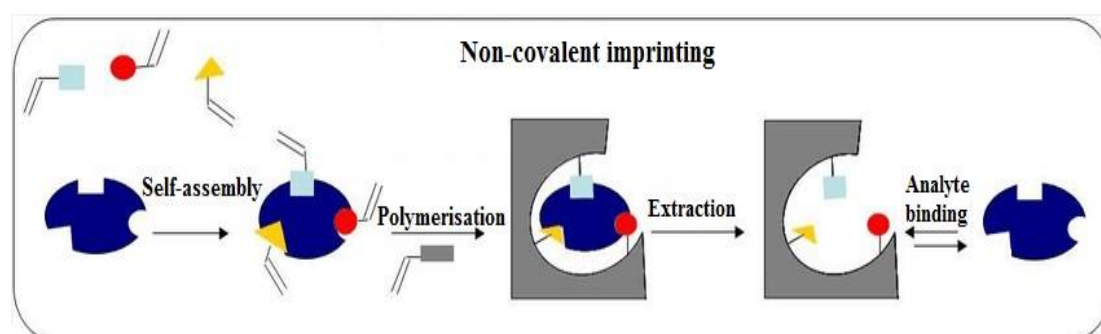


Fig.1.10. Schematic explaining the mechanism of non covalent imprinting.

In this technique, little segments of polymer structure having different useful groupings start to fold over the template particle after the development of a pre-polymerization complex between the desired template or target and practical monomers. Therefore, as against single monomer-template interaction, a mutual impact is created because of the different interactions. As polymerisation continues, these structures further create and change their shape depending on the quantity of monomer added. This results in higher affinity of the target molecule in the receptor site until it develops to a fully framed polymerized network. Non covalent imprinting procedure can be done either with a single monomer or blend of monomers.

### **A. Single functional monomer**

This method is the first one that was proven working and is usually considered the easiest and the most widely spread in various literature. The idea of the polymerization complex and the reasonable bindings between the monomer and the template with crosslinkers must be considered. This is on the grounds that the template may assume a significant job in characterizing or refining useful receptor, while the monomer can move the equilibrium from the ideal template-monomer complexes. Problems may be faced due to the self associative properties of the monomer, for example, carboxylic acids have a propensity to dimerise. Additionally, potential interactions with the initiator should be considered as they are regularly present, at least at first. Essentially, in their structure, the monomer, vinyl pyridine interacts strongly with electron rich  $\pi$ -electron ring network with their aromatic rings which has inadequate number of electrons. These monomers frequently associate strongly with templates and are subsequently, hugely productive in imprinting. Although useful, these monomers might sometimes be counter-productive as they yield solid interactions. This causes a huge burden to high levels of non-specific binding sites. As a result, both the imprinting and the non-imprinting polymer show the same affinity towards the template molecule. Other essential monomers include the group of tertiary amino monomers.

### **B. Combination of monomers**

Although it appears to be interesting to combine the particular interface potential of a wide variety of monomers for a particular work yet it is based on the considerable number of equilibria present in a pre-polymerization mixture. An on-

going work has shown that, to accomplish appropriate imprinting [77], the monomers are not required when the cross linker is properly functionalized. To be effective, the cohesion between the monomers and the target molecule should be way stronger than any interaction among the monomers. Additionally, computational virtual imprinting can anticipate imprinting plans that have functioned well in the experiments.

### **1.8.1.3. Semi covalent imprinting**

In the earlier sections, it has been elucidated that in case of covalent imprinting, the template molecule must be artificially changed with functional monomers and then evacuated through the cleavage of the covalent bonds. A more convenient methodology is the non-covalent imprinting wherein relatively weak forces of attraction, namely, electrostatic interactions, hydrogen bonding,  $\pi$ - $\pi$  bonding, hydrophobic interactions, etc. help attach the template to the monomer. This strategy overcomes the disadvantages of covalent imprinting by including the covalent attachment during the polymerization and hydrogen bond development during recognition. The hybrid amalgamation of both the covalent and the non-covalent imprinting process is termed as semi covalent imprinting. Herein, while polymerization, the template and functional monomer shares covalent bonding and utilizes the non covalent interactions.

In the previous segments, it has been seen that if there should be an occurrence of covalent imprinting, the template molecule must be artificially changed with the functional monomer and must be evacuated by the cleavage of the covalent bonds, so shaped. Then again, a more convenient methodology is the non-covalent strategy wherein relatively weak forces of attraction, namely, electrostatic interactions, hydrogen bonding,  $\pi$ - $\pi$  bonding, hydrophobic interactions, etc., serves the desirable purpose of attachment of the template to the monomer. This strategy includes the covalent attachment during the polymerization and hydrogen bond development during recognition, thus overcoming the disadvantages of covalent imprinting. Yet, this kind of imprinting is not appreciated because of the absence of direct template hydrolysis.

### **1.8.1.4. Imprinting with sacrificial spacers**

During the polymer formation, the group which links, performs both the role of connecting the template to the respective monomer and bridges the gap between the template and the polymer. This helps to prevent crowding in the rebinding



process [78-83]. Salicylate (2 hydroxybenzoate) was also used as a spacer group between the residue of polymerizable methacrylic acid and the template's primary amine [84]. This method of imprinting is efficient because intra-molecular hydrogen-bonding between the reactive groups in the non-covalent binding stage has maintained a close proximity and the phenyl methacrylate ester is easily split than the corresponding amide.

In this thesis, non-covalent imprinting method has been chosen despite the fact that covalent imprinting is much more stable because the template removal process of non-covalent bonding is much easier,

### 1.9. Literature survey based on MIP sensors

The on-going improvements in MIP based detection identified with target analyte and various areas of utilization have been detailed in this section. This is on the ground that the transduction system majorly affects the determination of the monomers and advancement of the polymerization procedure. Table 1.4 depicts a portion of the ongoing researches corresponding to the MIP strategy utilizing electrochemical transduction followed by a detailed description of some important research works.

*Table. 1.4. Literature survey on MIP technology.*

S. No.	Target analyte	Components of MIP	Polymerization method	Principle of operation	Refs
1	CAF	a) Monomer: Methylacrylic acid (MAA) b) Crosslinker: EGDMA: Ethylene Glycol Dimethacrylate (EGDMA) c) Initiator: 2,2'-Azobisisobutyronitrile (AIBN)	Bulk polymerization (MIP) Modifier- TiO <sub>2</sub> NPs	CV, DPV	[85]
2	CAT	a) Monomer: Acrylonitrile (AN) b) Crosslinker: EGDMA c) Initiator: Benzoyl peroxide (BP)	Bulk polymerization (MIP)	CV, DPV	[86]
3	EGCG	a) Monomer: AN b) Crosslinker: EGDMA c) Initiator: BP	Bulk polymerization (MIP)	CV, DPV	[87]
4	Q	Monomer: aminobenzoic acid	Electro-polymerization process	CV, DPV, Electrochemical impedance	[88]



				spectroscopy (EIS)	
5	GA	a) Monomer: MAA b) Crosslinker: EGDMA c) Initiator: 2,2-azobis (2-methyl propionitrile)	Precipitation polymerization	DPV	[89]
6	TF	a) Monomer: Acrylamide b) Crosslinker: EGDMA c) Initiator: BP	Bulk polymerization (MIP)		[90]
7	Atrazine	a) Monomer: Acetic acid thiophene b) Crosslinker: 3,4-ethylenedioxythioph-ene	Electrodeposition on Pt electrode	CV	[91]
8	Cadmium (II)	a) Monomer: MAA b) Crosslinker: EGDMA c) Initiator: AIBN	Bulk polymerization	Differential Pulse Anode Stripping voltammetry	[92]
9	Curcumin	a) Monomer: MAA b) Crosslinker: EGDMA c) Initiator: AIBN	Thermally induced Precipitation polymerization	CV	[93]
10	Melatonin	Monomer: 4-amino-3-hydroxy-1-naphthalenesulfonic acid and Melamine	Electropolymerization	CV, SWV	[94]
11	Emodin	a) Monomer: Allobarbital b) Crosslinker: EGDMA c) Initiator: AIBN	In -Situ photopolymerization	CV, DPV	[95]
12	Glucose	a) Monomer: MAA b) Crosslinker: EGDMA c) Initiator: AIBN	-	CV	[96]
13	Diphenylamine	a) Monomer: MAA b) Crosslinker: EGDMA c) Initiator: AIBN	-	DPV	[97]
14	Chlorpyrifos	Monomer: p Amino thiophenol	Photoelectrochemical process	CV	[98]
15	Manganese (II) ions	a) Monomer: MAA b) Crosslinker: EGDMA Initiator: AIBN	-	Square wave anode stripping voltammetry	[99]
16	Thiamethoxam	a) Monomer: p-vinylbenzoic acid b) Crosslinker: EGDMA	-	CV	[100]
17	Bovine serum albumin	a) Monomer: tetraethylene glycol 3-morpholin propionate acrylate. b) Crosslinker: diacryloyl urea	Free radical polymerization on the MWCNTs-ceramic electrode surface	CV and DPV	[101]

18	Lamotrigine	a) Monomer: MAA b) Crosslinker: EGDMA c) Initiator: AIBN	Bulk polymerization	CV, DPV	[102]
19	L-cysteine	a) Monomer: MAA b) Crosslinker: EGDMA c) Initiator: AIBN	Bulk polymerization followed by modification of CPE	CV, DPV and EIS	[103]
20	Methyl parathion	Monomer: Phenol	Electropolymerization	CV	[104]
21	Trimethoprim	Monomer: Pyrrole	Electropolymerization on the surface of GCE	EIS, CV	[105]
22	Carbofuran	a) Monomer: MAA b) Crosslinker: Ethylene glycol maleic rosinat acrylate	Electropolymerization after modification of GCE by reduced grap-hene oxide modified gold nanoparticles	CV and EIS	[106]
23	Ochratoxin A	Monomer: Pyrrole	Electropolymerization on the surface of MWCNT modified glassy carbon electrode (GCE).	CV and DPV	[107]
24	Norfloxacin	Monomer: Pyrrole	Electropolymerization on the surface of MWCNT modified GCE	CV and SWV	[108]
25	Melamine	a) Monomer: Pyrrole	Bulk polymerization using carbon nanotube- ionic liquid as carrier	CV and SWV	[109]
26	Sunset Yellow	a) Monomer: MAA b) Crosslinker: EGDMA c) Initiator: AIBN	Precipitation polymerization	CV	[110]
27	Estrone 3-sulfate sodium salt	a) Monomer: Acrylamide (AAM) Crosslinker: EGDMA Initiator: AIBN	-	CV	[111]
28	Thiamethoxam	a) Monomer: <i>p</i> -vinylbenzoic acid b) Crosslinker: EGDMA c) Initiator: AIBN	Graphite modified MIP prepared by bulk polymerization and dropcasted on GCE	CV, EIS, LSV	[112]
29	EGCG	a) Monomer: $\beta$ -cyclodextrin	Electropolymerization on graphene	CV, DPV	[113]

			oxide (GO) modified GCE		
30	Testosterone	Monomer: o-phenylenediamine	Electropolymerization on the surface of GO modified electrode	CV, EIS	[114]
31	Imidacloprid	a) Monomer: vinyl benzoic acid b) Crosslinker: EGDMA c) Initiator: AIBN	Bulk polymerization followed by the deposition of MIP/Gr on GCE	LSV	[115]
32	Thiamine	a) Monomer: N-methacryloylglutamic acid b) Initiator: AIBN	Free radical polymerization	DPASV, CV	[116]
33	Simazine	Monomer: o-aminothiophenol	Electropolymerization after modification with gold nanoparticles	CV, EIS	[117]
34	Sulfanilamide	a) Monomer: MAA b) Crosslinker: Di-Vinyl Benzene c) Initiator: AIBN	Bulk polymerization followed by modification with GO and deposition on GCE	CV, EIS	[118]
35	17- $\beta$ -estradiol	Monomer: Poly(3,6-diamino-9-ethylcarbazole (DAEth))	Electropolymerization	CV and EIS	[119]
36	Salbutamol	Monomer: o-phenylenediamine, 3-aminophenylboronic acid	Electrocopolymerization (graphene and screen printed electrodes)	CV, DPV	[120]
37	Dopamine	Monomer: py-PBA	Electropolymerization on the surface of GCE	CV and DPV	[121]
38	Glucose	Monomer: polyvinyl acetate	Bulk polymerization followed by modification with MnO <sub>2</sub> @GO/CuO nanocomposite	CV	[122]

As for example in [86], *Trisita et.al.* investigated on the detection of CAT using MIP technology. A stable electrode has been synthesized by obtaining recognition sites of catechin in a nano-composite of graphite and co-polymer of polyacrylonitrile. The cross-linking agent that has been used is EGDMA. On studying the sensory parameters, the electrode proved to be repeatable, reproducible and selective. A linear range from

5  $\mu\text{M}$  – 100  $\mu\text{M}$  was offered by the electrode having limit of detection (LOD) of 37 nM. Also, similar to [92], prediction accuracy of more than 90% was observed in this case.

In [87], *Trisita et.al.* describes a route for the synthesis of MIP modified with Ni(OH)<sub>2</sub> nano-petals to make it easier to detect EGCG in green tea in a selective and effective manner. The MIP created by co-polymerizing AN, EGDMA, and graphite was combined with the Ni(OH)<sub>2</sub> nanopetals that were made via a straightforward solution approach. Using cyclic voltammetry, it was possible to notice a significant improvement in the modified electrode's electrochemical characteristics over its unmodified counterpart. Results from DPV showed a range of linearity from 10 nM to 100 nM and a LOD of 7 nM which is the lowest among those reported in the literature. The electrode displayed reasonable analytical features and partial least squares analysis was used to satisfactorily validate its performance with samples of green tea.

Also in [90], *Trisita et. al.* described a convenient way for the synthesis of a MIP-based electrode for determination of total theaflavins. Using co-polymer of acrylamide and di-vinyl benzene as the cross linking agent, the electrode is prepared. Base of the polymer sheet is graphite wherein TF molecule has been imprinted. CV and DPV analysis were carried out to check the functioning of the electrode. Investigations revealed that the synthesized electrode has a linear range of 20–100  $\mu\text{M}$  and lower detection limit of 14 $\mu\text{M}$ . The synthesized electrode is used to determine the total TF present in tea by regression techniques and by correlating the experiment data with the HPLC values. In terms of determining the TF content, the electrode achieved a prediction accuracy of 94%.

In a report by *Pardieu et al.* [91], the authors have employed the MIP technique for the detection of atrazine. Here in this work, acetic acid thiophene has been selected as the monomer owing to its ability of hydrogen bond formation with the target molecule. Though 3,4-ethylenedioxythiophene cannot form hydrogen bonding, it is selected as the crosslinker here due to its hydrophilic properties, very well suitable to counteract with the hydrophobic characteristics of the acetic acid thiophene molecule ensuring electroactivity in the aqueous media. The copolymer has been synthesized electrochemically on to the Pt electrode based on the principle of association of the template molecule to acetic acid thiophene by hydrogen bonding and subsequent removal of atrazine from the polymer thereby creating enough reactive sites for binding with atrazine. In this work, the successful detection of atrazine was carried out from the

concentration range of  $10^{-9}$  mol/L to  $1.5 \times 10^{-2}$  mol/L and the corresponding LOD was found to be  $10^{-7}$  mol/L.

In the work by *Sebastian et al.* [92], a sensitive electrochemical sensor was designed to detect the lead ions using multiwalled carbon nanotube as the base material. The recognition sites for lead particles were etched with lead particle as the template and N,N'-methylene bis(acrylamide)-crosslinked polyacrylamide as the strong matrix on MWCNTs for the detection of lead ions with high selectivity. The ion imprinted polymer indicated high selectivity towards lead ion. CV and DPV were utilized to comment on the electrochemical properties of the sensor towards the detection of the lead ion.

A novel method for determination of melatonin by using MIP sensor has been highlighted by *Pankaj et al.* [94]. The sensor material was synthesized by using a composite of graphene and 4-amino-3-hydroxy-1-naphthalenesulfonic acid and melamine. The fabrication of the MIP film was done by depositing a layer of graphene layer on a GCE. Electro-polymerizing of 4-amino-3-hydroxy-1-naphthalenesulfonic acid and melamine was carried out in the presence of melatonin. The linearity range of the melatonin sensor was found to be 0.05 to 100  $\text{mM L}^{-1}$ . The detection limit of the sensor was examined and is found to be as low as  $60 \times 10^{-10}$   $\text{mol L}^{-1}$ .

In the report proposed by *Sun et al.* [97], using the MIP based technology the detection of chlorpyrifos was proposed for its sensitive and efficient detection. Based on titanium dioxide nanorods, a photo electrochemical sensor utilizing MIP was fabricated. MIP preparation was done through electro polymerization wherein hydrogen-bonding occurred. The sensor so developed had a high selectivity and high stability towards the detection of chlorpyrifos in presence of other pesticides.

*Liu et al.* [109] designed a MIP sensor using carbon nanotube-ionic liquid composite for the selective and sensitive determination of melamine. Melamine contains a considerably high proportion of nitrogen and thus added by unscrupulous manufactures in various milk products in order to enhance their protein content. Due to its unique property of large specific surface area, good mechanical stability and high electronic conductivity, CNTs have been preferred in this work. Moreover, ionic liquids are also advantageous due to good ionic conductivity, high viscosity and high chemical and thermal stabilities. Therefore, the composite of CNT and ionic liquid acted as a carrier material towards increase of sensitivity of MIP. The authors prepared the MIP using pyrrole as the monomer by means of bulk polymerization. CV and SWV

technique revealed linearity in the concentration of melamine from 0.4 to 9.2  $\mu\text{M}$  with the corresponding LOD being 0.11  $\mu\text{M}$ .

In another study [114], *Liu et al.* designed an ultrasensitive sensor for the detection of testosterone, an anabolic androgenic steroid. The regulation of testosterone levels is essential, as it is associated with prostate cancer and is also used by athletes as dopants for improvement of their performance. In pursuit of the development of the sensor, the authors have used o-phenylenediamine as the monomer and electropolymerized it on the surface of graphene oxide modified electrode. The electrochemical characterizations were performed using CV and EIS techniques. A linear range from 1 fM to 1  $\mu\text{M}$  of concentration was observed under optimized experimental conditions with the LOD being 0.4 fM.

In pursuit of its detection of dopamine, an important neuro transmitter, using the MIP technique, *Zhong et al.* [121] synthesized a novel monomer pyrrole-phenylboronic acid such that it can enable cyclic boronic ester formation with dopamine. The resultant boronic ester in combination with the imprinted cavities endowed double recognition capacities towards the detection of dopamine. A linear range of concentration was observed between the values of  $5 \times 10^{-8}$  mol/L to  $1 \times 10^{-5}$  mol/L. The results also indicated an LOD of  $3.3 \times 10^{-8}$  mol/L.

An enzyme free novel MIP sensor was developed by *Farid et al.* [122] for the selective detection of glucose. Here, the sensor was prepared using polyvinyl acetate as the monomer and subsequently modified by Manganese oxide/copper oxide loaded graphene oxide nanoparticles. The results indicated a linear range for concentration values from 0.5 to 4.4 mM. The corresponding LOD was calculated as 53  $\mu\text{M}$ .

## 1.10. Objectives

The present work focuses on the usage of the MIP procedure for the sensitive detection and quantification of health beneficial compounds in tea viz., CAF, GA, EC, separately. With regard to the development of the sensors, several exploratory parameters have been thoroughly examined, including the effects of pH, buffer, and scan rate. These three parameters (pH, buffer and scan rate) are our matter of interest because it is necessary for us to investigate under which combination the synthesized electrodes give optimal performance.

The following summarizes the goals of the thesis work:

- Optimization of monomers, modifiers and cross-linking agents for the development of MIP sensors for CAF, GA and EC.
- Characterization of the sensor materials in terms of their dimensions, structural and morphological variations.
- Thorough investigation of the electrochemical properties of the electrodes and optimization of the experimental conditions.
- Investigation of various electro-analytical characteristics of the developed electrodes, followed by a short literature review on MIP based sensing using conventional techniques.
- Include a light of potentiostat development. The chapter ends with the summarized objectives and scope of the work.

### 1.11. Thesis layout

In view of the abovementioned objectives, the entire work has been divided into five chapters. A brief chapter wise organization of the thesis is presented below.

*Chapter 1* describes the purpose of this work and exemplifies the goals of this thesis work. The human gustatory system is explained in details. Introduction to origin of tea along with its various compositions have been included. The electrochemical principle of transduction has been discussed. It also focuses on numerous electrochemical techniques used for detection of CAF, GA and EC. It was followed by a description of how MIP-based recognition systems can be used to overcome the challenges posed by conventional electrochemical identification techniques. Different types of imprinting have also been discussed. Literature survey regarding the usage of MIP technique for detection of various molecules has been done thoroughly.

*Chapter 2* discusses the MIP based TiO<sub>2</sub> nanoparticles embedded CAF electrode. This electrode has been synthesized with AN and graphite nanocomposite for the determination of CAF in green tea. The comparative study of CAF determination with other research reports is presented in this chapter. The electrochemical characteristics of the developed electrode and the experimental parameters for the detection CAF are discussed here in detail followed by analysis of real samples.

*Chapter 3* presents the MIP based sensor for GA in green tea samples. Here, MIP is synthesized by utilizing itaconic acid as the monomer, EGDMA as a crosslinker and graphite as the leading material. The experimental and characterization details are elucidated in this chapter. The electrode has been imbibed in green tea samples for validation of their practicality for real-time applications.

*Chapter 4* proposes an MIP based sensor for estimation of EC in tea. In this work, the detection of EC has been done using two different techniques. In the first case, EC molecule has been used as the template and in the second case, dummy template, i.e., quercetin, has been used for the synthesis of the MIP materials. The detection of EC using the dummy template appeared to be an economical solution towards the quality of tea. The comparative study with other research reports of EC determination has been presented in this chapter.

*Chapter 5* presents an approach adopted to develop a low-cost three electrode cyclic voltammetry system. The developed system consists of a triangular waveform generator, a potentiostat circuit and the digital signal oscilloscope has been used as the storage and display unit. The responses obtained in the standard solution using the developed system and the commercial potentiostat has been shown in this chapter as comparison.

*Chapter 6* shows a general outline of the work done and highlights the finishing up comments. The important points and weaknesses of the proposed framework have been examined here with certain suggestions and a few proposals are presented which may be taken up later.

## **References**

- [1] Q. Ping Dou, “Tea in Health and Disease” *Nutrients* 2019, 11(4), 929
- [2] L. R. Juneja, M. P. Kapoor, T. Okubo, T. P. Rao, “Green Tea Polyphenols: Nutraceuticals of Modern Life”, Boca Raton, FL, USA: CRC Press, 2013.
- [3] N. Bhattacharyya, R. Bandyopadhyay, M. Bhuyan, B. Tudu, D. Ghosh, A. Jana, “Electronic nose for black tea classification and correlation of measurements with tea taster marks”, *IEEE Trans. Instrum. Meas.* 57 (2008) 1313–1321.
- [4] C. A. Blanco, R. Fuente, I. Caballero, M. L. Rodriguez-Méndez, “Beer discrimination using a portable electronic tongue based on screen printed electrodes”, *J. Food Eng.* 157 (2015) 57-62.



- [5] Y. Zuo, H. Chen, Y. Deng, “Simultaneous determination of catechins, caffeine and gallic acids in green, Oolong, black and pu-erh teas using HPLC with a photodiode array detector”, *Talanta*, 57 (2002) 307–316.
- [6] H. Horie, T. Mukai, K. Kohata, “Simultaneous determination of qualitatively important components in green tea infusions using capillary electrophoresis”, *J. Chromatogr. A*, 758 (1997) 332–335.
- [7] E. A. H. Roberts, R. Smith, “Phenolic substances of manufactured tea. IX. Spectrophotometric evaluation of tea liquors”, *J. Sci. Food Agric.* 14 (1963) 689–700
- [8] V. Pavithra, “Review Article on Caffeine Activity”, *J. of Nanotechnology Res.* 3 (2021) 001-005.
- [9] G. Richards, A. Smith, “Caffeine consumption and self-assessed stress, anxiety, and depression in secondary school children”, *J. Psychopharmacol.* 29 (2015) 1236–1247.
- [10] U. L. Peri-Okonny, S. X. Wang, R. J. Stubbs, N. A. Guzman, “Determination of caffeine and its metabolites in urine by capillary electrophoresis-mass spectrometry”, *Electrophoresis* 26 (2005) 2652–2663.
- [11] R. Hursel, W. Viechtbauer, M. S. Westerterp Plantenga, “The effects of green tea on weight loss and weight maintenance: A meta-analysis”, *Int. J. Obesity* 33 (2009) 956–961.
- [12] R. N. Goyal, S. Bishnoi, B. Agrawal, “Electrochemical sensor for the simultaneous determination of caffeine and aspirin in human urine samples”, *J. Electroanal. Chem.* 655 (2011) 97-102
- [13] X. Chen, O. Ghribi, J. D. Geiger, “Caffeine protects against disruptions of the blood-brain barrier in animal models of Alzheimer’s and Parkinson’s diseases”, *J. Alzheimers Disease* 20 (2010) S127–S141.
- [14] Y. Dong, L. F. He, X. H. Zhang, X. R. Jiang, “Preparation and properties of caffeine molecular composite imprinted membranes,” *Dig. J. Nanomaterials Biostructures* 11 (2016) 1319–1326.
- [15] L. M. Juliano, R. R. Griffiths, “A critical review of caffeine withdrawal: Empirical validation of symptoms and signs, incidence, severity, and associated features”, *Psychopharmacology* 176 (2004) 1–29.

- [16] Y. Zuo, “Simultaneous determination of catechins, caffeine and gallic acids in green, oolong, black and pu-erh teas using HPLC with a photodiode array detector”, *Talanta*, 57 (2002) 307–316.
- [17] H. G. Valery, A. Chtaini, B. Loura, “Voltammetric sensor based on electrodes modified by Poly (vinyl alcohol)-natural clay film, for the detection of gallic acid”, *Port. Electrochimica Acta* 37 (2019) 327–333.
- [18] S. Sarafraz, H.A. Rafiee Pour, M. Khayatkashani, A. Ebrahimi, “Electrochemical determination of gallic acid in *Camellia sinensis* by MWCNTs-COOH Modified CPE”, *J. Nanostruct.*, 9 (2019) 384–395.
- [19] V. Armoskaite, K. Ramanauskiene, A. Maruska, A. Razukas, A. Dagilyte, A. Baranauskas, V. Briedis “The analysis of quality and antioxidant activity of green tea extracts”, *J. Med. Plants Res.* 5 (2011) 811–816.
- [20] L. Wang, M. S. Halquist, D. H. Sweet, “Simultaneous determination of gallic acid and gentisic acid in organic anion transporter expressing cells by liquid chromatography–tandem mass spectrometry”, *J. Chromatogr. B* 937 (2013), 91–96.
- [21] W. Ma, D. Han, S. Gan, N. Zhang, S. Liu, T. Wu, Q. Zhang, X. Donga, Li Niu, “Rapid and specific sensing of gallic acid with a photoelectrochemical platform based on polyaniline-reduced grapheme oxide-TiO<sub>2</sub>”, *Chem. Commun.* 49 (2013) 7842–7844.
- [22] R. V. Lith, G. A. Ameer, “Antioxidant polymers as biomaterials”, *Oxidative stress Biomater.* 10 (2016) 251–296.
- [23] Y. Fujimura, H. Tachibana, K. Yamada, “Lipid raft-associated catechin suppresses the Fc $\alpha$ RI expression by inhibiting phosphorylation of the extracellular signal-regulated kinase1/2”, *FEBS Lett.*, 556 (2004) 204–210.
- [24] F. D. S. Dias, M. P. Lovillo, C. G. Barroso, J. M. David, “Optimization and validation of a method for the direct determination of catechin and epicatechin in red wines by HPLC/fluorescence”, *Microchem. J.* 96 (2010) 17–20.
- [25] J. D. Langdon, B. J. Moxham, “Tongue, In: Susan Standring, Gray’s Anatomy”, Thirty ninth edition, Elsevier Churchill Livingstone, 1980.
- [26] S. D. Roper, “Signal transduction and information processing in mammalian taste buds”, *PFLUG ARCH EUR J PHY.* 454 (2007) 759-776.
- [27] M.K Meegahakumbura, M.C Wambulwa, M.M Li, K.K Thapa, Y.S Sun, M Möller, J.C Xu, J.B Yang, J Liu, B.Y Liu, D.Z Li, L.M Gao, “Domestication

- Origin and Breeding History of the Tea Plant (*Camellia sinensis*) in China and India Based on Nuclear Microsatellites and cpDNA Sequence Data”, *Front Plant Sci.* 8 (2018) 2270.
- [28] N. Khan and H. Mukhtar, “Tea and Health: Studies in Humans”, *Curr Pharm Des.* 19 (2013) 6141–6147.
- [29] D. Eric Conte , H. Rubinstein, “Determination of Caffeine in Beverages by Capillary Zone Electrophoresis: An Experiment for the Undergraduate Analytical Laboratory”, *Chem. Educ.* 73 (1996) 1169
- [30] M. Musa Ali, M. Eisa, M. Idrees Tah, B. Ahmed Zaka, A. Ahmed Elba, “Determination of caffeine in some sudanese beverages by high performance liquid chromatography”, *Pakistan J. Nutrition*, 11 (2012) 336–342.
- [31] X. Wang, J. Wang, N. Yang, “Flow injection chemiluminescent detection of gallic acid in olive fruits”, *Food Chem.* 105 (2007) 340–345.
- [32] K. Dhalwal, V. M. Shinde, Y. S. Biradar, K. R. Mahadik, “Simultaneous quantification of Bergenin, catechin, and gallic acid from *Bergenia ciliata* and *Bergenia ligulata* by using thin-layer chromatography”, *J. Food Composition Anal.* 21 (2008) 496–500.
- [33] R. de Queiroz Ferreira, L. A. Avaca, “Electrochemical determination of the antioxidant capacity: The ceric reducing/antioxidant capacity (CRAC) assay”, *Electroanalysis* 20 (2008) 1323–1329.
- [34] Y. Jaiswal, P. Tatke, S. Gabhe, A. Vaidya, “Rapid high performance thin layer chromatographic method for quantitation of catechin from extracts of cashew leaves—A short report”, *Polish J. Food Nutrition Sci.* 63 (2013) 49–54.
- [35] P. R. Machonis, M. A. Jones, B. T. Schaneberg, C. L. Kwik-Urbe, “Method for the determination of catechin and epicatechin enantiomers in cocoa-based ingredients and products by high-performance liquid chromatography: single-laboratory validation”, *J. AOAC Int.* 95 (2013) 500–507.
- [36] J. Xia, D. Wang, P. Liang, D. Zhang, X. Du, D. Ni, Z. Yu “Vibrational (FT-IR, Raman) analysis of tea catechins based on both theoretical calculations and experiments”, *Biophys. Chem.* 256 (2020) Art. no. 106282.
- [37] I. Berregi, J. I. Santos, G. D. Campo, J. I. Miranda, “Quantitative determination of (–)-epicatechin in cider apple juices by <sup>1</sup>H NMR”, *Talanta*, 61 (2003) 139–145

- [38] T. Dias, M. R. Silva, C. Damiani, F. A. da Silva, “Quantification of catechin and epicatechin in foods by enzymatic-spectrophotometric method with tyrosinase”, *Food Anal. Methods*, 10 (2017) 3914–3923.
- [39] Y. H. Cao, X. Zhang, X. H. Ding, Y. Z. Fang, J. N. Ye, “Determination of caffeine, epicatechin and ascorbic acid in tea samples by capillary zone electrophoresis with electrochemical detection”, *Chin. J. Anal. Chem.*, 21 (2001) 1072–1075.
- [40] H. G. Valery, A. Chtaini, B. Loura, “Voltammetric sensor based on electrodes modified by Poly (vinyl alcohol)-natural clay film, for the detection of gallic acid”, *Port. Electrochimica Acta*, 37 (2019) 327–333.
- [41] S. Pradhan, S. Biswas, D. K. Das, R. Bhar, R. Bandyopadhyay, P. Pramanik, “An efficient electrode for simultaneous determination of guanine and adenine using nano-sized lead telluride with graphene”, *New J. Chem.*, 42 (2018), 564-573.
- [42] K. Toko, Taste Sensor, In: A. G. Gaonkar (Eds.), “Characterization of Food: Emerging methods”, Elsevier, (1995) 377-401.
- [43] C. Di Natale, F. Davide, A. D. Amico, A. Legin, A. Rudinitskaya, B. L. Selezenev, Y. Vlasov, “Applications of an electronic tongue to the environmental control”, *Technical digests of Eurosensors X*, Leuven, Belgium, (1996) 1345-1348.
- [44] K. Toko, “Taste sensor with global selectivity”, *Materials Science and Engineering: C*, 4 (1996), 69-82.
- [45] F. Winqvist, “Voltammetric electronic tongues - basic principles and applications”, *Microchimica Acta*, 163 (2008), 3-10.
- [46] M. Palit, B. Tudu, P. K. Dutta, A. Dutta, A. Jana, J. K. Roy, N. Bhattacharyya, R. Bandyopadhyay, A. Chatterjee, “Classification of black tea taste and correlation with tea taster’s mark using voltammetric electronic tongue”, *IEEE Trans. Instrum. Meas.* 59 (2010) 2230-2239.
- [47] B. J. Privett, J. H. Shin, M. H. Schoenfisch, “Electrochemical sensors”, *Anal. Chem.* 80 (2008) 4499-4517.
- [48] F. Scholz, “Voltammetric techniques of analysis: the essentials”, *Chem Texts* 1 (2015) 1-24.
- [49] Autolab application note EC08, “Basic overview of the working principle of a potentiostat/galvanostat (PGSTAT)-Electrochemical cell setup”, (2011) 1-3.

- [50] Y. Xie, Y. Ju, Y. Toku, Y. Morita, “Fabrication of Fe<sub>2</sub>O<sub>3</sub> nano wire arrays based on oxidation-assisted stress-induced atomic-diffusion and their photovoltaic properties for solar water splitting”, RSC Adv. 7 (2017) 30548-30553.
- [51] <https://www.zimmerpeacocktech.com/knowledge-base/faq/cyclic-voltammetry/>
- [52] H. H. Willard, Jr. L. L. Merrit, J. A. Dean, Jr. F. A. Settle, “Instrumental methods of analysis”, 6th Edn. D. Van Nostrand, Princeton, 1981.
- [53] [https://www.basinc.com/manuals/EC\\_epsilon/Techniques/Pulse/pulse](https://www.basinc.com/manuals/EC_epsilon/Techniques/Pulse/pulse)
- [54] F. H. Dickey, “The preparation of specific adsorbents”, Proc. Natl. Acad. Sci. U.S.A. 35 (1949) 227-229.
- [55] F. H. Dickey, “Specific adsorption”, J. Phys. Chem. 59 (1955) 695-707.
- [56] L. Pauling, “A theory of the structure and process of formation of antibodies”, J. Am. Chem. Soc. 62 (1940), 2643-2657.
- [57] A. G. Mayes, M. J. Whitcombe, “Synthetic strategies for the generation of molecularly imprinted organic polymers”, Adv. Drug. Del. Rev. 57 (2005) 1742-1778.
- [58] S. Li, Y. Ge, S. Piletsky, J. Lunec “Molecularly imprinted sensors: Overview and applications”, Elsevier (2012) ISBN No. 978-0-444-56331-6.
- [59] L. Chen, S. Xu, J. Li, “Recent advances in molecular imprinting technology: current status, challenges and highlighted applications”, Chem. Soc. Rev. 40 (2011) 2922-2942.
- [60] P. Wang, X. Sun, X. Su, T. Wang, “Advancement on molecularly imprinted polymers in food safety field”, Analyst 141 (2016) 3540-3553.
- [61] G. Wulff, S. Schauhoff, “Enzyme-analog-built-polymers: Racemic-resolution of free sugars with macroporous polymers prepared by molecular imprinting-selectivity dependence on the arrangement of functional group versus requirements”, J. Org. Chem. 56 (1991) 395-400.
- [62] A.G. Mayes, M.J. Whitcombe, “Synthetic strategies for the generation of molecularly imprinted organic polymers”, Advanced Drug Delivery Reviews, Volume 57, Issue 12, 2005, Pages 1742-1778, <https://doi.org/10.1016/j.addr.2005.07.011>.
- [63] T. Sajina, B. Mathew, “A brief overview of molecularly imprinted polymers: Highlighting computational design, nano and photo-responsive imprinting”

- Talanta Open, Volume 4, December 2021, 100072,  
<https://doi.org/10.1016/j.talo.2021.100072>
- [64] S. H. Gao, W. Wang, B. H. Wang, "Building fluorescent sensors for carbohydrates using template-directed polymerizations", *Bioorg. Chem.* 29 (2001) 308-320.
- [65] S. A. Piletsky, K. Piletskaya, E. V. Piletskaya, K. Yano, A. Kugimiya, A. V. Elgersma, R. Levi, U. Kahlow, T. Takeuchi, I. Karube, T. I. Panasyuk, A. V. Elskaya, "A biomimetic receptor system for sialic acid based on molecular imprinting", *Anal. Lett.* 29 (1996) 157- 170.
- [66] W. Wang, S. H. Gao, B. H. Wang, "Building fluorescent sensors by template polymerization: the preparation of a fluorescent sensors for D-fructose", *Org. Lett.* 1 (1999) 1209-1212.
- [67] Y. Kanekiyo, M. Sano, R. Iguchi, S. Shinkai, "Novel nucleotide-responsive hydrogels designed from copolymers of boronic acid and cationic units and their application as a QCM resonator system to nucleotide sensing", *J. Polym. Sci. A Polym. Chem.* 38 (2000) 1302-1310.
- [68] A. Bossi, S. A. Piletsky, E. V. Piletska, P. G. Righetti, A.P.F. Turner, "Surface-grafted molecularly imprinted polymers for protein recognition", *Anal. Chem.* 73 (2001) 5281- 5286.
- [69] G. Wulff, R. Dederichs, R. Grotstollen, C. Jupe, "On the chemistry of binding sites: II. Specific binding of substances to polymers by fast and reversible covalent interactions in: T.C.J. Gribnau, J. Visser, R.J.F. Nivard (Eds.)", *Affinity Chromatography and Related Techniques*, Elsevier, Amsterdam, (1982) 207-216.
- [70] G. Wulff, "Selective binding to polymers via covalent bonds-the construction of chiral cavities as specific receptor sites", *Pure Appl. Chem.* 54 (1982) 2093-2102.
- [71] C. Alexander, C. R. Smith, M. J. Whitecombe, E. N. Vulfson, "Imprinted polymers as protecting groups for regioselective modification of polyfunctional substrates", *J. Am. Chem. Soc.* 121 (1999) 6640-6651
- [72] G. Wulff, W. Best, A. Akelah, "Enzyme-analogue built polymers: 17. Investigations on the racemic resolution of amino acids", *React. Polym.* 2 (1984) 167-174.

- [73] K. J. Shea, T. K. Dougherty, "Molecular recognition on synthetic amorphous surfaces-the influence of functional group positioning on the effectiveness of molecular recognition", *J. Am. Chem. Soc.* 108 (1986) 1091-1093.
- [74] K. J. Shea, D. Y. Sasaki, "On the control of microenvironment shape of functionalized network polymers prepared by template polymerization", *J. Am. Chem. Soc.* 111 (1989) 3442-3444.
- [75] K. J. Shea, D. Y. Sasaki, "An analysis of small-molecule binding to functionalized synthetic polymers by C-13 CP/MAS NMR and FT-IR spectroscopy", *J. Am. Chem. Soc.* 113 (1991) 4109-4120.
- [76] G. Wulff, G. Wolf, "On the chemistry of binding sites: On the suitability of various aldehydes and ketones as binding sites of monoalcohols", *Chem. Ber.* 119 (1986) 1876- 1889
- [77] M. Sibrian-Vazquez, D. A. Spivak, "Molecular imprinting made easy", *J. Am. Chem. Soc.* 126 (2004) 7827-7833.
- [78] M. J. Whitcombe, M. E. Rodriguez, P. Villar, E. N. Vulfson, "A new method for the introduction of recognition site functionality into polymers prepared by molecular imprinting-synthesis and characterization of polymeric receptors for cholesterol", *J. Am. Chem. Soc.* 117 (1995) 7105-7111.
- [79] M. Lübke, M. J. Whitecombe, E. N. Vulfson, "A novel approach to the molecular imprinting of polychlorinated aromatic compounds", *J. A. Chem. Soc.* 120 (1998) 13342- 13348.
- [80] A. Katz, M. E. Davis, "Molecular imprinting of bulk, microporous silica", *Nature* 403 (2000) 286-289.
- [81] A. L. Graham, C. A. Carlson, P. L. Edmiston, "Development and characterization of molecularly imprinted sol-gel materials for the selective detection of DDT", *Anal. Chem.* 74 (2002) 458-467.
- [82] C. J. Percival, S. Stanley, A. Braithwaite, M. I. Newton, G. McHale, "Molecular imprinted polymer coated QCM for the detection of nadrolone", *Analyst* 127 (2002) 1024- 1026.
- [83] M. Petcu, J. Cooney, C. Cook, D. Lauren, P. Schaare, P. Holland, "Molecular imprinting of a small substituted phenol of biological importance", *Anal. Chim. Acta* 435 (2001) 49- 55.



- [84] J. U. Klein, M. J. Whitecombe, F. Mulholland, E. N. Vulfsen, "Template-mediated synthesis of apolymeric receptor specific to amino acid sequences", *Angew. Chem. Int. Ed.* 38 (1999) 2057-2060.
- [85] T. Alizadeh, M. R. Ganjali, M. Zare, P. Norouzi, "Development of a voltammetric sensor based on a molecularly imprinted polymer (MIP) for caffeine measurement", *Electrochim. Acta* 55 (2010) 1568-1574.
- [86] T.N. Chatterjee, D. Das, R.B. Roy, B. Tudu, S. Sabhapondit, P. Tamuly, P. Pramanik, R. Bandyopadhyay, "Molecular Imprinted Polymer Based Electrode for Sensing Catechin (+C) in Green Tea", *IEEE Sens. J.* 18 (2018) 2236-2244.
- [87] T.N. Chatterjee, D. Das, R.B. Roy, B. Tudu, A.K. Hazarika, S. Sabhapandit, P. Tamuly, R. Bandyopadhyay, "Development of a nickel hydroxide nanopetal decorated molecular imprinted polymer based electrode for sensitive detection of epigallocatechin-3-gallate in green tea", *Sens and Actuators B Chem* 283 (2019) 69-78.
- [88] L. Yang, B. Xu, H. Ye, F. Zhao, B. Zeng, "A novel quercetin electrochemical sensor based on molecularly imprinted poly (para-aminobenzoic acid) on 3D Pd nanoparticles-porous graphene-carbon nanotubes composite", *Sens. Actuators B Chem.* 251 (2017) 601–608.
- [89] S. Shojaei, N. Nasirizadeh, M. Entezam, M. Koosha, M. Azimzadeh, "An electrochemical nanosensor based on molecularly imprinted polymer (MIP) for detection of gallic acid in fruit juices", *Food Anal. Methods* 9 (2016) 2721-2731.
- [90] T.N. Chatterjee, R.B. Roy, B. Tudu, P. Pramanik, H. Deka, P. Tamuly, R. Bandyopadhyay, "Detection of theaflavins in black tea using a molecular imprinted polyacrylamide-graphite nanocomposite", *Sens Actuators B Chem* 246 (2017) 840-847.
- [91] E. Pardieu, H. Cheap, C. Vedrine, M. Lazerges, Y. Lattach, F. Garnier, S. Remita, C. Pernelle, "Molecularly imprinted conducting polymer based electrochemical sensor for detection of atrazine", *Anal. Chim. Acta* 649 (2009) 236-245.
- [92] M. Sebastian, B. Mathew, "Ion imprinting approaches for the fabrication an electrochemical sensor and sorbent for lead ions in real samples using modified multiwalled carbon nanotubes", *J. Mater. Sci.* 53 (2018) 3557–3572.



- [93] Q. Zhou, H. Y. Zhai, Y. F. Pan, K. Lia, “A simple and sensitive sensor based on a molecularly imprinted polymer-modified carbon paste electrode for the determination of curcumin in foods”, *RSC Adv.* 7 (2017) 22913–22918.
- [94] P. Gupta, R. N. Goyal, “Graphene and Co-polymer composite based molecularly imprinted sensor for ultra-trace determination of melatonin in human biological fluids”, *RSC Adv.* 5 (2015) 40444–40454.
- [95] Z. Yu, J. Yang, J. Zhong, S. Wu, Z. Xu, Y. Tang, “Emodin voltammetric sensor based on molecularly imprinted polymer membrane-modified electrode using a multiple hydrogen bonds strategy”, *J. Appl. Polym. Sci.* 126 (2013) 1344–1350.
- [96] S. Alexander, P. Baraneedharan, S. Balasubrahmanyam and S. Ramaprabhu, “Highly sensitive and selective non enzymatic electrochemical glucose sensors based on Graphene oxide-molecular imprinted polymer”, *Mater. Sci. Eng. C* 78 (2017) 124–129.
- [97] P. E. Hande, A. B. Samui, P. S. Kulkarni, “An efficient method for determination of the diphenylamine (Stabilizer) in propellants by molecularly imprinted polymer based carbon paste electrochemical sensor”, *Propellants Explos. Pyrotech.* 42 (2017) 376–380.
- [98] X. Sun, C. Gao, L. Zhang, M. Yan, J. Yu, S. Ge, “Photoelectrochemical sensor based on molecularly imprinted film modified hierarchical branched titanium dioxide nanorods for chlorpyrifos detection”, *Sens. Actuators B Chem.* 251 (2017) 1–8.
- [99] M. Roushani, Z. Saedi, F. Hamdi, B. Z. Dizajdizi, “Preparation an electrochemical sensor for detection of manganese (II) ions using glassy carbon electrode modified with multi walled carbon nanotube chitosan-ionic liquid nanocomposite decorated with ion imprinted polymer”, *J. Electroanal. Chem.* 804 (2017) 1–6.
- [100] T. Xie, M. Zhang, P. Chen, H. Zhao, X. Yang, L. Yao, H. Zhang, A. Dong, J. Wang, Z. Wang, “A facile molecularly imprinted electrochemical sensor based on graphene: application to the selective determination of thiamethoxam in grain”, *RSC Adv.* 7 (2017) 38884–38894.
- [101] B. B. Prasad, A. Prasad, M. P. Tiwari, “Multiwalled carbon nanotubes-ceramic electrode modified with substrate-selective imprinted polymer for ultra-trace detection of bovine serum albumin”, *Biosens. Bioelec.* 39 (2013) 236-243.

- [102] M. B. Gholivand, G. Malekzadeh, M. Torkashvand, "Determination of lamotrigine by using molecularly imprinted polymer carbon paste electrode", *J. Electroanal. Chem.* 692 (2013) 9-16.
- [103] K. K. Aswini, A. M. V. Mohan, V. M. Biju, "Molecularly imprinted polymer based electrochemical detection of L-cysteine at carbon paste electrode", *Mater. Sci. Eng. C* 37 (2014) 321-326.
- [104] X. Xue, Q. Wei, D. Wu, H. Li, Y. Zhang, R. Feng, B. Du, "Determination of methyl parathion by a molecularly imprinted sensor based on nitrogen doped graphene sheets", *Electrochim. Acta* 116 (2014) 366-371.
- [105] H. Da Silva, J. G. Pacheco, J. MCS. Magalhães, S. Viswanathan, C. Delerue-Matos, "MIP-graphene modified glassy carbon electrode for the determination of trimethoprim", *Biosens. Bioelec.* 52 (2014) 56-61.
- [106] X. Tan, Q. Hu, J. Wu, X. Li, P. Li, H. Yu, X. Li, F. Lei, "Electrochemical sensor based on molecularly imprinted polymer reduced graphene oxide and gold nanoparticles modified electrode for detection of carbofuran", *Sens. Actuators B Chem.* 220 (2015) 216-221.
- [107] J. G. Pacheco, M. Castro, S. Machado, M. F. Barroso, H. P. A. Nouws, C. Delerue-Matos, "Molecularly imprinted electrochemical sensor for ochratoxin A detection in food samples", *Sens. Actuators B Chem.* 215 (2015) 107-112.
- [108] H. Da Silva, J. Pacheco, J. Silva, S. Viswanathan, C. Delerue-Matos, "Molecularly imprinted sensor for voltammetric detection of norfloxacin", *Sens. Actuators B Chem.* 219 (2015) 301-307.
- [109] B. Liu, B. Xiao, L. Cui, M. Wang, "Molecularly imprinted electrochemical sensor for the highly selective and sensitive determination of melamine", *Mater. Sci. Eng. C* 55 (2015) 457-461.
- [110] C. Qin, W. Guo, Y. Liu, Z. Liu, J. Qiu, J. Peng, "A novel electrochemical sensor based on graphene oxide decorated with silver nanoparticles-molecularly imprinted polymers for determination of sunset yellow in soft drinks", *Food Anal. Methods* 10 (2017) 2293-2301.
- [111] H. Song, Y. Wang, L. Zhang, L. Tian, J. Luo, N. Zhao, Y. Han, F. Zhao, X. Ying, Y. Li, "An ultrasensitive and selective electrochemical sensor for determination of estrone 3-sulfate sodium salt based on molecularly imprinted polymer modified carbon paste electrode", *Anal. Bioanal. Chem.* 409 (2017) 6509-6519.

- [112] T. Xie, M. Zhang, P. Chen, H. Zhao, X. Yang, L. Yao, H. Zhang, A. Dong, J. Wang, Z. Wang, "A facile molecularly imprinted electrochemical sensor based on graphene: application to the selective determination of thiamethoxam in grain", *RSC Adv.* 7 (2017) 38884-38894.
- [113] Y. Liu, L. Zhu, Y. Hu, X. Peng, J. Du, "A novel electrochemical sensor based on a molecularly imprinted polymer for the determination of epigallocatechin gallate", *Food Chem.* 221 (2017) 1128-1134.
- [114] W. Liu, Y. Ma, G. Sun, S. Wang, J. Deng, H. Wei, "Molecularly imprinted polymers on graphene oxide surface for EIS sensing of testosterone", *Biosens. Bioelec.* 92 (2017) 305- 312.
- [115] M. Zhang, H. T. Zhao, T. J. Xie, X. Yang, A. J. Dong, H. Zhang, J. Wang, "Molecularly imprinted polymer on graphene surface for selective and sensitive electrochemical sensing imidacloprid", *Sens. Actuators B Chem.* 252 (2017) 991-1002.
- [116] B. B. Prasad, R. Singh, K. Singh, "Development of highly electrocatalytic and electroconducting film using Ni nanomer for ultra-trace detection of thiamine", *Sens. Actuators B Chem.* 246 (2017) 38-45.
- [117] J. Zhang, C. Wang, Y. Niu, S. Li, R. Luo, "Electrochemical sensor based on molecularly imprinted composite membrane of poly(o-aminothiophenol) with gold nanoparticles for sensitive determination of herbicide simazine in environmental samples", *Sens. Actuators B Chem.* 249 (2017) 747-755.
- [118] X. Wei, X. Xu, W. Qi, Y. Wu, L. Wang, "Molecularly imprinted polymer/graphene oxide modified glassy carbon electrode for selective detection of sulfanilamide", *Pro. Nat. Sci. Mater. Int.* 27 (2017) 374-379.
- [119] W. Liu, H. Li, S. Yu, J. Zhang, W. Zheng, L. Niu, G. Li, "Poly(3,6-diamino-9-ethylcarbazole) based molecularly imprinted polymer sensor for ultra-sensitive and selective detection of 17- $\beta$ -estradiol in biological fluids", *Biosens. Bioelec.* 104 (2018) 79- 86.
- [120] D. Dechtriat, B. Sookcharoenpinyo, P. Pranjogtat, C. Sriprachuabwong, A. Sanguankiat, A. Tuantranont, S. Hannongbua, "An electrochemical MIP sensor for selective detection of salbutamol based on a grapheme /PEDOT: PSS modified screen printed carbon electrode", *RSC Adv.* 8 (2018) 206-212.

- [121] M. Zhong, Y. Teng, S. Pang, L. Yan, X. Kan, "Pyrrole-phenylboronic acid: A novel monomer for dopamine recognition and detection based on imprinted electrochemical sensor", *Biosens. Bioelec.* 64 (2015) 212-218.
- [122] M. M. Farid, L. Goudini, F. Piri, A. Zamani, F. Saadati, "Molecular imprinting method for fabricating novel glucose sensor: Polyvinyl acetate electrode reinforced by MnO<sub>2</sub>/CuO loaded on graphene oxide nanoparticles", *Food Chem.* 194 (2016) 61-67.

# Chapter 2

## Development of titanium oxide nanoparticles modified MIP electrode for determination of caffeine in green tea

This chapter discusses the molecular imprinted polymer based TiO<sub>2</sub> nanoparticles embedded caffeine electrode. This electrode has been synthesized with acrylonitrile and graphite nanocomposite for the determination of caffeine in green tea. The comparative study of caffeine determination with other research reports is presented in this chapter. The electrochemical characteristics of the developed electrode and the experimental parameters for the detection caffeine are discussed here in detail followed by analysis of real samples.

### List of sections

- Introduction
- Experimental section
- Preparation of the MIP-TiO<sub>2</sub> caffeine electrode
- Preparation of the green tea liquor for real sample analysis
- Data analysis techniques
- Results and discussions
- Analysis of green tea samples
- Validation and prediction using the regression models
- Comparison of the proposed technique with the reported methods
- Conclusion

**Contents of this chapter are based on following publication:**

**Debangana Das**, Trisita Nandy Chatterjee, Runu Banerjee Roy, Bipan Tudu, Ajanto Kr. Hazarika, Santanu Sabhapondit, Rajib Bandyopadhyay, "Titanium oxide nanocubes embedded molecularly imprinted polymer based electrode for selective detection of caffeine in green tea," *IEEE Sensors Journal*, vol. 20, no.12, pp. 6240-6247, 2020.



## Chapter 2

# Development of titanium oxide nanoparticles modified MIP electrode for determination of caffeine in green tea

---

### 2.1. Introduction

Caffeine (CAF) belonging to *N*-methyl derivatives of xanthine, is an ingrained alkaloid found in tea, coffee and cocoa beans [1,2]. The chemical structure of CAF as shown in Fig.2.1 reveals the presence of methyl groups ( $-\text{CH}_3$ ) at 1,3,7 and dione ( $=\text{O}$ ) at (2,6). In green tea, The CAF content varies from 11 to 20 mg/g of dry matter [3-5].

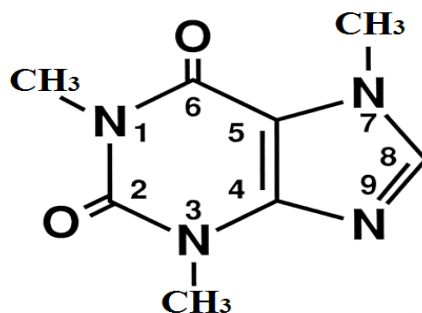


Fig.2.1. Chemical structure of caffeine.

The benefits of CAF, as mentioned in Section 1.1, are limited to 250 mg consumption of CAF per day. Its overconsumption can lead the person may suffer from several side-effects like insomnia, anxiety, increased heart rate, fatigue and high blood pressure [6-8]. Hence, regulating the amount of CAF in any food or beverage is of utmost importance and thus urges the development of a low-cost reusable sensor for its detection.

As highlighted in section 1.4.1, to date, analytical methods such as mass spectrometry, gas chromatography and other spectroscopic analyses have been proposed by a number of researchers [9, 10]. However, their complex operation, time consumption, requirement of skilled personnel and bulky weight undermine their

## Chapter 2: Development of titanium oxide nanoparticles modified MIP electrode for determination of caffeine in green tea

good sensitivities. On the contrary, researchers have proposed electrochemical methods wherein the electrodes are easily fabricated, sensitive and accurate [2, 11]. Simple carbon paste electrodes and fabrication of electrodes by addition of different modifiers have been proposed by a number of researchers [12-16]. These sensors lack selectivity because of absence of analyte specific sites on their surface though their designing is simple. As discussed in Section 1.8, MIP based sensor materials have been offering faithful solution to the above-mentioned hindrances. On exposure of the analyte to the polymer matrix externally, the analyte gets trapped within the cavities of the polymer and thus gets recognized [17-18].

The aforementioned methodology has been utilized in our research laboratory to detect theaflavin, catechin, epigallocatechin-3-gallate in tea quite successfully [19-21]. Moreover, molecularly imprinted photonic hydrogels [22], voltammetric detection using a MIP embedded carbon paste electrode [2], MIP based on graphene nanoparticles modified multi walled carbon nanotubes (MWCNTs) have been also proposed by the researchers for the detection of CAF [23].

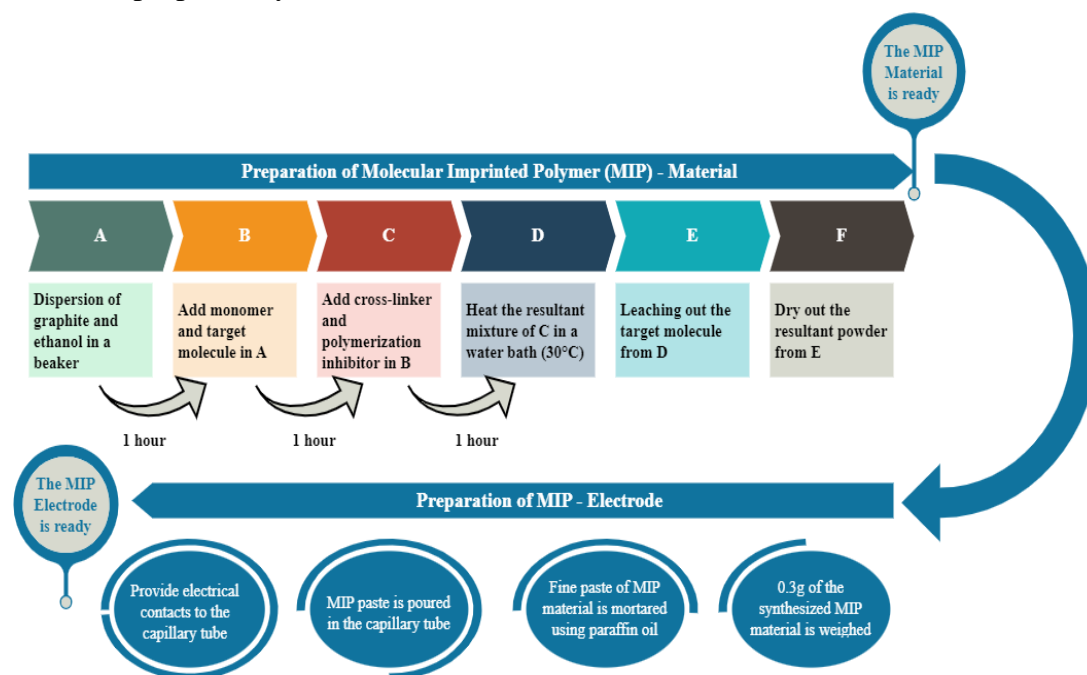


Fig.2.2. Step-wise preparation of the MIP Electrode.

Herein, we intend to fabricate an economic and reusable electrode for efficient tracing of CAF in green tea samples using the principle of MIP. the Copolymerization of acrylonitrile and EGDMA has been done to prepare the MIP material. The sample has been further modified by TiO<sub>2</sub> nanocubes in order to achieve



## Chapter 2: Development of titanium oxide nanoparticles modified MIP electrode for determination of caffeine in green tea

high oxidation efficiency, non-toxicity, enhanced photocatalytic activity, biocompatibility, high mechanical, thermal and chemical stability [24-26]. CV and DPV measurements have revealed an enhanced electron transfer using the proposed MIP-TiO<sub>2</sub> sensor accompanied by an acceptable detection limit and linear range. The sensor was also reasonably selective to its target analyte i.e., CAF and was also repeatable, stable and reproducible in nature. Moreover, in this work we have also tried to develop a model to predict the quantity of CAF in the tea samples. Towards this direction, firstly different tea samples were distinguished from each other on the basis of their CAF content by means of PCA. Additionally, two different linear regression techniques, viz., PLSR and PCR model were developed and tested to predict the quantity of CAF present in green tea. The performances of both the models were also validated for unknown samples and a comparative study has also been presented. The flowchart of MIP material synthesis and electrochemical studies and electrochemical studies attempted so as to optimize the properties of the electrode are shown in Fig. 2.2 and Fig. 2.3, respectively.

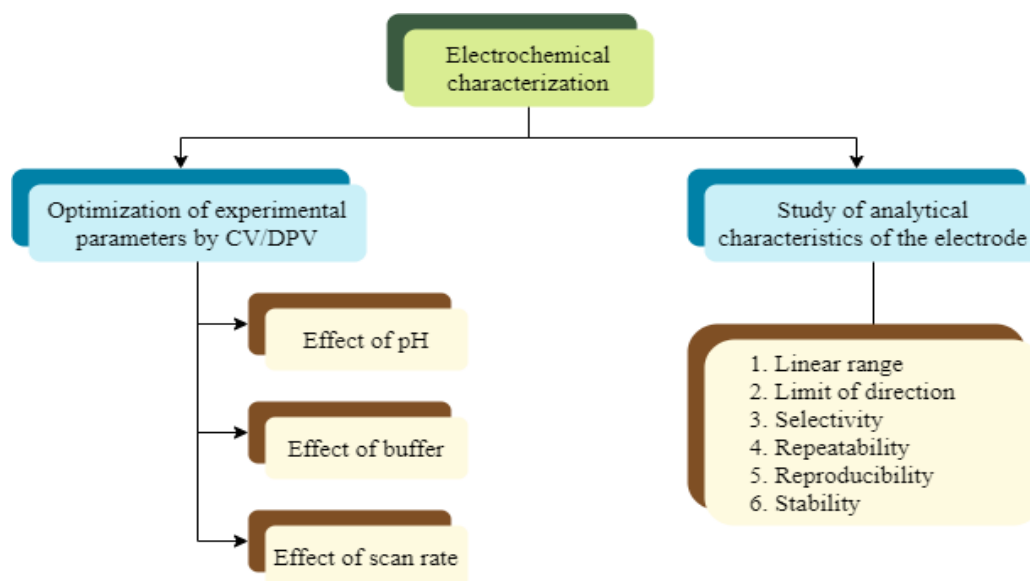


Fig.2.3. Optimizations and experimentations performed post-development of the electrode.

## 2.2. Experimental section

### 2.2.1. Reagents and materials

Acrylonitrile, EGDMA, CAF, ascorbic acid (AA), theophylline (TP), theobromine (TBr) and commercial graphite powder (99% pure) were procured from Sigma Aldrich, India. Hydrofluoric acid (HF), polyethylene glycol (PEG), ammonium

hydroxide ( $\text{NH}_4\text{OH}$ ), paraffin oil and ethanol were obtained from Merck, India. Benzoyl peroxide was supplied by Sisco Research Laboratories Pvt. Ltd., India. All the reagents used in the experiment were of analytical grade and used without further purification. Millipore water (Resistance = 18 M $\Omega$ ) was used throughout the entire experimentation and rinsing of the fabricate electrodes. The electrochemical experiments were performed at ambient temperature ( $25\pm 2^\circ\text{C}$ ).

### **2.2.2. Equipment and characterization**

Using a Phillips PW 1710 X-ray diffractometer (Eindhoven, The Netherlands) operated at 40 kV and 40 mA voltage and current, respectively, with CuK radiation (= 0.15406 nm) in a continuous scan mode from  $10^\circ$  to  $75^\circ$ , powder X-ray diffraction (PXRD) of the  $\text{TiO}_2$  nanoparticles was carried out. A twin beam Shimadzu UV-3600 spectrometer was used to measure the UV-visible absorption spectrum. A JEOL JEM6700F field emission scanning electron microscope (FESEM), run at an acceleration voltage of 10 kV, was used to characterise the sample's morphology. Utilizing the Autolab Potentiostat/Galvanostat 101, a three electrode system was used to conduct the electrochemical tests (Netherlands). As the reference electrode and counter electrode, respectively, Ag/AgCl and platinum electrodes have been employed. The measurements DPV and CV were taken in the same potential window of 1.0 V to 2.0 V.

### **2.2.3. Synthesis of $\text{TiO}_2$ nanoparticles**

The synthesis of  $\text{TiO}_2$  nanoparticles was performed in our laboratory following a similar technique as stated in [26]. At first, 10g of titanium dioxide was added to 50ml of HF followed by mixing with 10ml of PEG. The resultant solution was then stirred well for 1 h with cautious addition of 40 ml of  $\text{NH}_4\text{OH}$  till the formation of a white precipitate. The solution was further filtered and washed with distilled water followed by drying at room temperature. The dried sample was then calcined for 4 h at  $500^\circ\text{C}$  in air. Consequently, a yellowish powder of crystalline  $\text{TiO}_2$  nanoparticles was collected and preserved.

### **2.2.4. Synthesis of the MIP and non-imprinted polymer (NIP)**

The procedure for the synthesis of MIP electrode is given in Section 2.1, Fig. 2.2. Briefly, in 10 ml of ethanol, 0.95 g of commercial graphite powder was sonicated for 1 h. Then, 0.05g of acrylonitrile was added to it followed by 0.05g

addition of CAF. The solution was left under constant stirring for 2 h. After that, 400  $\mu\text{L}$  of EGDMA and 1 mg of benzoyl peroxide (polymerization initiator) were added to the same. The polymerization was carried out by heating the mixture in a water bath at 30°C. The polymerized sample produced as a result, was collected and dried under ambient conditions. The template molecule was leached out of the polymerized sample using a mixture of ethanol and water (80:20) to prepare the MIP. The resultant MIP sample was dried and preserved. The NIP sample was also synthesized similarly, except with the addition of CAF during its preparation.

#### **2.2.5. Preparation of the $\text{TiO}_2$ modified MIP and the NIP electrodes**

The previously synthesized  $\text{TiO}_2$  nanocubes were used for the preparation of both the MIP and NIP electrodes.  $\text{TiO}_2$  nanocubes were added to both the synthesized MIP and NIP samples keeping the ratio of 1:4. A fine paste of 0.3g of the respective powders was further prepared with the drop wise addition of paraffin oil. The paste was then poured into a 2.5 mm diameter fine capillary glass tube with Pt wires as electrical contacts (Fig. 2.4(a)). The surface of the electrodes were smoothed with  $\text{Al}_2\text{O}_3$  slurry and rinsed carefully with Millipore water before each measurement. Fig. 2.4 (b) shows the three-electrode configuration in the laboratory.

### **2.3. Preparation of the green tea liquor for real sample analysis**

The performance of the imprinted electrodes was validated using the tea samples, and the results, so obtained, were correlated with that of the HPLC data. The green tea samples were obtained from Tocklai Tea Research Institute, Jorhat, Assam, India. For all the imprinted electrodes in this thesis, green tea samples were considered as real samples and the same procedure for preparation of the tea liquor was followed. A thermoflask containing 200 mg of the tea samples had 40 ml of boiling water added to it. It underwent a ten-minute infusion before being sieved to extract the fluid. 20 ml of the liquor samples were poured into beakers after reaching room temperature, and using the manufactured MIP electrode, replicated voltammetric readings were taken from each of them.

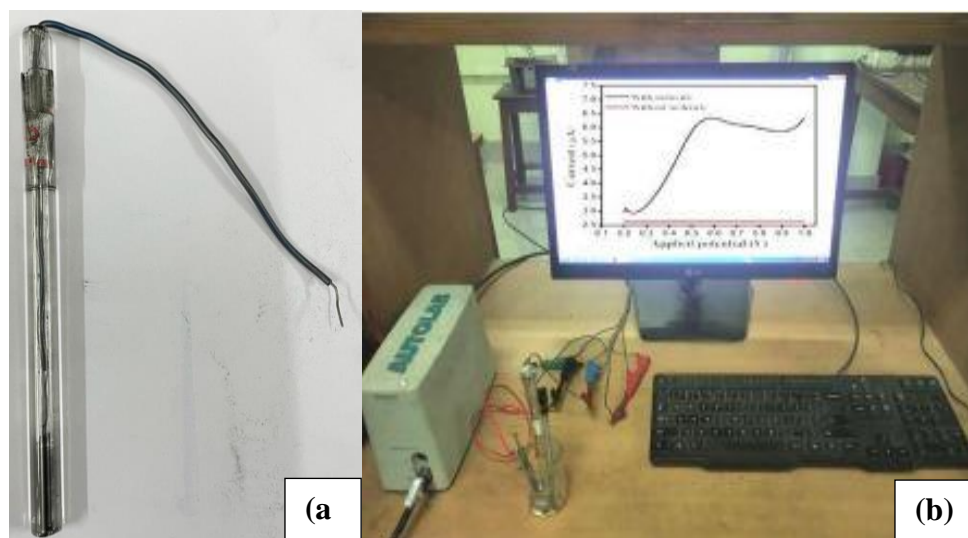


Fig. 2.4 (a) Fabricated MIP- electrode (b) Three-electrode configuration along with AutoLab.

## 2.4. Data analysis techniques

In this chapter, in order to discriminate amongst the green tea samples PCA has been implemented. PLSR and PCR technique has been implemented in order to correlate the electrode's response profile with that of the HPLC data of green tea samples. The flow chart depicted in Fig. 2.5 describes the data analysis techniques that were implemented post-development of the electrode.

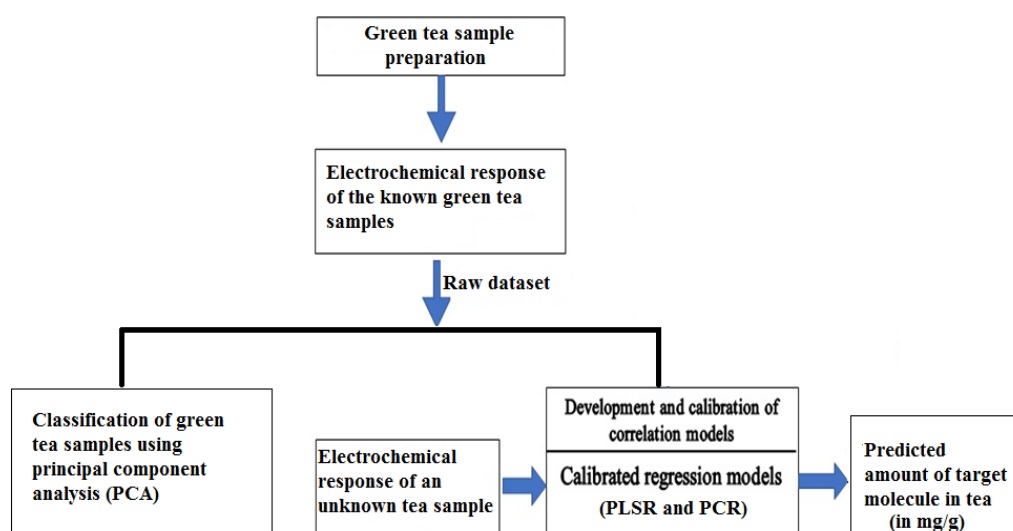


Fig.2.5. Operational flow chart.

### 2.4.1. Principal component analysis (PCA)

PCA is a dimensionality reduction tool where the data is represented as a linear combination of principal components. It is used to reduce a large set of variables into informative rich smaller data sets by transforming a number of correlated variables into a number of uncorrelated variables called principal components [27,28]. The amount of information linked with each principal component directions are measured in terms of the variance associated with them. The first principal component reveals the maximum variability in the dataset and the succeeding components account for the remaining variability [29]. Hence, a distinction between classes can be clearly established by visualizing the PCA score plots.

Let  $X$  is a matrix of size  $n \times m$  obtained from  $m$  no. of sensors.

$$X = \begin{pmatrix} X_{11} & \dots & X_{1m} \\ \vdots & \ddots & \vdots \\ X_{n1} & \dots & X_{nm} \end{pmatrix}$$

**Step 1:** The multidimensional dataset is taken and the mean is subtracted from each of the data dimensions. So,  $\bar{x}$  (mean value) is subtracted from all  $X$  values i.e.,  $[x_i - \bar{x}]$ . This produces a dataset with 0 mean values. Let the new matrix be denoted by  $Y$ .

$$Y = \begin{pmatrix} Y_{11} & \dots & Y_{1m} \\ \vdots & \ddots & \vdots \\ Y_{n1} & \dots & Y_{nm} \end{pmatrix}$$

where,  $Y_i = [x_i - \bar{x}]$

**Step 2:** The co-variance matrix can now be computed as:

$$\text{cov} = \frac{Y^T Y}{n - 1}$$

It is a square matrix of size  $m \times m$  for 'm' dimensional data.

$$C = \begin{pmatrix} C_{11} & \dots & C_{1m} \\ \vdots & \ddots & \vdots \\ C_{n1} & \dots & C_{nm} \end{pmatrix}$$

The main feature of the covariance matrix is that it is symmetrical about the main diagonal.

**Step 3:** The Eigen vectors and Eigen values are calculated from the covariance matrix from the Eigen value equations.

$$[C-\lambda I] Z=0$$

The solution of the above equation gives the value of  $\lambda$ , i.e. the eigen values. After obtaining the Eigen values, the Eigen vectors can be calculated. The Eigen values are arranged in descending order to form the column matrix.

$$E= [eig_1 eig_2 \dots \dots \dots eig_k \dots \dots eig_m]$$

The Eigen vectors are of unit length and are orthogonal, i.e., perpendicular to each other. The Eigen vectors are then arranged in the order of eigen values, from highest to lowest. This gives us the components in the order of their importance. The eigen vector with the highest eigen value forms the first principal component of the dataset. We can choose two or three eigen vectors with maximum eigen values for PCA plot. This will lead to loss of some information but that is negligible. The n dimensional dataset will be reduced to two or three dimensions as per requirement.

**Step 4:** Now, if we take only the k important eigenvectors and form a matrix with these eigen vectors in column, we may construct a feature vector as

$$\text{Feature vector } F= [eig_1 eig_2 \dots \dots eig_k]$$

where,  $k \ll m$

**Step 5:** Now, Row feature Matrix is formed with the eigenvectors in the column transposed i.e.

$$\text{Row Feature Vector } F = \begin{pmatrix} eig_1 \\ eig_2 \\ eig_3 \\ \dots \\ \dots \\ eig_k \end{pmatrix}$$

Row data adjust matrix is formed with the mean adjusted data transposed, i.e., rows representing the dimensions and columns representing the data items as shown below:

$$Y^T = \begin{pmatrix} Y_{11}, Y_{21}, & \dots & Y_{n1} \\ \vdots & \ddots & \vdots \\ Y_{1m}, Y_{2m}, & \dots & Y_{nm} \end{pmatrix}$$

So, final data is the product of the Row Feature Vector and the row data  $Y^T$ :

$$Final\ Data = \begin{pmatrix} eig_1 \\ eig_2 \\ \dots \\ \dots \\ eig_k \end{pmatrix} \begin{pmatrix} Y_{11} & \dots & Y_{k1} \\ \vdots & & \vdots \\ \dots & \ddots & \vdots \\ \dots & & \vdots \\ Y_{1m} & \dots & Y_{km} \end{pmatrix}$$

Final data is the dataset with items in column and dimensions in rows. Thus, after performing PCA, the dimensions get reduced.

#### **2.4.2. Partial least square regression (PLSR)**

Partial least square (PLS) is a widely used technique in chemometrics, especially in the case where the number of independent variables are significantly larger than the number of data points. The PLS regression reduces the number of predictors by extracting set of components that describe the maximum correlation between the predictors and response variables [30]. Herein, the leave one out cross validation (LOOCV) technique has been used in order to examine the predictive ability of the electrode. The parameters that reflect the degree of concurrence between the predicted and actual values are the root mean square error of calibration (RMSEC), root mean square error of validation (RMSEV) and root mean square error of prediction (RMSEP), respectively. PLSR is used to relate two data matrices namely, the predictor matrix  $\mathbf{X}$  and the response matrix  $\mathbf{Y}$ , by means of a linear multivariate model. A traditional multivariate model only relates the response variables with the predictor variables, whereas; the structure of  $\mathbf{X}$  and  $\mathbf{Y}$  can also be modelled by PLSR. PLSR is normally implemented when the datasets of  $\mathbf{X}$  and  $\mathbf{Y}$  consist of noisy, collinear and incomplete variables. The precision of the model parameters depends upon the relevant variables and increases on increasing their number. The central part of the model estimation deals with the calculation of the model parameters as the slopes of bivariate regression of partial components of predictors and the responses in the form of least squares.

The PLSR algorithm is as follows:

- a) Given the predictor matrix  $\mathbf{X}$  of  $N$  observations each of  $K$  variables and response matrix  $\mathbf{Y}$  of  $N$  observations each with  $M$  response elements. Let the number of PLS components be  $A$ . The index of the response elements can be represented by  $m$ , such that  $m = 1, 2, \dots, M$ . The corresponding index of PLS components can be represented by  $a$ , such that  $a = 1, 2, \dots, A$ .
- b) Perform the scaling and centering of  $\mathbf{X}$  and  $\mathbf{Y}$  data.

c) Perform initialization of the processing steps for the first response vector (first column) of  $\mathbf{Y}$ , i.e.  $y_m$  with  $m = 1$ .

d) Perform initialization of the processing steps for the PLS component, i.e.,  $p_1$ .

e) Obtain the starting vector of  $\mathbf{u}_a$ , such that  $\mathbf{u}_a$  is one of the columns of  $\mathbf{Y}$ , i.e.  $\mathbf{u}_a = \mathbf{y}_m$ . For univariate  $\mathbf{Y}$ ,  $\mathbf{u}_a = \mathbf{y}_1$ .

f) Calculate the X-weights  $\mathbf{w}_a$  such that

$$\mathbf{w}_a = X' \mathbf{u}_a / \mathbf{u}_a' \mathbf{u}_a$$

Modify  $\mathbf{w}_a$  such that norm of  $\mathbf{w}_a$  is 1.

g) Calculate X-scores,  $\mathbf{t}_a$ , i.e.,

$$\mathbf{t}_a = X \mathbf{w}_a$$

h) Calculate Y-weights,  $\mathbf{c}_a$ , i.e.,

$$\mathbf{c}_a = Y' \mathbf{t}_a / \mathbf{t}_a' \mathbf{t}_a$$

### 2.4.3. Principal Component Regression (PCR)

The principal component regression (PCR) model is designed to handle a large number of correlated independent variables. The idea behind PCR is to evaluate the principal components on the design matrix [31]. The components hence evaluated are sorted on the basis of their correlations which are used as predictors in a linear regression model fitted using the least squares procedure. In PCR, the directions in which the predictors show the maximum variance are the exact directions associated with the response variables. In this work, the validation of the PCR model is done using LOOCV technique [32] and here also RMSEC, RMSEV and RMSEP have been used to optimize the number of components best suitable for a good prediction. The number of principal components used to train the regression or prediction equation may vary depending upon the ability of the principal components to express the variation in the data. Now in ordinary least square technique there may be multi-collinearity present in the features. It can be seen that correlation for two or more data features may reach 80 to 90 percent then training a regression model becomes difficult.

The prediction equation will be Eq. 2.1:

$$y = b_0 + X^T b + error \quad (2.1)$$



X is the data matrix.  $b_0$  and b is the intercept and coefficients respectively. For getting the prediction equation the least square solution is used. If y is the output, then the predicted output is going to be

$$y_{pred} = (X^T X)^{-1} X^T y$$

Taking the output y and the data X,  $y_{pred}$  is found.

The prediction error or residual standard error is calculated by using the predicted output and the actual output. The error is termed as mean square error.

$$\sqrt{\sum_{all-y} (y - y_{pred})^2}$$

## 2.5. Results and discussions

### 2.5.1. XRD analysis of the prepared TiO<sub>2</sub> nanoparticles

The powder X-ray diffraction pattern was performed in order to confirm the phase purity and crystallinity of the prepared TiO<sub>2</sub> nanoparticles. The well-defined spectra obtained from the XRD pattern of the sample in Fig. 2.6 corresponds to the tetragonal anatase phase of TiO<sub>2</sub> (JCPDS 841286). Diffraction peaks obtained at 25.45°, 36.93°, 37.98°, 47.99°, 54.06°, 55.25°, 62.63°, 68.95°, 70.28°, 75.30°, 80.71° and 82.81° can be attributed to the (101), (103), (004), (200), (105), (211), (204), (116), (220), (215), (008), (303) planes of TiO<sub>2</sub> structure.

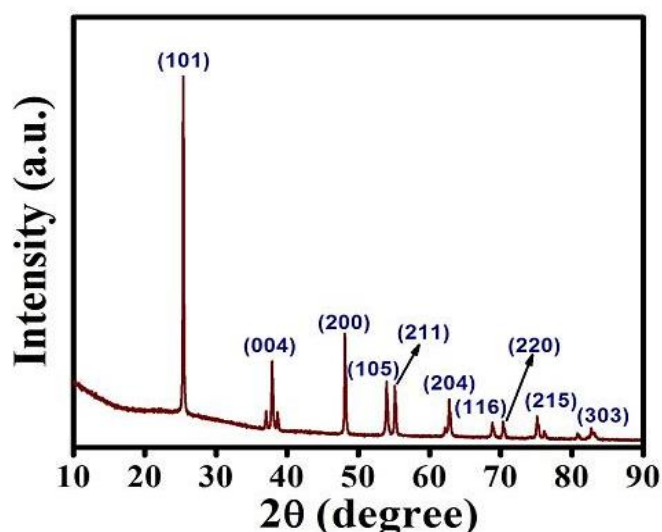


Fig. 2.6 Powder X-ray diffraction pattern of TiO<sub>2</sub>.

The broadened diffraction peaks and high intensity indicate good crystalline nature. The absence of other peaks confirms the absence of any impure phases in the sample.

The average crystallite size of the sample was calculated using the Debye-Scherrer method [33] considering the diffraction pattern of the most intense peaks and the particle size was found to  $38.6 \pm 9.86$  nm.

### 2.5.2. UV-visible spectroscopy

The removal of CAF from the polymer matrix was evidenced by means of UV-vis absorption spectroscopy performed in the wavelength region of 200-800 nm as shown in Fig. 2.7. The spectrum reveals visible absorption peaks corresponding to CAF at 273 nm for the CAF stock solution and also for the sample before CAF removal (BRT). However, the peak is absent from the material produced as a result of removal of CAF (ART) and thus confirms the successful removal of the template.

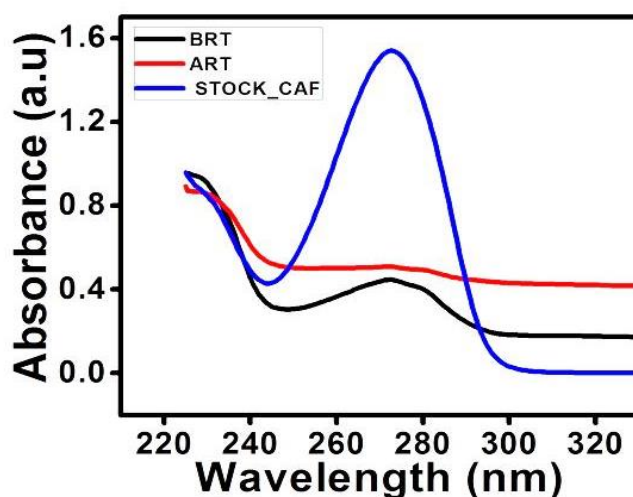


*Fig.2.7. Ultra violet visible absorption spectra of the 1mM CAF solution, before removal of template (BRT) and after removal of the template (ART).*

### 2.5.3. FESEM studies

The morphological images of the TiO<sub>2</sub>, MIP-TiO<sub>2</sub> and the NIP-TiO<sub>2</sub> samples are given in Fig. 2.8 (a), (b) and (c) respectively. It may be noted from Fig.2.8 (a) that TiO<sub>2</sub> nanoparticles are mostly cubical in nature. Fig. 2.8 (b) and 2.8 (c) depicts that the surface of the MIP-TiO<sub>2</sub> sample is rough and wrinkled as compared to the surface of the NIP material.

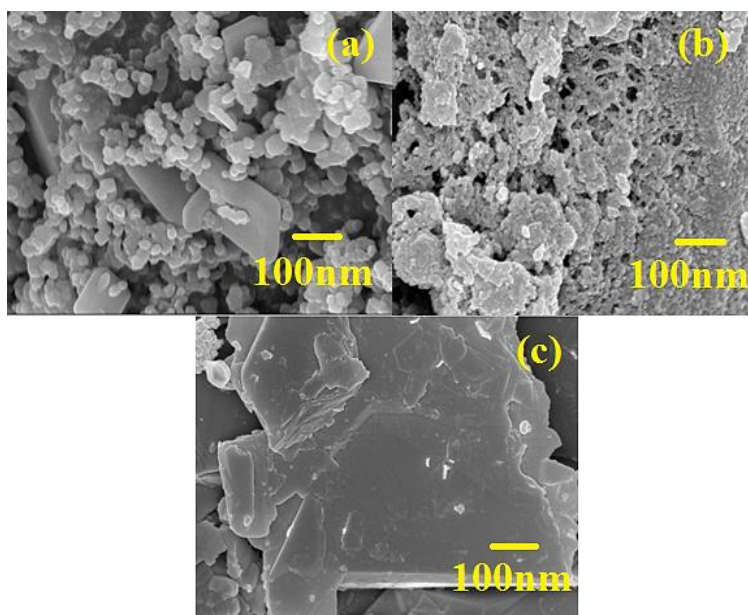


*Fig.2.8. Field Emission Scanning Electron Microscope images of (a) TiO<sub>2</sub> nanoparticles (b) MIP- TiO<sub>2</sub> and (c) NIP- TiO<sub>2</sub>.*

This change in smoothness is the result of the extraction of CAF molecule from the polymer sheet. This is consistent with the studies in literature [34, 35].

## **2.5.4. Optimization of the experimental conditions**

### **2.5.4.1. Supporting electrolyte and pH**

The choice of a suitable buffer for analysing the electrochemical performance of the fabricated electrode is vital. The electrode has been subjected to 1 mM CAF in three different buffers, viz., acetate buffer (ABS), phosphate buffer (PBS) and phthalate buffer (PTh) respectively, each of pH 5. The corresponding CV responses have been recorded (shown in Fig. 2.9 (a)). On comparison of the voltammetric peaks, it can be observed that the oxidation peak current ( $I_p$ ) of the MIP-TiO<sub>2</sub> electrode is highest (393.69  $\mu$ A) for phosphate buffer.

The impact of pH on the MIP-TiO<sub>2</sub> electrode has been analyzed by means of cyclic voltammetry tests has been carried out in 1 mM CAF using PBS of pH values 5, 6 and 7, respectively. The response curves are shown in Fig. 2.9(b). It may be inferred from the figure that maximum current intensity of 43.10  $\mu$ A has been observed in case of PBS 5. Hence, PBS 5 is chosen to be the test solution for the entire experiment.

Further, in order to study the electrochemical performance of the MIP-TiO<sub>2</sub> electrode over the unmodified MIP and the NIP- TiO<sub>2</sub> electrode, CV responses were obtained in 1 mM CAF solution using the respective electrodes. The corresponding response

profile, as shown in Fig.2.9 (c) reveals that the MIP-TiO<sub>2</sub> electrode showed an intuitive rise in peak current at 1.66 V than that offered by the unmodified MIP electrode. This sharp increment in the peak current using the MIP-TiO<sub>2</sub> electrode can be attributed to the high surface to volume ratio of the TiO<sub>2</sub> nanocubes, their high photocatalytic activity and magnetic property [26].

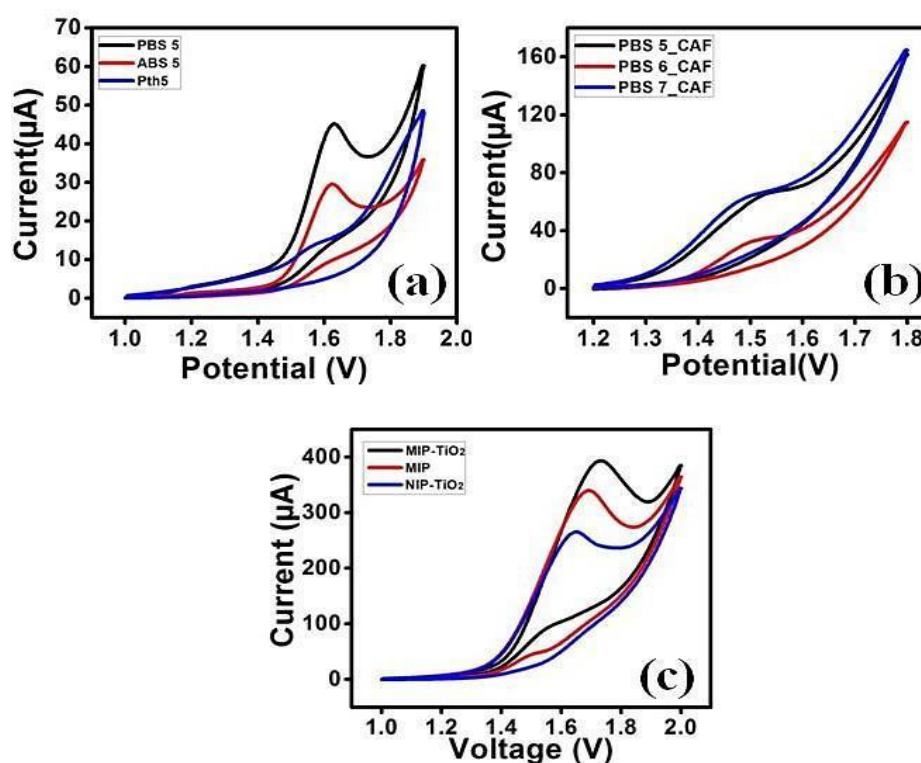


*Fig. 2.9. Cyclic voltammogram obtained for (a) 1 mM CAF in phthalate, phosphate and acetate buffer solutions (b) 1 mM CAF using PBS of pH values 5, 6 and 7, respectively (c) Comparative cyclic voltammetry response of 1 mM CAF solution using MIP-TiO<sub>2</sub>, MIP and NIP-TiO<sub>2</sub> electrode.*

The three dimensional surface of the crystalline TiO<sub>2</sub> nanocubes offers numerous active sites [26]. In the active sites, the inherent magnetic property of the TiO<sub>2</sub> nanocubes contributes to the fast electron transfer by attracting the polar CAF molecule towards it. However, due to the absence of the magnetic TiO<sub>2</sub> nanocubes, the rate of electron transfer is considerably reduced in case of the unmodified MIP electrode. Moreover, it can be seen from the figure that though the NIP-TiO<sub>2</sub> electrode responded proportionately to CAF, however, the corresponding peak current is relatively lower than that of the MIP-TiO<sub>2</sub> electrode. This may be due to the presence of lower active sites on the electrode surface due to the absence of the cavities having similar orientation as that of CAF.

#### **2.5.4.2. Influence of scan rate**

The effect of the scan rate on the electrochemical properties the MIP-TiO<sub>2</sub> electrode was investigated by means of CV. The electrode was imbibed in 1mM CAF stock solution at different scan rates (10 to 100 mVs<sup>-1</sup>) and the corresponding voltammogram are depicted in Fig. 2.10 (a). As predicted for a surface-controlled process [36], it can be clearly deduced from Fig. 2.10 (b) that the oxidation peak currents ( $I_p$ ) are directly proportional to the scan rate with  $R^2=0.98$ . Moreover, in the work, a detailed study of the kinetics of the reaction system involved in the oxidation of CAF has been analyzed. The surface concentration of the CAF and the number of electrons transferred has been calculated using the following equation

$$I_p = \frac{nFQv}{4RT} = \frac{n^2F^2Av\Gamma_c}{4RT} \quad (2.2)$$

where,  $n$ ,  $F$ ,  $A$ ,  $\Gamma_c$  and  $Q$  are the number of electrons transferred, Faraday's constant, area of the electrode, surface concentration and quantity of charge consumed during the oxidation process, respectively. The value of  $n$  and  $\Gamma_c$  calculated from equation (2.2) are 1.11 and  $11.12 \times 10^{-8}$  mole cm<sup>-2</sup>, respectively. The relationship between oxidation potential ( $E_p$ ) and logarithm of the scan rate ( $\log v$ ) is depicted in Fig. 2.10 (c). The value of  $E_p$  shifts in the positive direction and also increases linearly along with  $\log v$ .

$$E_p = 0.146 \log v + 1.7609 \quad (2.3)$$

The electron transfer coefficient ( $\alpha$ ) was calculated from the slope of the calibration curve of Eq. (2.4) and found to be 0.63 [37]. The value of  $n= 1.11$  and the presence of a single oxidation peak in the voltammogram, reveals that the developed electrode exhibits only one electron transfer process [38-40], which is the rate determining step in this work. Hence, experimental and analytical results are at par with each other.

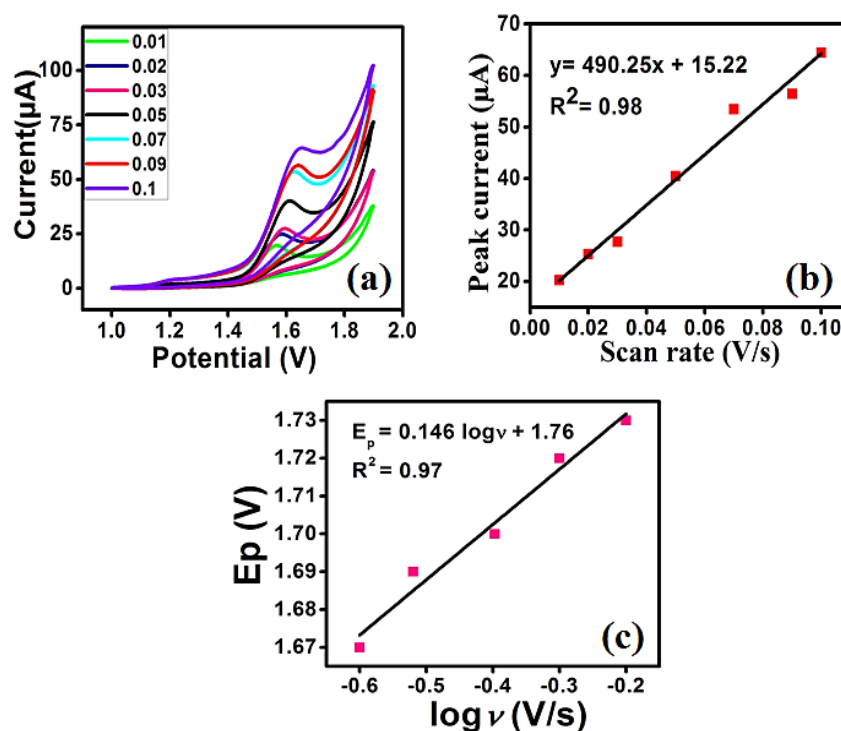


Fig. 2.10. a) Cyclic voltammogram indicating the variation of peak currents with different scan rates (10 to 100 mVs<sup>-1</sup>) b) Variation of the anodic peak current with the scan rate c) Relationship between oxidation potential ( $E_p$ ) and logarithmic scan rate ( $\log v$ ).

#### 2.5.4.3. Concentration variation and linearity

In order to study the dependence of current profile of the synthesized electrode DPV measurements were performed on varying concentration of CAF. The potential window for the entire DPV experiment was set from 1.0 V- 2.0 V. The modulation time, modulation amplitude and step potential were maintained at 0.2 s, 0.005V and 0.01 V, respectively. The scan rate and the interval time were kept fixed at 0.05 V/s and 0.4 s, respectively. It may be seen from Fig. 2.11 (a) oxidation peak current ( $I_p$ ) increases with the corresponding increase of CAF concentration from 5µM to 120µM. The calibration curve (shown in Fig. 2.11 (b)) obtained from the response profile is linear in nature as shown in equation (2.4).

$$I_p (\mu A) = 0.004x(\mu M) + 0.172 \quad (2.4)$$

with  $R^2=0.99$ . The limit of detection (LOD) of CAF was calculated as 0.6µM based on  $3S_y/x/m$  [42-43].



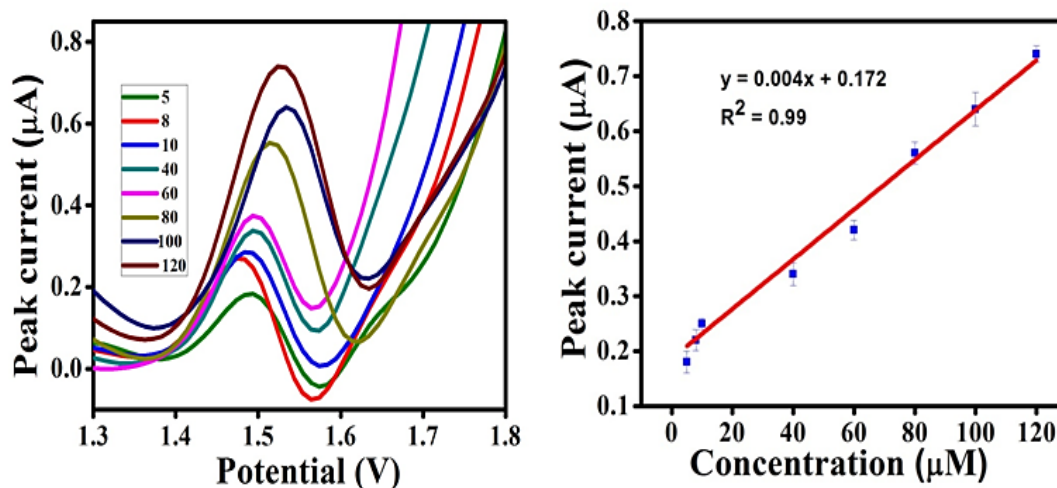


Fig. 2.11 (a) Concentration variation of CAF in PBS 5 buffer (DPV) using the MIP- TiO<sub>2</sub> electrode & (b) Linear dependency of peak current with concentration.

#### 2.5.4.4. Sensory characteristics of the MIP- TiO<sub>2</sub> electrode

For the measurement of selectivity of the proposed MIP-TiO<sub>2</sub> electrode, it has been exposed to 10<sup>-3</sup> M of THP, TBR, and AA, respectively. The electrode delivered no response towards the AA. The peak current of the corresponding analytes has been plotted in the form of bar graph shown in Fig. 2.11 (a). From the figure, it may be observed that the current response in presence of CAF was higher than that of the other three constituents, revealing that the electrode has the best selectivity towards its target analyte. It illuminated that the modified MIP-TiO<sub>2</sub> electrode was able to detect CAF effectively and the detection ability of other structural isomers are relatively less. To investigate the repeatability, twelve repetitive CV measurements in presence of 1 mM CAF in PBS 5 were performed using the electrode. The voltammogram as shown in Fig. 2.11 (b) are repeatable in nature with the relative standard deviation (RSD) of 2.08% indicating that the electrode's response is excellently repeatable. Consecutive voltammetric measurements were carried out in presence of 1 mM CAF solution using the proposed electrode under ambient conditions in order to obtain information regarding its stability. It may be observed from Fig. 2.11 (d), the sensitivity of the MIP-TiO<sub>2</sub> electrode decreased by 1.2% after 15 days and 10.25% after 3 months, thereby suggesting that the electrode is reusable. The reproducibility of the electrode has been studied by three similar electrodes followed by obtaining

CV response in presence of 1 mM CAF solution (Fig. 2.12 (c)). The electrodes showed moderately good reproducibility having RSD 5.49%.

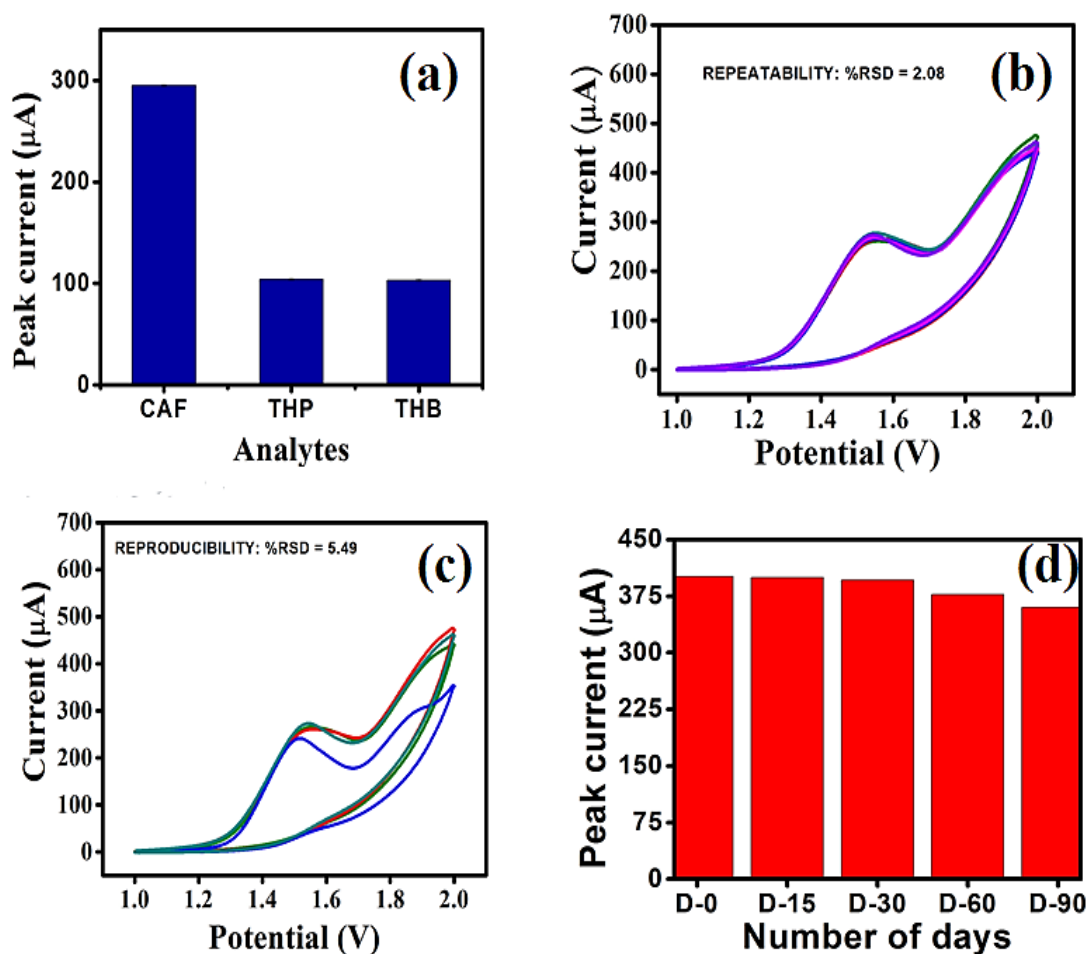


Fig. 2.12 (a) Bar plot indicating the selectivity of the MIP-TiO<sub>2</sub> electrode (b) repeatability of the MIP-TiO<sub>2</sub> electrode (c) reproducibility of the MIP-TiO<sub>2</sub> electrode (d) stability of the MIP-TiO<sub>2</sub> electrode.

## 2.6. Analysis of green tea samples

The primary objective of this study is to quantify the amount of CAF present in green tea using suitable prediction algorithms. This is a very important step in view of the deployment of the electrode to the tea industries. Ten varieties of green tea samples, along with their corresponding HPLC data, were obtained from Tocklai Tea Research Institute in Jorhat, Assam. The samples were prepared according to the method described in literature [20-21]. After attaining room temperature, few drops of NaOH were added to 20 ml of the tea liquor for carrying out the DPV experiments. Six duplicated DPV responses in the potential window of 1 V-2 V from each of the tea samples were obtained and the corresponding data matrix formed of the order of



(100×60). This dataset was further subjected to PCA [27], PLSR [41] and PCR [42] analysis using MATLAB 10.

### **2.6.1. Principal component analysis (PCA)**

From the PCA plot (shown in Fig. 2.13), it can be inferred that well defined clusters of the ten variants of the green tea samples are formed. The first three PC loadings added up to 98.65 % of the total variance in the samples; with PC1, PC2 and PC3 being 77.95%, 17.65% and 3.06%, respectively. The class separability measure has been calculated and a separability index (SI) of 47.82 is obtained. This significant high SI value implies the vivid discrimination of the ten varieties of green tea samples on the basis of their CAF content.

### **2.6.2. Partial least square regression analysis (PLSR)**

PLSR model incorporated with leave-one-out cross validation (LOOCV) technique [32] has been employed in order to measure the predictive ability of the electrode. Six repetitive DPV readings of 10 samples were taken. The obtained data matrix of the DPV response as well as the HPLC data were designed into two subsets, i.e., training and testing in the ratio of 80:20, respectively. The prediction performance was estimated by observing correlation coefficient ( $R^2$ ) and root mean square error (RMSE) between predicted and experimental values. The optimal number of factor used in the PLSR models was selected on the basis of the lowest value of root mean square error of calibration (RMSEC) in the cross validation process. The change in RMSEC values along with the latent variables is plotted in Fig.2.13 (a). It is observed that RMSEC value (0.0754) is lowest for eight latent variables. From Table 1 it can be inferred that the prediction accuracy using the PLSR model was found to be 92.94%. A comparative study of the predicted and actual value has been represented in form of a bar graph shown in Fig. 2.13 (b). The plot clearly indicates good agreement between the actual and the predicted values of CAF in green tea samples that have been used.

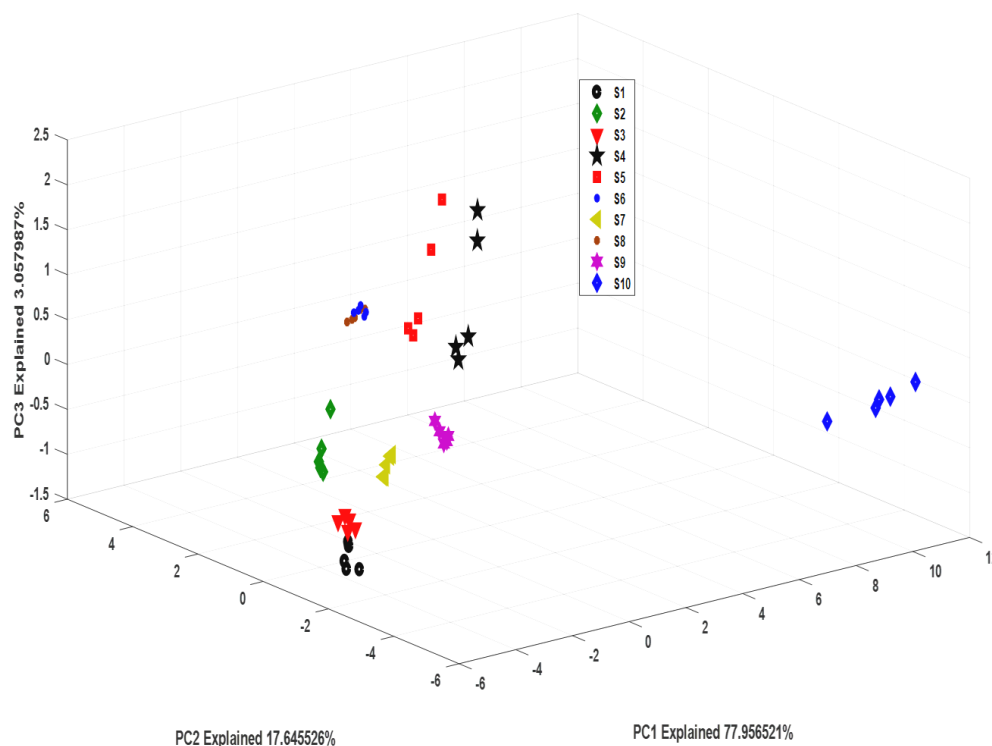


*Fig. 2.13. PCA plot showing cluster of ten green tea samples.*

### 2.6.3. Principal component regression analysis

A PCR model has also been used to predict the CAF content in the same green tea samples. The optimal number of factors or latent variable used in the PCR model, has been chosen on the basis of the lowest value of predicted RMSEC. Fig.2.13 (c) reveals that the lowest RMSEC (0.0733) has been obtained for nine components. The corresponding average prediction accuracy obtained from the PCR model is 93.75% (Table 2.1). The PCR results for calibration, validation and prediction has been tabulated in Table 2.2. The bar plot in Fig. 2.14 (d), reveals that the CAF content in 10 samples can be accurately predicted. Therefore, the overall prediction accuracy obtained from both the PLSR and the PCR analysis were more or less similar with only difference being the number of latent variables that are required to attain a constant minimum variance.

## Chapter 2: Development of titanium oxide nanoparticles modified MIP electrode for determination of caffeine in green tea

*Table 2.1. Actual and predicted CAF content (PLSR and PCR model)*

Sl. No.	Actual CAF (mg/g)	Predicted CAF (mg/g)		Prediction accuracy (%)	
		PLSR	PCR	PLSR	PCR
1	4.21	4.20	4.17	<b>99.83</b>	<b>99.11</b>
2	4.51	5.14	5.13	86.05	86.25
3	4.50	4.28	4.30	<b>95.11</b>	<b>95.66</b>
4	4.66	4.86	4.88	<b>95.73</b>	<b>95.31</b>
5	4.34	4.60	4.60	94.18	94.07
6	5.42	5.07	5.15	93.51	95.06
7	4.32	4.44	4.41	<b>97.17</b>	<b>97.87</b>
8	6.16	5.63	5.58	91.38	90.58
9	4.74	4.38	4.59	92.40	<b>96.73</b>
10	4.04	3.40	3.51	84.04	86.89
<b>Average prediction accuracy</b>				92.94	93.75

*Table 2.2. Prediction of CAF concentration in unknown tea samples\**

Regression Method	Latent Variable	Calibration		Validation		Prediction	
		RMSEC	R <sub>c</sub> <sup>2</sup>	RMSEV	R <sub>v</sub> <sup>2</sup>	RMSEP	R <sub>p</sub> <sup>2</sup>
<b>PLSR</b>	8	<b>0.07</b>	0.91	0.41	0.76	0.31	0.81
<b>PCR</b>	9	<b>0.07</b>	0.90	0.18	0.77	<b>0.13</b>	<b>0.82</b>

\*R<sub>c</sub><sup>2</sup>: Coefficient of determination for calibration; RMSEV: Root mean square of validation; R<sub>v</sub><sup>2</sup>: Coefficient of determination for validation; RMSEP: Root mean square error of prediction; R<sub>p</sub><sup>2</sup>: Coefficient of determination for prediction.

### 2.6.4. Validation and prediction using the regression models

An external dataset has been given as an input to the calibrated PLSR and PCR linear regression models. Validation and prediction of both the models have been carried out using this external dataset and the results are listed in Table 2.2. The validation results reflected that for PLSR, the RMSEV was found to be 0.4162 with coefficient of determination for validation R<sup>2</sup> = 0.7687 with eight latent variables; whereas, for PCR, the RMSEV was found to be R<sup>2</sup> = 0.7767 with nine latent variables. From the validation results, it can be concluded that the PCR model can provide better prediction for any unknown tea sample. Also, the prediction results with RMSEP = 0.1321 and R<sub>p</sub><sup>2</sup> being in unity with validation results implying that PCR model is best suited for predicting the CAF content in any unknown sample.

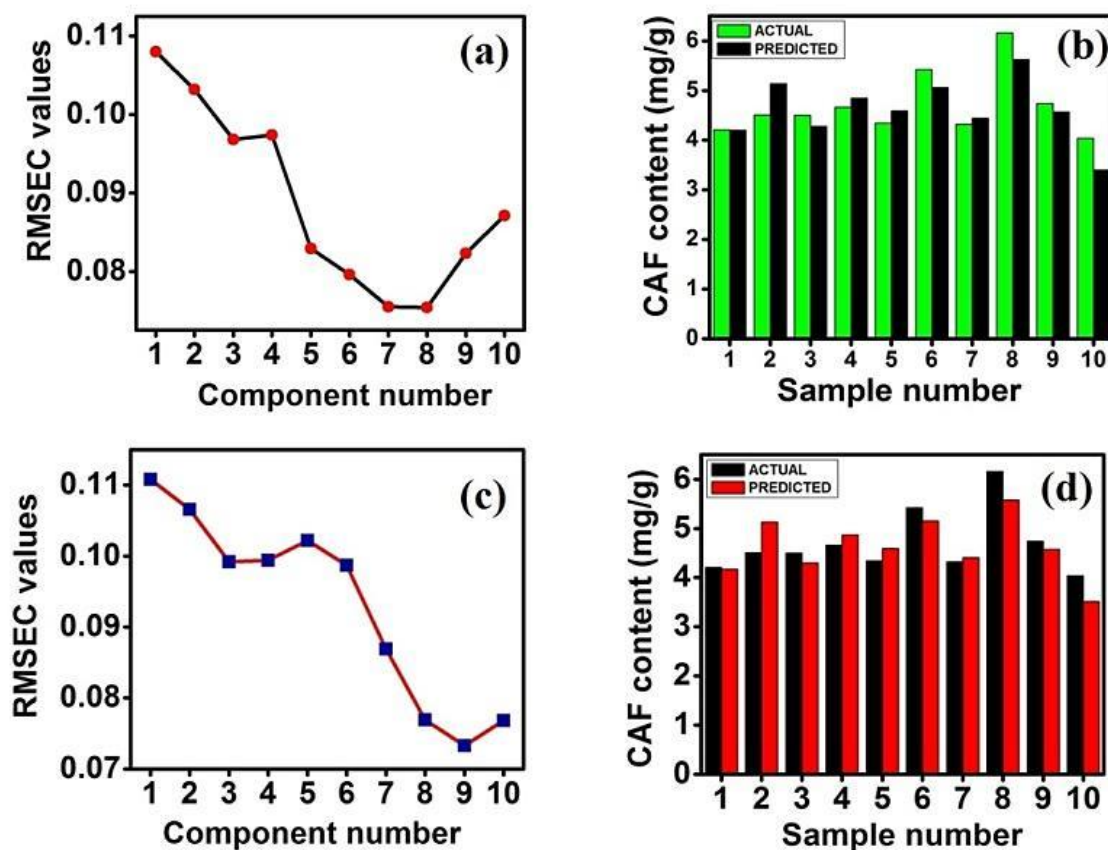


Fig. 2.14. For PLSR: (a) RMSEC values of ten components (b) Bar plot indicating the actual and predicted values of CAF; For PCR: (c) RMSEC values of ten PCR components (d) Bar plot indicating the actual and predicted values of CAF.

## 2.7. Comparative analysis

Our limited literature survey yielded a number of studies in which the individual electrochemical detection of CAF has been pursued. The results obtained are reported in Table 2.3. It may be observed from the table that though some of the electrochemical methods resulted in a lower value of LOD; but the processes related to the preparation of the electrodes are either tedious or the precursors involved are costly. Further, the selectivity of the electrodes is not discussed vividly in some of the reports. Moreover, the mechanism of detection involved in one such work is also indirect resulting into suppression of the oxidation current of the analyte due to the presence of modifying agent. However, in this work we have used less costly precursors and also the TiO<sub>2</sub> modifier used for the preparation of MIP is biocompatible and environment friendly. Further, the amount of CAF present in green

## Chapter 2: Development of titanium oxide nanoparticles modified MIP electrode for determination of caffeine in green tea

tea ranges from 11 to 20 mg/g in dry weight basis; which roughly accounts to be 56  $\mu\text{M}$  -102.99  $\mu\text{M}$ ; much higher than the LOD (0.6  $\mu\text{M}$ ) obtained in this study. Therefore, all in all, the MIP-TiO<sub>2</sub> electrode proposed in this work can serve as an efficient eco-friendly sensor for the detection of CAF in green tea.

*Table 2.3. Comparison of the proposed method with existing techniques.*

Methods	Linear Range	LOD	Ref.
Square wave voltammetry (SWV) and CV using carbon paste electrode (CPE) modified with 1,4 benzoquinone	0 – 0.5 mM/L 0.5 -8 mM /L	0.3 $\mu\text{M}$ /L 5.1 $\mu\text{M}$ /L	[12]
CV and DPV using carbon nanotubes (CNT) and gold nanoparticles MIP-based sensor	$5 \times 10^{-10} - 1.6 \times 10^{-7}$ M/L	$9 \times 10^{-11}$ M/L	[23]
DPV using modified glassy carbon electrode (GCE) multiwalled CNT/vinyl trimethoxy-silane based sensor	0.75 - 40 $\mu\text{M}$ /L	0.22 $\mu\text{M}$ /L	[16]
CV using anthroquinone modified based CPE	$2 \times 10^{-6} - 8 \times 10^{-4}$ M	$1.43 \times 10^{-7}$ M	[14]
CV using methyl orange modified based CPE.	10 -50 $\mu\text{M}$ 60- 1500 $\mu\text{M}$	0.5 $\mu\text{M}$	[16]
CV and DPV using MIP- CPE	0.06-25 $\mu\text{M}$ /L	15 nM/L	[23]
<b>DPV and CV using TiO<sub>2</sub> nano-cubes modified MIP -based electrode</b>	<b>5-120 <math>\mu\text{M}</math></b>	<b>0.6<math>\mu\text{M}</math></b>	<b>This work</b>

## 2.8. Conclusion

Monitoring the content of CAF in daily diet is necessary, as its overconsumption may be detrimental to human health. The present study reports the development of a low cost sensor by means of MIP technique for the detection and quantification of CAF in green tea. The sensing material has been synthesized using the copolymer of AN and EGDMA followed by impregnation of TiO<sub>2</sub> nanocubes into it during the preparation of the sensor. The sensor demonstrated a linear range from 5  $\mu\text{M}$  to 120  $\mu\text{M}$  with the LOD being 0.6  $\mu\text{M}$ . The sensory parameters revealed reasonable selectivity, repeatability, stability and reproducibility. Herein, further practical application of the prepared sensor has been ascertained in presence of ten variants of green tea. The PLSR model and PCR model have been developed to estimate the predictive ability of the electrode in terms of the caffeine content by correlating the response of the obtained DPV datasets for the ten green tea samples with that of HPLC data. In case of PLSR technique, an average prediction accuracy of 92.94% is

obtained with root mean square error of calibration (RMSEC) value being as low as 0.07. Additionally for PCR, an average prediction accuracy of 93.75% is acquired with RMSEC value being 0.07. Consequently, the MIP-TiO<sub>2</sub> electrode proposed in this work can serve as an efficient eco-friendly sensor for the detection of caffeine in green tea.

## References

- [1] L.R. Juneja, M.P. Kapoor, T. Okubo, T.P. Rao, "Green tea polyphenols: nutraceuticals of modern life", CRC press (2013).
- [2] T. Alizadeh, M.R. Ganjali, M. Zare, P. Norouzi, "Development of a voltammetric sensor based on a molecularly imprinted polymer (MIP) for caffeine measurement", *Electrochim. Acta* 55 (2010) 1568-1574.
- [3] S. Khokhar, S.G. Magnúsdóttir, "Total phenol, catechin and caffeine contents of teas commonly consumed in the United Kingdom", *J. Agric. Food Chem.* 50 (2002) 565-570.
- [4] R. Hursel, "The effects of green tea on weight loss and weight maintenance: a meta-analysis", *Int. J. Obes* 33 (2009) 956–961.
- [5] X. Chen, O. Ghribi, J.D. Geiger, "Caffeine Protects Against Disruptions of the Blood-Brain Barrier in Animal Models of Alzheimer's and Parkinson's Diseases", *J Alzheimers Dis.* 20 (2010) 127–141.
- [6] Y. Dong, L.F. He, X.H. Zhang, X.R. Jiang, "Preparation and properties of caffeine molecular composite imprinted membranes", *Dig. J.Nanomater.Biostruct.* 11 (2016) 1319-1326.
- [7] L.M. Juliano, R.R. Griffiths, "A critical review of caffeine withdrawal: empirical validation of symptoms and signs, incidence, severity, and associated features", *Psychopharmacology* 176(1) (2004) 1–29.
- [8] G. Richards, A. Smith, "Caffeine consumption and self-assessed stress, anxiety, and depression in secondary school children", *J Psychopharmacol* 29(12) (2015) 1236-1247.
- [9] U.L.P. Okonny, S.X. Wang, R.J. Stubbs, N.A. Guzman, "Determination of caffeine and its metabolites in urine by capillary electrophoresis-mass spectrometry", *Electrophoresis* 26 (2005) 2652-2663.

- [10] M.M. Ali, M. Eisa, M.I. Taha, B.A. Zakaria, A.A. Elbashir, “Determination of caffeine in some Sudanese beverages by means of High-Performance Liquid Chromatography”, *Pakistan J Nutr.* 11(4) (2012) 336-342.
- [11] A.C. Torres, M.M. Barsan, C.M.A. Brett, “Simple electrochemical sensor for caffeine based on carbon and Nafion-modified carbon electrodes”, *Food Chem.* 149 (2014) 215–220.
- [12] M. Aklilu, M. Tessema, M.R. Abshiro, “Indirect voltammetric determination of caffeine content in coffee using 1,4-benzoquinone modified carbon paste”, *Talanta* 76 (2008) 742–746.
- [13] W.J.R. Santosa, M. Santhiago, I.V.P. Yoshida, L.T. Kubota, “Electrochemical sensor based on imprinted sol–gel and nanomaterial for determination of caffeine”, *Sens Actuators B Chem* 166-167 (2012) 739– 745.
- [14] Y. Tadesse, A. Tadese, R.C. Saini, R. Pal, “Cyclic Voltammetric Investigation of Caffeine at Anthraquinone Modified Carbon Paste Electrode”, *Int. J. electrochem.* (2013) 1-7.
- [15] H. Wu, D.H. Bremner, H. Li, Q. Shi, J. Wu, R. Xiao, L. Zhu, “A novel multifunctional biomedical material based on polyacrylonitrile: Preparation and characterization”, *Mater. Sci. and Eng.* 6 (2016) 702-709.
- [16] J.G. Manjunatha, C. Raril, “Cyclic Voltammetric Investigation of Caffeine at Methyl Orange Modified Carbon Paste Electrode”, *Biomedical Journal of Scientific & Technical Research (BJSTR)* 9 (2018) 1 – 6.
- [17] F. Deng, E. M. Goldys , G. Liu, “Molecularly imprinted polymer-based reusable biosensing device on stainless steel for spatially localized detection of cytokine IL-1 $\beta$ ”, *Sens Actuators B Chem*, 292(2019) 277-283
- [18] M.C.Díaz-Liñán, A.I.López-Lorente, S.Cárdenas, R.Lucena, “Molecularly imprinted paper-based analytical device obtained by a polymerization-free synthesis”, *Sens Actuators B Chem* 287 (2019) 138-146
- [19] T.N. Chatterjee, R.B. Roy, B. Tudu, P. Pramanik, H. Deka, P. Tamuly, R. Bandyopadhyay, “Detection of theaflavins in black tea using a molecular imprinted polyacrylamide-graphite nanocomposite”, *Sens Actuators B Chem* 246 (2017)840-847.

- [20] T.N. Chatterjee, D. Das, R.B. Roy, B. Tudu, S. Sabhapandit, P. Tamuly, P. Pramanik, R. Bandyopadhyay, "Molecular Imprinted Polymer Based Electrode for Sensing Catechin (+C) in Green Tea", *IEEE Sens. J.* 18 (2018) 2236-2244.
- [21] T.N. Chatterjee, D. Das, R.B. Roy, B. Tudu, A.K. Hazarika, S. Sabhapandit, P. Tamuly, R. Bandyopadhyay, "Development of a nickel hydroxide nanopetal decorated molecular imprinted polymer based electrode for sensitive detection of epigallocatechin-3-gallate in green tea", *Sens Actuators B Chem* 283 (2019) 69-78.
- [22] S. Xu, J. Li, X. Song, J. Liu, H. Lu, L. Chen, "Photonic and magnetic dual responsive molecularly imprinted polymers: preparation, recognition characteristics and properties as a novel sorbent for caffeine in complicated samples", *Anal. Methods* 5 (2013) 124-133.
- [23] X. Kan, T. Liu, C. Li, H. Zhou, Z. Xing, A. Zhu, "A novel electrochemical sensor based on molecularly imprinted polymers for caffeine recognition and detection", *J Solid State Electrochem.* 16 (2012) 3207-3213.
- [24] L.C. Chuang, C.H. Luo, S.W. Huang, Y.C. Wu, Y.C. Huang, "Photocatalytic Degradation Mechanism and Kinetics of Caffeine in Aqueous Suspension of Nano-TiO<sub>2</sub>", *Adv. Mater.* 214 (2011) 97-102.
- [25] S. Bagheri, N.M. Julkapli, S.B.A. Hamid, "Titanium Dioxide as a Catalyst Support in Heterogeneous Catalysis", *Sci. World J* (2014).
- [26] S. Biswas, S. Pradhan, H. Naskar, R. Bandyopadhyay, P. Pramanik, "Sol-gel synthesis of cubic titanium dioxide nanoparticle using poly (ethylene glycol) as a capping agent: voltammetric simultaneous determination of uric acid and guanine", *Microchimica. Acta* 185: 513 (2018) 1-10.
- [27] M. Palit, B. Tudu, K.P. Dutta, A. Dutta, J. Jana, K. Roy, N. Bhattacharyya, R. Bandyopadhyay, A. Chatterjee, "Classification of black tea taste and correlation with tea taster's mark using voltammetric electronic tongue", *IEEE Trans. Instrum. Meas.* 59 (2010) 2230-2239.
- [28] S. Rezzi, D.E. Axelson, K. Héberger, F. Reniero, C. Mariani, C. Guillou, "Classification of olive oils using high throughput flow HNMR fingerprinting with principal component analysis, linear discriminant analysis and probabilistic neural networks", *Anal. Chim. Acta*, 2005552(1-2) (2005) 13-24.



## **Chapter 2: Development of titanium oxide nanoparticles modified MIP electrode for determination of caffeine in green tea**

---

- [29] I.T. Jolliffe, "Principal Component Analysis, Second edition", Springer, New York, 1986.
- [30] S. Wold, M. Sjostrom, L. Eriksson, "PLS-regression: a basic tool of chemometrics", *Chemom. Intell. Lab. Syst.* 58 (2001) 109–130
- [31] U. Depczynski, V.J. Frost, K. Molt, "Genetic algorithms applied to the selection of factors in principal component regression", *Anal. Chim. Acta*, 420(2) (2000) 217–227.
- [32] S. Kar, B. Tudu, A.K. Bag, R. Bandyopadhyay, "Application of Near-Infrared Spectroscopy for the Detection of Metanil Yellow in Turmeric Powder", *Food Anal. Methods.* 11 (2018) 1291–1302.
- [33] B.D. Cullity, S.R. Stock, "Elements of X-ray diffraction", *Math J.* (2001).
- [34] S. Yang, Y. Wang, M. Xu, M. He, M. Zhang, D. Ran, X. Jia, "Synthesis of modified chitosan-based molecularly imprinted polymers for adsorptive protein separation", *Anal. Methods* 5 (2013) 5471-5477.
- [35] X. Shi, A. Wu, G. Qu, R. Li, D. Zhang, "Development and characterization of molecularly imprinted polymers based on methacrylic acid for selective recognition of drugs", *Biomaterials* 28 (2007) 3741- 3749.
- [36] M. Amar, S. Admassi, "Polymer modified glassy carbon electrode for the electrochemical determination of caffeine in coffee", *Talanta* 93 (2012) 122– 128.
- [37] B. Habibi, M. Abazari, M. Hossein, P. Azar, "A Carbon Nanotube Modified Electrode for Determination of Caffeine by Differential Pulse Voltammetry", *Chin. J. Catal.* 33 (2012) 1783-1790.
- [38] A.J. Bard, L.R. Faulkner, "Electrochemical Methods: Fundamentals and Applications", New York: Wiley, 2001
- [39] G.A.M. Mersal, "Experimental and Computational Studies on the Electrochemical Oxidation of Caffeine at Pseudo Carbon Paste Electrode and Its Voltammetric Determination in Different Real Samples, *Food Anal. Methods*", 5 (2012) 520-529.
- [40] M.M. Farid, L. Goudini, F. Piri, A. Zamani, F. Saadati, "Molecular imprinting method for fabricating novel glucose sensor: Polyvinyl acetate electrode reinforced by MnO<sub>2</sub>/CuO loaded on graphene oxide nanoparticles", *Food Chem.* 194 (2016) 61-67.

## **Chapter 2: Development of titanium oxide nanoparticles modified MIP electrode for determination of caffeine in green tea**

---

- [41] D.A. Armbruster, T. Pry, “Limit of detection and limit of quantitation”, *Clin. Biochem.Rev.* 29 (2008) S49-S52.
- [42] K. Sivashanmugan, K. Squire, A. Tan, Y. Zhao, J.A. Kraai, G.L. Rorrer, A.X. Wang, “Trace Detection of Tetrahydrocannabinol in Body Fluid via Surface-Enhanced Raman Scattering and Principal Component Analysis”, *ACS Sens.* 4 (2019) 1109–1117.

# Chapter 3

## Development of copper oxide nanoparticles embedded MIP electrode for tracing gallic acid in green tea

This chapter presents the MIP based sensor for gallic acid detection in green tea samples. Here, MIP material is synthesized by utilizing itaconic acid as the monomer, EGDMA as a crosslinker and graphite as the leading material. The experimental and characterization details are elucidated in this chapter. The electrode has been imbibed in green tea samples for validation of their practicality for real-time applications.

### List of sections

- Introduction
- Experimental section
- Fabrication of MIP-CuO electrode
- Results and discussions
- Analysis of green tea samples
- Validation and prediction using linear regression models.
- Comparison of the present method with existing literature
- Conclusion

**Contents of this chapter are based on following publication:**

**Debangana Das**, Don Biswas, Ajanto Kumar Hazarika, Santanu Sabhapondit, Runu Banerjee Roy, Bipan Tudu, Rajib Bandyopadhyay, “CuO nanoparticles decorated MIP-based electrode for sensitive determination of gallic acid in green tea,” *IEEE Sensors Journal*, vol. 21, no.5, pp.5687-5694, 2021



## Chapter 3

### Development of copper oxide nanoparticles embedded MIP electrode for tracing gallic acid in green tea

---

#### 3.1. Introduction

Out of all the polyphenols, GA is the prime phenolic acid present in tea [1-2] and significant contributor towards health benefits of tea [3-4]. The chemical structure of 3,4,5- trihydroxybenzoic acid (GA) is shown in Fig. 3.1. Due to three hydroxyl groups (-OH) and the property of allowing straightforward copolymerization through its carboxylic (-COOH) group [5], it serves as a strong anti-oxidant.

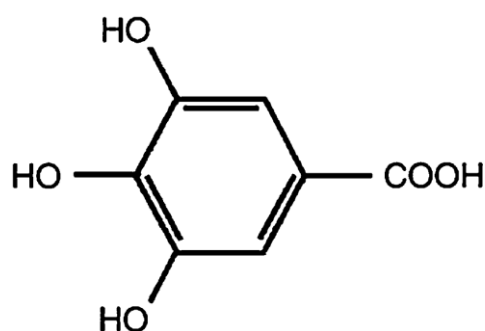


Fig. 3.1. Chemical structure of GA.

As discussed in Section 1.1, the traditional ways of determining GA content in tea include reversed phase high- pressure liquid chromatography, resonance light scattering, thin-layer chromatography, etc. [6-8]. Due to certain limitations, electrochemical methods for the detection of GA have been sought which serve as better alternatives owing to their intrinsic properties of good selectivity [9]. Carbon paste electrodes and electrodes modified with nanomaterials have previously been put forward for detection of GA [9-12, 14]. These electrodes exhibited instability, low sensitivity, reliability and the precursors used were costly, and thus necessitating the adoption of MIP technology for the determination of GA came into foray [15-17]. On subjecting these MIPs to the target analyte, molecules get trapped in the cavities and thus get detected [15-16]. Successful determinations of catechins and caffeine have

been reported using MIP technique [18-19]. Researchers have proposed methods using MIP which include incorporation of the synthesized MIP material in the multi-walled carbon nanotube modified carbon paste electrode (MWCNT–CPE) [11] and glassy carbon electrode embedded with polypyrrole film [15].

This work aims to develop an economic and reproducible electrode for the effective determination of GA in green tea samples utilizing MIP technology. The MIP matrix has been synthesized by co-polymerisation of itaconic acid (IA) and EGDMA using benzoyl peroxide (BP) as the polymerisation initiator. The sample has been modified with CuO NPs to increase the oxidation efficiency, the surface area of the electrode which in turn enhances the electrochemical performance of the sensor, stability of the sensor, biocompatibility and thermal stability [20-22]. On performing voltammetry, the synthesized electrode exhibited two linear ranges and a more sensitive detection limit as compared to other studies was observed [13,15, 23-25].

Novelty of the proposed method is its low cost, quick synthesis, availability of the precursors and the reproducible nature of the MIP- CuO electrode. Also, the thermal stability of CuO NPs contributes towards the usage of the MIP-CuO electrode in any environmental condition. The sensory parameters of the electrode were found to be selective, repeatable, stable and reproducible. On the basis of GA content, varieties of green tea samples were distinguished using PCA. The quantitative measure of separability amongst the samples has been established by calculating the separability index (SI). PLSR and PCR models have been developed to explore the ability of the electrode in predicting the amount of GA. After calibration, these models were utilized to quantify the amount GA in unknown green tea samples.

## **3.2. Experimental section**

### **3.2.1. Reagents and materials**

Graphite powder (99%), EGDMA, GA, IA, maleic acid (MA), catechin (CAT) and ascorbic acid (AA) were purchased from Sigma Aldrich, India. BP was obtained from Sisco Research Laboratories Pvt. Ltd, India. Copper chloride (CuCl<sub>2</sub>), ethanol, cetylpyridinium chloride (C<sub>21</sub>H<sub>38</sub>NCl), sodium hydroxide (NaOH), and paraffin oil were purchased from Merck & Co, India. Reagents used were of the highest grade and was not modified further. In every stage of electrode preparation, deionized water (Resistance 18 MΩ), obtained from Mili-Q water purification system was used.

### **3.2.2. Equipment and characterization**

A Phillips PW 1710 X-ray diffractometer is used to obtain PXRD patterns of CuO samples. The diffractometer is operated at 40kV and 40 mA with CuK $\alpha$  radiation ( $\lambda = 1.5406 \text{ \AA}$ ) in a continuous scan mode from  $10^\circ$  to  $75^\circ$ . The ultra violet-visible (UV-Vis) absorption measurements were done using Shimadzu UV-3600. The HPLC analysis was performed using UHPLC “DIONEX Ultimate 3000” for GA estimation. Scanning electron microscope (SEM) coupled with Oxford energy dispersive X-ray spectroscopy detector (EDX) (manufactured by ZEISS) were used to study the morphology and chemical composition. A three electrode system has been used to explore the behavior of electrode with Autolab Potentiostat/ Galvanostat 101 (Netherlands). As a CE, the platinum (Pt) electrode is used and Ag/AgCl electrode is used as RE. The DPV and CV were carried out in the voltage range of 0.0 V to 1.0 V.

### **3.2.3. GA estimation in HPLC**

The chromatographic separation of GA from tea samples was carried out at Tocklai Tea Research Institute, Assam, India. The column used was Phenomenex C18 (250mm x 4.6mm, 5  $\mu\text{m}$ ) phenyl hexyl ligand column. 9 % (volume fraction) acetonitrile, 2 % (volume fraction) acetic acid with 20  $\mu\text{g/ml}$  ethylenediamine tetraacetic acid was used as solvent A and 80 % (volume fraction) acetonitrile, 2 % (volume fraction) acetic acid with 20  $\mu\text{g/ml}$  ethylenediamine tetraacetic acid as solvent B. Flow rate of 1 ml/min was maintained. The chromatographic conditions were 100 % solvent A for initial 10 min, gradient elution over 15 min to 38% solvent B followed by 10 min in these conditions, i.e., 62 % solvent A + 38 % solvent B. The UV-Vis detector was set at 278 nm. The solvents used were filtered through 0.45-micron membrane filter. The peak of GA was identified and estimated by external standard method from response factor determined from GA standard [26].

### **3.2.4. Synthesis of CuO NPs**

The synthesis of porous CuO was carried out in the laboratory by sol gel method. 10gm of CuCl<sub>2</sub> was dissolved in 500 ml ethanol. To this solution, the surfactant C<sub>21</sub>H<sub>38</sub>NCl was added with continuous stirring for 30 minutes. 1 N NaOH solution was added to solution till the ‘pH’ of the solution becomes  $\sim 8-9$ , and a green colour precipitation was obtained. The precipitate was then filtered and dried in an electrical oven for 1 hour at  $50^\circ\text{C}$ . After calcination at  $400^\circ\text{C}$  for 3 hours, the black coloured CuO powder was obtained.

### **3.2.5. Synthesis of GA imprinted polymer and NIP**

The MIP samples were prepared following the standard method as described in Section 2.2. The polymer matrix was synthesized by the sonochemical treatment of an ethanolic dispersion of 0.90 g of commercial graphite powder and 0.05 g of IA for 1 hour. Then, 0.05 g of GA was added to the mixture and stirred continuously for 2 h. Later, EGDMA (400  $\mu$ l) and benzoyl peroxide (0.001 g) were added to the as-prepared-solution and left to stir for another 2 h. The mixture was then heated for 1 h in a water bath for the occurrence of polymerization. The polymerized powder, which was obtained as a final product was collected and dried. The GA imprinted sample was prepared by extraction of GA molecule from the powder by filtering it with a mixture of ethanol and deionized water (70:30) until indications of the presence of GA were completely nullified. This methodology was followed to synthesize the NIP sample excluding the mixing of GA.

### **3.2.6. Fabrication of CuO modified MIP and NIP electrodes**

For the purpose of fabricating the GA imprinted (MIP) and NIP electrodes, CuO NPs were added to both the MIP and NIP powder which were synthesized. The ratio of the polymerized powder to the CuO NPs was maintained to be 1:4. The respective mixtures were turned into a fine and smooth paste with the help of binder. The paste was delivered into capillary glass tubes having inner radius of 1.25 mm. To provide electrical contact to the electrode, copper wire was used.

## **3.3. Results and discussions**

### **3.3.1. UV-Visible Spectroscopy**

The removal of GA from the synthesized polymer network was affirmed by UV-Vis spectroscopy. The scanning of the instrument was done in the wavelength window of 200-800 nm. As observed from the spectrum (Fig. 3.2 (a)), two visible absorbance peaks are present corresponding to the GA molecule, one at 217 nm and other at 272 nm for the material before extraction of the target molecule (BRT). After extraction of GA (ART) from MIP network, both peaks are absent in spectrum ascertaining the complete removal of GA from MIP material.



### 3.3.2. XRD Analysis of the Prepared CuO NPs

The formation of CuO NPs was confirmed from JCPDS No. 80-1916, where diffraction peaks were obtained at 32.47°, 35.49°, 38.68°, 38.89°, 46.19°, 48.65°, 53.40°, 61.45°, 66.10°, 68.00°, 72.32° and 75.12°, respectively. These can be assigned to the (110), (111), (202), (020), (113), (311) and (222) planes and the structure of CuO is monoclinic in nature.

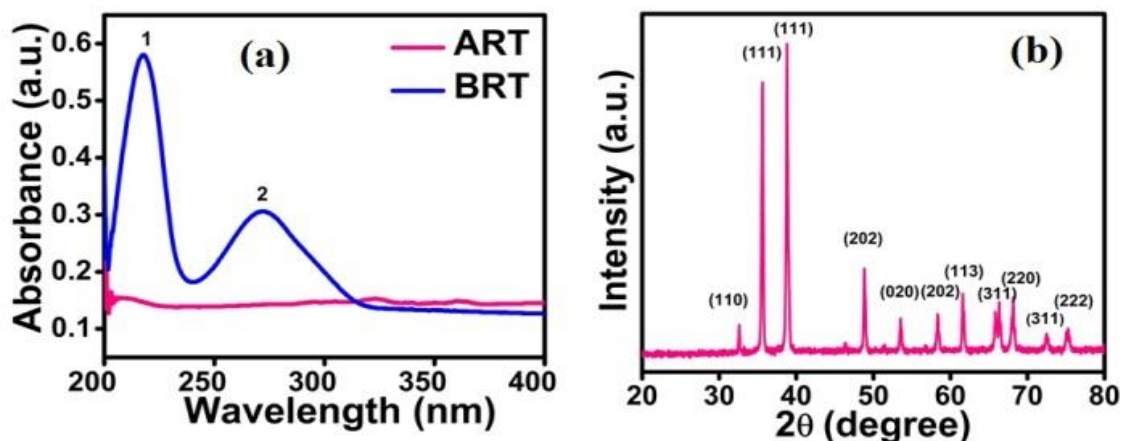


Fig. 3.2.(a) UV-vis absorption spectra of the 1mM GA solution before (BRT) and after (ART) removal of template (b) Powder XRD pattern of CuO NPs.

The absence of any other peaks in the XRD spectra of the samples shown in Fig. 3.2 (b) indicates that the corresponding CuO so formed is free from the impure phases. The approximate crystallite size of the NPs was calculated to be  $41.6 \pm 7.70$  nm applying the Debye-Scherrer method as stated in [27].

### 3.3.3. SEM and energy dispersive spectroscopy studies

SEM micrographs of MIP material, NIP material and CuO NPs (Fig. 3.3) are shown below. In Fig. 3 (a), the rough surfaces probably indicate that GA molecule, thus hampering the smooth surface of the polymer material. In Fig. 3.3 (b), the smooth surfaces of the NIP material reveal that no extraction process has been carried out.

Fig. 3.3 (c) shows the SEM image of the CuO NPs. The elementary composition and purity of CuO NPs were investigated by EDX analysis (Fig. 3.3 (d)).

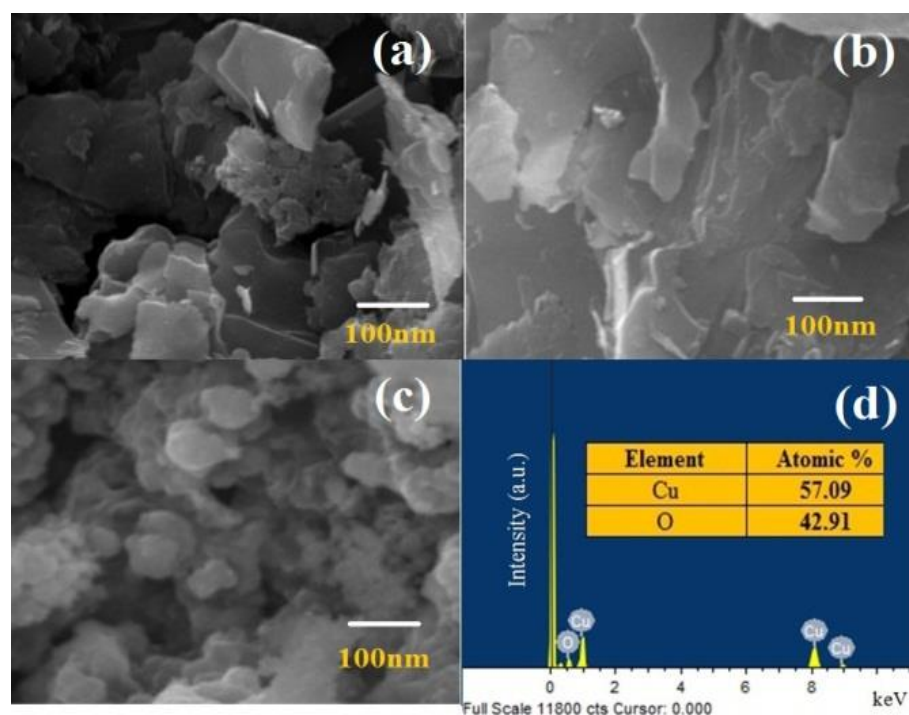


*Fig. 3.3. SEM image of a) MIP-CuO b) NIP-CuO c) CuO NPs and d) EDX spectrum of the as prepared CuO NPs.*

### **3.3.4. Optimization of the experimental conditions**

#### **3.3.4.1. Influence of buffer and pH**

The performance of electrode in electrochemical conditions by a suitable buffer is experimentally analysed. The electrode has been dipped in 1 mM GA in different buffers of pH 5, viz., citrate buffer (CB), phosphate buffer (PBS) and acetate buffer (ABS), respectively. As shown in Fig. 3.4 (a), the voltammetric responses have been plotted and it is observed that on being compared to voltammetric peaks, the oxidation peak current ( $I_p$ ) of the electrode is highest (26.17  $\mu$ A) for PBS. In presence of 1 mM GA, CV tests are performed to ascertain the impact of pH on the MIP-CuO electrode using PBS of pH values 5, 6 and 7, respectively.

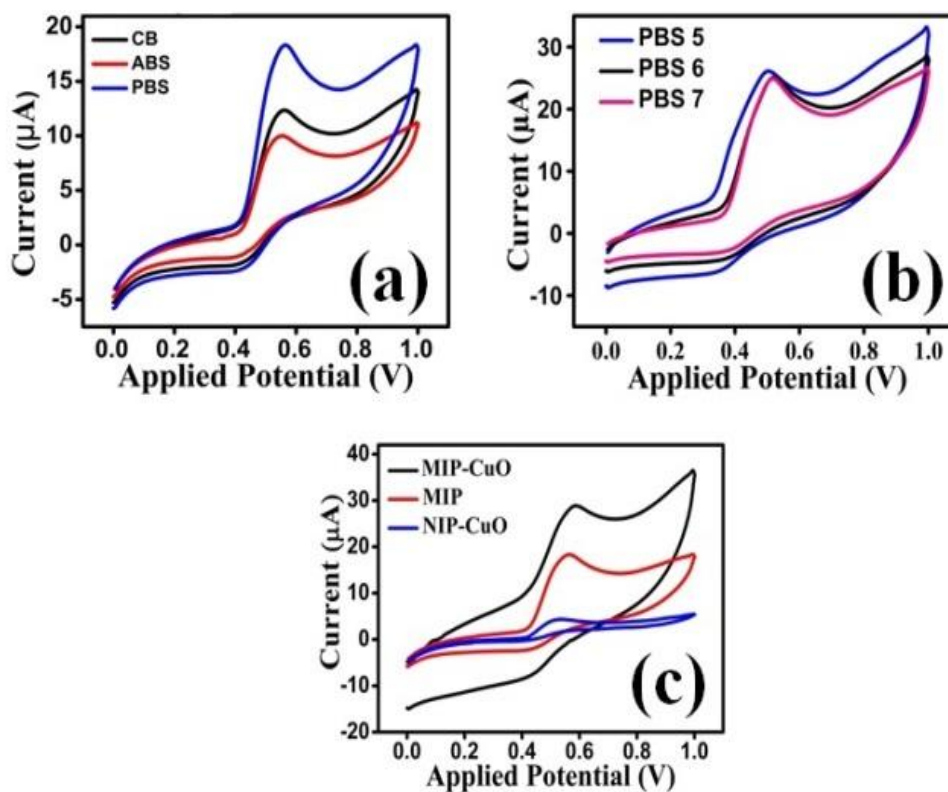


Fig. 3.4. Voltammograms obtained for 1 mM GA (a) in citrate, acetate and PBS solutions (b) with PBS of pH values 5, 6 and 7 (c) with MIP-CuO, MIP and NIP-CuO electrode.

Fig. 3.4 (c) portrays the current response profile wherefrom it is derivable that the MIP-CuO electrode showed a considerable rise in peak current (26.20  $\mu\text{A}$ ) at 0.50 V when compared to the unmodified MIP electrode (18.30  $\mu\text{A}$ ) at 0.56 V. This surge in the peak is observed due to the high specific surface area CuO NPs [20]. It is also observed from Fig. 3.4 (a) that the oxidation peak potential of the GA molecule on the MIP- CuO electrode surface is shifted negatively to 0.50 V as compared to that on the unmodified electrode. This phenomenon is observed possibly due to the presence of CuO NPs which facilitate faster transfer of electrons during any electrochemical process [22]. For the case of the simple MIP electrode, owing to the absence of the electrochemically active CuO NPs, the rate of electron transfer is assumed to considerably reduce. It can be inferred from Fig. 3.4 (c) that the corresponding peak current of the NIP-CuO electrode is comparatively lower than that of the MIP-CuO electrode even though the respective electrode has responded proportionately to GA. The probable reason behind this observation may be attributed to the lesser active sites on NIP- CuO electrode because of the absence of GA -like cavities.

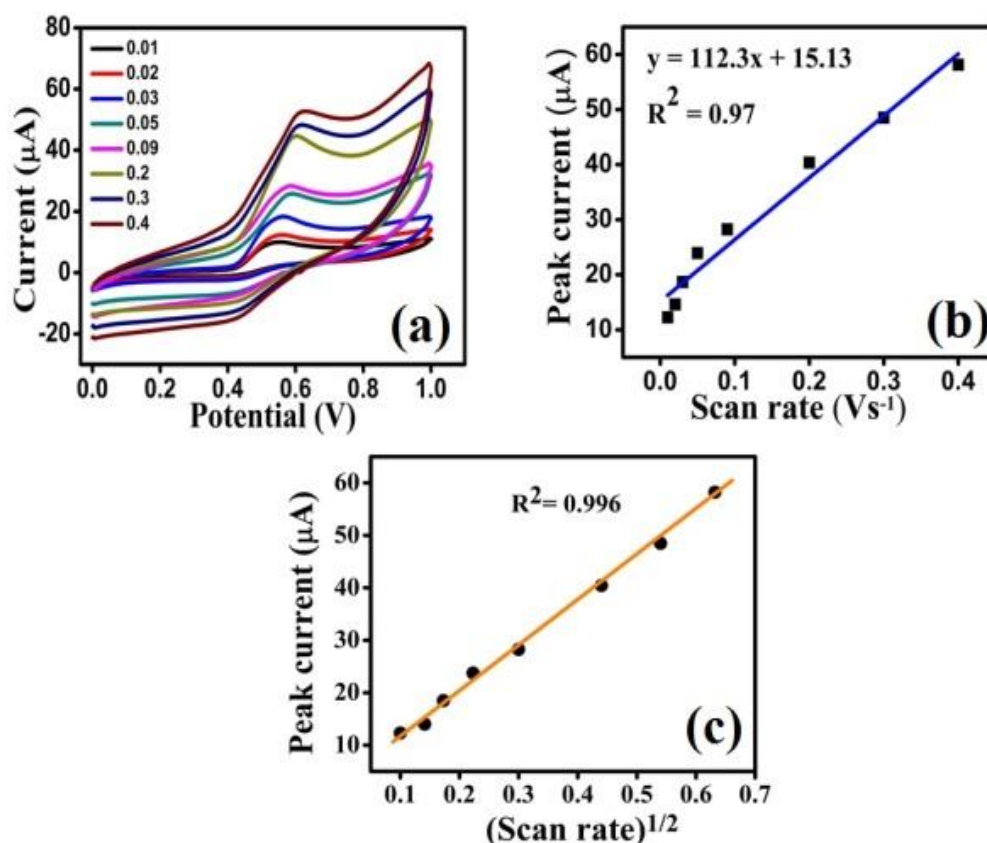


Fig. 3.5. a) Variation of peak currents with different scan rates (0.01- 0.4 Vs<sup>-1</sup>) b) Plot of peak current with scan rate c) Relationship between oxidation peak current ( $I_p$ ) and square root of scan rate.

### 3.3.4.2. Influence of scan rate

The impact of scan rate on the kinetics of the reaction system involved therein has been established by means of CV using the MIP-CuO electrode. The electrode was employed to 1 mM GA solution at varying scan rates ranging from 0.01 to 0.4 Vs<sup>-1</sup>, and the respective voltammograms are illustrated in Fig. 3.5 (a). The oxidation peak currents ( $I_p$ ) are proportional to that particular range of scan rate with  $R^2 = 0.97$  (Fig. 3.5 (b)) which demonstrates a surface-controlled process [28]. Also, it is evident from Fig. 3.5 (c) that the square root of scan rate and the corresponding peak current hold a linear relationship yielding  $R^2 = 0.996$ . This value of  $R^2$  is nearly equal to the numerical value of 1.0, which is normally the case for a surface-controlled process and thus satisfies the results so obtained.

### 3.3.4.3. Concentration Variation and Linearity

The current profile with increasing concentration of the GA in the analyte was monitored by performing DPV measurements using the MIP-CuO electrode. The voltage window for the DPV experiment was set to 0 - 1 V.

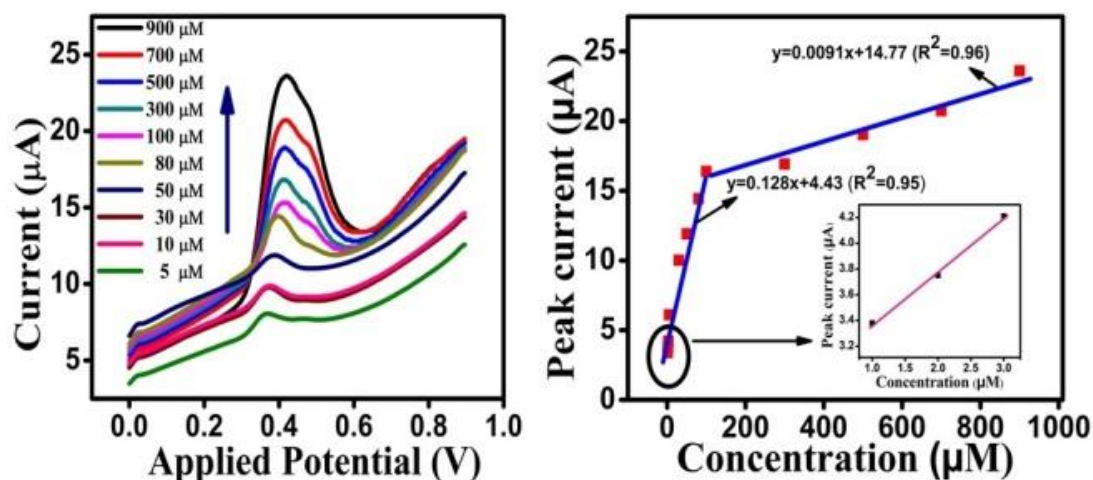


Fig. 3.6. DPV plots obtained on the surface of the MIP-CuO electrode containing different concentrations of GA in PBS 5 (b) Variation of the peak current with concentration; the inset shows the magnified image of the encircled portion.

The DPV experimental parameters viz., step potential, scan rate, modulation time, modulation amplitude and interval time were fixed at 0.01 V, 0.05 Vs<sup>-1</sup>, 0.2 s, 0.005 V, and 0.4 s respectively. It may be observed that a prominent increase in current is observed from Fig. 3.6 (a), as the concentration of GA increases. From the calibration curve of GA (Fig. 3.6 (b)), there are two linear segments: one linear segment is from 1 µM to 100 µM, which follows the regression equation of  $y = 0.128x + 4.43$  ( $R^2 = 0.95$ ). The second linear segment is within the range of 100 µM and 900 µM, and the corresponding regression equation is  $y = 0.0091x + 14.77$  ( $R^2 = 0.96$ ). The limit of detection (LOD) of the synthesized MIP-CuO electrode was calculated to be 12.6 nM based on  $3S_y/x/m$ .  $S_y/x$  and  $m$  are the standard deviation of the regression line and slope of the calibration curve, respectively [19].

### 3.3.5. Sensory characteristics of the MIP-CuO electrode

The MIP-CuO electrode has been subjected to 1mM of MA, AA and CAT, respectively in order to measure the selectivity of the electrode. The electrode showed a very little response when imbibed in MA and AA solutions. A negligible

response towards CAT was observed. The peak current obtained on imbibing the electrode to 1 mM GA, MA and AA have been plotted in Fig.3.7 (a). It can be deduced from the bar plot that the peak current in presence of GA was comparatively higher than rest of the analytes, exhibiting that the MIP-CuO electrode is the most selective towards GA. In presence of 1mM GA solution, CV responses were recorded to study the reproducibility of the electrode (Fig. 3.7 (b)) utilizing three similar electrodes. The electrodes showed acceptable reproducibility with relative standard deviation (% RSD) of 1.34. For repeatability, six CV measurements were recorded in presence of 1 mM GA in PBS 5 using this electrode. The nature of current response (Fig. 3.7 (c)) is repetitive with the % RSD of 4.22 indicating that the repeatability of the electrode is acceptable. To comment on the stability of the electrode, DPV measurements were carried out in presence of 1 mM GA solution at an interval of 10 days for almost 3 months under similar environmental conditions. Also, the sensitivity of the electrode decreased by 0.94 % after 15 days (Fig. 3.7 (d)) and 2.9 % after 3 months, thereby emphasizing that the electrode is highly stable and functional.

### **3.4. Analysis of green tea samples**

To comment on the practical application of the synthesized MIP-CuO GA electrode, it was employed to determine GA in ten varieties of green tea samples. GA content in all samples has been quantified by means of the developed PCR and PLSR models. The liquor to be used for experimentation was prepared following the method already described in Section 2.6. For each of the ten samples, eight repetitive DPV responses were recorded in the voltage range of 0.0 V – 1.0 V. The data matrix of dimensions [179 x 80] so obtained on imbibing the MIP-CuO electrode to the green tea samples was subjected to PCA [29,30], PLSR [31,32] and PCR [33,34] analysis using MATLAB R2014a.



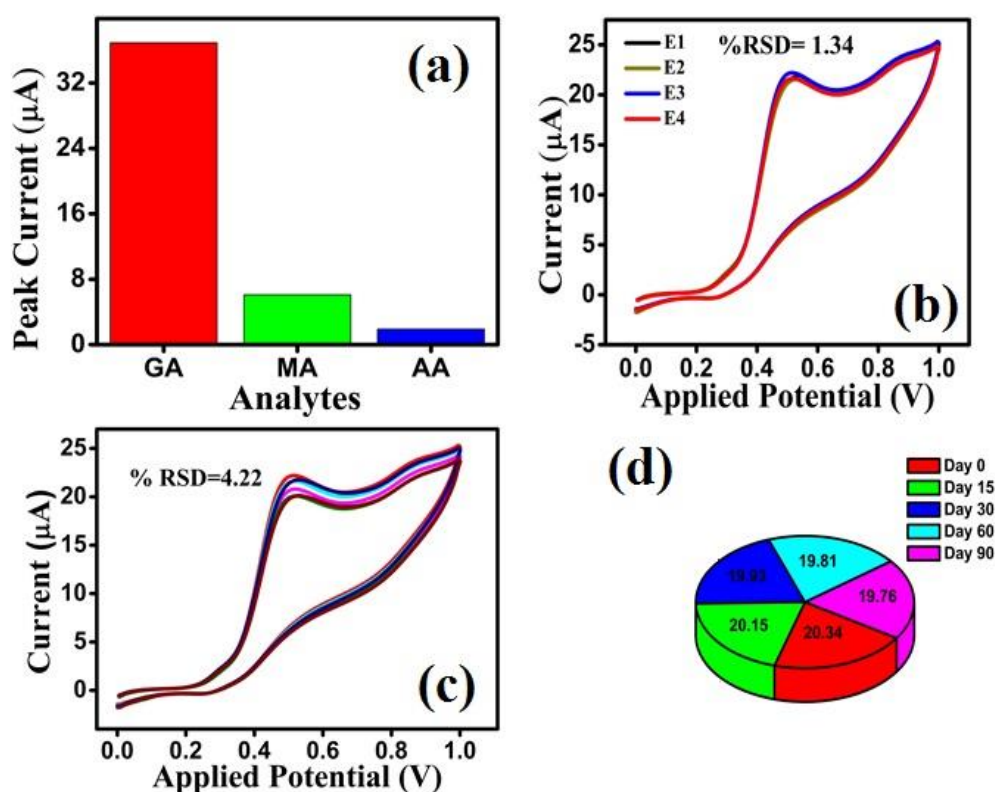
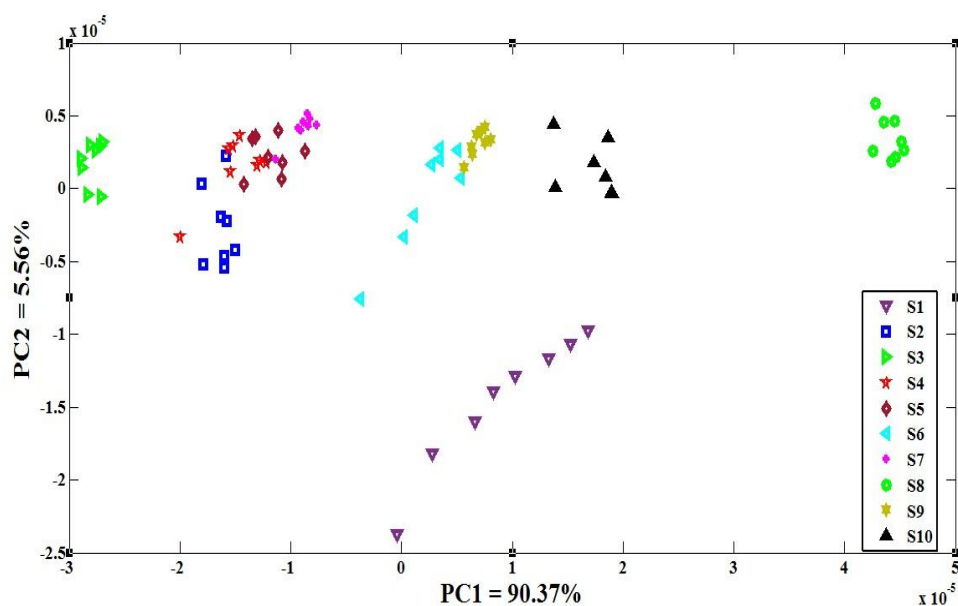


Fig. 3.7. Sensory characteristics of the MIP-CuO electrode showing (a) selectivity, (b) reproducibility, (c) repeatability and (d) stability.

### 3.4.1. Data clustering using PCA

Ten varieties of green tea samples were discriminated and were visualized by means of PCA analysis on the DPV datasets. It can be observed from Fig. 3.8 that samples belonging to a definite class have formed distinct and segregated clusters. The first two PC loadings explain 95.93 % of the total variance in the dataset with PC1 being 90.37 and PC2 being 5.56. On quantitative evaluation of the data nature, class separability index (SI) of 31.27 is obtained. This value of SI indicates the interclass separability of the samples is reasonably good using the MIP-CuO electrode.



*Fig. 3.8. PCA score plot showing cluster of ten GT samples based on their GA content.*

### **3.4.2. PLSR analysis**

The ability of the MIP-CuO electrode to predict the amount of GA has been analysed by developing PLSR model coupled with LOOCV technique. Eight repetitive DPV datasets were obtained for the designated GT samples. The matrix so obtained as a result of the DPV response and the corresponding HPLC data were divided into two subsets, i.e., training set and testing set in the ratio of 70:30. The performance of the model has been estimated by observing correlation coefficient ( $R^2$ ) and the RMSE between predicted and experimental values. The LV has been selected corresponding to the lowest value of RMSEC. As observed from Fig. 3.9 (a), the RMSEC value (1.36) is lowest for 14 LVs. For predicting the GA content (in mg/g) in green tea samples, the PLSR model has been used yielding a prediction accuracy of 88.97% on an average. Table 3.1 summarizes the comparison between the actual HPLC and predicted values of GA in the GT samples. The bar graph (shown in Fig. 3.9 (c)) illustrates the comparative study for precise visualization. This plot affirms a fair level of synonymity between the actual value and predicted value of GA content.

### **3.4.3. PCR analysis**

A relation has been established between the principal components of the data matrix of size [179×80] and the corresponding HPLC data. As can be seen from Fig. 3.8 (b), the lowest RMSEC (1.37) has been obtained for 17 LVs and hence it has



### Chapter 3: Development of copper oxide nanoparticles embedded MIP electrode for tracing gallic acid in green tea

been optimized for the prediction of GA content. The average prediction accuracy obtained in this case is 87.24% (Table 3.1). This has been graphically illustrated in Fig. 3.8 (c). Table 3.2 summarizes the statistical parameters, i.e., coefficient of determination for calibration ( $R_c^2 = 0.93$ ), coefficient of determination of validation ( $R_v^2 = 0.02$ ), RMSEC for both PLSR and PCR regression models. Hence, barring the sole dissimilarity of lesser quantity of LVs required for PLSR (14 LVs), both PCR and PLSR models furnish similar prediction accuracies.

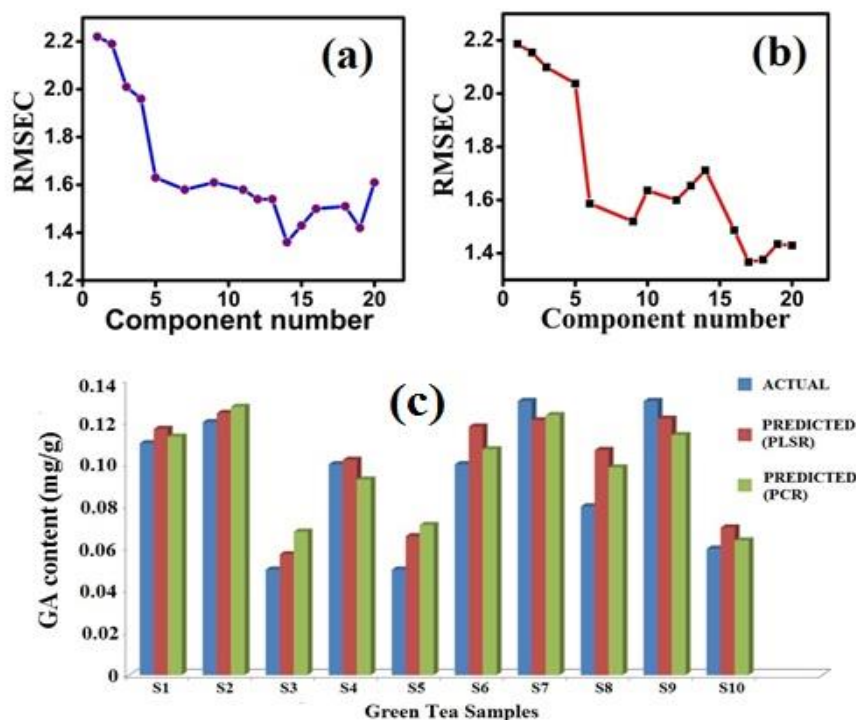


Fig. 3.9. RMSEC versus number of components (a) PLSR (b) PCR and (c) Plot depicting the actual and predicted contents of GA by employing both PLSR and PCR model.

### Chapter 3: Development of copper oxide nanoparticles embedded MIP electrode for tracing gallic acid in green tea

*Table 3.1. Actual and predicted GA content from PLSR and PCR models.*

S. No.	Actual GA (mg/g)	Predicted GA (mg/g)		Prediction accuracy (%)	
		PLSR	PCR	PLSR	PCR
1	0.11	0.116	0.113	94.54	97.27
2	0.12	0.124	0.127	96.66	94.16
3	0.05	0.057	0.068	86.00	80.00
4	0.1	0.102	0.092	98.00	92
5	0.05	0.065	0.071	80	60
6	0.1	0.11	0.107	90	93
7	0.13	0.12	0.123	92.30	94.16
8	0.08	0.10	0.098	75	77.5
9	0.13	0.121	0.113	93.84	87.6
10	0.06	0.07	0.062	83.33	96.66
<b>Average prediction accuracy</b>				<b>88.967</b>	<b>87.235</b>

*Table 3.2. Prediction of GA concentration in unknown tea samples.*

Method	LV	Calibration		Validation		Prediction	
		RMSEC	$R_c^2$	RMSEV	$R_v^2$	RMSEP	$R_p^2$
<b>PLSR</b>	<b>14</b>	1.35	0.93	0.021	0.84	0.023	<b>0.81</b>
<b>PCR</b>	17	1.38	0.82	0.022	0.77	0.024	0.74

#### 3.4.4. Validation and prediction using linear regression models

Prediction was performed using an unknown dataset of size [179×20] by employing both the developed PLSR and PCR models. The results are tabulated in Table 3.2. The prediction results showed that on using the PLSR model, the RMSEP was found to be 0.023 with the coefficient of determination for prediction ( $R_p^2$ ) as 0.816 with fourteen LVs. Likewise for PCR, the RMSEP was established to be 0.024 with  $R_p^2$  being 0.741 with seventeen LVs. The unknown dataset prediction results are in sync with the validation results, thereby suggesting that the PLSR model is the best option for analysing the GA content in any sample.

### 3.5. Comparative analysis

The deep insight into literature has revealed a number of studies in which detection of GA has been sought (Table 3.3). In this work, owing to the modification of the MIP sensor with CuO NPs, the detection limit has considerably improved in comparison to previous literatures [12,13,16,24-25,35]. Also, the synthesized MIP –

### Chapter 3: Development of copper oxide nanoparticles embedded MIP electrode for tracing gallic acid in green tea

CuO sensor exhibited two linear ranges unlike those reported by other authors. Though some of the literature report low LOD or sensitive detection, yet the precursors and the processes involved in the preparation of the material are either costly, scarcely available or time consuming [36-37]. Some studies aimed to detect GA using MIP technology; however, they have no detailed analysis of the analytical parameters, calculation of LOD or analysis of the linear range [6, 15]. In this work, the usage of excellently stable CuO NPs for the modification of the electrode contributed to an acceptable response in GT samples. The quantity of GA in tea samples roughly accounts to be 0.039- 6.7 mg/g; this is approximately 0.229  $\mu\text{M}$  – 39.38  $\mu\text{M}$ , noticeably higher than the LOD (12.6 nM) calculated. In essence, the p electrode can be deployed as an efficient, cost-effective and electrochemically stable electrode for GA detection in any industry.

*Table 3.3. Comparison of the present method with existing literature.*

Techniques and electrode material	Linear range ( $\mu\text{M}$ )	LOD (nM)	Refs
DPV using electrode modified with Zirconia-choline chloride-gold NPs.	0.22–55	25	[36]
DPV using modified carbon nanotubes electrode	0.5–15	300	[25]
CV and DPV Fe <sub>2</sub> O <sub>3</sub> /electro-reduced graphene oxide electrode	1 - 100	150	[9]
DPV using GA imprinted MIP sensor	0.12–380.0	47	[16]
CV and DPV using poly-(glutamic acid): graphene electrode	0.03–480	10	[28]
DPV using SiO <sub>2</sub> NPs modified electrode	0.8–100	250	[24]
<b>CV and DPV using MIP-CuO electrode</b>	<b>1-100 and 100-900</b>	<b>12.6</b>	<b>This work</b>

### 3.6. Conclusion

The present work elucidates a method for the economic development of a reproducible electrode for sensitive determination and prediction of the amount of GA in green tea by MIP technology. In the present work, the MIP material has been implanted with electrochemically active CuO NPs for effective detection of GA in green tea by the concept of molecular imprinting. The electrode material has been synthesized by co-polymerization of poly (itaconic acid) and EGDMA followed by

implantation of CuO NPs. The electrode demonstrated two wide linear ranges, i.e., 1  $\mu\text{M}$  – 100  $\mu\text{M}$  and 100  $\mu\text{M}$  to 900  $\mu\text{M}$  with a low detection limit of 12.6 nM. The sensory parameters attested to their reasonable stability, selectivity and repeatability. The practical applicability of the electrode has been validated by quantifying the amount of GA in green tea samples. PCA has been performed and a separability index (SI) of 31.27 has been calculated. To explore the predictive ability of the electrode, PLSR and PCR models have been developed. This has been done by correlating the DPV signals from the electrode and the corresponding HPLC data. While with PLSR, average prediction accuracy of 88.81 % is obtained with RMSEC as low as 1.36, PCR results in an average prediction accuracy of 87.38 % with RMSEC being 1.37. Therefore, this study focuses on the development of a selective sensor and also on the quantitative analytical ability of the electrode. In a nutshell, this work puts a progressive step forward towards practical usability of the electrode as sensing material for qualitative estimation of tea in industries.

## References

- [1] G. Galati, A. Lin, A. M. Sultan, P. J. O'Brien, "Cellular and in Vivo Hepatotoxicity caused by green tea phenolic acids and catechins", *Free Radic. Biol. Med.* 40 (2006) 570-80.
- [2] Y. Zuo, H. Chen, Y. Deng, "Simultaneous determination of catechins, caffeine and gallic acids in green, Oolong, black and pu-erh teas using HPLC with a photodiode array detector", *Talanta*. 57 (2002) 307–316.
- [3] B. Boye, E. Brillas, A. Buso, G. Farnia, C. Flox, M. Giomo, G. Sandona, "Electrochemical removal of gallic acid from aqueous solutions", *Electrochim. Acta*. 52 (2006) 256–262.
- [4] P. Carloni, L. Tiano, L. Padella, T. Bacchetti, C. Customu, A. Kay, E. Damiani, "Antioxidant activity of white, green and black tea obtained from the same tea cultivar", *Food Res. Int.* 53(2013) 900-908.
- [5] R.V. Lith, G. A. Ameer, "Antioxidant polymers as biomaterials", *Oxidative stress and biomaterials*, 10 (2016) 251-296.
- [6] L. Wang, M. S. Haquist, D. H. Sweet, "Simultaneous determination of gallic acid and gentisic acid in organic anion transporter expressing cells by liquid

- chromatography-tandem mass spectrometry”, *J. Chromatogr. B.* 937 (2013) 91-96.
- [7] A. Andreu-Navarro, J. M. Fernandez-Romero, A. Gomez-Hens, “Determination of antioxidant additives in foodstuffs by direct measurement of gold nanoparticle formation using resonance light scattering detection”, *Anal. Chim. Acta.*, 695 (2011) 11–17.
- [8] K. Dhalwal, V. M. Shinde, Y. S. Biradar, K. R. Mahadik, “Simultaneous quantification of bergenin, catechin and gallic acid from *Bergeniaciliata* and *Bergenialigulata* by using thin-layer chromatography”, *J. Food Compos. Anal.* 21 (2008) 496–500.
- [9] F. Gao, D. Zheng, H. Tanaka, F. Zhan, X. Yuan, F. Gao, Q. Wang, “An electrochemical sensor for gallic acid based on Fe<sub>2</sub>O<sub>3</sub>/electro-reduced graphene oxide composite: Estimation for the antioxidant capacity index of wines”, *Mater. Sci.* 57 (2015) 279–287.
- [10] H. G. Valery, A. Chtaini, B. Loura, “Voltammetric Sensor Based on Electrodes Modified by Poly(vinyl alcohol)-Natural Clay Film, for the Detection of Gallic Acid”, *Port. Electrochim.* 37 (2019) 327-333.
- [11] S. Sarafraz, H.-A. Rafiee-Pour, M. Khayatkashani, A. Ebrahimi, “Electrochemical Determination of Gallic Acid in *Camellia sinensis*(L.) Kuntze, *Viola odorata*L., *Commiphora wightii*(Arn.) Bhandari, and *Vitex agnus-castus*L. by MWCNTs-COOH Modified CPE”, *J Nanostruct.* 9 (2019) 384-395.
- [12] F. Gao, D. Zheng, H. Tanaka, F. Zhan, X. Yuan, F. Gao, Q. Wang, “An electrochemical sensor for gallic acid based on Fe<sub>2</sub>O<sub>3</sub>/electro-reduced graphene oxide composite: Estimation for the antioxidant capacity index of wines”, *Mater. Sci.* 57 (2015) 279–287.
- [13] M. Chen, H. Lv, X. Li, Z. Tian, X. Ma, “Determination of Gallic Acid in Tea by a Graphene Modified Glassy Carbon Electrode”, *Int. J. Electrochem. Sci.* 14 (2019) 4852 – 4860.
- [14] P.A. Kilmartin, H. Zou, A. L. Waterhouse, “A Cyclic Voltammetry Method Suitable for Characterizing Antioxidant Properties of Wine and Wine Phenolics”, *J. Agric. Food Chem.* 49 (2001) 1957-65.

- [15] P. Jara-Ulloa, P. Salgado-Figueroa, R. Moscoso, J. A. Squella, “Polypyrrole Molecularly Imprinted Modified Glassy Carbon Electrode for the Recognition of Gallic Acid”, *J. Electrochem.* 160 (2013) 243-246.
- [16] S. Shojaei, N. Nasirizadeh, M. Entezam, M. Koosha, M. Azimzadeh, “An Electrochemical Nanosensor Based on Molecularly Imprinted Polymer (MIP) for Detection of Gallic Acid in Fruit Juices”, *Food Anal. Methods.* 9 (2016) 2721 – 2731.
- [17] T.V. Nicolescu, A. Sarbu, S. O. Dima, C. Nicolae, D. Donescu, “Molecularly Imprinted “Bulk” Copolymers as Selective Sorbents for Gallic Acid”, *J. Appl. Polym. SCI.* 127 (2013) 366-374.
- [18] T. N. Chatterjee, D. Das, R. B. Roy, B. Tudu, S. Sabhapondit, P. Tamuly, P. Pramanik, R. Bandyopadhyay, “Molecular Imprinted Polymer Based Electrode for Sensing Catechin (+C) in Green Tea”, *IEEE Sens. J.* 18 (2018) 2236-2244.
- [19] D. Das, T. N. Chatterjee, R. B. Roy, B. Tudu, A. K. Hazarika, S. Sabhapondit, R. Bandyopadhyay, “Titanium Oxide Nanocubes Embedded Molecularly Imprinted Polymer Based Electrode for Selective Detection of Caffeine in Green Tea”, *IEEE Sens. J.* 20 (2019) 6240-6247.
- [20] M. Ghaedi, S. Y. Shajaripour Jaber, S. Hajati, M. Montazerzohori, A. Asfaram, B. Mirtamizdoust, M. Zare, “CuO Nanoparticles Intermixed With Chemically Modified Multiwalled Carbon Nanotubes as a Novel Electrode for Cu<sup>2+</sup> Ion Determination”, *IEEE Sens. J.* 15 (2015) 2882-2890.
- [21] S. Cherevko, C.H. Chung, “The porous CuO electrode fabricated by hydrogen bubble evolution and its application to highly sensitive non-enzymatic glucose detection”, *Talanta.* 80 (2010) 1371–1377.
- [22] R. Khan, R. Ahmad, P. Rai, L.W. Jang, J.-H. Yun, Y.T. Yu, Y.-B. Hahn, I.H. Lee, “Glucose-assisted synthesis of Cu<sub>2</sub>O shuriken like nanostructures and their application as nonenzymatic glucose biosensors”, *Sens. Actuators B Chem.* 203 (2014) 471–476.
- [23] B.B. Petkov, D. Stankov, M. Milc, S.P. Sovil, D. Manojlov, “Dinuclear copper(II) octaazamacrocyclic complex in a PVC coated GCE and graphite as a voltammetric sensor for determination of gallic acid and antioxidant capacity of wine samples”, *Talanta.* 132 (2015) 513–519.

- [24] J. Tashkhourian, S.F. Nami-Ana, “A sensitive electrochemical sensor for determination of gallic acid based on SiO<sub>2</sub> nanoparticle modified carbon paste electrode”, *Mater. Sci. Eng. C*, 52 (2015)103–110.
- [25] L.P. Souza, F. Calegari, A.J.G. Zarbin, L.H. Marcolino-Júnior, M.F. Bergamini, “Voltammetric determination of the antioxidant capacity in wine samples using a carbon nanotube modified electrode”, *J. Agric. Food Chem.* 59 (2011) 7620–7625.
- [26] ISO 14502-2:2005. “Determination of substances characteristic of green and black tea — Part 2: Content of catechins in green tea —Method using high-performance liquid chromatography”
- [27] B.D. Cullity, S.R. Stock, “Elements of X-ray diffraction”, Boston, MA, USA: Addison Wesley (2001).
- [28] J. J. Feminus, R. Manikandan, S. S. Narayanan and P. N Deepa, “Determination of gallic acid using poly(glutamic acid): graphene modified electrode”, *J. Chem. Sci.* 131 (2019) 1-10.
- [29] M. Palit, B. Tudu, K. P. Dutta, A. Dutta, J. Jana, K. Roy, N. Bhattacharyya, R. Bandyopadhyay, A. Chatterjee, “Classification of black tea taste and correlation with tea taster's mark using voltammetric electronic tongue”, *IEEE Trans. Instrum. Meas.* 59 (2010) 2230-2239.
- [30] P. Beatriz Garcia-Allende, Olga M. Conde, Jesus Mirapeix, Ana M. Cubillas, and Jose M. Lopez-Higuera, “Data Processing Method Applying Principal Component Analysis and Spectral Angle Mapper for Imaging Spectroscopic Sensors”, *IEEE Sens. J.* 8 (2008) 1310-1316.
- [31] F. Harrou, Y. Sun , M. Madakyaru, and B. Bouyedou, “An Improved Multivariate Chart Using Partial Least Squares With Continuous Ranked Probability Score”, *IEEE Sens. J.* 18 (2018) 6715-6726.
- [32] S. Wold, M. Sjostrom, and L. Eriksson, “PLS-regression: a basic tool of chemometrics”, *Chemom. Intell. Lab. Syst.* 58 (2001) 109–130.
- [33] S. Kar, B. Tudu, A. K. Bag, R. Bandyopadhyay, “Application of Near-Infrared Spectroscopy for the Detection of Metanil Yellow in Turmeric Powder”, *Food Anal. Methods.* 11 (2018) 1291–1302.

- [34] U. Depczynski, V. J. Frost, K. Molt, “Genetic algorithms applied to the selection of factors in principal component regression”, *Anal. Chim. Acta.* 420 (2000) 217–227.
- [35] X. Hu, L.W. Xie, J. F. Guo, H. Li, X.Y. Jiang, Y. P. Zhang, S. Y. Shi, “Hydrophilic gallic acid-imprinted polymers over magnetic mesoporous silica microspheres with excellent molecular recognition ability in aqueous fruit juices”, *Food Chem.* 179 (2015) 206– 212.
- [36] S. A. Shahamirifard, M. Ghaedi, Z. Razmi, S. Hajati, “A simple ultrasensitive electrochemical sensor for simultaneous determination of gallic acid and uric acid in human urine and fruit juices based on zirconia-choline chloride-gold nanoparticles-modified carbon paste electrode”, *Biosens. Bioelectron.* 114 (2018) 30-36.
- [37] A. Pasahan, N. Ayhan, I. Ozcan, S. Titretir Duran, S. Koytepe, “Development of gallic acid sensors based on polyimide-modified platinum electrode”, *Polym-plast Technol.* 58 (2019) 1125-1139.



# Chapter 4

## Development of MIP electrode for tracing epicatechin in green tea

This chapter proposes an MIP based sensor for estimation of epicatechin in tea. In this work, the detection of epicatechin has been done using two different techniques. In the first case, epicatechin molecule has been used as the template and in the second case, dummy template, i.e., quercetin, has been used for the synthesis of the MIP materials. The detection of epicatechin using the dummy template appeared to be an economical solution towards the quality of tea. The comparative study with other research reports of epicatechin determination has been presented in this chapter.

### List of sections

- Introduction
- Detection of EC using EC as the target molecule
- Preparation of the electrodes
- Analysis with real samples
- Detection of EC using Q as the target molecule
- Preparation of the electrodes
- Analysis with real samples
- Comparison of the proposed technique with the reported methods
- Conclusion

### Contents of this chapter are based on following publication:

- ✓ **Debangana Das**, Shreya Nag, A. Adaval, A. K. Hazarika, S. Sabhapondit, A. R. Bhattacharyya, B. Tudu, R. Bandyopadhyay, R.B. Roy, "Amine Functionalized MWCNTs Modified MIP-Based Electrode for Detection of Epicatechin in Tea, *IEEE Sensors Journal*, vol. 22, no. 11, pp. 10323-10330, 2022, doi: 10.1109/JSEN.2022.3169169.
- ✓ **Debangana Das**, Shreya Nag, Shubham De, Ajanto Kumar Hazarika, Santanu Sabhapondit, Bipan Tudu, Rajib Bandyopadhyay, Panchanan Pramanik, Runu Banerjee Roy "Electrochemical Detection of Epicatechin in Green Tea Using Quercetin-Imprinted Polymer Graphite Electrode," in *IEEE Sensors Journal*, vol. 21, no. 23, pp. 26526-26533, 2021, doi: 10.1109/JSEN.2021.3122145.



## Chapter 4

### Development of MIP electrode for tracing epicatechin in green tea

#### 4.1. Introduction

The most pertinent flavonoids in green tea are the catechins [1-2]. Amongst them, EC is an important bioactive compound [2], naturally-occurring and one of the major flavonoids with strong antioxidant properties which contribute towards the quality of green tea [3]. The chemical structure of EC ( $C_{15}H_{14}O_6$ ) as shown in Fig. 4.1 (a) has two benzene rings (with resorcinol group in ring A and catechol group in ring B) and consists of dihydro-pyranheterocycle (the C-ring) along with a hydroxyl group on C-3. EC has two chiral centers on the C-2 and C-3 carbons and is an optically active molecule. EC being optically active appears to be a bit unstable and the cost of EC is high. Hence, on quest of better stability and low-cost, the study on detection of EC using quercetin (Q) (Fig 4.1 (b)) as the dummy template was investigated.

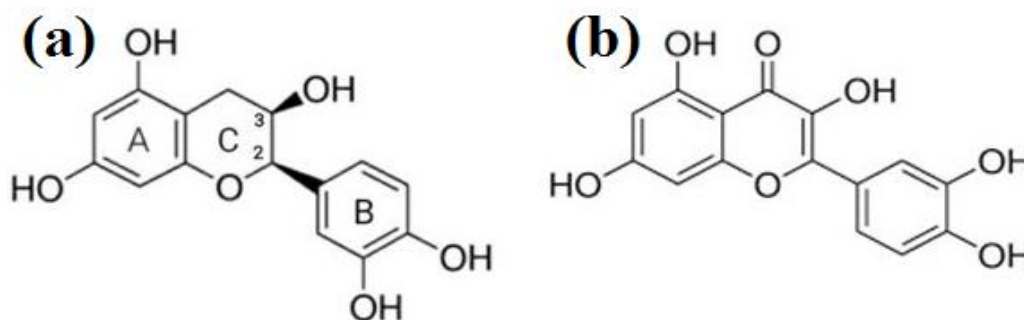


Fig. 4.1. Chemical structure of (a) EC (b) Q.

The chemical structure of EC is shown in Fig. 4.1 and it possesses resorcinol group in ring A and catechol group in ring B. As already mentioned in Chapter 1, for precise determination of EC, instrumental methods such as thin layer chromatography [4], infrared (IR) spectroscopy & Raman spectroscopy [5], NMR [6], HPLC [7], and electrophoresis [8] are being used. Electrochemical detection is a cost-effective, simple and less time-consuming process. In [9], on application of adsorptive stripping voltammetry, the detection of EC using poly (3, 4-ethylenedioxythiophene)-modified

Pt electrodes was studied. The process of EC oxidation on a GCE was also examined using both CV and square-wave voltammetry [10]. In [11], polyimide membrane-based electrodes were also developed for EC determination. However, the experimental results so obtained in [9-11] urged the researchers to adopt a better technique for development of the electrodes which could enhance the analytical parameters of the electrodes. Therefore, MIP technology has been adopted to improve upon the properties of selectivity, repeatability and reproducibility. To the best of our survey, no literature based on the development of voltammetric sensors using MIP technology for the detection of EC was reported in literature.

The first study in the present chapter puts forward the development of an MWCNTs modified MIP electrode, which is duly reproducible and selective for the sensitive determination of EC in green tea samples using the EC template for detection of EC. However, one of the major draw-back of the direct template imprinting is the unavoidable template leaking, which tends to influence the accuracy of determination and quantification of the analytes [12]. Template leaking leads to false positive results. A method to avoid template leaking is the use of a dummy template or structural isomer of target analyte [13].

This technique of imprinting a structurally similar molecule provides practical benefits as well as the ability to recognize the target compound and other structurally related molecules [14-16]. As mentioned, the second work in this chapter deals with the development of EC electrode using Q as the target molecule. To the best of our knowledge, there is no developed method concerning the template leaking of MISPE during the analysis of RAC residue [17]. The structure of the dummy molecule and its functional groups must be similar to the target analyte, and must not interfere in the test. To date, a dummy molecularly imprinted polymer has not been used for detection of EC. This method is promising as a rapid, simple, inexpensive, environmentally friendly, and highly selective method for detection of EC and has been investigated [18].

### **Procedure I:**

#### **4.2. Detection of EC using EC as the target molecule**

The current study focuses on the development of a highly stable and selective electrode for the proper detection and measurement of EC in green tea samples. BP,

the polymerization initiator enabled the matrix synthesis by co-polymerizing acrylamide (AAm) and ethylene glycol di methacrylate (EGDMA). Further, the modification of the MIP-EC electrode through incorporation of amine functionalized multi-walled carbon nanotubes (f-MWCNTs) enabled the increase in electrical conductivity and adsorption properties. f-MWCNTs are highly porous with large surface area, higher electrical conductivity and excellent chemical and thermal stability [9]. Further, f-MWCNTs are highly promising adsorbents as they exhibit superb adsorption properties [10]. The presence of carboxylic (-COOH), hydroxyl (-OH) and amine (-NH<sub>2</sub>) groups enhance the adsorption capacity of f-MWCNTs as these groups are responsible for initiating various interactions. Consequently, this work has been performed using the EC template for the preparation of MIP material. Also, for comparison purpose, the non-imprinted (NIP) polymer material was prepared where no template molecule was present. The novelty of the applied technology can be attested to its low detection limit thus enabling the detection of EC in green tea samples. Furthermore, the electrode can be fabricated relatively easily, which is another benefit of the current MIP preparation process. The large number of imprinted EC sites make the synthesized electrode fairly repeatable, highly reproducible, stable and widely compatible in various applications. In conjunction, the MIP-EC electrode has higher surface/volume ratio owing to the modification with f-MWCNTs, which further improves upon the number of imprinted sites vacant for binding. Pre-treatment of samples is redundant before electrochemical experiments as a consequence of which, the electrode may be submerged directly in the infusion. This makes the adoption of this technology a considerable benefit for industrial applications. The PLSR and PCR models were used to investigate the modified MIP-EC electrode's capacity to predict EC. After calibrating the regression models, they were utilized to calculate the EC concentration in unknown tea samples.

### 4.2.1. Chemicals and reagents

Sigma Aldrich (India) provided EGDMA, EC, acrylamide (AAm), CAT, EGCG, AA, and commercial graphite powder (99% pure). Amine (-NH<sub>2</sub>) functionalized MWCNTs (hereafter, referred as f-MWCNTs; NC-3152, purity of 95% and degree of NH<sub>2</sub> functionalization of <0.5%, diameter of ~9.5 nm and length of <1 μm, as per manufacturer specifications) were procured from Nanocyl S.A., Belgium. Sisco Research Laboratories Pvt. Ltd. (India) provided the benzoyl peroxide.

Millipore water (18 M $\Omega$ ) was used to rinse the electrodes. The electrochemical experiments were performed at ambient temperature (25 $\pm$ 2 °C).

### 4.2.2. Methods and measurement

FTIR spectroscopic analysis of the powder samples was carried out at room temperature using a Bruker 3000 Hyperion microscope with Vertex 80 FTIR at the resolution of 0.2 cm<sup>-1</sup> in the scanning range of 400 – 4000 cm<sup>-1</sup>. Transmission electron microscopy (TEM) was carried out with various powders using a Themis 300 G3 (Thermo Scientific) transmission electron microscope operating at 300 kV. Selected area electron diffraction (SAED) patterns were also recorded to witness the crystalline nature of the polymer and also the f-MWCNTs. The powders were thoroughly dispersed in ethanol via bath ultra-sonication for 2 h and were then deposited on lacy grids for analysis. A drop of the f-MWCNTs dispersion was casted on a glass slide and observed under a polarized optical microscope (Leica 2700LP, Germany). Powder samples were observed via scanning electron microscopic analysis FEG-SEM (JSM-7600F, JEOL, Japan). The samples were gold sputtered to avoid charging during measurements. Raman analysis for f-MWCNTs was carried out using a HR 800 micro Raman (Jobin Yvon, Israel) with a power of 10 MW and the scanning range of 600 to 3000 cm<sup>-1</sup>. The incident laser light of 514 nm was used. The electrochemical measurements were made with the use of a three-electrode setup using the Autolab Potentiostat/ Galvanostat 101 (Netherlands). A platinum electrode and an Ag/AgCl electrode were utilized as the counter electrode and reference electrode, respectively. The electrochemical measurements were recorded by cyclic voltammetry (CV) and differential pulse voltammetry (DPV) techniques within 0 - 1.2 V and 0 - 1.4 V applied potential window, respectively.

### 4.2.3. Synthesis of multi-walled carbon nanotubes

Approximately, 0.20 gm of f-MWCNTs were dispersed in 125 ml of tetrahydrofuran (THF) via ultra-sonication (in bath sonicator, Vibronics, frequency = 20 kHz) for 2 h and then centrifuged for 2 h. The resultant dispersion was dried on a hot plate and subsequently in vacuum over at 80 °C for 24 h.

### 4.2.4. Preparation of the molecularly imprinted polymer material

0.90 g of commercial fine graphite powder was sonicated for 1 h in 15 ml of ethanol. The monomer (AAm) and template molecule (EC) in a ratio of 1:1

(wt/wt) were added to the homogenized dispersion of graphite. After 2 h of stirring, 400  $\mu\text{L}$  of EGDMA and 1 mg of benzoyl peroxide (polymerization initiator) were introduced. The polymerization was carried out in a water bath at 30  $^{\circ}\text{C}$ . The EC molecule was extracted from the polymerized sample using an 80:20 mixture of ethanol and water to prepare the MIP after the sample was collected and dried. The resultant MIP sample was dried and preserved. Except for the inclusion of EC, the NIP material was synthesized in a similar way.

### 4.2.5. Preparation of the electrodes

The MIP and NIP samples were prepared in a similar way as mentioned in Section 2.5 using amine functionalised MWCNTs as the modifier. The MIP and NIP synthesized materials were embedded with f-MWCNTs in a 3:1 ratio. 0.2 g of the individual powders was mixed and a smooth paste was achieved with a calculated quantity of paraffin oil. After that, a capillary glass tube was filled with the paste with copper wire connected as an electrical conductor.

### 4.2.6. Results and discussions

#### 4.2.6.1. Morphological characterizations of MIP-EC material

##### A. Optical microscopy, Raman spectroscopy and TEM of the prepared MWCNTs

The optical microscopic image of the dispersion of f-MWCNTs in THF after centrifugation has been shown in Fig. 4.2(a). It is observed that f-MWCNTs are predominantly dispersed homogeneously. However, f-MWCNTs ‘agglomerates’ of average ‘agglomerate’ size of  $\sim 10 \mu\text{m}$  are also observed. Moreover, coiled and entangled ‘individualized’ f-MWCNTs of average diameter of  $\sim 10 \text{ nm}$  and length of  $\sim 1 \mu\text{m}$  are observed from TEM observation (Fig. 4.2(b)), which are homogeneously dispersed. Selected area electron diffraction (SAED) pattern of the f-MWCNTs exhibits circular ‘ring’ pattern indicating the polycrystalline nature of f-MWCNTs (Fig. 4.2(c)). Further, a dense network of coiled and entangled f-MWCNTs is observed via FEG-SEM observations (Fig. 4.2 (d) and Fig. 4.2 (e)). Raman spectroscopic analysis depicts the presence of D-band at  $\sim 1342 \text{ cm}^{-1}$ , G-band at  $\sim 1578 \text{ cm}^{-1}$  and 2D band at  $\sim 2673 \text{ cm}^{-1}$ . The corresponding  $I_{\text{D}}/I_{\text{G}}$  (intensity of D-band over G-band) value is observed to be 1.06, which is higher as compared to the corresponding purified and unfunctionalized MWCNTs (NC-3100) [19]. This

suggests that amine functionalization leads to defects in the ordered graphitic structure in f-MWCNTs. Raman spectroscopic analysis is important to understand the crystalline nature of f-MWCNTs. MWCNTs show characteristic Raman shifts at  $\sim 1342\text{ cm}^{-1}$  and  $\sim 1578\text{ cm}^{-1}$  in the tangential mode Raman spectrum (Fig. 4.2(f)), which are assigned to D-band and G-band respectively. The origin of D-band is due to the disorder induced phonon mode and G-band is assigned to vibration of  $\text{sp}^2$ -bonded carbon atoms in a two dimensional hexagonal lattice, which indicates ordered graphitic structure.

### B. SEM and TEM of the prepared MIP materials

FEG-SEM images of MIP and NIP samples are shown in Fig. 4.3. Sample 1 exhibits smooth surfaces corresponding to ‘flake-like’ structure of MIP (Fig. 4.3(a)). Sample 2 depicts porous nature of the ‘flake-like’ structure of MIP after the removal of EC (Fig. 4.3(b)). Fig. 4.3(c) shows network of f-MWCNTs, which are embedded with MIP in Sample 3. On the contrary, a higher ‘flake-like’ structure is observed in Sample 4 corresponding to NIP as compared to MIP (Fig. 4.3 (d)). Sample 5 indicates highly dense f-MWCNTs network, which are embedded with NIP (Fig.4.3 (e), Fig. 4.3 (f)). In order to have a deeper analysis on the morphological characteristics of the five samples, TEM investigation has been carried out and the TEM images along with their corresponding SAED patterns are shown in Fig. 4.4. It is observed that ‘Sample 1’ exhibits ‘flake-like’ structure of MIP (Fig. 4.4 (a) and Fig. 4.4 (b)), which is poly-crystalline in nature. The ‘ring pattern’ in the SAED pattern suggests poly-crystalline structure associated with one of the crystalline substances used during MIP preparation (Fig. 4.4 (c)).

As can be seen from Fig. 4.4 (d) and Fig. 4.4 (e), ‘Sample 2’ also exhibits ‘flake-like’ structure of MIP, which indicates ‘spot pattern’ in the SAED diffraction pattern suggesting ‘single-crystal’ structure associated with one of the crystalline substances used during MIP preparation (Fig. 4.4 (f)). On the other hand, ‘Sample 3’ indicates ‘flake-like’ structure of MIP along with coiled and entangled structure associated with f-MWCNTs (Fig. 4.4 (g)). Higher magnification TEM image of ‘Sample 3’ also suggests f-MWCNTs are embedded in MIP (Fig. 4.4 (h)). The corresponding SAED pattern exhibits a superposition of ‘spot pattern’ associated with MIP and ‘ring pattern’ corresponding to f-MWCNTs (Fig. 4.4 (i)). ‘Flake-like’ structures of NIP are observed in ‘Sample 4’ (Fig. 4.4(j), Fig. 4.4(k)), which shows



predominantly 'spot pattern', wherein the flakes are distributed in different orientations (Fig. 4.4 (l)). 'Sample 5' depicts 'flake-like' structures corresponding to NIP and coiled and entangled structure associated with f-MWCNTs in low magnification TEM image (Fig. 4.4 (m)). f-MWCNTs are observed to be embedded with the 'flake-like' structure of NIP in higher magnification TEM image (Fig. 4.4 (n)). The corresponding SAED pattern of 'Sample 5' shows predominantly 'ring-like' pattern (Fig. 4.4(o)), which suggests that SAED pattern is dominated by f-MWCNTs as they are embedded in the NIP.

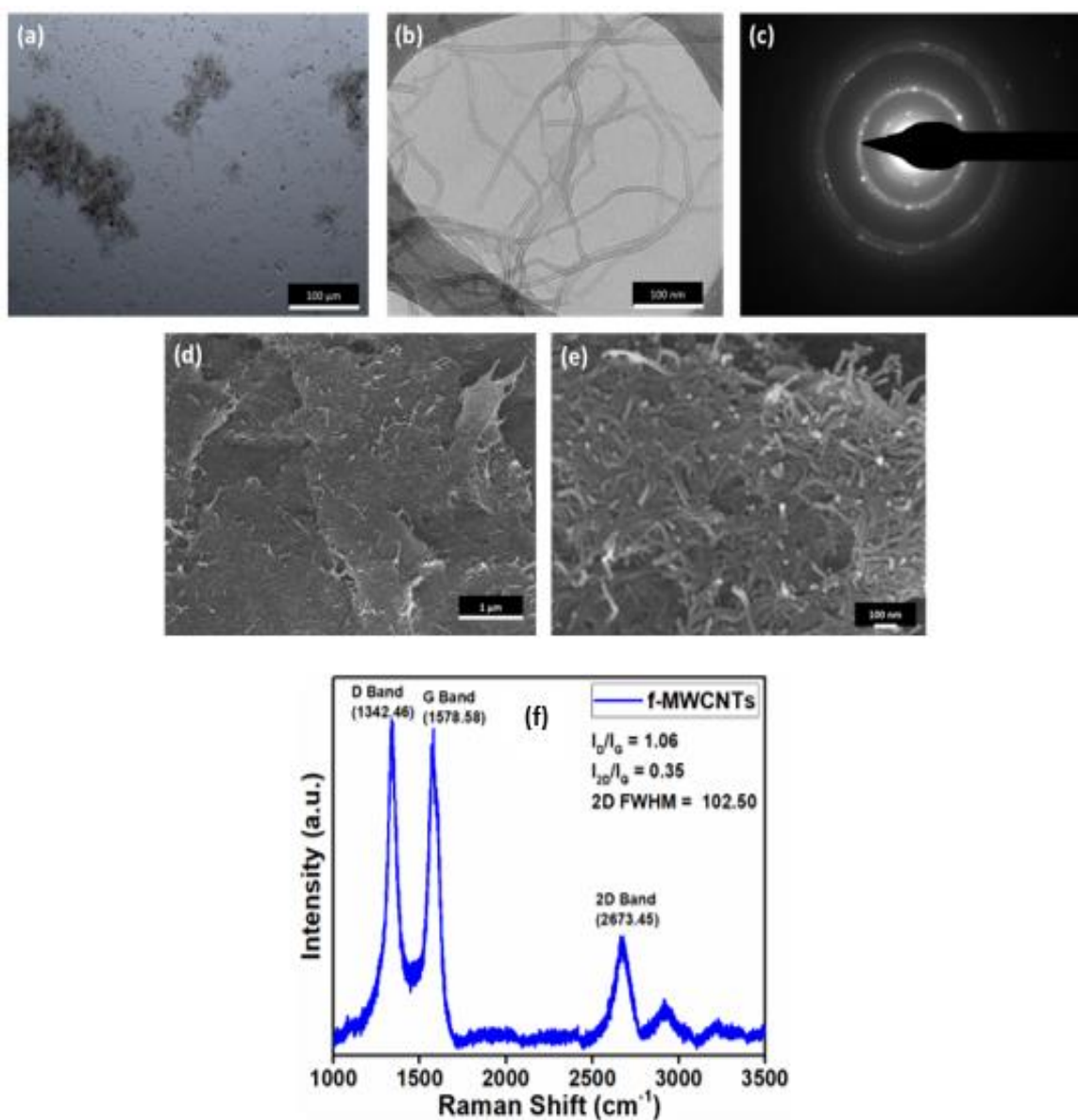
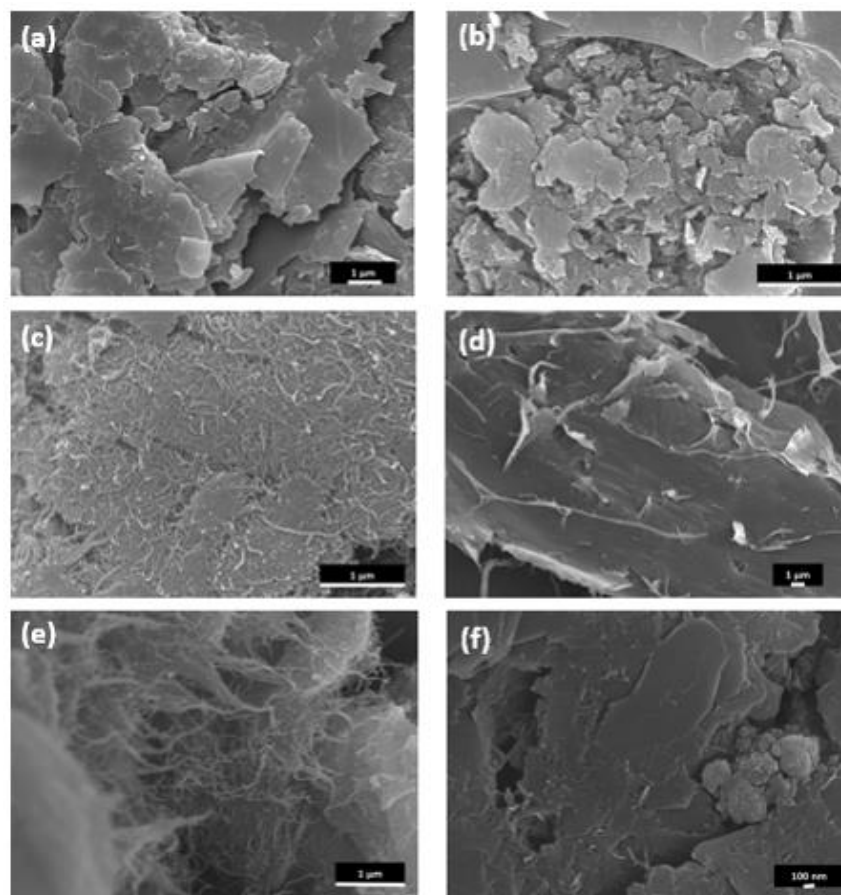


Fig. 4.2. Morphological characterizations of *f*-MWCNTs: (a) optical microscopic image (scale bar = 100  $\mu\text{m}$ ) showing homogeneously dispersed along with 'agglomerates' of *f*-MWCNTs, (b) TEM image (scale bar = 100 nm) of coiled and entangled 'individualized' *f*-MWCNTs, (c) the corresponding SAED 'ring pattern' associated with *f*-MWCNTs, (d,e) FEG-SEM images of highly dense *f*-MWCNTs network and (f) intensity versus Raman shift of *f*-MWCNTs.



*Fig. 4.3. FEG-SEM images of (a) MIP before wash (Sample 1), (b) MIP after wash (Sample 2), (c) MIP modified with f-MWCNTs (Sample 3), (d) NIP (Sample 4), (e) and (f) NIP modified with f-MWCNTs (Sample 5).*

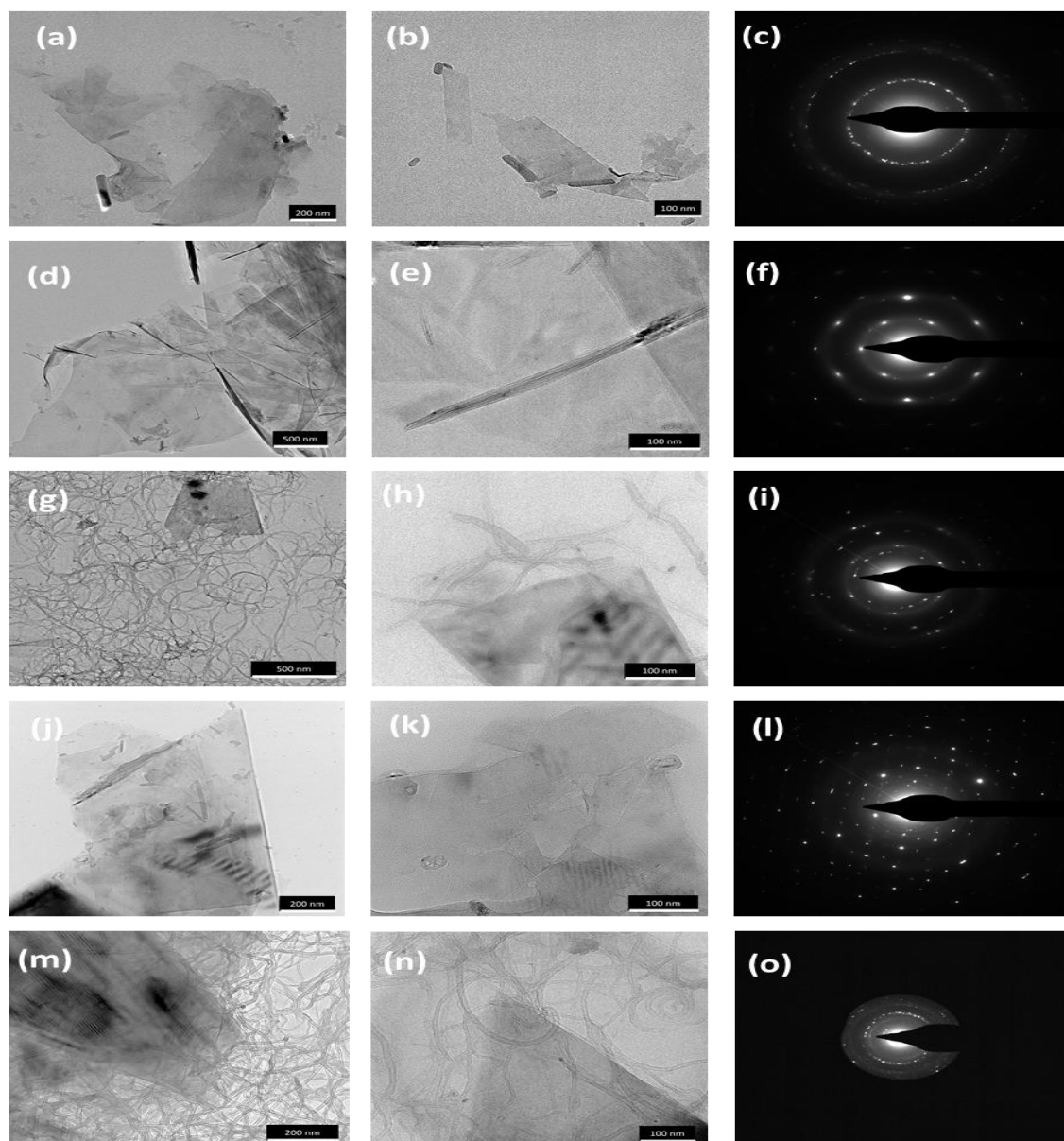


Fig. 4.4. TEM images and the corresponding SAED patterns of Sample 1: MIP before wash (a, b, c), Sample 2: MIP after wash (d, e, f), Sample 3: MIP modified with *f*-MWCNTs (g, h, i), Sample 4: NIP (j, k, l), and Sample 5: NIP modified with *f*-MWCNTs (m, n, o).

### C. FTIR analysis

FTIR spectra of the various samples of different compositions have been shown in Fig. 4.5. FTIR spectrum of ‘Sample 1’ shows strong signature corresponding to AAm, EGDMA and EC. AAm shows strong absorption bands at  $\sim 1637\text{ cm}^{-1}$  and  $3434\text{ cm}^{-1}$  corresponding to  $>\text{C}=\text{O}$  and  $-\text{CONH}$  stretching vibrations respectively in ‘Sample 1’. EGDMA exhibits strong absorption peaks at  $\sim 1723\text{ cm}^{-1}$  and  $1637\text{ cm}^{-1}$  corresponding to  $>\text{C}=\text{O}$  stretching vibrations in ‘Sample 1’.

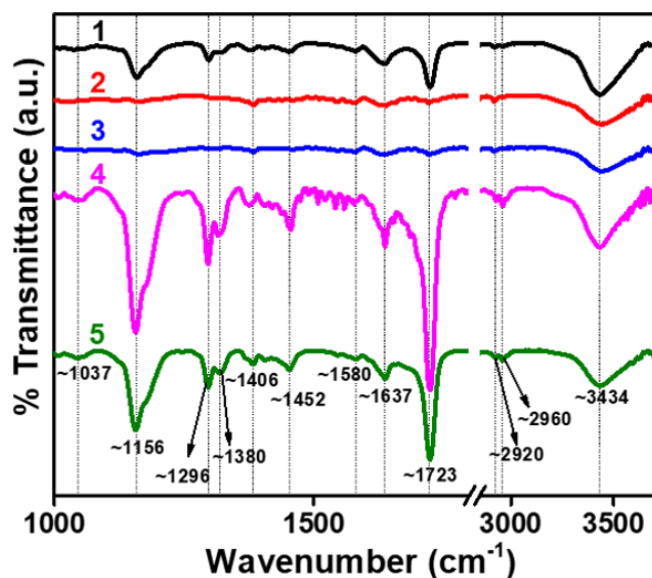


Fig. 4.5. FTIR spectra of MIP before wash (Sample 1), MIP after wash (Sample 2), MIP modified with MWCNTs (Sample 3), NIP (Sample 4), and NIP modified with MWCNTs (Sample 5).

Further, the stretching vibrations observed at  $\sim 1580\text{ cm}^{-1}$ ,  $\sim 1278\text{ cm}^{-1}$ , and  $\sim 1156\text{ cm}^{-1}$  are due to breathing mode vibrations of the three rings in the EC structure in 'Sample 1'. It is observed that FTIR spectrum of 'Sample 2' does not show any absorption bands corresponding to EC. However, the presence of absorption bands corresponding to AAm and EGDMA are observed, which suggests that 'Sample 2' does not contain any EC. Therefore, the complete removal of EC from the template may be justified from this observation. The presence of different absorption bands corresponding to AAm, EGDMA and EC molecules are observed in 'Sample 3', wherein an overall lower intensity corresponding to various stretching vibrations due to presence of f-MWCNTs is observed. The presence of amine group in f-MWCNTs can be detected from the absorption band corresponding to  $\sim 3158\text{ cm}^{-1}$ , which is shifted to  $\sim 3434\text{ cm}^{-1}$ . FTIR spectrum of 'Sample 4' shows strong absorption bands corresponding to AAm and EGDMA, which are corresponding to NIP. Similar intense absorption bands can be observed in 'Sample 5', which contains AAm, EGDMA and f-MWCNTs. However, the FTIR spectrum between 'Sample 4' and 'Sample 5' is hard to differentiate as AAm shows an intense absorption band at  $3434\text{ cm}^{-1}$  corresponding to  $-\text{CONH}$  stretching vibrations, which is overlapping with the absorption band corresponding to  $-\text{NH}_2$  functional groups in f-MWCNTs.

#### 4.2.6.2. Influence of buffer and pH

The modified MIP-EC electrode performance has been evaluated by using various buffer compositions at pH 5, viz., citrate buffer saline (CBS), acetate buffer saline (ABS), and phosphate buffer saline (PBS), respectively. Fig. 4.6(a) depicts the maximum peak current due to oxidation (36.04  $\mu\text{A}$ ) for PBS buffer in the presence of 1mM EC. The influence of PBS buffer pH variation on the modified MIP-EC electrode was affirmed using CV tests at pH 5, 6, 7, respectively. The PBS 5 was considered the optimized buffer throughout the experiment as it delivered the maximum peak current as shown in Fig. 4.6 (b). The CV responses of the MIP- EC modified with f-MWCNTs, MIP-EC, and NIP electrodes in 1 mM EC were investigated. The MIP-EC modified with f-MWCNTs electrode portrays a markable rise in peak current when compared to the unmodified MIP-EC electrode (15.20  $\mu\text{A}$ ) as represented in Fig.4.6(c). This phenomenon can be demonstrated due to the presence of f-MWCNTs, which might have triggered faster electron kinetics. It can be inferred from Fig. 4.6(c) that the NIP electrode has responded with comparatively lower peak current than that of the MIP-EC electrode. The absence of EC cavities and a lesser number of active sites at the NIP electrode attributed to this behaviour.

#### 4.2.6.3. Influence of scan rate

The electrochemical response of the modified MIP-EC electrode was obtained by subjecting it to the EC solution of 1 mM at scan rates varying from 0.005 to 0.3  $\text{Vs}^{-1}$  shown in Fig. 4.7(a). This certain range of scan rate has established a linear oxidation peak current versus scan rate profile with  $R^2 = 0.98$  (Fig.4.7 (b)). The linearity between the oxidation peak current and scan rate validates a surface controlled process [20]. A positive peak potential ( $E_p$ ) shift was evident during the study of the modified MIP-EC electrode adsorption kinetics with a linear rise along with  $\log v$  (Fig. 4.7(c)). Evaluation of the EC analyte surface concentration ( $\Gamma_c$ ) and the number of electrons ( $n$ ) transferred was performed using the Eq. (2.2). The value of  $n$  and  $\Gamma_c$  computed from Eq. (1) is 1.86 (approximately equals 2) and  $2.736 \times 10^{-3}$  mole  $\text{cm}^{-2}$ , respectively.



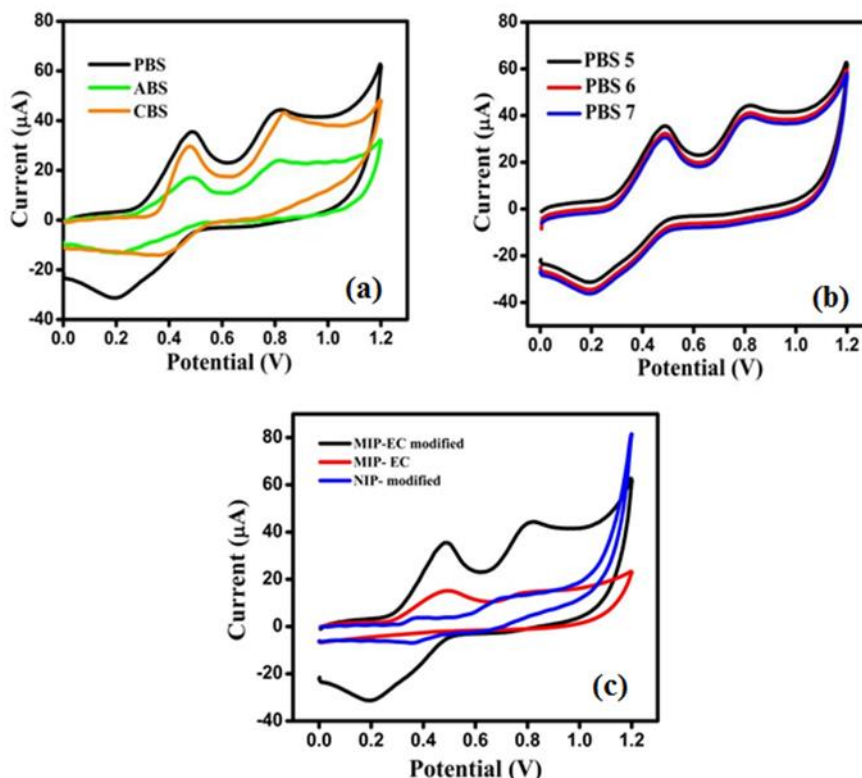


Fig. 4.6. Voltammograms obtained for 1 mM EC (a) in citrate, acetate and phosphate buffer solutions (c) with PBS of pH values 5, 6 and 7 (c) with MIP-EC modified, MIP-EC and NIP-modified electrode.

The  $n$  and  $\Gamma_c$  values so obtained designates that the MIP-EC electrode holds remarkable adsorption capability to the EC molecules. The linear regression equation (2) obtained with  $R^2 = 0.98$  is given as

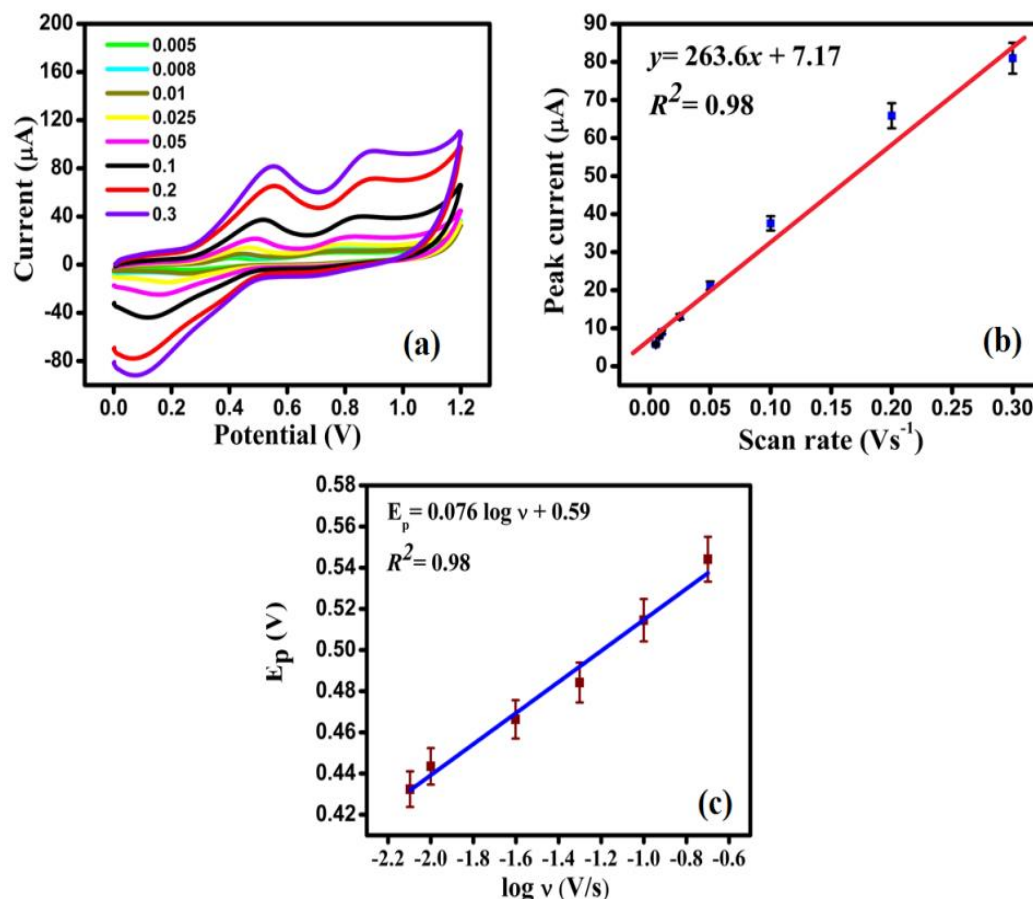
$$E_p = 0.07 \log v + 0.59 \quad (4.1)$$

The value of the electron transfer coefficient ( $\alpha$ ) was determined as 0.58 from the calibration curve slope of Eq. (4.1).

#### 4.2.6.4. Concentration variation and linearity

DPV measurements with the modified MIP-EC electrode were used to track the current profile as the concentration of EC in the analyte increased. The voltage window for the DPV experiment was set to 0 - 1.4 V, and the experimental parameters, such as step potential, scan rate, modulation time, modulation amplitude, and interval time, were set to 0.005 V, 0.08 Vs<sup>-1</sup>, 0.02 s, 0.04 V, and 0.0625 s, respectively.

In Fig. 4.8 (a), a notable increase in current was observed with increasing concentration of EC. The calibration curve for EC (Fig. 4.8 (b)) indicates two linear segments: one from 1  $\mu\text{M}$  to 30  $\mu\text{M}$ , with the regression equation  $y = 0.79x +$



4.54 having  $R^2 = 0.93$ ; the second linear segment is between 30  $\mu\text{M}$  and 300  $\mu\text{M}$ , with the regression equation  $y = 0.09x + 26.65$  having  $R^2 = 0.93$ . Based on 3  $\text{Sy}/x/m$  [21] and 10  $\text{Sy}/x/m$  [22], the LOD and LOQ of the MIP- EC electrode was determined to be 51.92 nM and 0.17  $\mu\text{M}$ .

Fig. 4.7. (a) CV obtained by varying scan rates (0.005 - 0.3 $\text{Vs}^{-1}$ ) (b) deviation of peak current with scan rate (c)plot of Oxidation potential ( $E_p$ ) versus logarithm of scan rate ( $\log v$ ).



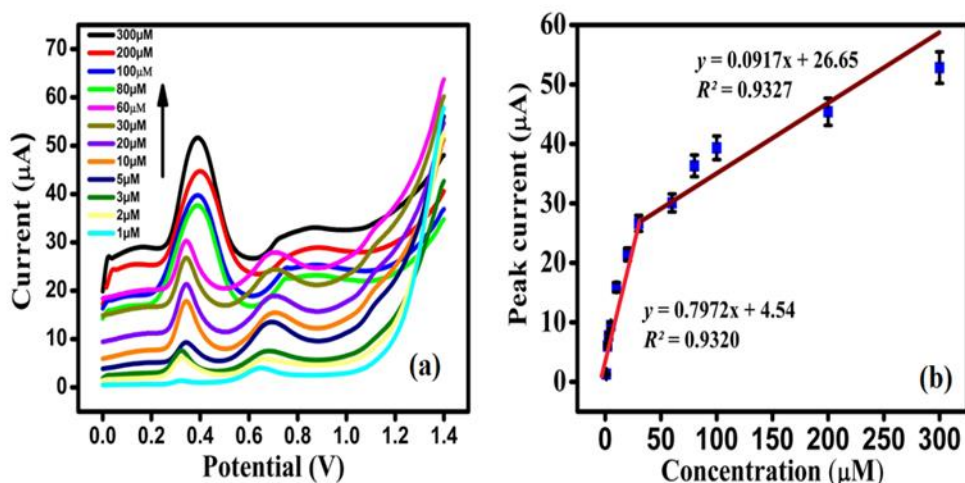


Fig. 4.8. (a) Voltammograms at the MIP-EC electrode surface with different EC concentrations in PBS 5 (b) Deviation of peak current with EC concentration.

#### 4.2.6.5. Sensory parameters of the MIP-EC electrode

To investigate selectivity, the modified MIP-EC electrode has been exposed to 1mM of EC, CAT and EGCG respectively.

It can be observed from Fig. 4.9 (a) that the electrode demonstrated a very poor response in CAT solution and almost a blunt response when in EGCG solution. A peak current of 35.40  $\mu\text{A}$  has been obtained for the case when the modified MIP-EC electrode was exposed to EC solution unlike the case of CAT where a peak current of 18.51  $\mu\text{A}$  has been obtained. Hence, it can be concluded that though EC and CAT are optical isomers, MIP technology integrated electrochemical sensors are capable to distinguish between the two, thereby, attesting to the high selectivity of the modified MIP-EC electrode. Repeatability studies were conducted and it has been found that the modified MIP-EC sensor shows good repeatability with %RSD of 4.06 (Fig. 4.9 (b)). The modified MIP-EC electrode CV performances were recorded to examine the reproducibility (Fig. 4.9 (c)) using four parallel electrodes. Adequate reproducibility was obtained with relative standard deviation (% RSD) of 4.30. For analyzing the stability of the modified MIP-EC electrode, in 1mM EC, DPV measurements were done at an interval of 15 days for almost 90 days. The peak current of the modified MIP-EC electrode reduced by 0.39% after next 15 days (Fig.4.9(d)) and 5.38 % after a span of 90 days.

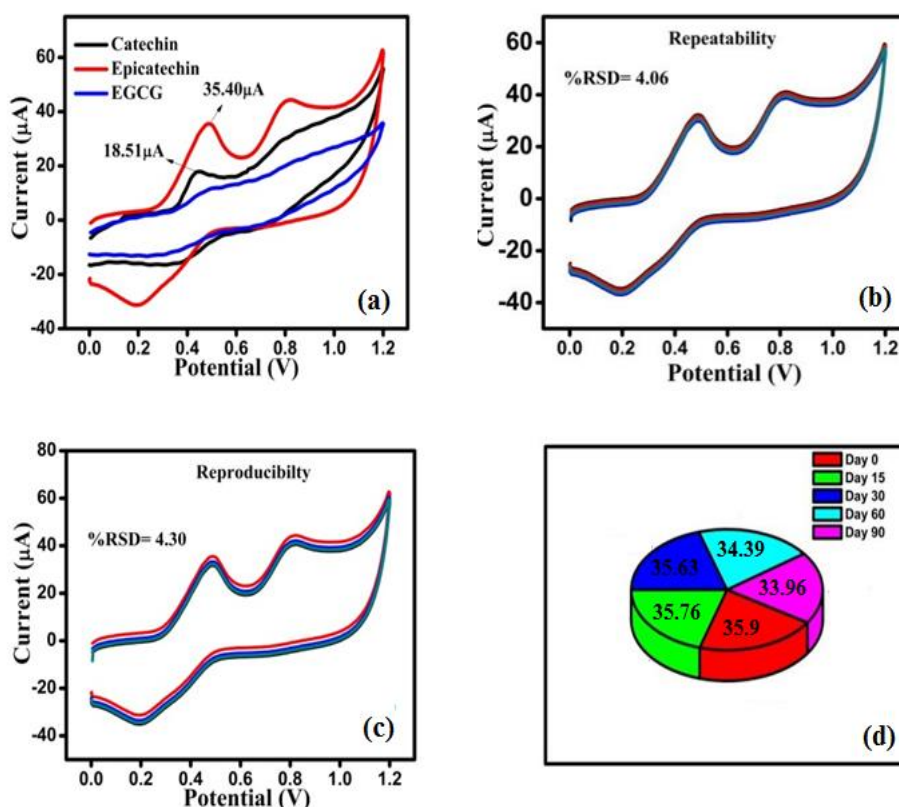


Fig. 4.9. MIP-EC electrode showing (a) selectivity, (b) repeatability, (c) reproducibility and (d) stability.

#### 4.2.7. Analysis with real samples

The f-MWCNTs modified MIP electrode was used to determine EC in fifteen different green tea samples using the created PLSR model in order to comment on its practical uses. The procedure that has been used to make the tea liquor is detailed in Section 2.6. In the potential range of 0.0 V – 1.4 V, ten repeating DPV responses were collected for each sample. The data matrix [279 x 150] acquired after infusing the modified MIP- EC electrode to the green tea samples was subjected to PLSR and PCR using MATLAB R2014a.

##### 4.2.7.1. PLSR analysis

The prediction capacity of the modified MIP-EC electrode to the EC quantity has been investigated using the PLSR model in conjunction with the LOOCV methodology. As a consequence of the DPV response and the related HPLC data, the matrix [279 x 150] was separated into two subsets in the ratio of 80:20: training set and testing set. The root mean square error (RMSE) and correlation

coefficient ( $R^2$ ) between predicted and experimental data have been used to estimate the model's performance. LV corresponds to the lowest RMSE obtained during the calibration (RMSEC). As shown in Fig. 4.10(a), the RMSEC value (0.29) is lowest for 6 LVs (a). When predicting the EC concentration (in mg/g) in green tea samples, the PLSR model had a prediction accuracy of 93.58% on average. A comparative assessment among the actual (HPLC) and the predicted EC values in the green tea samples is summarized in Table 4.1. The bar graph in Fig. 4.10 (c) depicts the comparative visualization. An acceptable degree of synchronization between the actual and expected values of EC content is confirmed by this plot.

*Table 4.1. EC content from PLSR and PCR Model.*

S. No.	Actual EC (mg/g) (HPLC)	Predicted EC (mg/g)		Prediction accuracy (%)	
		PLSR	PCR	PLSR	PCR
1	1.10	1.191	1.206	91.727	90.327
2	0.97	0.910	0.945	93.814	97.522
3	1.15	1.067	1.055	92.782	91.736
4	0.81	0.803	0.791	99.086	97.611
5	1.21	0.990	1.060	81.818	87.570
6	0.96	0.873	0.867	90.979	90.362
7	1.08	1.043	1.070	96.537	99.081
8	1.05	1.023	1.045	97.428	99.562
9	1.54	1.429	1.310	92.792	85.062
10	1.90	1.969	1.878	96.368	98.832
11	0.33	0.371	0.330	87.575	99.944
12	0.53	0.536	0.456	98.867	86.037
13	0.17	0.176	0.159	96.470	93.701
14	0.35	0.371	0.452	94.00	70.721
15	0.81	0.815	0.863	93.382	93.433
<b>Average prediction accuracy</b>				93.580	92.004

*Table 4.2. Prediction of EC concentration in unknown samples.*

Method	LV	Calibration		Validation		Prediction	
		RMSEC	$R_c^2$	RMSEV	$R_v^2$	RMSEP	$R_p^2$
PLSR	6	0.290	0.931	0.193	0.861	0.173	0.91
PCR	10	0.310	0.911	0.159	0.863	0.153	0.89

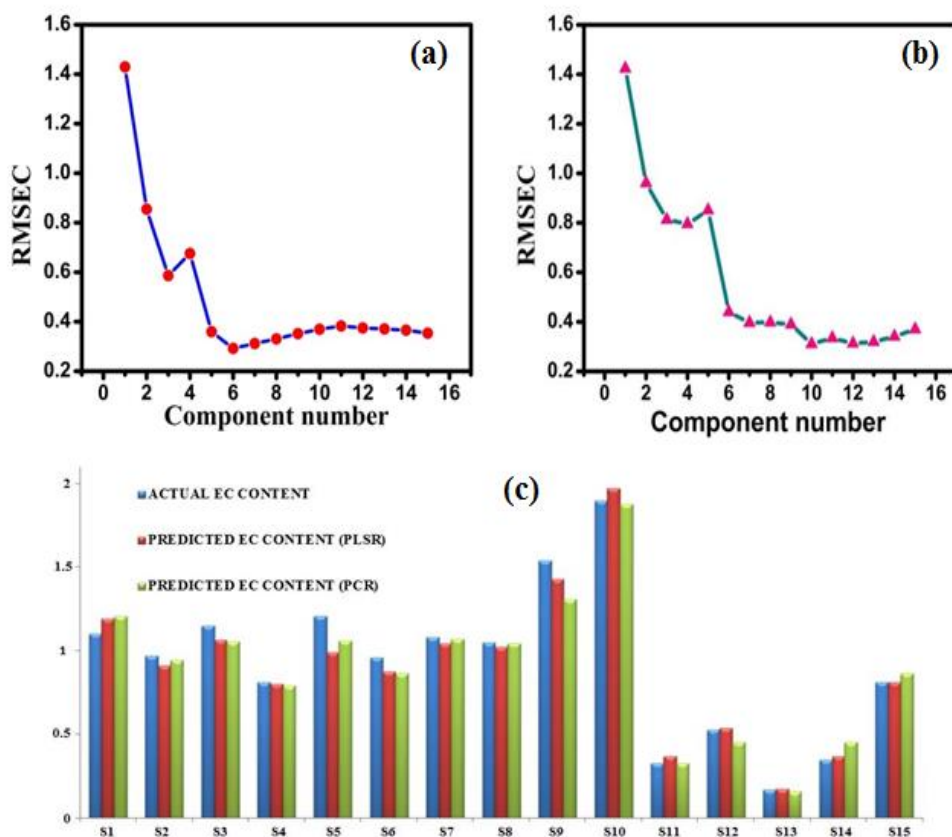


Fig. 4.10. RMSEC versus number of components (a) PLSR (b) PCR and (c) Plot depicting the actual and predicted contents of EC by employing both PLSR and PCR model.

#### 4.2.7.2. PCR analysis

The size of the principal components of the data matrix [279 x 150] and the HPLC data have been linked up using PCR analysis. The lowest RMSEC (0.31) was obtained for a total of ten LVs, as shown in Fig. 4.10 (b). The average prediction accuracy in this research was 92% (Table 4.1). Table 4.2 shows the statistical metrics for both the PLSR and PCR regression models, including the coefficient of determination for validation ( $R_v^2 = 0.863$ ), coefficient of determination for calibration ( $R_c^2 = 0.911$ ) and RMSEC for both the statistical models. With the exception of the smaller number of LVs needed for PLSR (6 LVs), both PLSR and PCR models have more or less the same prediction accuracies.

#### 4.2.7.3. Validation and prediction using the regression models

Prediction was performed using an unknown dataset of size [279×20] by employing both the developed PLSR and PCR models. The results are tabulated below (Table 4.2). The prediction results showed that on using the PLSR

model, the RMSEP was found to be 0.173 with the coefficient of determination for prediction ( $R_p^2$ ) being 0.91 with 6 LVs. Likewise for PCR, the RMSEP was established to be 0.153 with  $R_p^2$  being 0.89 with 10 LVs. The unknown dataset prediction results are in sync with the validation results using both the linear regression models. Both PLSR and PCR models have more or less the same prediction accuracies with the same number of LVs, thereby suggesting that any of the two developed models can be used for analysing the EC content in green tea samples.

### 4.3. Comparison of the present work with existing techniques

A review of the literature indicated in Table 4.3 has attempted to detect EC. In this present investigation, low LOD and LOQ values were found, as well as two large linear ranges of the developed modified MIP-EC electrode, which is advantageous. The resulting LOD is lower than that reported in earlier research [10], [11] [25] or equivalent to that achieved in [9]. However, some of the chemicals and processes employed in some of the works are expensive or the electrode synthesis takes a long time. The modified MIP-EC, which has high stability, was successfully used to test green tea samples. The calculated LOD in this work is notably lesser than the content of EC in green tea samples, which is approximately 0.2718 M-0.2738 M.

*Table 4.3. Comparison of the present technique with previous literature.*

Electrode	Methods	Linear range ( $\mu\text{M}$ )	LOD ( $\mu\text{M}$ )	Refs
GC	SWV	0.01-10	4.27	[9]
Pt	Ad-SV	0.69 - 8.6	0.34	[10]
Pt	DPV	50-300	1.8	[11]
MIP-EC	CV and DPV	1-30 and 30-300	0.05192	This work

## Procedure II:

### 4.4. Detection of EC using Q as the target molecule

In our previous investigation, EC molecule has been used as the template for the detection of EC. Nanomolar detection limit is exhibited only when EC template has been used for the detection of EC, with the use of f-MWCNTs rendering an added stability. Taking cost as an important parameter, the price of EC is approximately 12 times higher than Q. Hence, Q molecule has been chosen as the template because both

EC and Q have closely related chemical structures. Additionally, as mentioned in Section 4.1, in order to avoid template leakage and false positive results, the idea of using dummy template emerged.

In this work, the polymer matrix of the electrode material has been synthesized by co-polymerization of AAm and EGDMA by the use of benzoyl peroxide (BP) as a polymerization initiator. The novelty of the envisaged method lies in its cost effectiveness and selectivity, which leads to the synthesis of a simple electrode for EC detection in green tea samples. The present methodology of preparation of MIP is therefore cheap and the electrode is fairly simple to fabricate. In addition, the prepared electrode has desirable repeatability, reproducibility, stability and wide compatibility in large domains of application. Prior to the electrochemical experimentation, no pre-treatment is required. As a result, the electrode can be directly immersed in any infusion, which is a significant advantage for industrial use. The prediction capacity of the MIP-Q@G electrode has been thoroughly explored using the PLSR and PCR models. The above models were used to compute the EC content in unknown tea samples after they were calibrated.

### 4.4.1. Chemicals and reagents

Quercetin ( $C_{15}H_{10}O_7$ ), EGDMA, CAT, EGCG, AAm and fine graphite powder (99%) were bought from Sigma Aldrich, India. EC was bought from TCI Chemicals Pvt. Ltd., India. BP was taken from Sisco Research Laboratories Pvt. Ltd, India. Binder (paraffin oil) and ethanol were obtained from Merck & Co., India. Distilled water ( $R=18\text{ M}\Omega$ ) was used for washing the electrode during the experiment which was acquired from millipore water purification system.

### 4.4.2. Methods and measurement

A double beam Shimadzu UV-3600 spectrometer was used for UV-visible absorption spectral measurements. The HPLC analysis was carried out using UHPLC DIONEX Ultimate 3000 for EC estimation in the Tocklai Tea Research Institute, Jorhat, Assam, India. The morphological study was accomplished by scanning electron microscope (SEM), ZEISS-EVO 18 (United States) with acceleration voltage of 15 kV. To investigate the behavior of MIP-Q@G electrode, a three electrode system has been used with Autolab Potentiostat/ Galvanostat 101 (Netherlands). In the three electrode system, Ag/AgCl electrode is used as the

reference electrode and platinum (Pt) electrode is used as a counter electrode. The DPV and cyclic voltammetry (CV) measurements were performed within a potential window of 0.0 V-1.2 V.

### 4.4.3. Preparation of the MIP material

The similar protocol as explained in section 2.4 has been followed for the preparation of the MIP material. Briefly, 0.90 g of commercial fine graphite powder was sonicated for 1 h in 15 ml of ethanol. The monomer (AAm) and template molecule (Q) in a ratio of 1:1 (wt/wt) were added to the homogenized dispersion of graphite. After 2 h of stirring, 400  $\mu$ L of EGDMA and 1 mg of benzoyl peroxide (polymerization initiator) were introduced. The polymerization was carried out in a water bath at 30 °C. The EC molecule was extracted from the polymerized sample using an 80:20 mixture of ethanol and water to prepare the MIP after the sample was collected and dried. The resultant MIP sample was dried and preserved. Except for the inclusion of EC, the NIP material was synthesized in a similar way.

### 4.4.4. Preparation of the electrodes

The polymerized powders of both materials were mortared into a fine and smooth paste using 1 ml of the binder to develop the MIP-Q@G and NIP@G electrodes. The paste was delivered into glass capillary tubes (2.5 mm diameter). Copper wire was utilized to provide the electrical contact with the electrode.

### 4.4.5. Results and discussions

#### 4.4.5.1. Electrochemical Properties of the MIP-Q@G Electrodes and NIP@G Electrodes

CV was used to evaluate the electrochemical oxidation behavior of the EC molecule at the surfaces of MIP-Q@G and NIP@G electrodes. Phosphate buffer saline of pH 5 (PBS 5) was used as the test buffer solution. The electrolyte had 9 ml of buffer and 1 ml of EC from  $10^{-2}$  M stock solution of EC. As can be seen from Fig. 11 (a), the peak current so obtained by using MIP-Q@G electrode was approximately two times higher (38.61  $\mu$ A) than that obtained in case of NIP@G electrode (15.73  $\mu$ A). This is probably because the MIP-Q@G electrode has Q-imprinted sites which were not present on the NIP@G electrode.



#### 4.4.5.2. UV visible spectroscopy

The UV-vis spectroscopy was carried out in the wavelength window of 200-800 nm. The spectrum in Fig. 11 (b) depicts the absorption spectra of the polymer sample before washing the template molecule (BW) and after washing the template molecule (AW). An absorbance peak corresponding to Q molecule is visible around 277.03 nm in case of the before washing (BW) the material, whereas, this peak is absent in the spectrum after the removal of Q (AW) from the BW material. The absence of the peak affirms the absolute removal of the Q template from the MIP material.

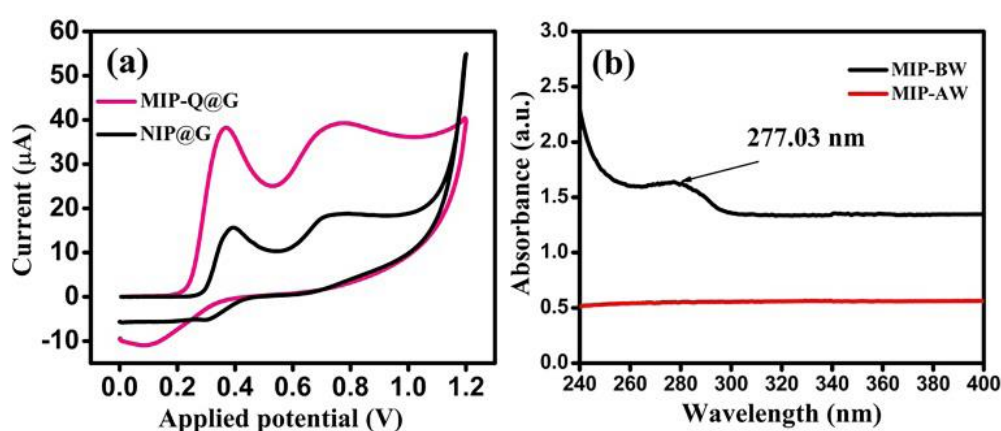


Fig. 4.11. (a) CVs of MIP-Q@G and NIP@G electrode in 0.1 M buffer containing 1mM EC (b) UV-vis absorption spectra of the MIP material before (BW) and after (AW) washing the template.

#### 4.4.5.3. Morphological characterizations of MIP-Q material

SEM micrographs of MIP-Q@G and NIP@G materials are shown in Fig.4.12. In Fig. 4.12 (a), the rough surfaces indicate the continuous etching out of the Q molecule, thus impeding the fine surface of the polymer. Smooth and fine surfaces of the NIP material in Fig. 4.12 (b) reveal that there was an absence of extraction process [23].

The MIP-Q@G electrode was immersed in 1 mM EC in different buffers viz., phosphate buffered saline (PBS), acetate buffered saline (ABS) and citrate buffered saline (CBS), respectively, to observe the effect of buffer solution and pH.



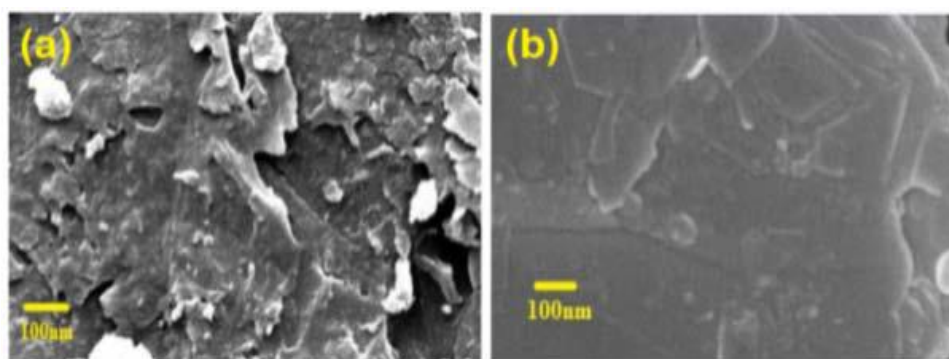


Fig. 4.12. SEM image of (a) MIP material and (b) NIP material.

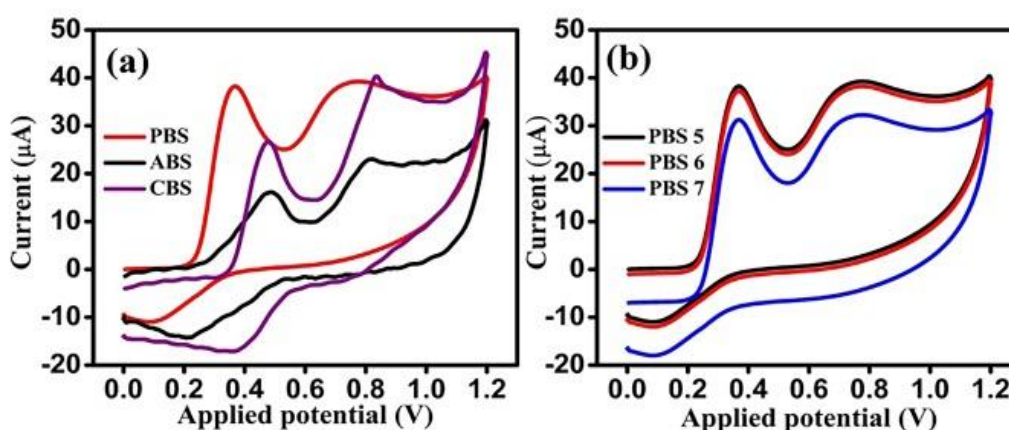


Fig.4.13. Voltammograms obtained for 1 mM EC (a) in PBS, acetate and citrate buffer solutions (b) with PBS of pH values 5, 6 and 7.

#### 4.4.5.4. Effect of buffer and pH

After performing CV, from Fig. 4.13 (a), it is derivable that the oxidation peak current ( $I_p$ ) of the MIP-Q@G electrode is highest (38.61  $\mu\text{A}$ ) for PBS. By using PBS of pH 5, 6 and 7, the effect of pH on MIP- Q@G electrode was investigated. The response curves shown in Fig. 4.13 (b) imply that maximum current (38.61  $\mu\text{A}$ ) was recorded for PBS-5. The oxidation of the EC molecule can be rendered easily when it is negatively charged through elevation of highest occupied molecular orbital (HOMO). The studied molecule (EC) has five phenolic groups and the molecule behaves as weak organic acid. Ionization of phenolic group through dissociation is facilitated with increasing pH producing phenolate ion. At pH =5 of PBS, the abundant phenolate is sufficient for efficient detection of the analyte molecule through electrochemical principle. So, PBS-5 was selected to be the test solution during the whole experiment.

**4.4.5.5. Influence of scan rate**

The scan rate was varied from 0.025 to 0.30 Vs<sup>-1</sup> for better visibility of the electrochemical mechanisms involved in the reactions. Fig. 4.14 (a) shows the CV of 1 mM EC in PBS 5 buffer for varying scan rates. The surface-controlled process [20] can be concluded from Fig.4.14 (b), which shows that the oxidation peak ( $I_p$ ) is directly proportional to that particular window of scan rate with  $R^2 = 0.91$ . Calculations for the surface concentration of Q molecule ( $\Gamma_c$ ) and the number of electrons ( $n$ ) transferred have been done using Eq. (2.2). The number of electrons transferred ( $n$ ) and surface concentration ( $\Gamma_c$ ) are calculated and found to be 1.94 (approximately 2) and  $1.37 \times 10^{-3}$  mole cm<sup>-2</sup> respectively. The relation between oxidation potential ( $E_p$ ) and logarithm of the scan rate ( $\log v$ ) is shown in Fig. 4.14 (c). The  $n$  and  $\Gamma_c$  values so obtained show that the MIP-Q@G electrode holds remarkable adsorption capability to the EC molecules. The equation of the curve is

$$E_p = 0.060 \log v + 0.40 \quad (4.2)$$

Using the slope of Eq. (4.2), the electron transfer coefficient ( $\alpha$ ) was determined to be 0.493 which indicates a simple electron transfer process.

**4.4.5.6. Concentration variation and linearity**

By performing DPV measurements, the dependence of current profile with varying concentration of EC was observed using MIP-Q@G electrode. After optimization, the experimental parameters: interval time, modulation time, scan rate, modulation amplitude and step potential were fixed at 0.0625 s, 0.02 s, 0.08 Vs<sup>-1</sup>, 0.04 V, and 0.005 V respectively. The DPV was performed within 0.0 V- 1.2 V potential ranges.

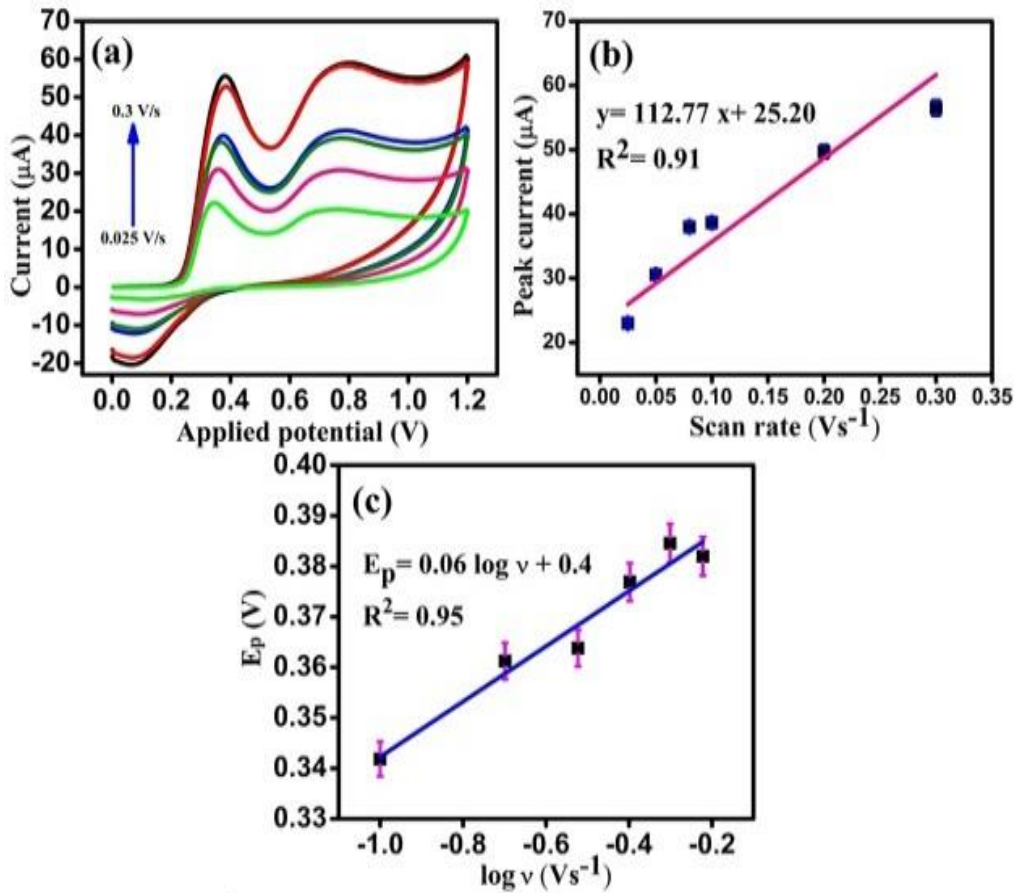


Fig. 4.14. (a) Effect of varying scan rates (0.025 - 0.3 Vs<sup>-1</sup>) over peak current (b) Peak current deviation with scan rate (c) Oxidation potential vs logarithm of scan rate ( $\log v$ ).

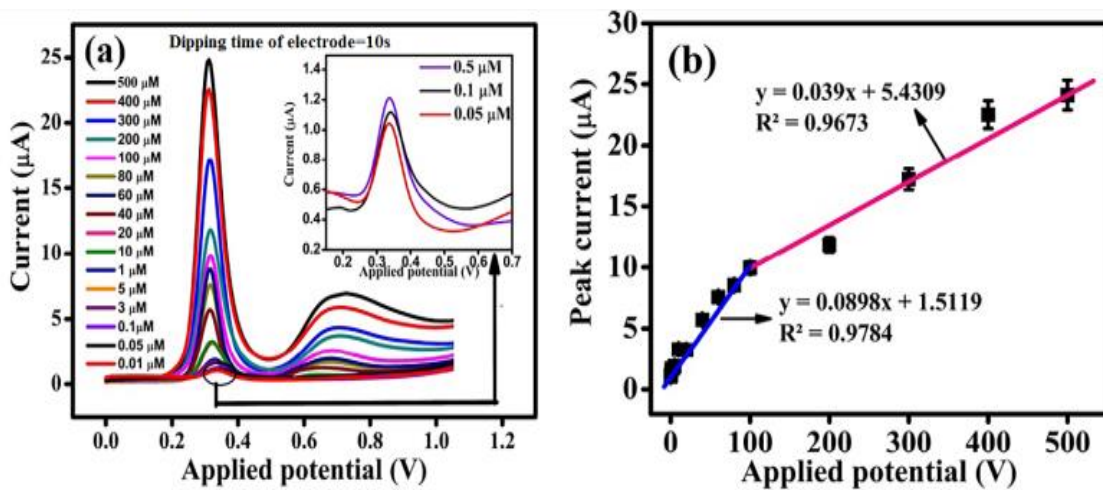


Fig. 4.15. (a) DPV responses at the MIP-Q@G electrode surface with different EC concentrations in PBS 5 (dipping time 10s before each measurement) (b) Peak current deviation with concentration.

Additionally, the LOD calculated at this particular scan rate, i.e., 0.33  $\mu\text{M}$  is quite low, thereby, suggesting very low signal to background ratio. Thus, scan rate of 0.08  $\text{Vs}^{-1}$  was optimized. A notable increase in current was observed with increasing concentration of EC in Fig. 4.15 (a). The calibration curve for EC (Fig. 4.15 (b)) indicates two linear segments: one from 1  $\mu\text{M}$  to 100  $\mu\text{M}$ , with the regression equation  $y = 0.08x + 1.51$  ( $R^2 = 0.97$ ), the second linear segment is between 100  $\mu\text{M}$  and 500  $\mu\text{M}$ , with the regression equation being  $y = 0.03x + 5.43$ ,  $R^2 = 0.96$ . Using 3  $\text{Sy}/\text{x}/\text{m}$  [21] and 10  $\text{Sy}/\text{x}/\text{m}$  [22], the LOD and LOQ of the MIP-Q@G electrode were determined to be 0.33  $\mu\text{M}$  and 1.09  $\mu\text{M}$ .

#### 4.4.5.7. Sensory characteristics of the developed MIP electrode

To investigate selectivity, the MIP-Q@G electrode has been dipped in 1mM of EC, Q, CAT and EGCG respectively. In Fig. 4.16 (a), the MIP-Q@G electrode demonstrated a sharp response towards EC and CAT where the peak current of EC obtained was notably greater than rest of the analytes. Owing to the same number of H bonds donors, a better match of EC in the cavities of MIP-Q@G material induced by Q. The difference in the peak current for EC and CAT using MIP-Q@G electrode is probably because the  $\gamma$ -phenolic hydroxyl group has non-identical spatial distribution which carries to a different matching in the recognition sites of the MIP-Q@G material. It can be observed that the response of MIP-Q@G electrode towards EGCG molecule is quite poor. Hence, it can be concluded that the MIP-Q@G electrode is most selective towards EC.

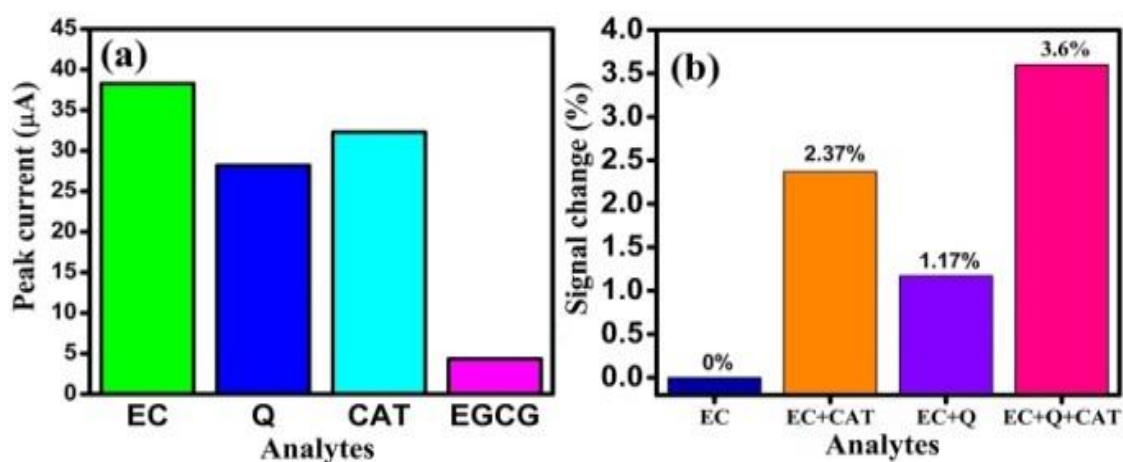


Fig. 4.16. MIP-Q@G electrode showing (a) selectivity, (b) interference profile.

Additionally, the MIP-Q@G has been subjected to CAT and Q (possible interferents) in the presence of 100  $\mu\text{M}$  EC. The responses were recorded in the presence of 10-folds of CAT and Q interfering to 100  $\mu\text{M}$  EC. Fig. 4.16 (b) depicts the interference profile of MIP-Q@G electrode. The relative change of signal (tolerance limit of less than  $\pm 5\%$ ) due to presence of CAT, Q and both of the interferents together has been plotted with respect to the response obtained only for EC. These observations justifies that even if CAT and Q are in high concentrations, EC has much higher affinity towards the recognition sites of the MIP-Q@G electrode. Repeatability studies were conducted and it has been found that the MIP-Q@G electrode shows good repeatability with %RSD of 4.12 (Fig. 4.17(a)). The CV responses of the MIP-Q@G electrode was recorded to examine the reproducibility (Fig. 4.17(b)) using four similar electrodes. Acceptable reproducibility was obtained with relative standard deviation (% RSD) of 1.76. For analyzing the stability, in 1mM EC, DPV measurements were done at an interval of 7-15 days for almost 45 days. The peak current of the MIP-Q@G electrode reduced by 0.104% after next 7 days (Fig.4. 17(c)) and 1.253 % after a span of 45 days.

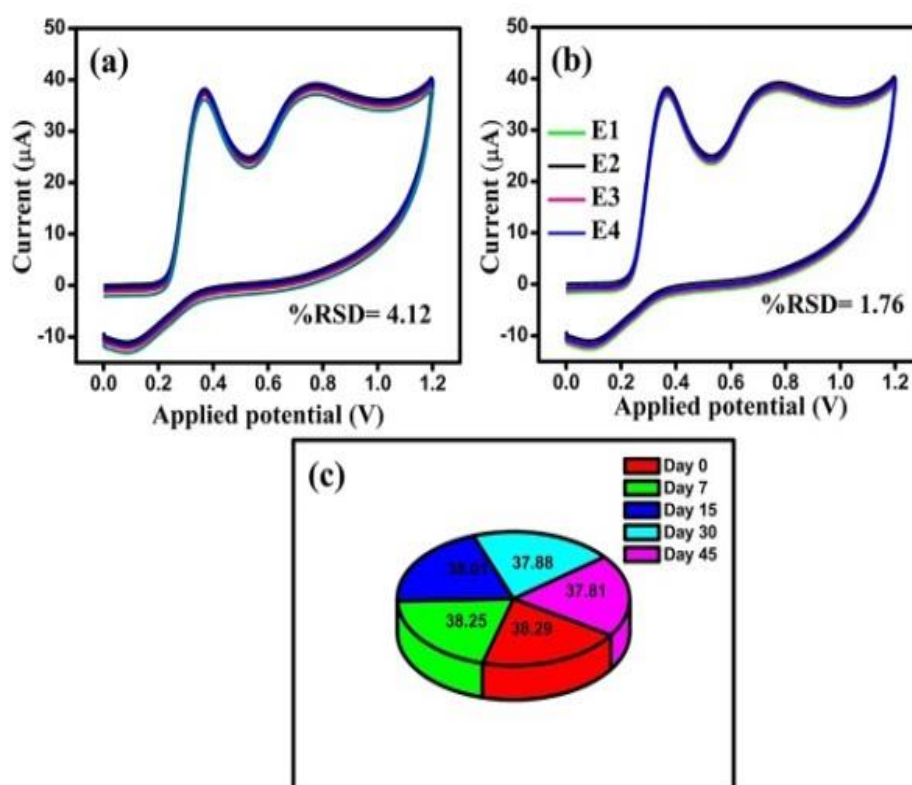


Fig.4.17. MIP-Q@G electrode showing (a) repeatability (b) reproducibility, and (c) stability.

#### 4.4.6. Analysis with real samples

##### 4.4.6.1. Partial least square regression

The practical applicability of the MIP-Q@G electrode was ascertained by measuring the amount of EC in green tea samples. This has been investigated by using the PLSR model in conjunction with the LOOCV methodology. As a consequence of the DPV response and the related HPLC data, the matrix [279 x 100] was separated into two subsets in the ratio of 80:20, training set and testing set. The RMSE and correlation coefficient ( $R^2$ ) between the predicted and experimental data have been used to estimate the performance of the model. The number of LV was chosen as 10 that correspond to the lowest RMSEC of 0.113. When predicting the EC concentration (in mg/g) in green tea samples, the PLSR model had a prediction accuracy of 94.54% on average. An acceptable degree of accuracy between the expected and actual values of EC content is confirmed from Table 4.4.

**Table 4.4.** Prediction of EC content from PLSR and PCR model

S. No.	Actual EC (mg/g) (HPLC)	Predicted EC (mg/g)		Prediction accuracy (%)	
		PLSR	PCR	PLSR	PCR
1	0.81	0.794	0.790	98.02	97.53
2	1.1	0.947	0.931	86.09	84.63
3	0.97	0.960	0.957	98.96	98.65
4	0.81	0.897	0.888	89.25	90.37
5	1.08	1.008	1.004	93.34	92.96
6	1.05	1.021	1.024	97.23	97.52
7	0.96	1.097	1.092	85.72	86.25
8	1.21	1.208	1.208	99.83	99.83
9	1.15	1.171	1.190	98.17	96.52
10	1.9	1.877	1.897	98.78	99.83
Average prediction accuracy (%)				94.54	94.41

**Table 4.5.** Prediction of EC concentration of unknown samples

Method	Calibration		Validation		Prediction	
	RMSEC	$R_c^2$	RMSEV	$R_v^2$	RMSEP	$R_p^2$
PLSR	0.113	0.96	0.08	0.94	0.079	0.944
PCR	0.119	0.95	0.09	0.92	0.082	0.940



#### 4.4.6.2. Principal component regression

A link has been found by PCR analysis between the size of the data matrix's primary components [279×100] and the HPLC data. Like PLSR, the lowest RMSEC has been observed for 10 LVs, i.e., 0.119. The average prediction accuracy that has been achieved is 94.41% (Table 4.4). Table 4.5 presents the statistical metrics for both PLSR and PCR regression models, including coefficient of determination for calibration ( $R_c^2$ ), coefficient of determination for validation ( $R_v^2$ ) and RMSEC for both the statistical models.

#### 4.4.6.3. Validation and prediction using the developed models

By using PLSR and PCR models, prediction was done on an unknown dataset of size [279 x 20]. The results are listed in Table 4.5. The results of the prediction showed that when the PLSR model was used, the RMSEP obtained was 0.079 with the coefficient of determination for prediction ( $R_p^2$ ) being 0.944 with 10 LVs. Similarly for PCR, with 10 LVs, the RMSEP was determined to be 0.082 and  $R_p^2$  to be 0.940. The findings of the unknown dataset prediction match with the validation results using both linear regression models. With the same number of LVs, both PLSR and PCR models exhibit nearly identical prediction accuracies, implying that any of the two generated models can be utilized for EC determination in green tea samples.

*Table 4.6. Comparison of the present technique with previous literature*

Electrode	Techniques used	Linear range( $\mu\text{M}$ )	LOD ( $\mu\text{M}$ )	Refs
Pt	Ad-SV	0.69 - 8.6	0.34	[9]
GC	SWV	0.01-10	4.27	[10]
Pt	DPV	50-300	1.8	[11]
MIP-Q@G	CV and DPV	1-100 and 100-500	0.33	This work

### 4.5. Comparative analysis

A thorough examination of the literature reveals some studies listed in Table 4.6 where the detection of EC has been pursued. Low values of LOD and LOQ were observed in this study along with two wide linear ranges of the MIP- Q@G electrode which is desirable. The LOD so obtained is comparatively lower than the previous studies [10] [11] or comparable to that obtained in [9]. This study on highly selective

and stable electrochemical detection of EC using a low cost Q-based MIP was found to be an economical solution to commercialization. Green tea samples were successfully examined with MIP-Q@G which has excellent stability. EC content in tea samples is estimated to be in the range of 7.89-7.95 mg/g; this is approximately equivalent to 0.2718 M- 0.2738 M, which is higher than the LOD (0.33  $\mu$ M) calculated. Therefore, the electrochemically stable and cost- effective MIP-Q@G electrode can be used for EC detection in any industry.

### 4.6. Conclusion

In this work, two electrodes were developed for the detection of EC. In the first investigation, the target molecule itself was used as template. In the second work, in order to achieve a low-cost electrode, dummy template, i.e., quercetin was used for imprinting. For the first case, the MIP sensing material has been embedded with electrochemically activated f-MWCNTs for successful recognition of EC in green tea in this study. The electrode has two distinct linear ranges (1  $\mu$ M to 30  $\mu$ M and 30  $\mu$ M to 300  $\mu$ M). The detection of EC at nanomolar levels has been proven, and the LOD was predicted to be 51.92 nM, which is significantly lesser than the quantity of EC in any infusion. The LOQ was determined to be 0.17  $\mu$ M. The electrode was established to be repeatable, selective, and reproducible, with three-month stability. The conception and comparative prediction of the findings achieved through the use of PLSR and PCR by means of reference HPLC data have been completed. As a consequence, the average prediction accuracy of PLSR and PCR was 93.58% and 92%, respectively. The MIP-Q@G electrode has been developed in this work for successful recognition of EC in green tea. The electrode has two distinct linear ranges (1  $\mu$ M to 100  $\mu$ M and 100  $\mu$ M to 500  $\mu$ M). The LoD of the electrode was calculated to be 0.33  $\mu$ M, which is significantly lesser than the quantity of EC in any infusion. The electrode revealed an excellent LoQ of 1.09  $\mu$ M. on the other hand, the MIP-Q@G electrode was observed to be repeatable, selective and reproducible with acceptable stability. The PCA plot validated the clear segregation of green tea samples. The average prediction accuracy of the MIP-Q@G electrode was 94.54% and 94.41%, respectively by means of PLSR and PCR models. The focus of this research is on the development of a low-priced and highly selective electrode with the further aim of investigating the electrode's quantitative prediction capability. Summarizing, this research advances the electrode's practical applicability as a sensor



material designed for qualitative evaluation of tea or any other food or beverage based on its EC content.

### References

- [1] S. A. Khan, S. Priyamvada, N. A. Aivarasu, S. Khan, A. N. K. Yusufi, "Influence of green tea on enzymes of carbohydrate metabolism, antioxidant defense, and plasma membrane in rat tissues", *Nutr. J.* 23 (2007) 687-695.
- [2] H. Wang, G. J. Provan, K. Helliwell, "Tea flavonoids: their functions, utilisation and analysis", *Trends Food Sci. Technol.* 11 (2000) 152-160.
- [3] L. Ding, H. Li, F. Tang, S. Yao, "Molecularly imprinted solid phase extraction of epicatechin from tea beverage", *Anal. Lett.* 39 (2006) 2373-2385.
- [4] Y. Jaiswal, P. Tatke, S. Gabhe, A. Vaidya, "Rapid High Performance Thin Layer Chromatographic Method for Quantitation of Catechin from Extracts of Cashew Leaves – a Short Report", *Pol. J. Food Nutr. Sci.* 63 (2013) 49-54.
- [5] J. Xia., D. Wang, P. Liang, D. Zhang, X. Du, D. Ni, Z. Yu, "Vibrational (FT-IR, Raman) analysis of tea catechins based on both theoretical calculations and experiments", *Biophys. Chem.* 256 (2020).
- [6] I. Berregi, J. I. Santos, G. D. Campo, J. I. Miranda, "Quantitative Determination Of (-) Epicatechin In Cider Apple Juices by  $^1\text{H}$  NMR", *Talanta.* 61 (2003) 139-145.
- [7] P. R. Machonis, M. A. Jones, B. T. Schaneberg, and C. L. Kwik-Urbe, "Method for the Determination of Catechin and Epicatechin Enantiomers in Cocoa-Based Ingredients and Products by High-Performance Liquid Chromatography: Single Laboratory Validation", *J. AOAC Int.* 95 (2013) 500-507.
- [8] Y. H. Cao, X. Zhang, X. H. Ding, Y. Z. Fang, J. N. YE, "Determination of Caffeine, Epicatechin and Ascorbic Acid in Tea Samples by Capillary Zone Electrophoresis with Electrochemical Detection", *Chinese J. Anal. Chem.* 21 (2001) 1072-1075.
- [9] L. Pigani, R. Seeber, A. Bedini, E. Dalcanale, M. Suman, "Adsorptive-stripping voltammetry at PEDOT-modified electrodes. Determination of epicatechin", *Food Anal. Methods.* 7 (2014) 754-760.

- [10] I. Novak, M. Šeruga, Š. Komorsky-Lovrić, “Square-wave and cyclic voltammetry of epicatechin gallate on glassy carbon electrode”, *J. Electroanal. Chem.*, 631 (2009) 71–75.
- [11] S. Titretir Duran, “Preparation of poly (pyromellitic dianhydride-cothionin) modified voltammetric sensor for the determination of epicatechin”, *J. Turkish Chem. Soc. Chem.* 5 (2018) 1021–1028.
- [12] F. G. Tamayo, E. Turiel, E., A. Martin “Molecularly imprinted polymers for solid-phase extraction and solid-phase microextraction: Recent developments and future trends” *J. of Chrom. A*, 1152 (2007) 32-40.
- [13] Y. M. Yin, Y.P. Chen, X.F. Wang, Y. Liu, H.L. Liu, M. X. Xie, “Dummy molecularly imprinted polymers on silica particles for selective solid-phase extraction of tetrabromobisphenol A from water samples”, *J. of Chrom. A*. 1220 (2012) 7-13.
- [14] B. Danylec, L. Schwarz, S. Harris, R. Boysen, M. Hearn, “The application of template selectophores for the preparation of molecularly imprinted polymers”, *Molecules* 20 (2015) 17601–17613.
- [15] P. Parmpi, P. Kofinas, “Biomimetic glucose recognition using molecularly imprinted polymer hydrogels”, *Biomaterials*, 25 (2004) 1969–1973.
- [16] M. D. M. C. Lopez, M. C. C. Perez, M. S. D. Garcia, J. M. L. Vilarino, M. V. G. Rodriguez, and L. F. B. Losada, “Preparation, evaluation and characterization of quercetin-molecularly imprinted polymer for preconcentration and clean-up of catechins”, *Analytica Chim. Acta*, 721 (2012) 68–78.
- [17] W. Du, Q. Fu, G. Zhao, P. Huang, Y. Jiao, H. Wua, Z. Luo, C. Chang, “Dummy-template molecularly imprinted solid phase extraction for selective analysis of ractopamine in pork”, *Food Chem.* 139 (2013) 24-30.
- [18] X. Ma, H. Lin, J. Zhang, X. Zhou, J. Han, Y. She, C. Qiu, Q. He, J. Wang & T. Rabah, “Preparation and characterization of dummy molecularly imprinted polymers for separation and determination of farrerol from *Rhododendronaganniphum* using HPLC”, *Green Chem Lett Rev.* 11 (2018) 513-522.
- [19] J. Bannerjee, Ajay S. Panwar, K. Mukhopadhyay, A. Saxena, Arup. R. Bhattacharyya, “Deagglomeration of multi-walled carbon nanotubes via an

- organic modifier: structure and mechanism”, *Physical Chemistry Chemical Physics* 38 (2015) 25365-25378.
- [20] J. J. Feminus, R. Manikandan, S. S. Narayanan and P. N Deepa, “Determination of gallic acid using poly (glutamic acid): graphene modified electrode”, *J. Chem. Sci.* 131 (2019) 1-10.
- [21] S. Nag, S. Pradhan, H. Naskar, R. B. Roy, B. Tudu, P. Pramanik, and R. Bandyopadhyay, “A simple nano cerium oxide modified graphite electrode for electrochemical detection of formaldehyde in mushroom”, *IEEE Sens. J.* 21(2021) 12019-12026.
- [22] S. Kar, B. Tudu, A. K. Bag, R. Bandyopadhyay, “Application of near-infrared spectroscopy for the detection of metanil yellow in turmeric powder”, *Food Anal. Methods.* 11 (2018) 1291-1302.
- [23] D. Das, S. Nag, S. De, A. K. Hazarika, S. Sabhapondit, B. Tudu, R. Bandyopadhyay, P. Pramanik, R.B. Roy, “Electrochemical Detection of Epicatechin in Green Tea Using Quercetin-Imprinted Polymer Graphite Electrode”, *IEEE Sens. J.* 21 (2021) 26526-26533.
- [24] D. Das, T. N. Chatterjee, R. B. Roy, B. Tudu, A. K. Hazarika, S. Sabhapondit, R. Bandyopadhyay, “Titanium oxide nanocubes embedded molecularly imprinted polymer based electrode for selective detection of caffeine in green tea”, *IEEE Sens. J.* 20 (2019) 6240-6247.



# Chapter 5

## Towards development of a function generator and signal conditioning circuit for voltammetric purpose

This chapter presents an approach adopted to develop a low-cost three electrode cyclic voltammetry system. The developed system consists of a triangular waveform generator, a potentiostat circuit and the digital signal oscilloscope has been used as the storage and display unit. The responses obtained in the standard solution using the developed system and the commercial potentiostat has been shown in this chapter as comparison.

### List of sections

- Introduction
- The three electrode potentiostat
- Components of the developed cyclic voltammetry three electrode system
- Overview of the complete circuit
- Comparison of data
- References
- Conclusion





## Chapter 5

### Towards development of a function generator and signal conditioning circuit for voltammetric purpose

---

#### 5.1. Introduction

The principle of voltammetry is frequently used to collect large amounts of information about the target analyte from the current responses of WEs. Given the fact that tea liquor is a mixture of large number of chemical species, the use of voltammetry technique stands justified. The voltammetry technique provides numerous adjustable parameters to probe the test sample making it suitable for the analysis of complex liquids [1]. The application of voltammetric principle also requires the electrodes to be arranged in a three-electrode configuration where the voltage applied to the WE is measured and controlled by an instrument called a *potentiostat*. The commercial potentiostats are expensive and hence a step towards development of a low cost potentiostat has been taken. The potentiostat also collects the current responses from the electrode array and stores them for future analysis. “DStat”, in [1], is designed as a general-purpose open-source potentiostat that can be used alone or in conjunction with other instruments. DStat features picoampere current measurement, a small USB-powered architecture, and cross-platform software that is easy to use. DStat is simple and affordable to create, can be freely customized, and performs reasonably well at low current levels that other laboratory-fabricated devices cannot. The “EcoStat” designed in [2] is a low-cost, digitally controlled potentiostat with various advantages over other low-cost instruments, including lower noise and a more steady output signal thanks to a digital PI controller. Furthermore, a user-friendly PC interface named “POTCON” controls data collecting, display, and filtering. In [3], the fabrication and design of a simple potentiostat has been done that is capable of resolving a current of the order of a few microamperes ( $\mu\text{A}$ ). The device, when compared to commercial equipment, makes it a viable alternative for places where electrochemical experiments are conducted using computer software or web-

based simulators. In [4], the potentiostat designed is used for determination of pH, which is an important parameter for the initiation of any electrochemical experiment. To correctly measure the voltage between a pH sensor electrode and a RE, a potentiometric apparatus with extremely low input bias current is required. The hardware consists mostly of an Arduino Nano microcontroller, a 16-bit analog-to-digital converter, two electrical buffer amplifiers, a temperature sensor and a bluetooth module, all of which cost roughly \$50. The device was tested against a commercial pH meter using a regular glass electrode and a bespoke palladium/palladium oxide pH detecting electrode. The accuracy and precision of the developed device were found to be adequate for industrial purposes. In [5], the paper demonstrates a unique gadget made by combining a miniature potentiostat with an electronic micropipette. The micropipette battery powers the mini-potentiostat, which is operated by a smartphone through Bluetooth wireless connection. With the help of an adapter, a set of three electrodes is inserted into the tip of the micropipette, allowing electrochemical measurements to be performed without impairing the precision and trueness of handling small amounts of liquid. The device has shown to improve portability, versatility, agility and analytical techniques in studies. This process needs a minimal number of samples and reagents, as well as offers the possibility of recovery after analysis. In [6], the KAUSTat is a wireless, wearable, open-source potentiostat. It enables the use of cyclic voltammetry for a variety of solutions. The MIT App Inventor interface was used to create the app. The user-friendly interface makes parameter definition simple. Wireless connection and a testing distance of up to 16-20 meters are available with the bluetooth low energy (BLE). This allows for easy access to the user's database and error-free point-to-point examination. The gadget has been proved to work more efficiently with a high current, approximately around 10  $\mu\text{A}$ . Experiments suggest that the KAUSTat can work at 500  $\mu\text{A}$  and could be an efficient commercial potentiostat for use in laboratories.

The work reported in this chapter describes the development of a CV three electrode potentiostat with the help of which, in future, we can capture the responses of the electrodes that have been developed in Chapter 2, Chapter 3 and Chapter 4. In order to compare the developed instrument with the commercial one, we have used the caffeine sensor, the description of which has been elucidated in Chapter 2.



Herein, the three-electrode cyclic voltammetry system has been developed. It consists of a triangular wave-form generator, the potentiostat circuit, the three electrodes, (viz., WE, RE, CE) and a digital storage oscilloscope for storing the data and displaying the voltammogram.

## 5.2. The three electrode potentiostat

A potentiostat, as the name suggests (*Potentio* means voltage; *stat* means to keep constant) is an electronic device that maintains a constant voltage difference between the RE and WEs [7, 8]. The role of a potentiostat in an electrochemical system is analogous to that of a controlled voltage source in an electrical system. The voltage applied at the WE is measured and controlled with respect to the applied voltage. The voltage at the WE then induces the redox reactions that in turn generate the current, which contains useful information about the concentration of reaction species [9]. The task of potentiostat is not only to control the potential difference of WE with respect to the RE but also to measure the current flowing through the WE and CE.

In a two electrode potentiostat consisting of WE and CE, the actual voltage between WE and CE differs from the applied voltage due to many sources of variations [10]. These sources include the solution resistance, convection effects, electrode polarization and changes in temperature. The effect of solution resistance becomes more acute with electrolytes of higher resistance. A three electrode system has been proposed to overcome this problem. In a three electrode system, the task of CE is divided between two electrodes, a RE and a CE. RE is such that it is almost an electrochemical half-cell by itself with fixed potential that remains constant with time as long as the concentrations of electro-active species within the cell remain constant. The potential of RE is thus treated as the reference level of the electrochemical system. The potential of the WE specified with respect to that of the RE. The purpose of the CE is only to provide the return path of currents due to electrochemical processes. The CE is expected to have large surface area in order to provide easy passage of charges and has very low voltage developed around it. All the electrochemical reactions occur at the surface of WE. The current flowing between WE and CE is a measure of redox reactions occurring at the WEs.

The developed system is capable of detecting specific target analytes in food and beverage samples. The system setup comprises of: a) the specifically developed MIP electrochemical sensors for target analytes and b) the quality assessment instrumentation using DSO as the display unit. The overview of the proposed system is depicted in Fig. 5.1. The system comprises of Arduino UNO based triangular function generator with a second order filter circuit, a potentiostat circuit and a DSO for display through CRO. In this, the system is instigated over quantitative analysis of epicatechin present in tea.

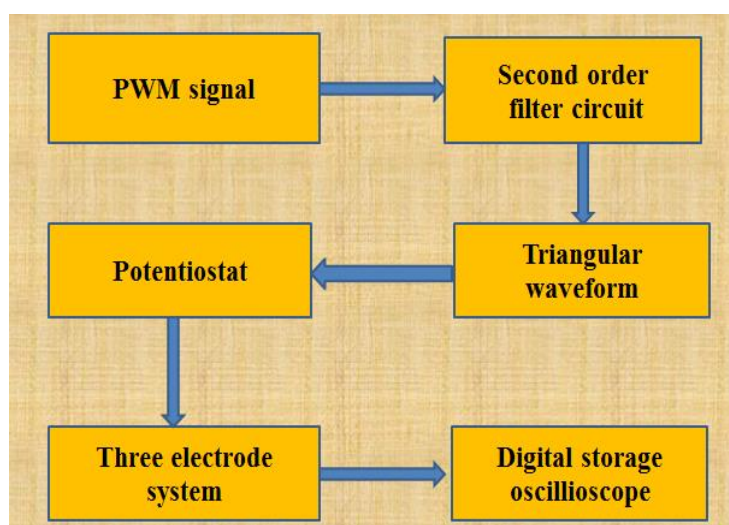


Fig. 5.1. Block diagram of the developed system.

The function of CA is to maintain the potential of WE at the level of applied voltage [11]. It measures the difference between the applied voltage and the voltage at the RE; it then forces current through the CE so that the difference between the applied voltage and the voltage at RE becomes zero. This leads to the potential at WE being the same as the applied voltage, provided the RE is placed very close to the WE.

### 5.3. Components of the developed CV three electrode system

#### 5.3.1. Triangular function generator

This component is used to generate a triangular wave of variable scan rate (user selectable) from -0.5V to +0.5V. The generated triangular wave is fed to the potentiostat circuit (acts as the input of the circuit). Arduino UNO is selected to realize this component. Since UNO does not have a digital to analog converter (DAC), triangular waves output cannot be obtained from any UNO Pin. Instead, UNO is used to generate PWM waves of variable duty cycle (varying from 0 to 20%) and

2nd order low pass filter is utilized to get the low frequency DC component (which is proportional to the duty cycle). As the PWM duty cycle can be easily controlled and varied from the UNO, the filter output will vary in a controlled manner. UNO is also incapable of generating negative voltages, so the required negative half of the triangular wave is achieved by shifting the filtered wave output. From UNO, 0  $\rightarrow$  ( $V_+$  -  $V_-$ ) is required; so, shifting down of the filtered output required is  $V_-$ .

### A. Wave generation parameters

The triangular wave parameters, such as, the scan rate which indicates the total voltage change in mV in one second, the minimum voltage in the triangular wave ( $V_-$ ), the maximum voltage in the triangular wave ( $V_+$ ), are tabulated below in Table 5.1.

*Table 5.1. Wave generation parameters.*

Parameters	Values
Scan rate	50 - 1250 mV/sec
$V_-$	-0.5V
$V_+$	+0.5V
Peak to peak voltage of the triangular waveform $-(-V_-+V_+)$	1V

### B. Step numbers and size

The wave is generated with variable PWM duty cycle. A voltage resolution of order 2-3 mV is required for moderate accuracy of the potentiostat circuit. Taking a voltage resolution of 2.5mV,  $(5000/2.5) = 2000$  steps are needed where each step corresponds to a fixed PWM duty cycle generating a particular voltage.

$$\text{Max required steps} = \frac{\text{Max required voltage}}{\text{Max voltage}} \text{ step numbers} = 400 \text{ steps}$$

### C. Step duration

Step duration is the time for which the system lasts a given step  $n$ . Using above step size,

$$\begin{aligned} \Delta V_{step} &= 2.5 \text{ mV} \\ \Rightarrow \text{Scan rate} &= \frac{\Delta V_{step}}{T_{step}} = \frac{2.5}{T_{step}} \\ \Rightarrow T_{step} &= \frac{2.5}{\text{Scan rate}} \end{aligned}$$

#### D. Algorithm for generation of PWM

The voltage generated in  $n^{\text{th}}$  step is  $(2.5n)$  mV

$$5000d_n = n(2.5)$$

$$\Rightarrow d_n = \frac{n}{2000}$$

If  $d_n$  is required to be generated using a PWM generator with duty cycle of the form  $gen = \frac{n}{F}$ , following is obtained;

$$\begin{aligned} d_{n1} &= gen_{n2} \\ \Rightarrow \frac{n_1}{2000} &= \frac{n_2}{F} \\ \Rightarrow n_2 &= n_1 \left( \frac{F}{2000} \right) \end{aligned}$$

Since,  $n_1$  is variable integer, if for every value of  $n_1$ , there exists an integer  $n_2$

$$\Rightarrow \frac{F}{2000} = k \text{ where } k \text{ is an integer} \quad (5.1)$$

So, F has to be an integral multiple of 2000

The default PWM generated by Arduino has 8 bit resolution. So, the  $n^{\text{th}}$  duty cycle for Arduino can be written as:

$$\begin{aligned} default_n &= \frac{n}{2^8} = \frac{n}{256} \\ \Rightarrow F_{default_n} &= 256 \end{aligned}$$

Thus,  $default_n$  cannot be used for generation of  $d_n$

The PWM can be custom-generated by alternating the Pin between HIGH and LOW after some time delays using the `delay()` function.

If a period of T and  $T_{HIGH}$  is considered to be the ON time (consequently  $T_{LOW} = T - T_{HIGH}$ ):

$$gen_n = \frac{T_{HIGH}}{T}$$

Let us generate  $T_{HIGH}$  as some integer multiple of a fundamental delay

$$T_{HIGH} = nT_{fundamental}$$

$$gen_n = \frac{nT_{fundamental}}{T}$$

$$F_{gen_n} = \frac{T}{T_{fundamental}}$$

$$\text{Thus, } \frac{T}{T_{fundamental}} = k \cdot 2000 \text{ (using (1))}$$

$$\Rightarrow T_{fundamental} = \frac{T}{k \cdot 2000} \quad (5.2)$$

A single step using the above generation scheme would at least take T units of time (since there has to be at least one PWM cycle in a step), thus,

$$T_{step} \geq T$$

Unit step duration,

$$\Rightarrow \frac{2.5}{Scan\ rate} \geq T$$

$$\Rightarrow T \leq \frac{2.5}{Scan\ rate}$$

For the above equation to satisfy for all scan rates,

$$T \leq \frac{2.5}{(Scan\ rate)_{max}}, \text{ substituting}$$

$$\Rightarrow T_{fundamental} \leq \frac{2.5}{(Scan\ rate)_{max} \cdot k \cdot 2000}$$

Atmega 328P has a minimum possible delay of (DELAY\_LOOP\_CYCLE), 4 clock cycles. The microcontroller runs at 16 MHz, so a clock cycle is 1/16 μsec. So, minimum possible delay is (DELAY\_LOOP\_CYCLE) μsec, that is, 1/16 μsec.

$$\frac{1}{4} \mu\text{sec} \leq T_{fundamental} \leq \frac{2.5}{(Scan\ rate)_{max} \cdot k \cdot 2000}$$

Since maximum possible  $ScanRate_{max}$  is needed to be generated using Arduino, the lesser equal to equal is changed and considering k=1:

$$T_{fundamental} = \frac{2.5}{Scan\ rate_{max} \cdot 2000} = \frac{1}{4} \mu\text{sec}$$

$$Scan\ rate_{max} = 5000\ mV/sec$$

$$T = k \cdot 2000 \cdot T_{fundamental} = \frac{2.5}{Scan\ rate_{max}} = 500 \mu\text{sec}$$

**Hold loops-** This represents the number of fixed duty PWM cycles per step of the generation. That is, number of PWM cycles of duty  $gen_n$  required in  $n^{\text{th}}$  step.

$$Holdloops = \frac{T_{step}}{I} = \frac{2.5}{ScanRate} \frac{2.5}{ScanRate_{max}} = \frac{ScanRate_{max}}{ScanRate}$$

Now fractional PWM cycles cannot be generated using our algorithm, so Holdloops must be an integer. The above can be rewritten as,

$$Scan\ rate = \frac{Scan\ rate_{max}}{Holdloops}$$

Thus, all possible *ScanRate* are multiples of *ScanRate<sub>max</sub>* (5000mV/s)

### 5.3.2. Filter and level shifter circuit

The higher frequencies need to be filtered out from the output PWM to get the low frequency components (average DC value) of the signal. A first order filter was first used (Fig. 5.2) with response time comparable to the highest step duration required, that is, 2.5/50mV/sec = 50msec.

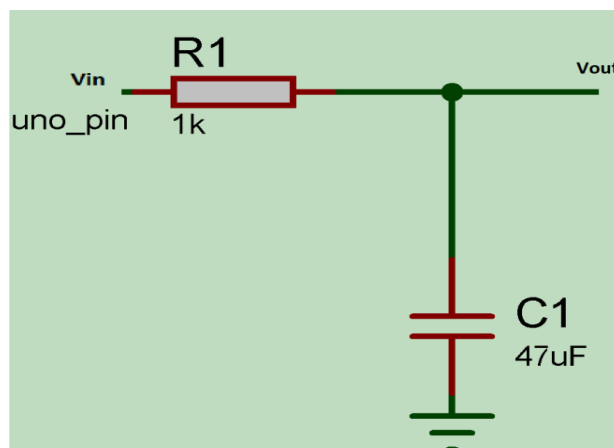


Fig. 5.2. First order filter circuit.

But the ripples observed in the above circuit were in the order of 100mV which is way beyond our required voltage resolution of 2.5 mV. The response time for 1st order filter with ripples around 2.5mV is in the order of seconds, which is slower by many orders than required for generating the scan rates. So, a second order filter was used as shown in Fig. 5.3. On using this, it was observed that the triangular wave was produced satisfactorily.

Additionally, the level shifter circuit has been appended because the Arduino cannot produce negative voltage and the  $V_{pp}$  for our case is 0V- 1V. However, the scanning of the voltage from -0.5 V to 0.5 V is desired, keeping  $V_{pp}$  fixed. Hence, a level shifter circuit was utilised to fulfil this requirement.

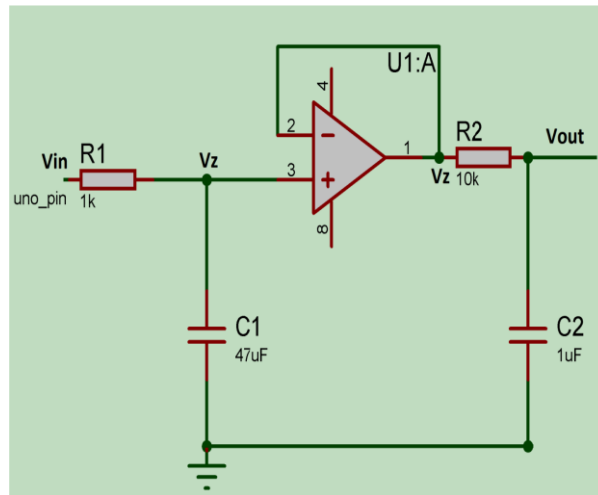


Fig. 5.3. Second order filter circuit.

### 5.3.3. Potentiostat circuit

The triangular signal generated, as can be seen from the Fig. 5.4. is fed to the control amplifier of the potentiostat circuit. The main function of the control amplifier is to shift the RE potential  $180^\circ$  with the applied potential. Using negative feedback, the control amplifier senses the RE potential and then makes the difference between applied potential and RE potential to be applied by forcing current through an CE. The voltage buffer is used mainly to overcome the current loading effect without changing the input voltage. It also provides very high input impedance. As the Arduino cannot measure current directly, it can only measure voltage as an input, so we also need a current to voltage (I to V) converter. The potentiostat is divided into four major blocks and then a collective view of all these parts is appended for overall understanding. Also, op-amp LF347 is used as it very high i/p impedance, high slew rate, low bias current (pA) and with low cost [3].

Three major blocks:

- i. Control amplifier
- ii. Voltage buffer
- iii. I to V converter

#### 5.3.3.1. Control amplifier

The main function of the CA is to shift the RE potential by  $180^\circ$  with respect to the applied potential. Using negative feedback, the control

amplifier senses the RE potential and then makes the difference between applied potential and RE potential by forcing current through CE.

$$V_{ref} = -V_{applied} \quad (5.3)$$

In Fig 5.4,  $1\text{k}\Omega$  (yellow resistor) is the solution potential between CE and RE; the purple signal and the green signal are nothing but the  $V_{applied}$  and  $V_{ref}$  respectively. As can be seen in the graph, RE potential is shifted  $180^\circ$  from the applied potential. Although it's a small part of the full potentiostat circuit, yet it is very important.

### 5.3.3.2. Voltage buffer

In electronic circuit, voltage buffer is used mainly to overcome current loading effect without changing the input voltage, as can be seen in Fig 5.5,  $V_{out} = V_{Non-inverting}$ . The circuit has high input impedance.

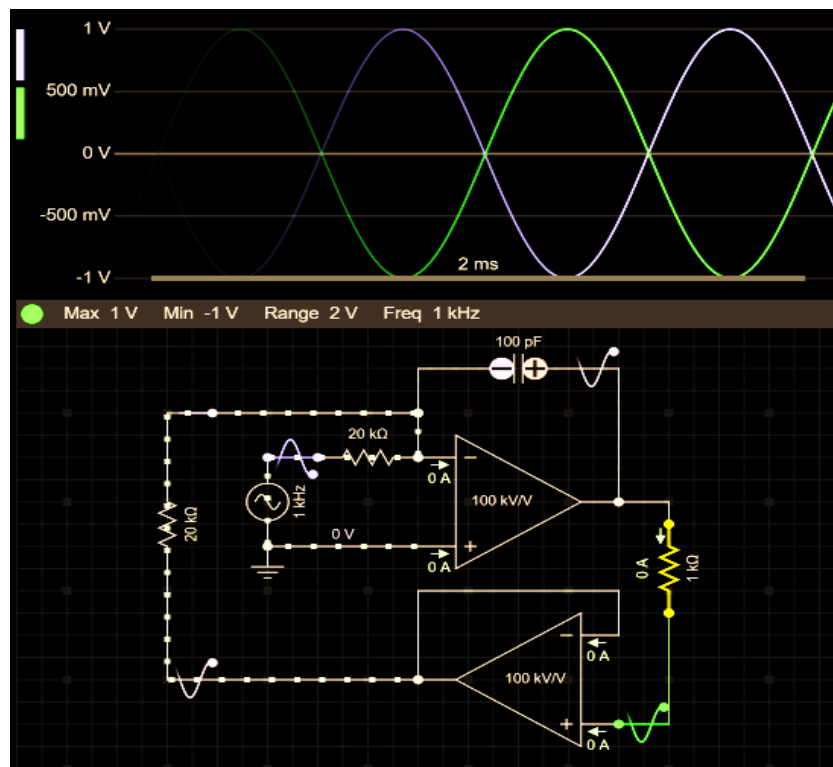


Fig. 5.4. Control amplifier circuit.



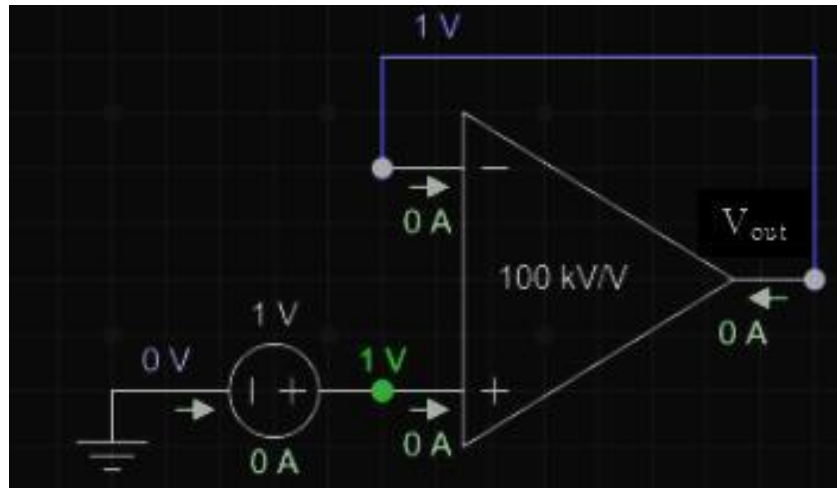


Fig. 5.5. Voltage buffer circuit.

$$V_{out} = V_{Non-inverting} \quad (5.4)$$

### 5.3.3.3. I to V converter

As the Arduino cannot measure current directly, it can only measure voltage as an input, so a current to voltage (I to V) converter is needed.

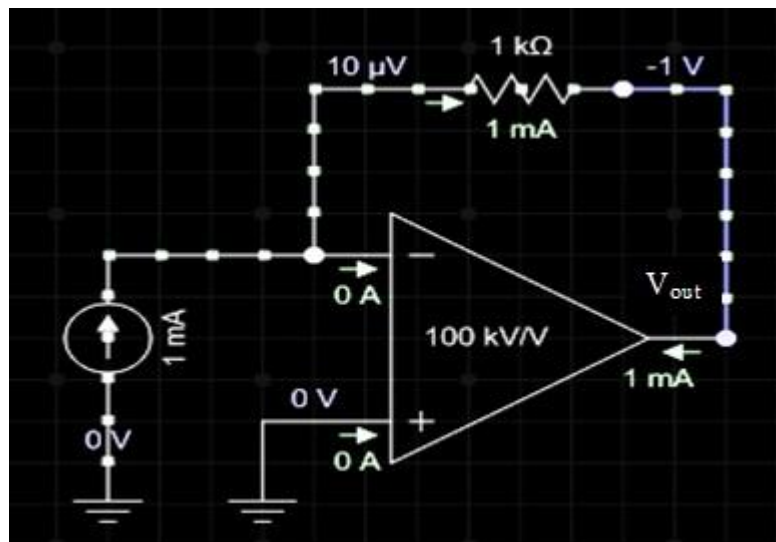


Fig. 5.6. I to V converter.

$$V_{out} = V_{Non-inverting} - R_f I_{Inverting} \quad (5.5)$$

In Eq. 5.5, if the value of  $V_{Non-inverting}$  is put 0,  $R_f=1K$  and the current and output voltage can be given as,  $I_{Inverting} = 1 mA$ ,  $V_{out} = 1 V$ , as can be seen in Fig 5.6.

### 5.3.4. Potentiostat circuit design

As can be seen from Fig. 5.7., from Pin 5 of Arduino Uno, the PWM signal is generated. The PWM signal is then fed as input to the second order filter circuit for generation of the triangular function. The output of the second order filter circuit is then connected to the input of the level shifter. There is a need for shifting the level because Arduino cannot generate negative voltage. To check the input signal or the final signal, there are dedicated pins to measure. Now, it is important to understand how the control amplifier works and the derivation of Eq. 5.5.

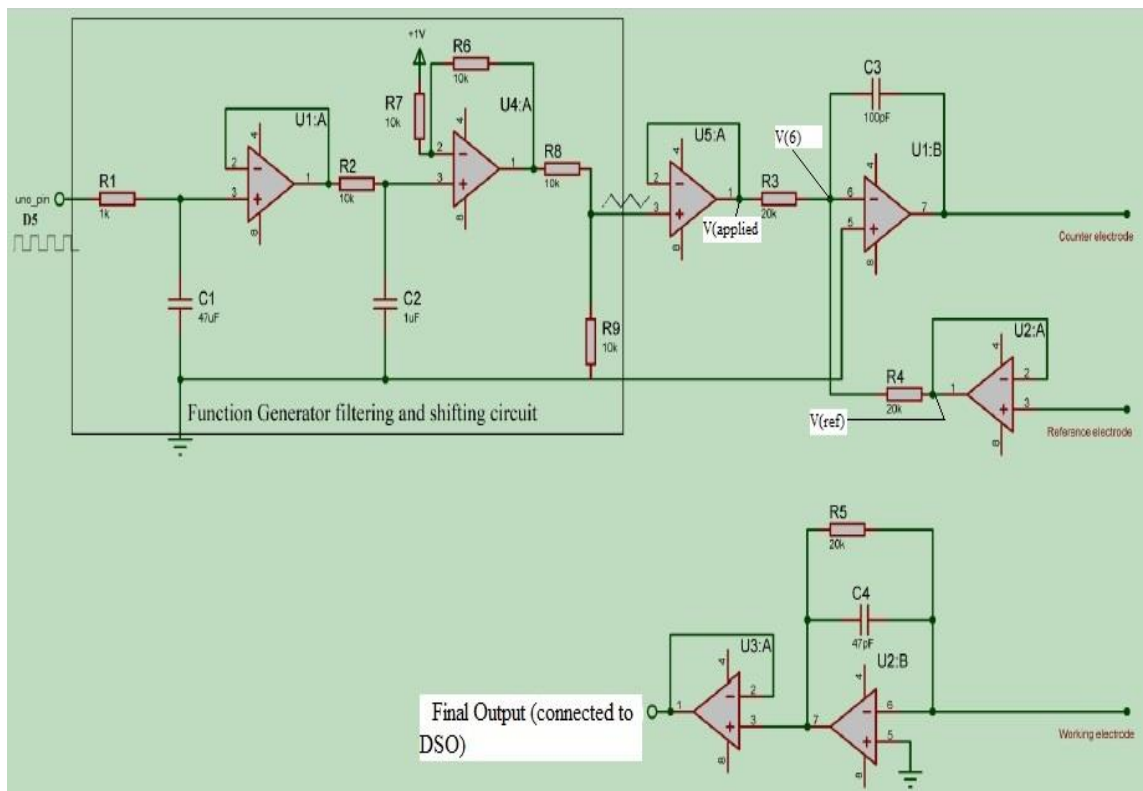


Fig.5.7. Potentiostat circuit design.

As the op-amp U1:B is having negative feedback, potential of the node near pin 6. (V(6)) of UC:B will be zero due to virtual short and owing to high input impedance, there will be no current going into the op-amp; therefore,

$$V_{applied} = -V_{ref} \quad [as R_3 = R_5 = 20 K\Omega]$$

Now to maintain the relation between  $V_{(applied)}$  and  $V_{(ref)}$ , the control amplifier forces current into the system, which flows through the solution potential between CE and WE. This current is then being measured, later. As

the RE and WE is put so close together and WE potential is at zero potential for virtual short of op-amp U2:A, this gives rise to Eq. 5.6.

$$V_{WE} - V_{RE} = V_{applied} \quad (5.6)$$

The feedback capacitors 100 pF and 47 pF are used so that with sudden changes in  $V_{applied}$ , the system does not start to oscillate and it also acts as phase correction capacitor. Till now, one of the major parts has been elucidated, which is applying potential between WE and RE. Now another part is to measure the current, which is being generated by control amplifier and is converted to voltage using the I to V converter. After converting the current to voltage, it is passed through a buffer circuit to avoid current loading and then there is a high voltage protection circuit for securing our microcontroller and other electronic components.

### 5.3.5. PCB routing

Fig 5.8 is the routing diagram which has been done using “Proteus 8 professional”. The size of the board is 45 mm x 42.5 mm.

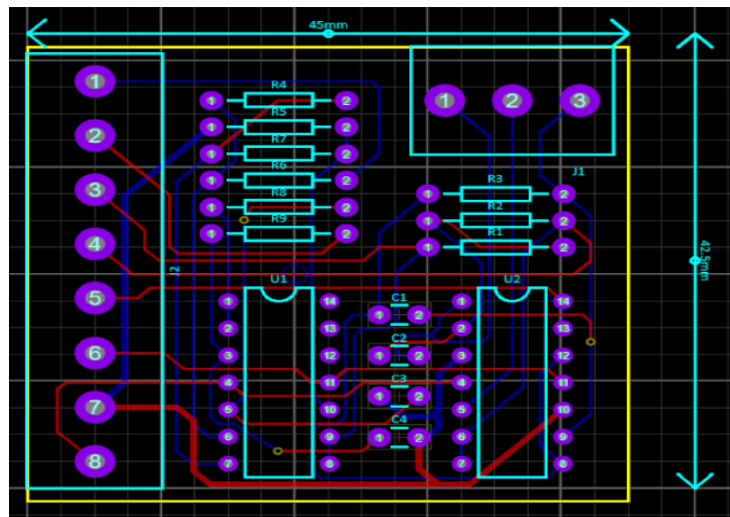


Fig.5.8. PCB routing in Proteus 8.

### 5.3.6. Snapshots of the developed system

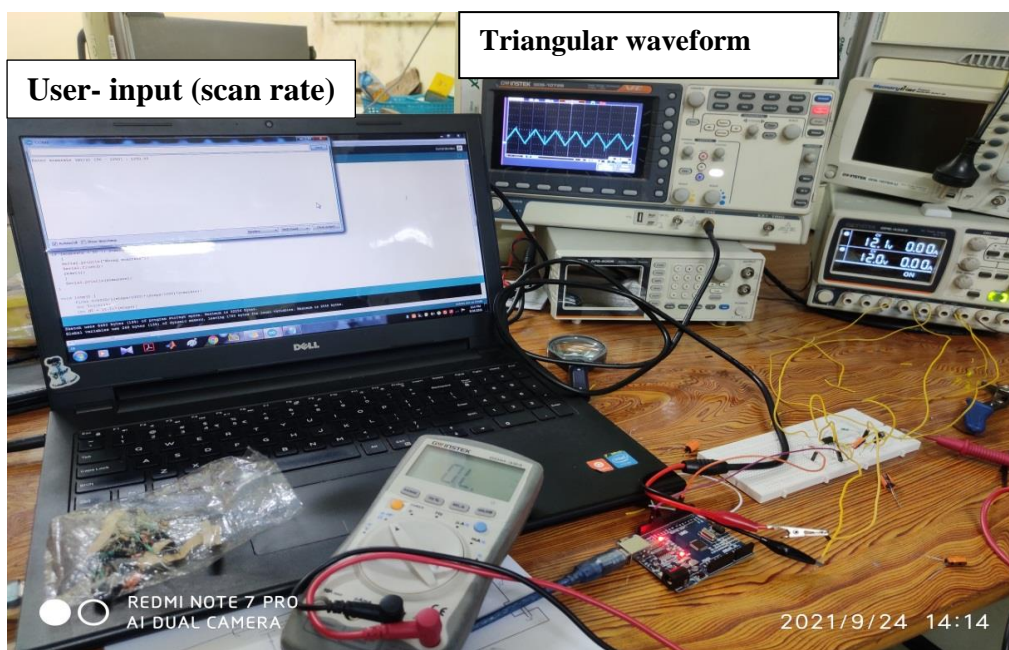


Fig. 5.9. Display of the triangular-waveform.

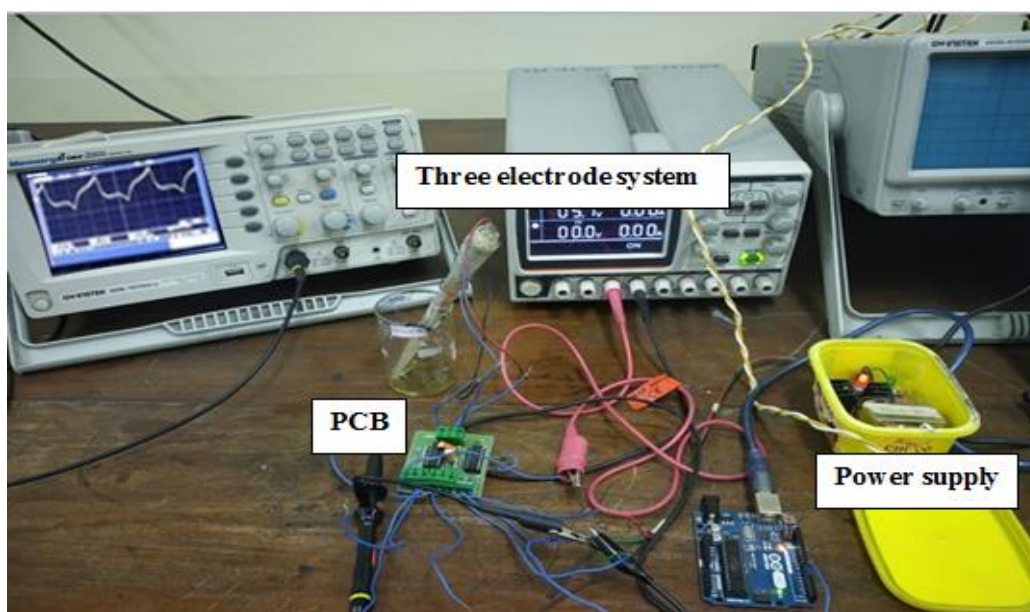


Fig. 5.10. Electrochemical response using the developed potentiostat

### 5.3.7. Power supply circuit

Voltage supplier is needed to power the op-amps and other circuit parts. In the work,  $+V_{sat}$  and  $-V_{sat}$  of op-amp LF347 are set as +12V and -

12V, respectively. So, we need to generated +12V and -12V. The power supply circuit, given in Fig. 5.11., has four stages.

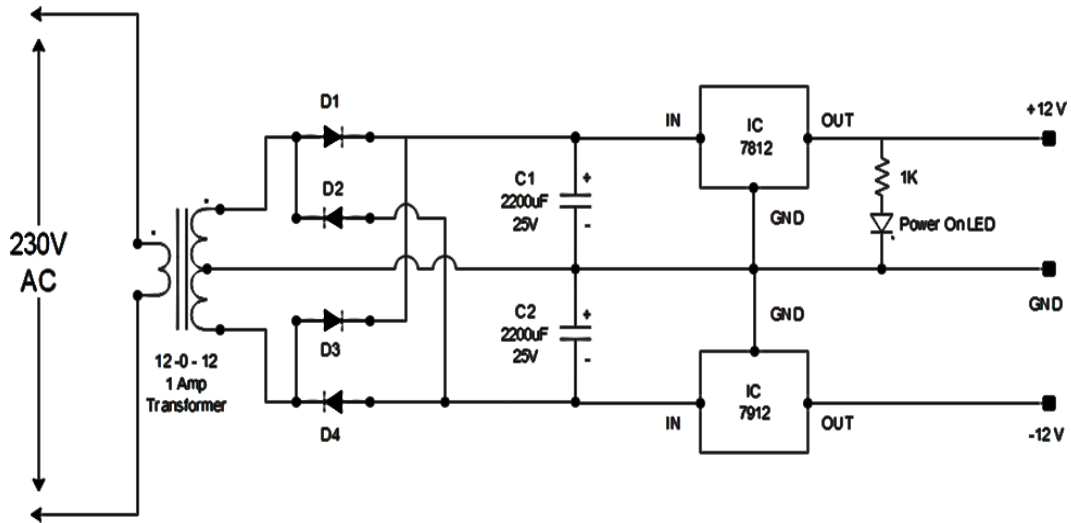


Fig. 5.11. Power supply circuit.

First is the transformer: it is a 24V 1 A center tapped transformer, which steps down 230V AC to 12V AC. It will measure 24V AC across the outer taps of the two secondary coils and 12V AC from each tap to the center-tap of the secondary coil. These two 12V AC supplies are 180° out of phase with each other [11]. Therefore,  $\pm 12V$  power supply can be made out of it.

Second is the full wave rectifier circuit which is made of four power diode (D1, D2, D3, D4) of 6 A: it converts AC into DC. Third is the 2200 $\mu F$  capacitor (C1 and C2) which is used to filter out ripples in DC. Fourth is the voltage regulator IC, which regulates the voltage at +12V (IC 7812) and 12V (IC 7912). Lastly there is the power on led. The ground is earthed to protect the circuit.

#### 5.4. Scan rate variation using the developed system

The scan rate was varied from 0.05V/s to 1.25V/s. It is observed from Fig. 5.12. that the peak-to-peak voltage is increasing on increasing the scan rate. Voltage and current being directly proportional, it may be concluded that the current will increase. This is at par with the response obtained in the previous chapters.

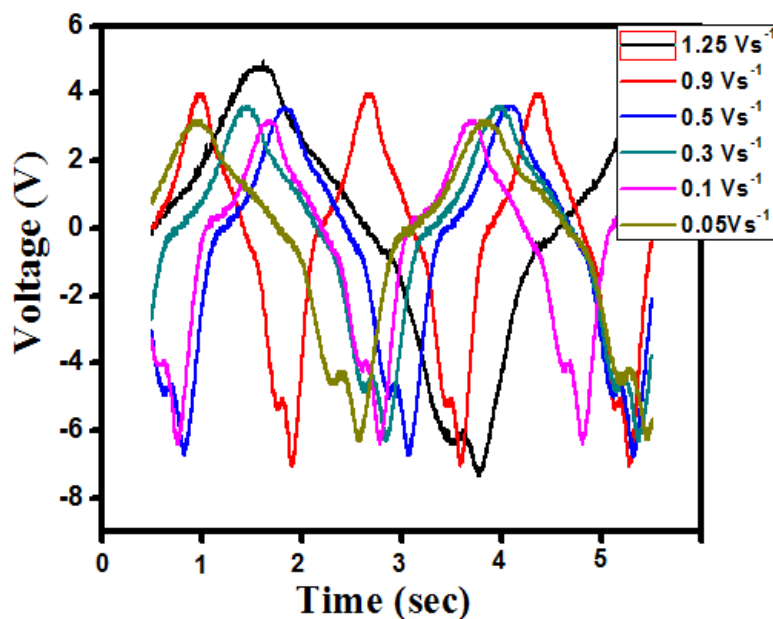


Fig. 5.12. Scan rate variation.

### 5.5. Comparison of data

The performance of the developed potentiostat has been initially tested with the MIP-caffeine electrode. At first, the electrode was subjected to the 1 mM stock solution of caffeine using commercial Autolab Potentiostat (PGSTAT 101). On imbibing, acceptable results were found as in Fig 5.14, with a peak current of 167.4  $\mu\text{A}$ . In order to compare the instrument that has been developed in this project work with the Autolab potentiostat, the same electrode was dipped in the caffeine solution of concentration 1 mM and a peak current of 161.56  $\mu\text{A}$  has been observed (Fig 5.15). The scan rate in both the cases of the Autolab potentiostat and for the developed potentiostat was  $0.1 \text{ Vs}^{-1}$ .



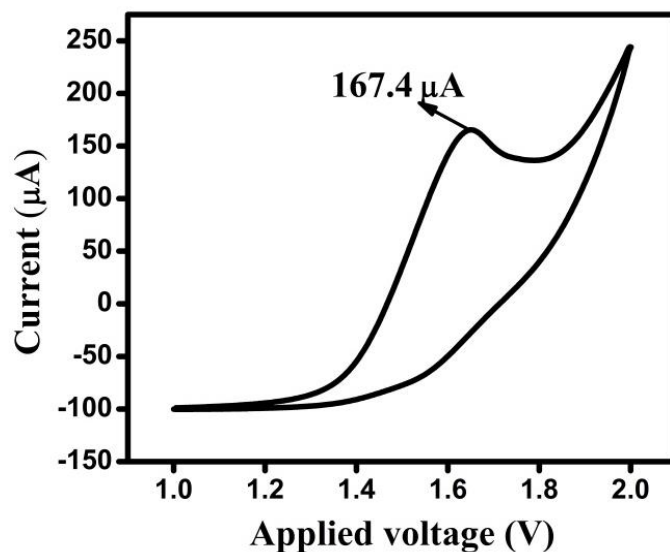


Fig.5.13. Voltammogram obtained with commercial Autolab potentiostat using MIP- caffeine electrode.

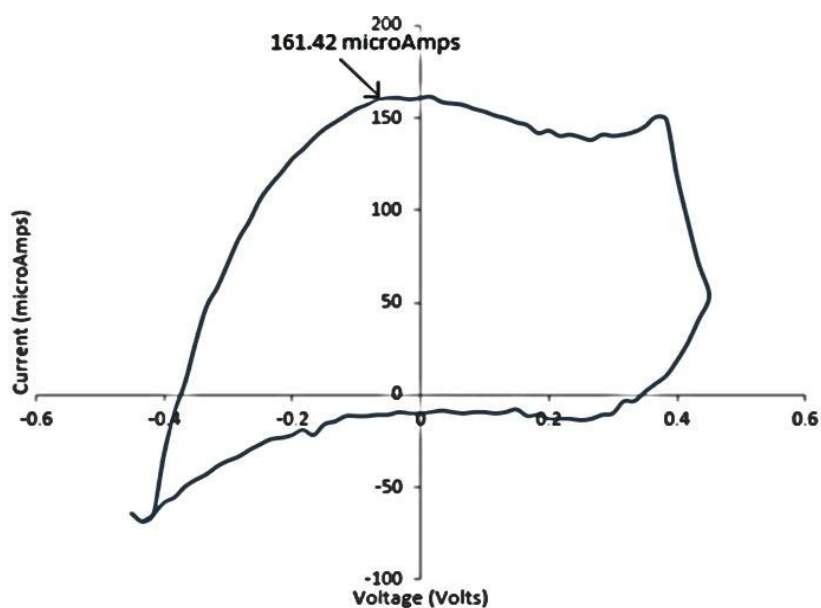


Fig.5.14. Voltammogram obtained with the developed system using the same electrode.

## 5.6. Conclusion

In this work, the performance of the developed potentiostat has been initially tested with the MIP-CAF electrode. At first, the electrode was subjected to the commercial Autolab Potentiostat (PGSTAT 101) to test the performance of the sensor. On imbibing the electrode, acceptable results were found with a peak current of 167.4  $\mu\text{A}$ . In order to compare the instrument that has been developed in this work

with the Autolab potentiostat, the same sensor was dipped in the CAF stock solution of concentration 1 mM and a peak current of 161.42  $\mu\text{A}$  has been observed. Hence, we can say that the device which has been developed this work is providing acceptable results. It is on the initial stage and needs several improvements to be made portable and commercial.

## References

- [1] M. D. Dryden and A. R. Wheeler, "Dstat: A versatile, open-source potentiostat for electroanalysis and integration", *PloS one* 10 (2015) e0140349.
- [2] K. Kellner, T. Posniecek, J. Ettenauer, K. Zuser, and M. Brandl, "A new, low-cost potentiostat for environmental measurements with an easy-to-use pc interface", *Procedia engineering*", 120 (2015) 956-960.
- [3] G. N. Meloni, "Building a microcontroller based potentiostat: A inexpensive and versatile platform for teaching electrochemistry and instrumentation", *Chem.Educ.* 93 (2016) 1320-1322.
- [4] H. Jin, Y. Qin, S. Pan, A. U. Alam, S. Dong, R. Ghosh, and M. J. Deen, "\Open- source low-cost wireless potentiometric instrument for ph determination experiments", (2018).
- [5] J. T. Barragan and L. T. Kubota, "Minipotentiostat controlled by smartphone on a micropipette: A versatile, portable, agile and accurate tool for electroanalysis", *Electrochimica Acta.* 341 (2020) 136048.
- [6] R. Ahmad, S. G. Surya, J. B. Sales, H. Mkaouar, S. Y. C. Catunda, D. R. Belfort, Y. Lei, Z. L. Wang, A. Baeumner, O. S. Wolfbeis et al., "Kaustat: A wireless, wearable, open-source potentiostat for electrochemical measurements:", *IEEE sensors*, (2019) 1-4.
- [7] J. B. Allen and R. F. Larry, "Electrochemical methods fundamentals and applications", John Wiley & Sons. (2001).
- [8] D. A. Skoog, F. J. Holler, and S. R. Crouch, "Principles of instrumental analysis", Cengage learning, (2017).
- [9] <https://www.ti.com/lit/ds/symlink/lf147.pdf?ts=1623910870261&refurl=https%253A%252F%252Fwww.google.com%252F>



- [10] S.-Y. Lu, S.-S. Shan, T.-H. Lu, Y.-H. Yeh, S.-C. Kuo, Y.-C. Chen, and Y.-T. Liao, "A review of cmos electrochemical readout interface designs for biomedical assays", IEEE Sensors Journal, 21 (2021) 12 469-12 483.
- [11] Van Brussels, Potentiostats: Principles of operation, Autolab Instruments (<http://ebookbrowse.net/vanbrussel-autolab-ppt-d20379686>).
- [12] A. Ghosh, "Electronic tongue based detection of important bio-chemical quality descriptors of black tea", Jadavpur University, PhD thesis, (2014).
- [13] S. Sarkar and M. Bhattacharya, "Sstat: Wi-and bluetooth integrated multimodal- do-it-yourself" electrochemical potentiostat," in IECON 2020 The 46th Annual Conference of the IEEE Industrial Electronics Society. IEEE, (2020) 5249-5254.



# Chapter 6

## Conclusion and future scopes

This chapter presents the review of the work and summary of the findings. It also presents some important recommendations for the developed methodology and the instrument developed towards various applications in industries. The future directions of research are discussed along with some concluding comments emphasizing the importance and implications of the reported research.

### **List of sections**

- Review of the work
- Summary of the findings
- Recommendations
- Future scope of this work
- Conclusion
- References





## Chapter 6

### Conclusion and future scope

---

#### 6.1. Introduction

First off, the thesis introduces a novel paradigm for qualitatively evaluating tea in terms of the components that contribute to its flavour. Currently, the tea industries mostly use two types of quality evaluation methodologies. The first is the appointment of tea tasters, in which a group of human panellists evaluates the tea and assigns a score between 1 and 10 based on a range of its various characteristics. The installation of analytical tools, which can precisely estimate the many biochemical factors contained in tea and afterwards assess its quality, is the second way. However, the expensive cost of these equipment prevents them from being used in remote businesses. The third technique, called E-tongue, is an improvised variation of the previous one in which an electronic circuitry array of sensors is used to simulate the human sense of taste. Thus, it is possible to eliminate human subjectivity and inconsistencies with this technique, which makes response patterns or qualitative judgements naturally repeatable. recurring in nature.

The use of non-specific or low-specific sensing elements is the main drawback of an E-tongue, despite the fact that it is objective and less expensive than analytical instruments. In an E-tongue, the general pattern of response collected from a variety of noble metal electrodes is analysed using the right pattern recognition algorithms to deliver the qualitative information of tea. The quality of other liquid samples can also be estimated using this set of electrodes. As a result, this method cannot evaluate the chemical information of the many analytes contained in tea and their contribution. E-tongue also gets a little pricey because it uses a lot of noble metal electrodes as sensing components.

In this thesis, a potential way of preparing the sensing elements has been proposed in order to get over the aforementioned restrictions of an E-tongue and in search of sensors with high affinity and sensitivity. The idea is to create imprinted cavities inside a polymer matrix that are comparable to the target molecule's orientation and form. This is known as a molecular imprinted polymer-based

approach. As a result, the electrode's sensitivity rises when it is exposed to that specific analyte, and a response profile is produced. The following benefits [1-3] of this methodology make it beneficial for the tea industries:

- a. Compared to the recently employed E-tongue, the overall cost of the instrument with MIP-designed electrodes will be significantly lower. This is due to the fact that the precursors used in a MIP-based technique are less expensive than noble metal electrodes.
- b. The procedure used to prepare the electrodes is incredibly straightforward and simple to repeat.
- c. The MIP approach uses a specific component of a substance as the target analyte during the electrode fabrication process. As a result, this technology makes it simple to gather specific information about the reaction kinetics of the system and the redox characteristics of the biochemical components.

Considering the above advantages, we understand that determination of the taste-affecting compounds is of utmost necessity and the molecularly imprinted polymer technique has been adopted for developing the electrodes. In the thesis, CAF has been chosen as the first chemical to be investigated in tea. GA has been chosen as the second molecule. GA is the only free phenolic acid found in tea and acts as a potent antioxidant. EC, the third molecule that has been selected, is the most significant bioactive compound of all and competes in the race to be served tea as a high-quality health beverage. For cost-efficiency, the epicatechin electrode has been fabricated in two different ways.

## 6.2. Summary of the findings

### 6.2.1. Development of titanium oxide nanoparticles modified MIP electrode for determination of caffeine in green tea

Regulating the amount of CAF in any food or beverage is of utmost importance and thus necessitates the development of a low-cost reusable sensor for its detection. The MIP sample has been prepared by copolymerization of AN and EGDMA of CV and DPV has been employed to study the electrochemical characteristics of the electrode. The electrochemical characteristics of the sensor have been detailed in chapter 2 and a

possible reason behind the superior performance of the proposed electrode has been cited. Real time application of the electrode has been ascertained by subjecting the synthesized electrode in ten variants of green tea. A separability index (SI) of 47.82% has been established on performing the PCA on the obtained DPV datasets. The PLSR model and PCR model have been developed to estimate the predictive ability of the electrode in terms of the CAF content by correlating the response of the obtained DPV datasets for the ten green tea samples with that of HPLC data. In the case of PLSR technique, an average prediction accuracy of 92.94% is obtained with root mean square error of calibration (RMSEC) value being as low as 0.07. For PCR, an average prediction accuracy of 93.75% is acquired with RMSEC value being 0.07. The performances of both the models have been compared in this study. Additionally, both the linear regression models have been validated with external datasets wherein acceptable prediction accuracy has been obtained.

### **6.2.2. Development of copper oxide nanoparticles embedded MIP electrode for tracing gallic acid in green tea**

The present work elucidates a method for the economic development of a reproducible electrode for sensitive determination and prediction of the amount of GA in green tea by MIP technology. The electrode material has been synthesized by co-polymerization of poly (itaconic acid) and EGDMA followed by implantation of CuO NPs. The electrochemical characteristics of the sensor have been detailed in chapter 3 and a possible reason behind the superior performance of the proposed electrode has been cited. The practical applicability of the electrode has been validated by quantifying the amount of GA in green tea samples. Principal component analysis (PCA) has been performed and class separability index (SI) of 31.27 has been calculated. While with PLSR, average prediction accuracy of 88.97 % is obtained with RMSEC as low as 1.35, PCR results in an average prediction accuracy of 87.24 % with RMSEC being 1.38.

### **6.2.3. Development of molecularly imprinted polymer-based electrode for detection of epicatechin in green tea**

To the best of the literature survey, this is the first work related to fabrication of MIP-EC electrode. EC is an important bioactive compound and

naturally-occurring flavonoid with strong antioxidant properties which contribute towards the quality of green tea.

*i) Electrochemical detection of epicatechin in tea using amine functionalized MWCNTs modified MIP-based electrode (Using epicatechin as template molecule)*

The polymer-graphite composite embedded with amine functionalized multi-walled carbon nanotubes (f-MWCNTs) has been synthesized to fabricate the MIP-EC electrode. Briefly, benzoyl peroxide (BP), the polymerization initiator enabled the matrix synthesis by co-polymerizing acrylamide (AAm) and EGDMA. Further, the modification of the MIP-EC electrode through incorporation of amine functionalized multi-walled carbon nanotubes (f-MWCNTs) enabled the increase in conductivity and adsorption properties. The electrode material was thoroughly mortared and a fine paste was poured in the capillary tube. The real time application of this electrode was tested in green tea samples. Two linear regression models have been developed, using the experimental DPV data and HPLC data as reference data to predict the EC. Prediction accuracies of 92% using PCR and 93.58 % using PLSR were obtained. The root mean square error of calibration (RMSEC) for PLSR and PCR is 0.29 and 0.31.

*ii) Electrochemical detection of epicatechin in green tea using quercetin-imprinted polymer electrode (Using quercetin as template molecule)*

In this work, we intend to develop a cost-effective reusable sensor for efficient detection of EC in green tea samples using the principle of MIP. Acrylamide (AAm) co-polymerized with EGDMA and optically inactive quercetin (Q) as the template has been used to make the electrode (sensor) material. The voltammetric experiment has been performed using the MIP-Q electrode with the help of a three-electrode configuration which comprises of the working electrode, reference electrode and counter electrode. PLSR and PCR models have been developed to investigate the predictive ability of the synthesized MIP-Q@G electrode using the DPV signals and the HPLC data. Both PLSR and PCR models achieved prediction accuracies of 94.54 % and 94.41% with a root mean square error of calibration (RMSEC) of 0.113 and 0.119, respectively. The electrochemical characteristics of the sensor have been detailed in chapter 4 and a possible reason behind the superior performance of the proposed electrode has been cited.



The analytical characteristics of all the electrodes synthesized in this work for the detection of CAF, GA and EC respectively has been summarized in the following Table 6.1. The predictive ability of the synthesized electrodes in terms of their average prediction accuracy using PLSR and PCR models have been tabulated in Table 6.2.

*Table 6.1 Summary of findings in the proposed work.*

Target	Electrode	Linear range	LOD	Repeatability (% RSD)	Reproducibility (% RSD)	Refs
CAF	MIP-TiO <sub>2</sub>	5-120 μM	0.6 μM	2.08	5.49	[1]
GA	MIP-CuO	1-100 μM 100-900 μM	12.6 nM	4.22	1.34	[2]
EC	MIP-EC	51 nM	0.051 μM	4.06	4.30	[3]
EC	MIP-Q@G	1-100 μM 100-500 μM	0.33 μM	4.12	1.76	[4]

*Table 6.2. Predictive ability of the fabricated electrodes.*

Target molecule	Fabricated Electrode	Average Prediction accuracy (%)	
		PLSR model	PCR model
CAF	MIP-TiO <sub>2</sub>	92.94	93.75
GA	MIP- CuO	88.96	87.23
EC	MIP-EC	93.58	92.00
EC (Dummy template: Q)	MIP-Q@G	94.54	94.41

#### **6.2.4. Towards development of a function generator and signal conditioning circuit for voltammetric purpose**

An additional step has been taken towards the development of a three electrode cyclic- voltammetry system. The commercial potentiostat is of very high cost because of its precision and provision of various types of voltammetric techniques. The three electrode cyclic voltammetry consists of a triangular wave-form generator, the potentiostat circuit, the three electrodes, namely, working electrode, counter electrode

and reference electrode and a digital storage oscilloscope for storing the data and the display of the voltammetric response.

### 6.3. Recommendations

The following applications in the tea business can be suggested for the proposed thesis study in its current form.

a) The MIP-TiO<sub>2</sub> electrode dedicated for CAF detection can be used by the tea industry to keep a check on the proper and safe caffeine content in tea. CAF concentrations of 3–6 mg/kg are considered safe. Concentrations of 80–100 mg/L are considered lethal. Psychiatric disorders have been related to large amounts and long-term use of caffeine. It acts as a trigger of psychiatric symptoms, from anxiety to depression and even psychosis. [5-8].

b) The CAF electrode and the GA electrode so developed can be used in food and as well as the pharmaceutical industries for measuring the content of CAF and GA content, respectively in certain medicines and food.

c) To increase the export worthiness, keeping a check on the antioxidants is of huge importance. This can be done by using the synthesized MIP- EC electrode.

### 6.4. Future scope of this work

There are several areas in which the proposed methodology discussed in the previous sections can undergo improvement. These are listed as follows:

a) The sensors should be made more commercially viable for implementation in the tea industries. It may be done using disposable sensors or sensors made using screen printed electrodes. By employing such types of methodologies, the problem of regenerating the surface every time the electrode is exposed to target analyte, may be dissolved. Moreover, those sensors will also be able to yield a greater level of precision.

b) All the sensors described herein, were tested using a limited number of tea samples supplied by Tocklai Tea Research Institute, Jorhat, Assam, India. To prepare an electrode that can be implemented in the industry level it must be trained with datasets corresponding to different types of tea samples from

different tea gardens. Therefore, there is a need to evaluate the performance of the sensors when it is exposed to different genres of tea corresponding to different tea gardens. Further, the electrodes should also be exposed to different variants of tea (black, oolong, etc.) to procure a wide range of samples for the performance validation of the electrodes.

c) In this thesis, though suitable protocols are described for the fabrication of the sensors, but only PLSR and PCR techniques have been used to evaluate them in terms of quantification of tea constituents and discrimination of different variants of tea. Consequently, there is a need for the application of different pattern recognition algorithms and various classification models in order to efficiently extract the information content of the electrodes.

d) In this thesis, only electrodes specific to CAF, GA and EC have been fabricated. In order to have a complete insight to the quality of tea liquor, electrodes specific to amino acids like L-theanine needs to be developed. This will enable to have a complete notion regarding the quality of tea.

e) It is realized that if specific electrodes can be designed for perceiving the tea aroma and brightness of tea liquor, a combinatorial approach consisting of E-tongue, E-nose and E-vision, respectively, can be pursued for performing the overall quality analysis of tea.

f) In this thesis, the MIP based sensors have been designed with a view to replace the noble metal-based E-tongue for more objective analysis of tea. Thus, an important future scope lies on the fabrication of tea specific electrodes so as to generate a portable device that can be used explicitly in the tea industries.

g) To make this device portable, some more future work needs to be done. Firstly, a function generator, which should have the provision of applying various types of voltammetric techniques should be there. Secondly an on-board power supplier like batteries or power banks with proper power rating needs to be placed and a proper charging circuit also needs to be designed. Third one, is to develop a useful user interference (UI) using raspberry pi, which will have the functionality to set the start-stop potential, scan rate, input waveform type and

last but not least is a voltammogram graph needs to be shown directly using the run time collected data. Apart from this a proper calibration of the device is needed to generate accurate results.

### 6.5. Conclusion

In order to develop a customized electronic tongue, we need a methodology to fabricate MIP-based sensors for qualitative tea liquor estimation. Even though the presented research is still in its nascent stages of development, it does pave the way for objective tea analysis. In addition to the obvious health benefits of these constituents, continued efforts in this direction can lead to the development of a very promising instrument that can not only be used by the tea industry, but also by the pharmaceutical industry.

### References

- [1] D. Das, T. N. Chatterjee, R.B. Roy, B. Tudu, A. K. Hazarika, S. Sabhapondit, R. Bandyopadhyay, “Titanium Oxide Nanocubes Embedded Molecularly Imprinted Polymer Based Electrode for Selective Detection of Caffeine in Green Tea”, *IEEE Sens. J.* 20(12) (2020), 6240-6247.
- [2] D. Das, D. Biswas, A.K. Hazarika, S. Sabhapondit, R. B. Roy, B. Tudu, R. Bandyopadhyay, “CuO Nanoparticles modified MIP-Based Electrode for Sensitive Determination of Gallic Acid in Green Tea”, *IEEE Sens. J.* 21 (2021) 5687-5694.
- [3] D. Das, S. Nag, A. Adaval, A. K. Hazarika, S. Sabhapondit, A. R. Bhattacharyya, B. Tudu, R. Bandyopadhyay, R.B. Roy, “Amine Functionalized MWCNTs Modified MIP-Based Electrode for Detection of Epicatechin in Tea”, *IEEE Sens. J.* 22(11), 2022, 10323-10330.
- [4] D. Das, S. Nag, S. De, A. K. Hazarika, S. Sabhapondit, B. Tudu, R. Bandyopadhyay, R.B. Roy, “Electrochemical Detection of Epicatechin in Green Tea Using Quercetin-Imprinted Polymer Graphite Electrode”, *IEEE Sens. J.* 21 (23) (2021) 265226- 265234.
- [5] N. Ogawa, H. Ueki, “Clinical importance of caffeine dependence and abuse”. *Psychiatry Clin. Neurosci.* 61 (2007) 263–268.

- [6] P. Broderick, A.B. Benjamin, “Caffeine and psychiatric symptoms: A review”, J. Okla. State Med. Assoc. 97 (2004) 538–542.
- [7] J.A. Greenberg, C. Dunbar, R. Schnoll, R. Kokolis, S.Kokolis, J. Kassotis, “Caffeinated beverage intake and the risk of heart disease mortality in the elderly: a prospective analysis”, Am. J. Clinical Nutrition. 85 (2007) 392-398.
- [8] J.V. Higdon, B. Frei, “Coffee and health: a review of recent human research”, Crit Rev Food Sci Nutr. 46(2) (2006) 101-123.



Professor  
Dept. of Instrumentation & Electronics Engg  
Jadavpur University  
Saltlake, 2nd Campus  
Kolkata-700 106

